

A MECHANISTIC AND KINETIC STUDY:
CONVERSION OF ICE NANOCRYSTALS
TO NANOPARTICLES OF THE
HYDRATES OF AMMONIA

By

NEVIN URAS

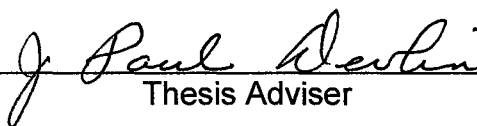
Bachelor of Science
Anadolu University
Eskisehir, Turkey
1993

Master of Science
Oklahoma State University
Stillwater, Oklahoma
1997

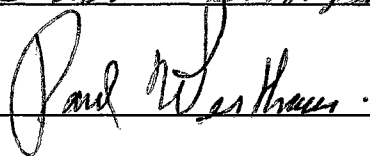
Submitted to the Faculty of the
Graduate College of the
Oklahoma State University
in partial fulfillment of
the requirements for
the Degree of
DOCTOR OF PHILOSOPHY
December, 2001

A MECHANISTIC AND KINETIC STUDY:
CONVERSION OF ICE NANOCRYSTALS
TO NANOPARTICLES OF THE
HYDRATES OF AMMONIA

Thesis Approved:


Thesis Adviser










Dean of the Graduate College

ACKNOWLEDGMENTS

I would first like to express my sincere thanks to my advisor Dr. J. Paul Devlin for his unending guidance, great patience, and invaluable advice. Without his mentoring, this work would not have been possible.

I would also like to thank my committee members, Dr. Donald Thompson, Dr. Nicholas Kotov, Dr. Lionel Raff, and Dr. Paul Westhaus. All have provided me with insightful comments and recommendations. Special thanks go out to Dr. Donald Thompson whose assistance with my work has enabled me to become a more knowledgeable Chemist. I cannot thank him enough for his endless encouragement and material support.

I would also like to express my gratitude to Dr. Victoria Buch of Hebrew University in Jerusalem. She has not only been given me much professional advice, but has also been a true friend.

I wish to extend my special appreciation to my parents, Ismail Uras and Mukadder Uras, for their love, faith and encouragement. My husband, Levent Aytemiz, has been a constant source of support. My daughter, Aylin Sila, has been an inspiration to me and I sincerely hope that she has the same opportunities as I had.

Finally, the financial support provided by the National Science Foundation is appreciated.

TABLE OF CONTENTS

Chapter	Page
I. LITERATURE REVIEW.....	1
Introduction.....	1
Ice Nanocrystals as a Sample for FTIR.....	4
Structure.....	4
Interactions of the Ice Nanocrystals with Adsorbates.....	8
IR spectrum of NH ₃	15
NH ₃ + H ₂ O Complexes.....	15
Hydrates of Ammonia.....	20
The Monohydrate of Ammonia.....	20
The Hemihydrate of Ammonia.....	26
The Dihydrate of Ammonia.....	26
Reactions in the Solid State and Deuterium Isotope Effects on Reaction Kinetics.....	31
Deuterium Isotope Effects on Reaction Kinetics.....	34
II. EXPERIMENTAL.....	38
Introduction.....	38
Experimental Equipment.....	38
Cryogenic System and Cryogenic Cell.....	38
Vacuum System.....	40
FTIR Instrument.....	41
Experimental Procedure.....	41
Procedure for the Conversion of the Ice Nanocrystals to the Monohydrate of Ammonia.....	42
Preparation of the Window Deposited Ice Nanocrystals.....	42
Adding NH ₃ (ND ₃) and Collecting FT-IR Spectra.....	43
Evaluation of the Data.....	43
Procedure for the Conversion of the Ice Nanocrystals to the Hemihydrate of Ammonia.....	46
Alternating Layers.....	46
Collecting Data.....	47
Methodology for Evaluation of Experimental Results for Conversion of Ice Nanocrystals to the Hemihydrate of Ammonia.....	51

Chapter	Page
III. CONVERSION OF ICE NANOCRYSTALS TO THE MONOHYDRATE OF AMMONIA.....	63
Introduction.....	63
Mechanism for the conversion of Ice Nanocrystals to the Monohydrate of Ammonia.....	64
Kinetics of Conversion of Ice Nanocrystals to the Ammonia Monohydrate.....	64
Introduction.....	64
Conversion of D ₂ O Ice Nanocrystals to NH ₃ .D ₂ O at Different Reaction Temperatures.....	66
Temperature Dependence of the Reaction Rates.....	69
Isotope Effects on Reaction Kinetics.....	69
D ₂ O versus H ₂ O.....	69
NH ₃ versus ND ₃	72
Effect of Size of the Ice Nanocrystals on the Reaction Kinetics.....	79
Changing Particle Size by Ostwald Ripening.....	79
Changing the Particle Size by Preparing Particles at 140 and 145 K.....	85
What is the Rate Determining Step for the Conversion of Ice Nanocrystals to the Monohydrate of Ammonia?	90
Major sources of Errors in Determination of the Reaction Rates.....	92
IV. CONVERSION OF ICE NANOCRYSTALS TO THE AMMONIA HEMIHYDRATE.....	94
Introduction.....	94
Mechanism for Conversion of Ice Nanocrystals to the Hemihydrate of Ammonia.....	95
NH ₃ on the Ice Surface.....	96
Penetration/Conversion to the Hydrates.....	96
Kinetics of Conversion of Ice Nanocrystals to the Ammonia Hemihydrate.....	100
Introduction.....	100
Conversion of D ₂ O Ice to 2NH ₃ .D ₂ O at Different Reaction Temperatures.....	102
Relation of the Subsurface Spectrum to the Initial Fraction of Reacted Ice.....	118
Evaluation of the kinetic results by using the product band intensities....	119
Isotopic effects on Reaction Kinetics.....	124
D ₂ O versus H ₂ O.....	124
NH ₃ versus ND ₃	130

Chapter	Page
V. KINETIC MODEL FOR THE CONVERSION OF ICE NANOCRYSTALS TO THE HEMIHYDRATE OF AMMONIA.....	139
Introduction.....	139
Diffusion Equations.....	140
Shrinking (Unreacted) Core Model for Spherical Particles.....	141
The Diffusion Kinetics of Reactions in Spherical Particles: Ginstling and Brounshtein's Derivation.....	145
Kinetic Model for Solid-State Reactions; Carter's Derivation.....	149
Analysis of NH ₃ +D ₂ O Results Using Shrinking Core Model.....	151
Conversion of Ice Nanocrystals to the Amorphous Hemihydrate.....	151
The temperature Dependence of Reaction Rates.....	154
Conversion of Ice Nanocrystals to the Crystalline 2NH ₃ .D ₂ O.....	155
Ginstling's Equation.....	159
Carter's Equation.....	159
Conversion of H ₂ O Ice Nanocrystals to the Amorphous 2NH ₃ .H ₂ O.....	163
Conversion of D ₂ O Ice Nanocrystals to 2ND ₃ .D ₂ O.....	163
Errors in the Results.....	167
Errors in Determination of Fraction of Reacted Ice.....	167
Errors in Determination of Constants in the Equation of (6bD _e C _{Ag} /ρ _B R ²)	168
Summary.....	168
VI. CONCLUSION AND DISCUSSION.....	170
Introduction.....	170
Conclusions.....	170
Literature Review for the Kinetic Studies with Ice.....	171
Diffusion of HDO in Ice.....	174
Future Studies.....	174
REFERENCES.....	176
APPENDIX.....	181

LIST OF TABLES

Table	Page
1. Positions for the major absorption bands of NH_3	17
2. Vibrational frequencies of $\text{NH}_3 \cdot \text{H}_2\text{O}$ and $\text{ND}_3 \cdot \text{D}_2\text{O}$	24
3. Frequencies of spectral features of $2\text{NH}_3 \cdot \text{H}_2\text{O}$, $2\text{NH}_3 \cdot \text{D}_2\text{O}$ and $2\text{ND}_3 \cdot \text{D}_2\text{O}$	29
4. Infrared spectral features of $\text{NH}_3 \cdot 2\text{H}_2\text{O}$ at 100 K.....	33
5. $2\text{NH}_3 \cdot \text{D}_2\text{O}$ at 102 K from the second method.....	121
6. Fraction of reacted ice versus time for $2\text{NH}_3 \cdot \text{D}_2\text{O}$ from the first method.....	181
7. Fraction of reacted ice versus time for $2\text{NH}_3 \cdot \text{D}_2\text{O}$ from the second method.....	182
8. Fraction of reacted ice versus time for $2\text{NH}_3 \cdot \text{H}_2\text{O}$ from the second method.....	183
9. Fraction of reacted ice versus time for $2\text{ND}_3 \cdot \text{D}_2\text{O}$ from the second method.....	184

LIST OF FIGURES

Figure	Page
1. Representation of an ice particle.....	4
2. Crystalline ice structure.....	6
3. A model crystalline cubic ice surface.....	7
4. The subsurface and surface spectra.....	9
5. Surface groups of an ice cluster.....	13
6. Difference spectra obtained by subtracting the spectra of adsorbate-coated ice nanocrystals from the spectrum of the bare ice nanocrystals.....	14
7. IR spectrum of solid ammonia.....	16
8. Structure of $\text{NH}_3\text{-H}_2\text{O}$ and B – structure of $\text{NH}_3\text{-2(H}_2\text{O)}$	19
9. The crystal structure of ammonia monohydrate.....	21
10. Infrared spectrum of $\text{NH}_3\text{.H}_2\text{O}$ at 100 K.....	22
11. Infrared spectrum of $\text{ND}_3\text{.D}_2\text{O}$ at 100 K.....	23
12. Structure of $2\text{NH}_3\text{.H}_2\text{O}$	27
13. Infrared spectra of hemihydrate of ammonia for the different isotopomers of water and ammonia.....	28
14. Infrared spectrum of $\text{NH}_3\text{.2H}_2\text{O}$ at 100 K.....	32
15. Potential energy diagram for a molecule with H and D.....	35
16. Main components of the experimental equipment.....	39
17. Standard spectra of $\text{NH}_3\text{.D}_2\text{O}$, $\text{ND}_3\text{.D}_2\text{O}$ and $\text{NH}_3\text{.H}_2\text{O}$	44

Figure	Page
18. Finding one datum for extent of formation of $\text{NH}_3 \cdot \text{D}_2\text{O}$	45
19. The spectrum of a network of $\text{NH}_3 + \text{H}_2\text{O}$ particles at 90 K.....	48
20. The spectrum of a network of $\text{ND}_3 + \text{D}_2\text{O}$ particles at 90 K.....	49
21. The spectrum of a network of $\text{NH}_3 + \text{D}_2\text{O}$ particles at 90 K: bottom.....	50
22. Spectra of NH_3 and ND_3	53
23. Finding one datum for extent of formation of amorphous $2\text{NH}_3 \cdot \text{D}_2\text{O}$	54
24. Subtracted spectra between zero-time ice and partially reacted ice spectra.....	55
25. Shows extent of reaction in the zero-time ice spectrum of $\text{NH}_3 + \text{D}_2\text{O}$	57
26. Spectra of the network of $\text{NH}_3 + \text{D}_2\text{O}$	59
27. Subtraction of the bare D_2O ice spectrum from itself.....	61
28. Finding one datum for extent of formation of amorphous $2\text{NH}_3 \cdot \text{D}_2\text{O}$	62
29. A simple picture of the mechanism of the transport of NH_3 to the ice nanocrystals.....	65
30. The monohydrate of ammonia ($\text{NH}_3 \cdot \text{D}_2\text{O}$) at 115 K.....	67
31. Plots of the fraction of reacted ice versus time (h) for the conversion of D_2O ice nanocrystals to $\text{NH}_3 \cdot \text{D}_2\text{O}$ at the different reaction temperature....	68
32. Arrhenius plot of the rate constant (k) of conversion of D_2O ice nanocrystals to $\text{NH}_3 \cdot \text{D}_2\text{O}$	70
33. The monohydrate of ammonia ($\text{NH}_3 \cdot \text{H}_2\text{O}$) at 115 K.....	71
34. Plots of the fraction of reacted ice versus time for the conversion of H_2O ice nanocrystals to $\text{NH}_3 \cdot \text{H}_2\text{O}$ at the different reaction temperature.....	73
35. Comparison of the formation rates for $\text{NH}_3 \cdot \text{D}_2\text{O}$ versus $\text{NH}_3 \cdot \text{H}_2\text{O}$ at 115, 117 and 123 K.....	74

Figure	Page
36. Arrhenius plot of the rate constant (k) of conversion of H ₂ O ice nanocrystals to NH ₃ .H ₂ O.....	75
37. The monohydrate of ammonia (NH ₃ .D ₂ O) at 117 K.....	76
38. Plots of the fraction of reacted ice versus time (h) for the conversion of D ₂ O ice nanocrystals to ND ₃ .D ₂ O at the different reaction temperature.....	77
39. Comparison of the formation rates for NH ₃ .D ₂ O versus ND ₃ .D ₂ O.....	78
40. Arrhenius plot of the rate constant (k) of conversion of D ₂ O ice nanocrystals to ND ₃ .D ₂ O.....	80
41. Shows decreasing d-D intensity with increasing annealing temperature.....	82
42. Difference spectra obtained by subtracting the spectrum of the bare ice nanocrystals from the spectra of NH ₃ -coated ice nanocrystals.....	83
43. Effect of the ice particle size on the reaction kinetics.....	84
44. Difference spectra obtained by subtracting the spectrum of the bare ice nanocrystals from the spectra of NH ₃ -coated ice nanocrystals.....	87
45. Plots of fraction of reacted ice versus time (hr) for the samples having the similar amount surface areas.....	88
46. Plots of fraction of reacted ice versus time (hr) for the samples having the different thickness of ice network.....	89
47. Proposed free energy diagram.....	98
48. The heterogeneous reaction of NH ₃ with spherical ice particles.....	100
49. Starting point of the reaction.....	102
50. The product spectra, from the difference spectra between the zero-time ice and the partially reacted ice.....	104
51. The plot for the conversion of D ₂ O ice nanocrystals to 2NH ₃ . D ₂ O at 100 K.....	105
52. The plot for the conversion of D ₂ O ice nanocrystals to 2NH ₃ .D ₂ O at 102 K.....	107

Figure	Page
53. The product spectra, from the difference spectra between the zero-time ice and the partially reacted ice.....	108
54. The product spectra, from the difference spectra between the zero-time ice and the partially reacted ice.....	109
55. The plot for the conversion of D ₂ O ice nanocrystals to 2NH ₃ .D ₂ O at 105 K.....	110
56. The product spectra, from the difference spectra between the zero-time ice and the partially reacted ice.....	111
57. The plot for the conversion of D ₂ O ice nanocrystals to 2NH ₃ .D ₂ O at 107 K.....	112
58. The plot for the conversion of D ₂ O ice nanocrystals to 2NH ₃ .D ₂ O at 110 K.....	113
59. The product spectra, from the difference spectra between the zero-time ice and the partially reacted ice.....	114
60. The sample spectra, after partial reaction, as a function of time at 112 K.....	116
61. The plot for the conversion of D ₂ O ice nanocrystals to 2NH ₃ .D ₂ O at 112 K.....	117
62. The sample spectra, after partial reaction, as a function of time at 102 K.....	120
63. The plot obtained from two methods.....	123
64. The sample spectra, after partial reaction, as a function of time at 105 K.....	125
65. The sample spectra, after partial reaction, as a function of time at 107 K.....	126
66. The plot for the conversion of D ₂ O ice nanocrystals to amorphous 2NH ₃ .D ₂ O at 105 and 107 K.....	127
67. The sample spectra, after partial reaction, as a function of time at 110 K.....	128

Figure	Page
68. The plot for the conversion of D ₂ O ice nanocrystals to crystalline 2NH ₃ .D ₂ O at 107,110 and 112 K.....	129
69. The plot for the conversion of H ₂ O and D ₂ O ice nanocrystals.....	131
70. The sample spectra, after partial reaction, as a function of time at 102 K.....	132
71. The sample spectra, after partial reaction, as a function of time at 105 K.....	133
72. The sample spectra, after partial reaction, as a function of time at 102 K.....	135
73. The plot for the reaction of NH ₃ and ND ₃ with the D ₂ O ice nanocrystals.....	136
74. The plot for the reaction of NH ₃ and ND ₃ with the D ₂ O ice nanocrystals....	137
75. A representation of a partially reacted particle.....	142
76. Diagram of the process.....	146
77. Model for the Carter's analysis.....	150
78. Plots of $[1-3(1-X_B)^{2/3}+2(1-X_B)]$ versus time for the conversion of D ₂ O ice nanocrystals to the amorphous 2NH ₃ .D ₂ O.....	152
79. Plot of lnD versus 1/T for the conversion of D ₂ O ice nanocrystals to the amorphous 2NH ₃ .D ₂ O.....	156
80. Plots of $[1-3(1-X_B)^{2/3}+2(1-X_B)]$ versus time for the conversion of D ₂ O ice nanocrystals to the crystalline 2NH ₃ .D ₂ O.....	157
81. Plot of lnD versus 1/T for the conversion of D ₂ O ice nanocrystals to the crystalline 2NH ₃ .D ₂ O.....	158
82. Comparison of Gingstling's and Carter's equations for the conversion of D ₂ O ice nanocrystals to 2NH ₃ .D ₂ O at 102 K.....	161
83. Comparison of Gingstling's and Carter's equations for the conversion of D ₂ O ice nanocrystals to 2NH ₃ .D ₂ O at 112 K.....	162

Figure	Page
84. Plots of $[1-3(1-X_B)^{2/3}+2(1-X_B)]$ versus time for the conversion of H ₂ O ice nanocrystals to the amorphous 2NH ₃ .H ₂ O.....	164
85. Plots of $[1-3(1-X_B)^{2/3}+2(1-X_B)]$ versus time for the conversion of D ₂ O ice nanocrystals to the amorphous 2ND ₃ .D ₂ O.....	165
86. Plots of $[1-3(1-X_B)^{2/3}+2(1-X_B)]$ versus time for the conversion of D ₂ O ice nanocrystals to the crystalline 2ND ₃ .D ₂ O.....	166

CHAPTER I

LITERATURE REVIEW

1. Introduction

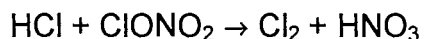
This study describes the “hydrogen bond chemistry” that takes place between crystalline ice and ammonia molecules (NH_3) within a mechanistic and kinetic perspective. More specifically, it considers, under given experimental conditions, how and how fast NH_3 molecules can convert ice particles to particles of the hydrates of ammonia, which are known hydrogen-bonded compounds. Furthermore, it shows how FTIR spectroscopic methods are used for this purpose.

Water is one of the unique molecule because of its ability to form four strong hydrogen bonds to four neighboring molecules as in ice. It also forms H-bonds with adsorbates, e.g., NH_3 , HCl .¹ Chemical and physical processes occurring with the adsorbates at the surface and in the bulk of the crystalline ice have gained particular attention, since, in addition to the biological applications², interaction of adsorbates with the ice is a particularly important subject of atmospheric science.

In recent years, heterogeneous reactions taking place with HCl , HNO_3 , N_2O_5 , and ClONO_2 on ice clouds have been studied extensively after the discovery of their part in the appearance of the ozone hole. Two types of polar stratospheric clouds (PSCs) have been reported; type I is thought to consist of

nitric acid trihydrate (NAT) particles and type II contains the water ice particles contaminated with small amounts of acids.^{3,4,5}

Although the overall chemistry that causes the ozone depletion is fairly well understood, the mechanism involved in these processes are still unclear. For instance, the reaction



is proposed as one of the key reactions for the ozone depletion, since it produces gaseous Cl_2 . The photodissociation of Cl_2 by sunlight produces chlorine (Cl) atoms that can attack and destroy ozone. Although this reaction is slow in the gas phase, it occurs very quickly on the surface of ice. The proposed first step for this reaction is the adsorption and reaction of HCl on the surface and in the ice.^{3,4,5} Therefore, this has been a subject for experimental^{6,7,8} and theoretical studies^{9,10,11}. There are unclear aspects that involve how HCl adsorbs on the ice surface, reacts with ice and converts ice to the hydrates of HCl. Moreover, the reaction kinetics for the conversion of ice to hydrates of HCl is the prime concern of most of these researchers.

Reports of studies that investigate HNO_3 and ice within these perspectives are also intensive in the literature.^{12,13}

This study is not undertaken to understand these processes. However, it will aid in understanding the mechanism of the reaction of the strong acids since NH_3 is a strong base that reacts with ice.

Moreover, this study contributes to knowledge of the heterogeneous reaction kinetics taking place between gas molecules and solid particles as in the

atmosphere.

Hydrogen bonds are also important cosmochemically. In the outer solar system, the most stable nitrogen and oxygen containing species at the ambient temperatures and pressures are ammonia and water. Ices and hydrates formed from these may play critical roles in the origin and evolution of the outer solar system bodies.¹⁴ For instance, Lewis¹⁵ modeled for Jupiter's clouds and used the model to study the clouds thermodynamic properties. The model predicted that solid phases of H₂O and NH₃ are important components of the atmosphere at high altitudes where the temperature is below a few hundred Kelvin. The thermodynamic studies of the NH₃-H₂O system showed that the hydrate forms of ammonia may be found under the clouds of NH₃. Therefore, a detailed understanding of the hydrate formation kinetics, phase diagrams and mechanical properties is of interest over a wide range of temperatures and pressures.

These examples are given to illustrate the potential applications of this study and they can be enlarged. Therefore, to understand the hydrogen bond chemistry, we studied the conversion of ice nanocrystals to the nanoparticles of the hydrates of ammonia, in terms of mechanism and kinetics, under laboratory conditions. Furthermore, this will be a basis of a computer simulation for the molecular-level investigation of this reaction, as the computer simulation technique will be adapted to understanding initial steps of NH₃ adsorption, penetration and hydrate formation.

2. Ice Nanocrystals as a Sample for FTIR

2.1. Structure

The structure of ice nanocrystals has been studied by both spectroscopic and computational methods; it is shown that a single particle has a surface, subsurface and interior (see Figure 1), but its spectrum is consistent with a largely crystalline ice structure.

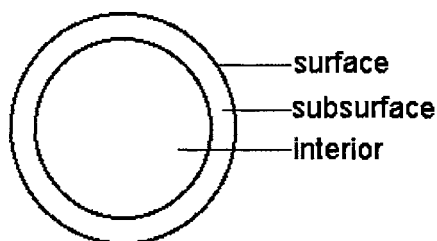


Figure 1. Representation of an ice particle.

The information about the structure of ice nanocrystals is usually derived from difference spectra. Useful difference spectra can be obtained from comparison of spectra of annealed and unannealed ice.¹⁶ When ice nanocrystals are annealed, the size of the particles become larger by the Ostwald ripening process. During this process, small particles vaporize and the vapor is added to the surface of larger ones. Further, one can control the particle size depending on the annealing temperature (generally, the size changes between 110-150 K). Some surface molecules are converted to interior ice during the ripening process. Consequently, after the annealing process, some of the surface molecule

absorption is lost due to this conversion. This can be followed by FTIR difference spectroscopy as decreasing peak intensities of the surface molecules. Although the total amount of ice does not change, different relative amounts of surface and interior absorption are obtained from the annealed and unannealed ice sample spectra that are taken at the same temperature.¹⁶

Difference spectra between the annealed and unannealed spectra and computational methods show that the surface of ice nanocrystals consists of 3-coordinated molecules with non-H-bonded atoms or dangling-H (D) (or d-H(D)), molecules with a dangling-O coordination (or d-O) and 4-coordinated surface (or s-4) water molecules (see Figure 2). Furthermore, the vibrational modes of surface molecules are assigned¹⁷ as follows: a) the out-of-phase stretch of the three-coordinated molecules with dangling-H (D) is 3692 (2725) cm^{-1} , the in-phase stretch 3110 (2300) cm^{-1} and the bending modes 1650 (1215) cm^{-1} , b) the out-of-phase stretch of the three coordinated molecules with dangling-O is 3560 (2640) cm^{-1} , the in-phase stretch 3350 (2480) cm^{-1} and the bending modes 1690 (1235) cm^{-1} , c) the out-of-phase of s-4 molecule is 3490 (2580) cm^{-1} .

Buch¹⁷ simulated a surface of an ice slab. She started with the crystalline ice surface (see Figure 3A) and then carried out classical MD heating simulations. The S3 (see Figure 3B) disordered surface was found to give the closest match to the experimental data. A similar disordered surface was observed in the computational work of Kroes.¹⁸

In the subsurface of ice particles, most water molecules are 4-coordinated and their coordination shells distorted with respect to tetrahedral symmetry. The

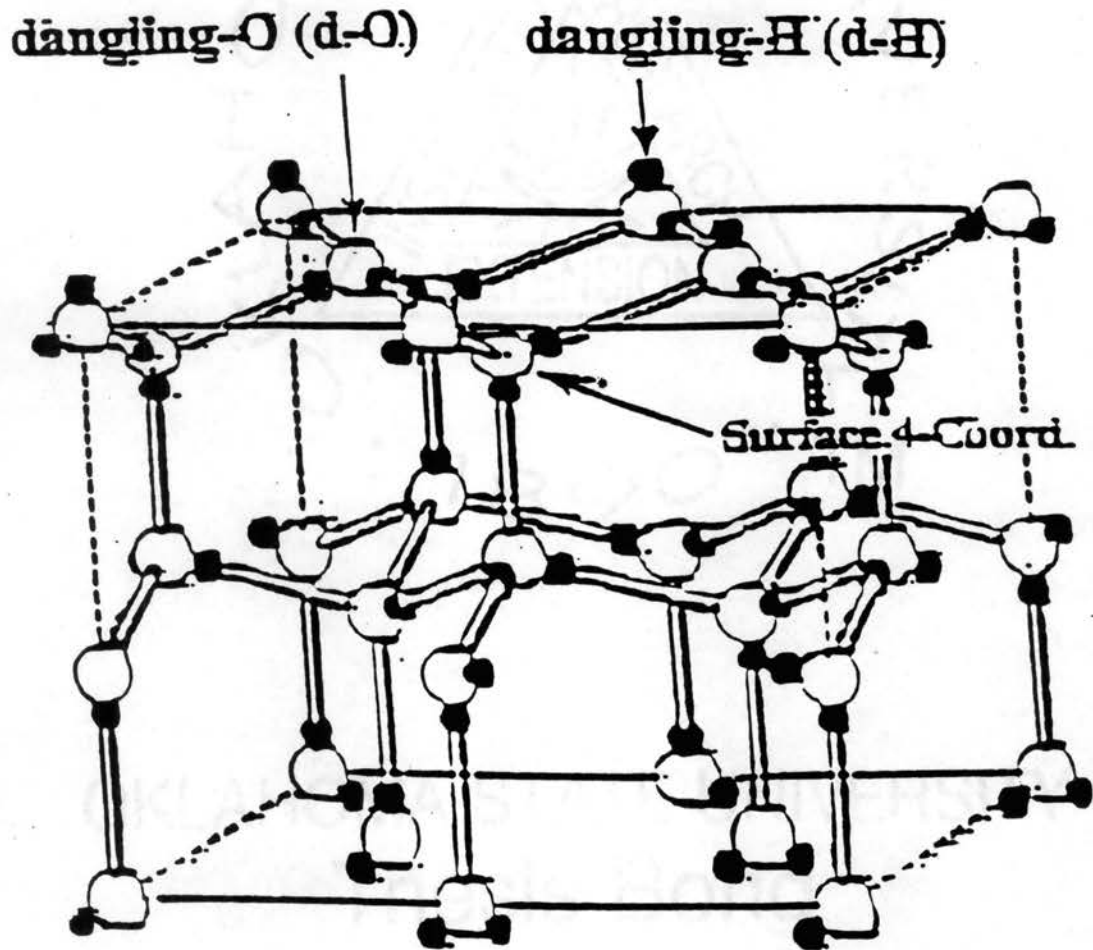
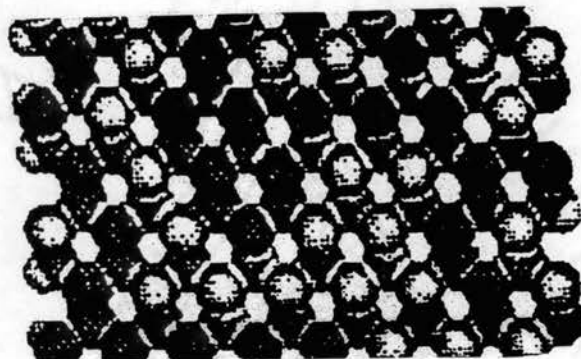


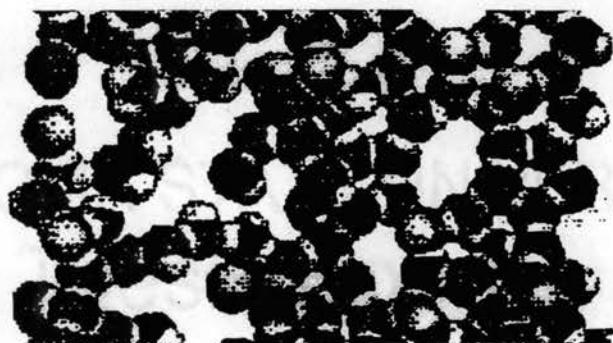
Figure 2. Crystalline ice structure.

A



cr(111)

B



S3

Figure 3. cr(111) a model crystalline cubic ice surface and S3 disordered surface model at 83 K.

subsurface is the transition region that connects the highly disordered surface to the crystalline interior.¹⁹

In addition to the conversion of the surface molecules to the interior ice, some subsurface is also converted to the interior ice during the Ostwald ripening process. Since there is a difference in the relaxation rates for the surface and subsurface molecules, the separation of the surface and subsurface spectra into individual components can be accomplished using the difference spectra obtained from subtraction of spectra of large nanocrystals from spectra of smaller nanocrystals. The resulting spectra of the surface and subsurface¹⁹ are shown in Figure 4.

In the interior of the crystalline ice, each water molecule is coordinated through four hydrogen bonds with a near tetrahedral structure; two of them are through the two hydrogen atoms and the others are through oxygens (see Figure 2). Interior D₂O ice gives absorption in the 2300-2500 cm⁻¹ spectral range.

2.2. Interactions of the Ice Nanocrystals with Adsorbates

The interaction of the adsorbates with the ice nanocrystals can also be examined by obtaining the difference spectra in two ways: one of them is between spectra of small and large ice particles coated with adsorbates and the other is between spectra of bare ice and adsorbate-coated ice.¹⁷

As mentioned above, the three parts of an ice nanocrystal are surface, subsurface, and interior. The adsorbates (used by our group) can be categorized as a) weak adsorbates, b) intermediate H-bonding adsorbates and c) penetrating

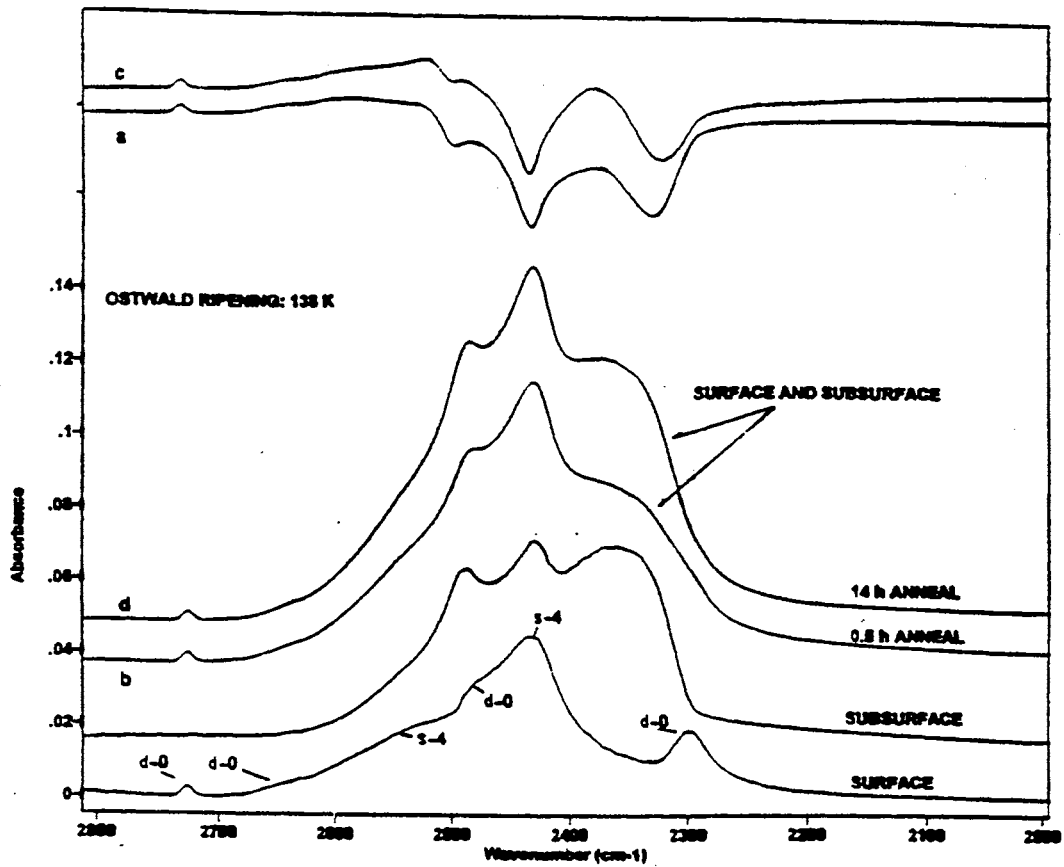


Figure 4. FTIR difference spectra for sequential periods at 138 K. Curves a and c are the difference between ice nanocrystal spectra before and after annealing for 0.5 and 14 h, respectively. Curves b and d are the same spectra with the bulk ice bands removed. The subsurface and surface spectra are from appropriate differences between b and d.

adsorbates, depending on their effect on the three parts of the ice nanocrystals. Since the subject of this study is focused on one of the strong penetrating adsorbates, namely NH_3 , they will be explained in detail. However, the intermediate H-bonding and the weak adsorbates, particularly, provide insight to the surface and subsurface structure of the ice nanocrystals. For this reason, they will be considered briefly.

a) Weak adsorbates: These molecules affect only vibrational modes of the surface molecules of ice nanocrystals; CH_4 , N_2 , CO , and H_2 are examples.^{17,20,21,22} Since these adsorbates do not have the capability to form significant H-bonds, they are called weak adsorbates. They do not affect the subsurface or the interior ice spectra. One more characteristic of these adsorbates is that they are easily desorbed below 100 K.

b) Intermediate H-bonding adsorbates: Among the intermediate H-bonding adsorbates are H_2S , SO_2 , HCN and acetylene. These adsorbates do not have a capability to break normal H-bond in the ice structure, but they can break the weakest and strained hydrogen bonds on the surface. Therefore, the weak hydrogen bonds are replaced by bonds to the adsorbate and they reverse the restructuring of the outer layer of ice. The net result of this process is the reordering of the surface molecules with an increase in the number of hydrogen bonds of the surface water molecules.²¹

Moreover, it is shown that the ordering process by these adsorbates on the surface of the ice nanocrystals causes a subsurface relaxation to a form that behaves spectroscopically as interior ice. The spectrum of the ice subsurface

was obtained from a difference spectrum achieved by subtracting the spectra of adsorbate-coated ice nanocrystals from spectra of the coated plus relaxed nanocrystals. The resulting spectrum for the subsurface ice, obtained from this procedure, matches the spectrum obtained from subtraction of spectra of the large nanocrystals from spectra of smaller ice nanocrystals.²¹

c) Strong (penetrating) adsorbates: These molecules react with ice to form hydrates at cryogenic temperatures. Ethylene oxide, HCl, HBr, HNO₃ and NH₃ are in this class of adsorbates. They affect all parts of the ice spectrum as they react with ice nanocrystals to form crystalline hydrates at the cryogenic temperatures. They do not undergo desorption at cryogenic temperatures (T<140 K).^{23,24,25}

Delzeit *et al.*²³ showed that ethylene oxide (EO) penetrates through ice crystals by virtue of its strong proton-acceptor character. Further, they concluded that EO converts the ice nanocrystals to the type I clathrate hydrate via a molecular mechanism. Firstly, the ice nanocrystals were exposed to EO(g) at 125 K at which temperature EO acts as an adsorbate. Then, the temperature was raised to 132 K for the hydrate formation. Total conversion time was found to be 3 hours at 132 K.

In the case of HCl, the conversion of ice nanocrystals to the hydrate of HCl proceeds via an ionic mechanism based upon formation of H₃O⁺ and Cl⁻ ions. HCl forms hydrates with the ratios 1, 2, 3, 4 and 6 to 1. The preferred hydrate is the hexahydrate but at high exposure levels and rates and low temperatures, lower hydrates are favored.²³⁻²⁵

Nitric acid (HNO_3), like HCl , converts ice to the ionic hydrates. The mono-, di-, and trihydrate of nitric acid have been reported.^{25, 26}

In our classification, NH_3 is also a penetrating adsorbate. The previous studies of ammonia and ice nanocrystals in our group have been limited to the surface of the ice nanocrystals. The behavior of NH_3 on ice nanocrystals was investigated in the work of Delzeit *et. al.*²³

It was shown that exposure of the ice nanocrystals to ammonia, at levels a less than a monolayer, resulted in strong hydrogen bonding of the ammonia to the dangling-hydrogen sites (saturation of d-H) while the limited uptake was observed for the d-O and s-4 surface sites (see Figure 5).

The multiple interactions were proposed for ammonia at levels less than a monolayer on the ice surface; interactions accomplished by moving away from the linear hydrogen-bonded structures. A linear hydrogen-bonded structure was gained by a complete monolayer coating of the ice surface with ammonia or adding acetylene vapor to the ammonia-coated ice surface. Since the acetylene is a relatively strong proton donor, it attaches at vacant d-O and s-4 sites of the surface. In Figure 6, the difference spectra between the spectra of adsorbate coated ice and the spectrum of the bare ice with subtraction factor 1.0 were shown for (a) N_2 (at 83 K), (b) ammonia (120 K), (c) the ammonia followed by acetylene (at 110 K). As seen from that figure, after acetylene addition, the band, marked with *, due to the ammonia linear binding to the d-D sites appeared.

In our adsorbate classification, the ammonia also has the capability to order the surface and subsurface. That is, as discussed in the intermediate

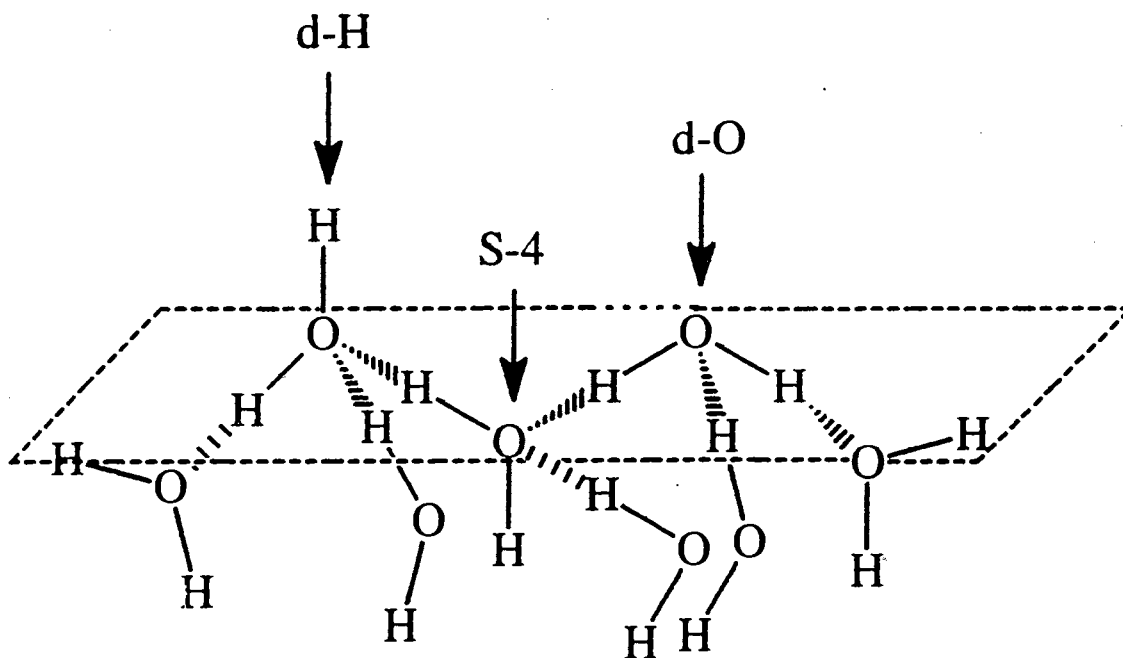


Figure 5. Surface groups of an ice cluster.

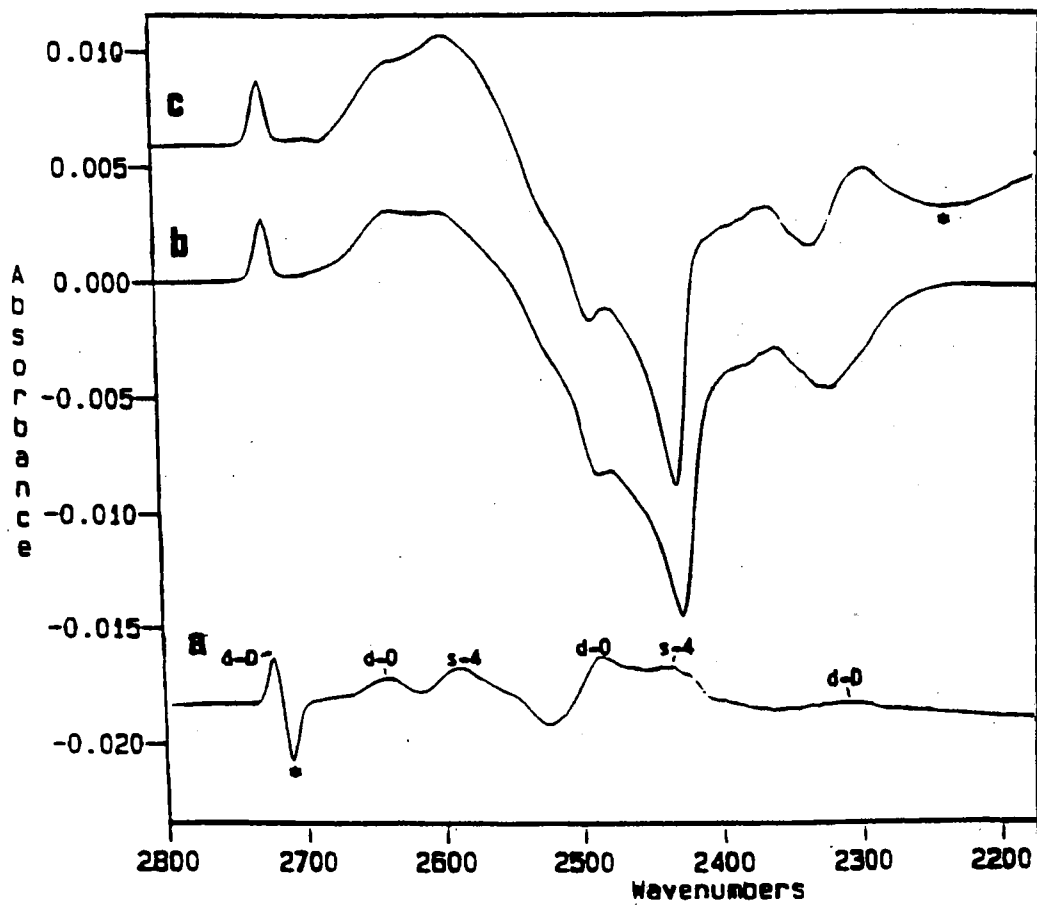


Figure 6. Difference spectra obtained by subtracting the spectra of adsorbate-coated ice nanocrystals from the spectrum of the bare ice nanocrystals, using a subtraction factor of 1.0: the adsorbate was (a) N_2 (83 K), (b) NH_3 (120 K) and (c) NH_3 followed by acetylene (110 K).

adsorbates part, NH_3 can reconstruct the surface, at levels of a monolayer, causing the subsurface relaxation to the interior ice. It should be noted here that a similar molecular adsorbate state was observed for the submonolayer amounts of strong acids, i.e. HCl , DBr , HNO_3 , at above 120 K by Devlin *et al.*^{24,25}

3. IR spectrum of NH_3

The infrared spectrum of NH_3 was studied by different researchers.²⁷⁻²⁹ The spectra of solid ammonia at 88 and 118.5 K obtained from a film of NH_3 ice is shown in Figure 7. The major absorption bands of NH_3 under different conditions are given in Table 1.²⁹

4. $\text{NH}_3 + \text{H}_2\text{O}$ Complexes

Hydrogen bonds play an important role in many areas, particularly in biological systems. Therefore, one of the most studied systems both experimentally and theoretically is the $\text{NH}_3\text{--H}_2\text{O}$ system since it serves as the simplest prototype of H-bonding between different molecules. In this system, both molecules can act as either proton donor or proton acceptor.

Latajka and Scheiner³⁰ studied theoretically the $\text{NH}_3\text{--H}_2\text{O}$ dimer. It was found that the hydrogen bond is very nearly linear with an O–N distance of 2.98. The binding energy is computed to be ~ 6 kcal/mol where the ammonia molecule is acting as a proton acceptor ($\text{H}_3\text{N}\dots\text{HOH}$).

A similar study by Langet, Caillet and Caffarel³¹ showed that, in a dimer structure of NH_3 and H_2O , the more stable electronic configuration occurs when

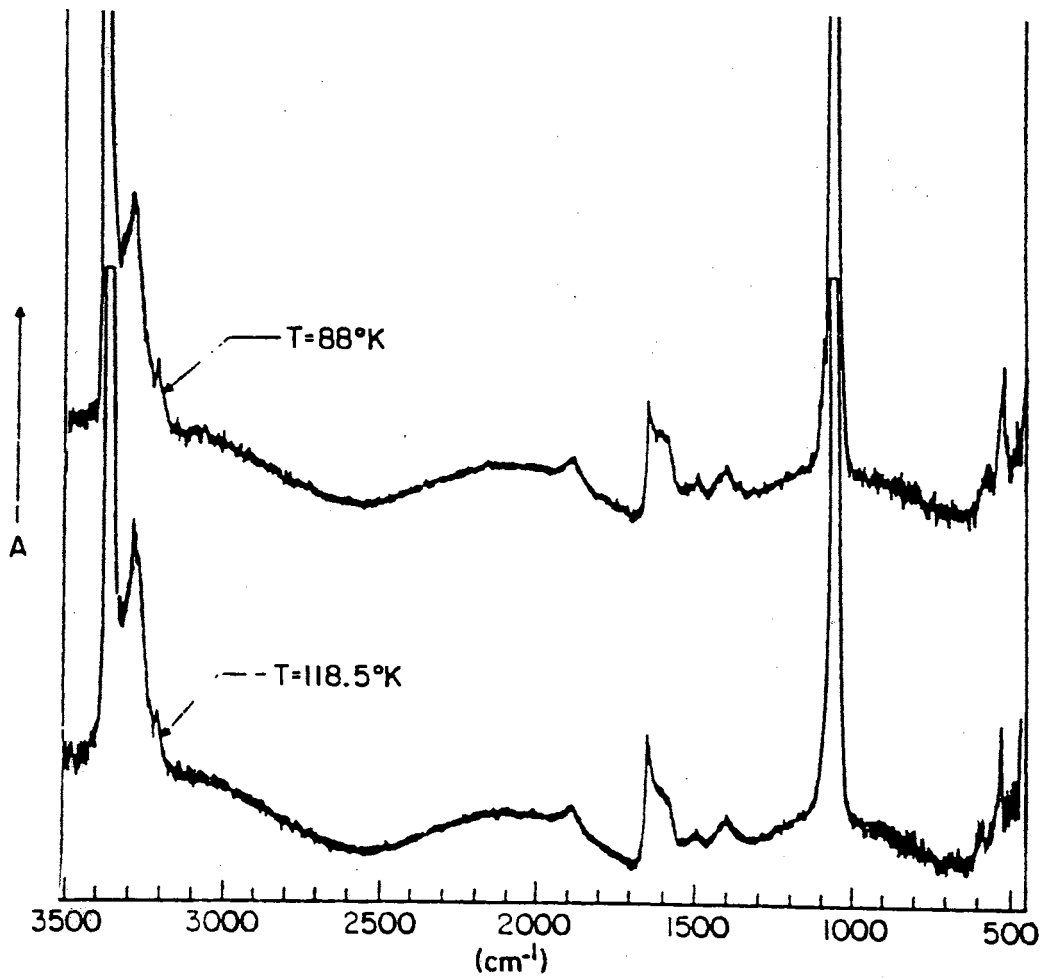


Figure 7. IR spectrum of solid ammonia (adapted from reference 29).

Table 1

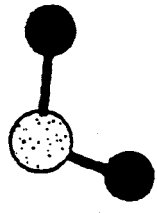
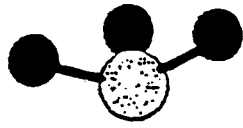
Positions for the major absorption bands of NH₃.

Assignment and identification	Gas		Liquid		Amorphous		Crystalline	
	Frequency	Intensity	Frequency	Intensity	Frequency	Intensity	Frequency	Intensity
ν_2	950.4		1058		1075		1057 1100	124 12
Total ν_2 region		164		100		128		125
ν_4	1626.8	29	1630	26	1625	32	1490 1592 1620 1650	23
$2\nu_4$	3219.1	~2			3290	30	3280	20
ν_1	3336.7	6.7	3230	40	3210	30	3210	5
ν_3	3443.8	4.5	3360	70	3375	100	3367 3374	168
Total $2\nu_4$, ν_1 , and ν_3 region		12		110		160		193

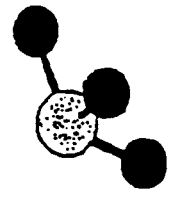
ammonia acts as the proton acceptor ($\text{H}_3\text{N}\dots\text{HOH}$) rather than a proton donor ($\text{H}_2\text{O}\dots\text{H}\text{NH}_2$). Further, they showed that since the stability of $\text{H}_3\text{N}\dots\text{HOH}$ is greater than that of $\text{H}_2\text{O}\dots\text{HOH}$, NH_3 is a better proton acceptor than H_2O .

The studies of the complex of water and ammonia discussed above were either experimental in the gas phase or theoretical. To our knowledge, a study by Donaldson³² is the only one in the literature in which the ammonia-water complex is examined at the air/water interface; and that has been studied both experimentally and theoretically. In the experimental part, the interfacial binding energies and evaporation rates are extracted from temperature and time dependent surface tension measurements of aqueous ammonia solutions. The standard Gibb's energy of adsorption of ammonia vapor to the water surface was calculated as ~ -19 kJ/mol and the Gibb's energy of activation for ammonia evaporation from the water surface was found in the range 13–18 kJ/mol at 298 K.

Donaldson also did *ab initio* calculations for the $\text{NH}_3\text{-H}_2\text{O}$ and $\text{NH}_3\text{-(H}_2\text{O)}_2$ complexes. The optimized geometries of these complexes are shown in Figure 8. The results of this study are that the principal interaction of NH_3 at the interface involves a hydrogen bond with a free OH. However, there may be multiple interactions with one ammonia and two water molecules. Indeed, he calculated a higher binding energy of ammonia hydrogen bonded to two water molecules, arising from the formation of a second hydrogen bond with NH_3 as the donor and the second H_2O molecule as the acceptor. It should be noted that a similar multiple-interaction was observed for the ammonia molecule at the ice surface in



A



B

Figure 8. A – structure of $\text{NH}_3\text{-H}_2\text{O}$ and B – structure of $\text{NH}_3\text{-2(H}_2\text{O)}$.

the work of Delzeit et al.²³ (see penetrating adsorbates section).

The complex formed at the surface of water was called a “critical cluster” in Donaldson’s work and the solvation of ammonia was explained with a nucleation process. That is, after this critical cluster formation, he found, based on the work of Davidovits³³, that NH_3 easily transfers to the bulk solution.

5. Hydrates of Ammonia

In the literature, three types of $\text{NH}_3\text{-H}_2\text{O}$ molecular solids have been described; the monohydrate ($\text{NH}_3\cdot\text{H}_2\text{O}$), hemihydrate ($2\text{NH}_3\cdot\text{H}_2\text{O}$) and dihydrate ($\text{NH}_3\cdot 2\text{H}_2\text{O}$).

5.1. The Monohydrate of Ammonia

The crystal structure of ammonia monohydrate has been determined by Olovsson and Templeton³⁴ from three-dimensional X-ray data. The crystal is orthorhombic and the unit cell constants are $a= 4.51$, $b= 5.587$ and $c= 9.7$. The crystal structure of the ammonia monohydrate is shown in Figure 9.

Bertie and Shehata³⁵ studied $\text{NH}_3\cdot\text{H}_2\text{O}$ and $\text{ND}_3\cdot\text{D}_2\text{O}$. They produced spectra of bulk forms of hydrates of ammonia by using the mull technique at 100 K, and assigned peak values of vibrational modes for the first time. Figure 10 and Figure 11 (adapted from reference 35) show FTIR spectra for both $\text{NH}_3\cdot\text{H}_2\text{O}$ and $\text{ND}_3\cdot\text{D}_2\text{O}$, respectively, with corresponding peak values in Table 2.

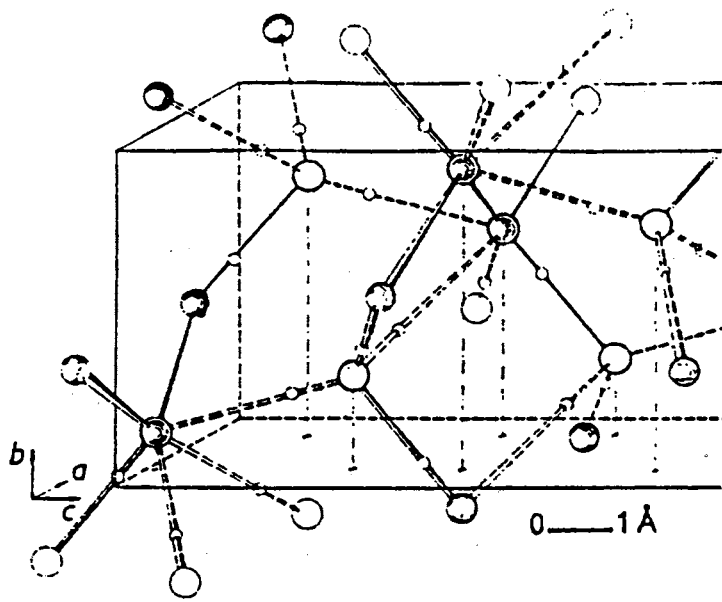


Figure 9. The crystal structure of ammonia monohydrate; shaded circles are oxygens and open circles are nitrogens (adapted from reference 34).

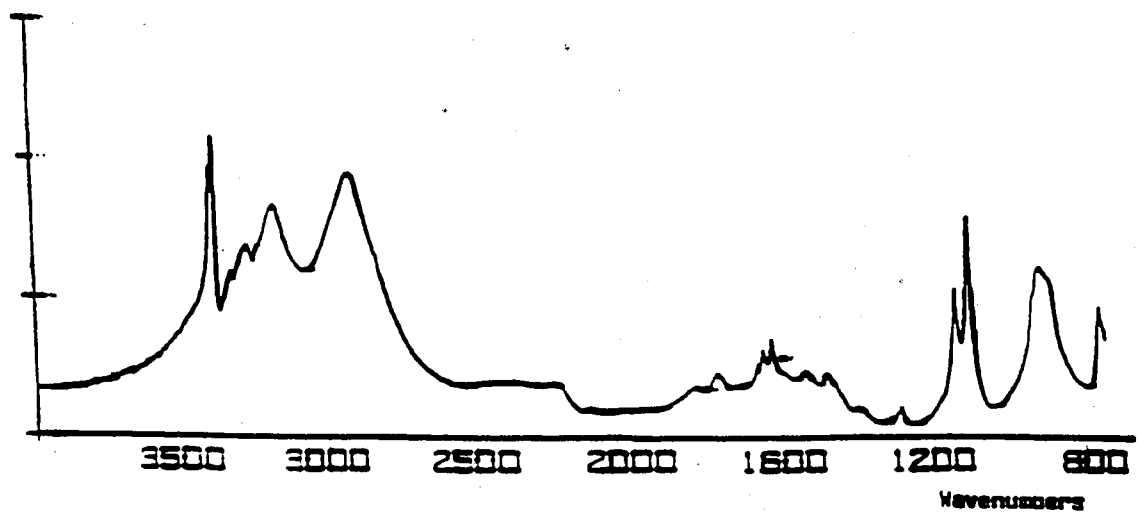


Figure 10. Infrared spectrum of $\text{NH}_3 \cdot \text{H}_2\text{O}$ at 100 K (adapted from reference 35).

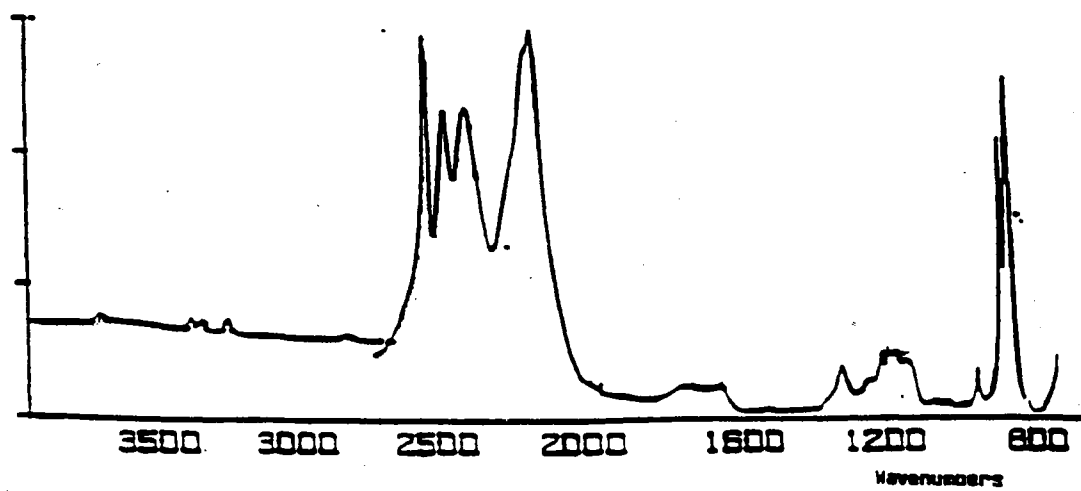


Figure 11. Infrared spectrum of ND₃.D₂O at 100 K (adapted from reference 35).

Table 2

Vibrational frequencies of $\text{NH}_3 \cdot \text{H}_2\text{O}$ and $\text{ND}_3 \cdot \text{D}_2\text{O}$.

$\text{NH}_3 \cdot \text{H}_2\text{O}^a$		$\text{ND}_3 \cdot \text{D}_2\text{O}^a$		Ratio	Assignment ^b
ν/cm^{-1}	Intensity	ν/cm^{-1}	Intensity		
~5210	vw				
5015(1)	w	3715(2)	w	1.350	$(\nu_3 + \nu_4)(a)$
~4953	sh				
~4800	w,br	~3610	sh	1.33	
		~3471	vw		
4515(4)	w	3392(2)	w	1.331	$(\nu_3 + \nu_2)(a)$
2471	w	3362	sh	1.360	$\nu_{\text{NH}}(\text{ND}_2\text{H})$
2467	w	3349.2(5)	w	1.358	or
2464	w	3344.9	sh	1.357	
2410	w	3259(2)	w	1.352	HDO, $\nu_{\text{O-HDI-O}}$
		~3135	vw		HDO
~4417	vvw				
~4366	vvw				
~4320	vvw				
~4240	vvw				
~4150	vvw	~3085	vw,br		
~3771	sh	2954	vvw		
3689	sh	2940	vvw		
3590	sh	2917	vvw		
3531	sh				
2197	w	2825(5)	w	1.285	HDO, $\nu_{\text{O-HDI-N}}$
3403.2(5)	vs	2534.3(5)	vs	1.343	$\nu_3(a), B_1, B_2, \text{ and } B_3$
3392.1(5)	vs	2526.1(5)	vs	1.343	
3387.3(5)	vs	2522.2(6)	vs	1.343	
3332(2)	s				
3294	sh				$\nu_1(a); 2\nu_4(a)$
3275(3)	s	2459(2)	vs	1.332	$\nu_{\text{O-H-O}}(B_2, \text{ out-of-phase})$
3235	sh	~2414	sh	1.340	
3182(2)	vs	2390(1)	vs	1.331	$\nu_{\text{O-H-O}}(B_3, \text{ in-phase})$
~2950	sh	~2260	sh	1.31	
		{ 2189(2)	vs	1.319	$\nu_{\text{O-H-N}}(B_1)$
2887(10)	vs	{ 2165(2)	vs	1.333	$\nu_{\text{O-H-N}}(B_2)$
		~1929	sh		$3\nu_R(W); \nu_R(W) + \nu_2(W)$
		~1836	sh		
~2430	w,br	1767(3)	mw,br	1.38	$\nu_4(a) + \nu_R(W)$
2260(3)	w,br	~1675	w,br	1.35	
2140.8(5)	vw	1667(1)	mw	1.284	$2\nu_2(a)$
2028(4)	vw,br	1534(2)	vw	1.322	$\nu_2(a) + \nu_R(W)$
1994(5)	vw,br			1.30	
		1467(2)	w		$\nu_2(\text{HDO})$
1834(3)	w	1319.5(9)	mw	1.390	$2\nu_R(W)$
1773(3)	w			1.340	
~1696	sh	1243(3)	mw	1.364	$\nu_2(W); \nu_R(W) + \nu_R(W)$
1665.5(5)	m	~1217	sh	1.369	$\nu_4(a)(B_2)$
1650.1(5)	m	1209.1(5)	mw	1.365	$\nu_4(a)(B_1)$
1627.0(5)	m	1192.6(5)	mw	1.364	$\nu_4(a)(B_3)$
~1594	sh	1169(1)	mw	1.363	$\nu_R(W) + \nu_R(W)$

Table 2 (continued)

NH ₃ -H ₂ O ^a		ND ₃ -D ₂ O ^a		Ratio	Assignment ^b
ν/cm^{-1}	Intensity	ν/cm^{-1}	Intensity		
1537(2)	w	1135(3)	mw	1.354	$\nu_R(W) + \nu_{R'}(W)$
1480(2)	w				$2\nu_{R'}(W)$
1439(4)	w	1060(4)	vw	1.358	$2\nu_{R'}(W)$
1402(2)	w	1023(2)	vw	1.370	$2\nu_{R'}(W)$
1287.1(5)	w	943.4(6)	mw	1.364	$2\nu_{R'}(W)$
1133.4(5)	s	870.6(9)	vs	1.302	$\nu_2(a)(B_1)$
1095.9(5)	vs	848.2(8)	vs	1.292	$\nu_2(a)(B_2)$
		~806	sh		
~932	sh				
915	s	682.3(6)	vs	1.340	$\nu_R(W)$
~893	sh	661(2)	s	1.35	
757.6(5)	s	554(1)	ms	1.368	
~750	sh	~548	s	1.37	$\nu_{R'}(W)$
709.9(5)	vs	516.3	s	1.375	
644.2(5)	m	466.7(5)	mw	1.380	$\nu_{R'}(W)$
~579	sh				
448(3)	m				$\nu_R(a)(B_2)$
420.4(5)	m				$\nu_R(a)(B_1)$
389(2)	s				$\nu_R(a)(B_3)$
308(3)	sh				
300(2)	w				$\nu_R(a) + \nu_T$
266.6(5)	mw				
243(2)	s				ν_T

5.2. The Hemihydrate of Ammonia

The crystal structure of the hemihydrate of ammonia obtained X-ray data by Siemons and Templeton³⁶ is shown in Figure 12. In the hemihydrate structure, there are two nonequivalent types of ammonia molecule; each ammonia molecule of type I forms bonds to three water molecules, as a proton donor (N–H...O), and receives an O–H...N bond from a fourth water molecule. The bond length of O–H...N is 2.835 and the N–H...O bond lengths are 3.11, 3.24, and 3.24 Å. The ammonia molecules of type II form an O–H...N bond of length 2.854 Å. The water molecules in the hemihydrate form O–H...N_I and O–H...N_{II} bonds, described above.

Bertie and Devlin³⁷ studied the infrared spectra of the hemihydrate of ammonia for the different isotopomer pairs of ammonia and water. The hemihydrate samples were prepared by deposition, from the gas phase of ammonia and water using the separate delivery nozzles, onto an IR transparent sample plate using an overall 2:1 mole ratio of ammonia to water.

The infrared spectra of the hemihydrate were obtained for different isotopomer pairs of ammonia and water at 15 and 90 K. The spectra of 2NH₃.H₂O, 2NH₃.D₂O and 2ND₃.D₂O are shown in Figure 13 and the assignments of the vibrational modes for these isotopomers are given in Table 3.

5.3. The Dihydrate of Ammonia

The dihydrate of ammonia was studied by x-ray diffraction and infrared spectroscopy by Bertie and Shehata³⁸. Like in the hemihydrate structure, there

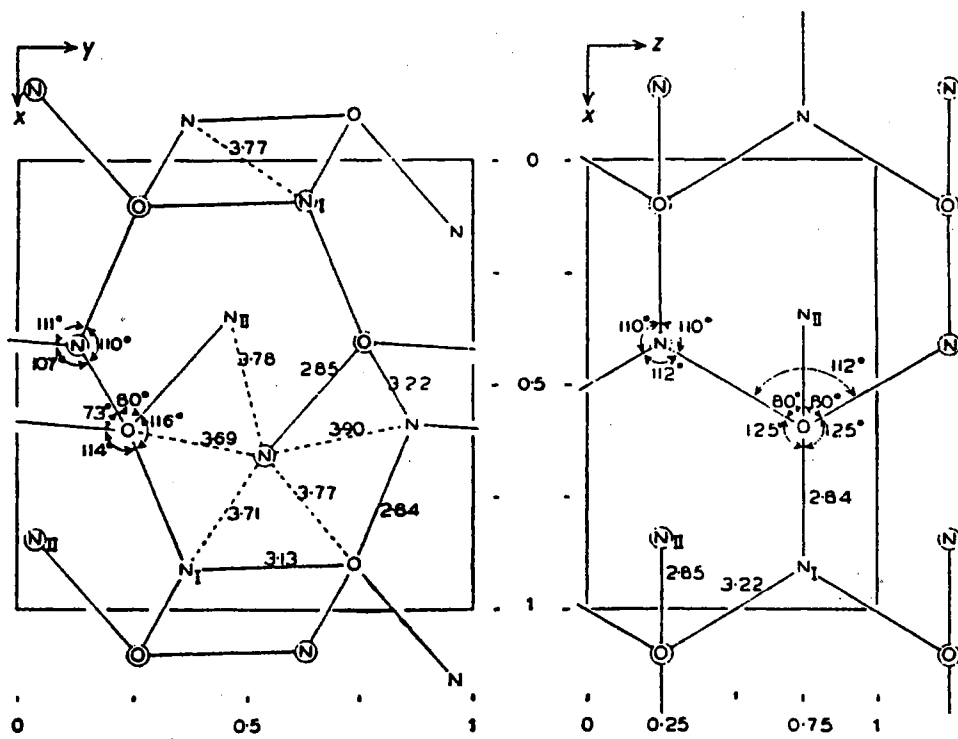


Figure 12. Structure of $2\text{NH}_3 \cdot \text{H}_2\text{O}$.

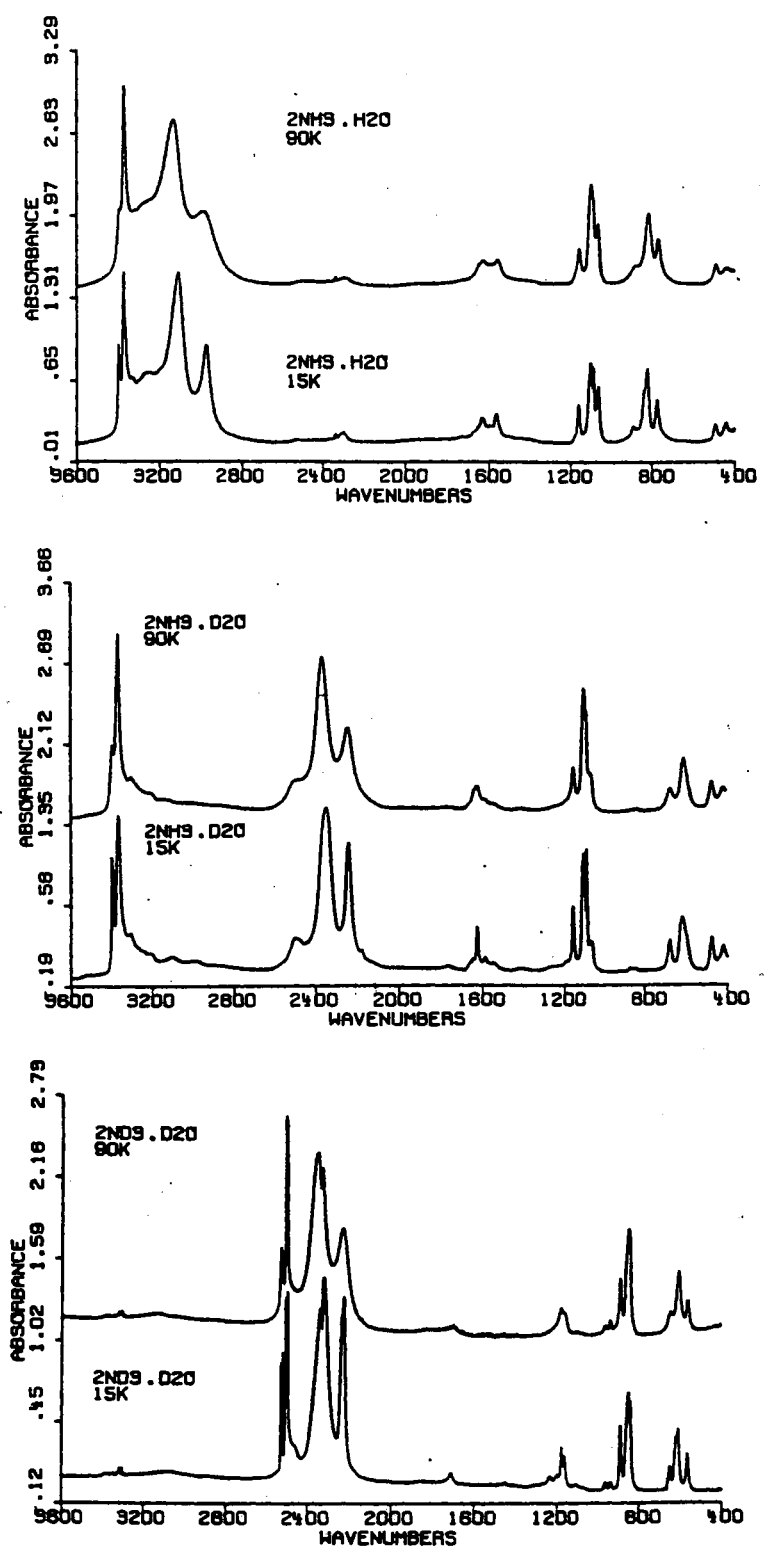


Figure 13. Infrared spectra of hemihydrate of ammonia for the different isotopomers of water and ammonia.

Table 3

Frequencies of spectral features of $2\text{NH}_3 \cdot \text{H}_2\text{O}$, $2\text{NH}_3 \cdot \text{D}_2\text{O}$ and $2\text{ND}_3 \cdot \text{D}_2\text{O}$.

Assignment	$2\text{NH}_3 \cdot \text{H}_2\text{O}$		$2\text{NH}_3 \cdot \text{D}_2\text{O}$		$2\text{ND}_3 \cdot \text{H}_2\text{O}$		$2\text{ND}_3 \cdot \text{D}_2\text{O}$	
	15 K	90 K	15 K	90 K	15 K	70 K	15 K	90 K
$\nu_3[\text{NH}_3(\text{II})]$	3402 3400 3396 3392.5	3397	3401 3399.5 3396 3392.5	3397				
$\nu_3[\text{NH}_3(\text{I})]$	3376 3368	3374	3372 3369 3366	3369				
NH_3	3304		3308	3306				
NH_3	3265		3240		3264 (3205)			
$\nu_1(\text{NH}_3)$	~3200		~3206	~3204				
$\nu_{\text{O-H-N}_1}$	3110	3125			3090	3112		
$\nu_{\text{OH-N}_1}$	2974	2975			2972	2974		
H_2O	2524	2500			~2650	~2650	~2650	
$\nu_3[\text{ND}_3(\text{II})]$					2532.7 2530.1 2526.7 2524.0	2532 2528	2532.8 2530.0 2527.5 2524.2	2530
$\nu_3[\text{ND}_3(\text{I})]$					2507 2502.2 2498.2	2509 2503 2500	2508.6 2503.8 2499.8	2502
$\nu_1(\text{ND}_3)$					2328.8	2330		
$\nu_{\text{OD-N}_1}$			2348	2367			2340 2322	2355 2326
$\nu_{\text{OD-N}_1}$							2237 2227	2230
H_2O	2303	2294	2241	2243	2292	2293		
NH_3	2186	2180	2180		2167			
ND_3					1855		1851	~1840
D_2O			1761	1754			1713	1705
$\text{ND}_3 + \text{D}_2\text{O}$							1693 sh	
$\nu_4[\text{NH}_3(\text{I})]$	1675		~1666					
$\nu_4[\text{NH}_3(\text{II})]$	1655		~1645	~1640				
$\nu_2(\text{H}_2\text{O})$					1642 sh			
$\nu_2(\text{H}_2\text{O})$	1634	1626	1626	1625	1635	1625		
$\nu_4[\text{NH}_3(\text{II})]$	1626							
NH_3	1595	1590	1587	1583				
$2\nu_R(\text{H}_2\text{O})$					1566			
$2\nu_R(\text{H}_2\text{O})$	1562	1555			1558	1552		
NH_3	~1545		1548	~1540				
NH_3	1499		~1500					
$\text{ND}_3 \cdot \text{H}_2\text{O}$					1488	1489	1488	
ND_3					1475	1477	1472	
ND_3					1451	1453	1453	
v.w.br.	~1438		~1415 ~1390	1405	1402			
ND_3					1272	1270	1271 sh	
$\text{D}_2\text{O}?$			1255	~1253			~1255 sh	~1250 sh
vvw					1258	1254		
$\text{ND}_3 + \text{D}_2\text{O}$							1237	
$\nu_4[\text{ND}_3(\text{I})]$					1212 sh		1211 sh	~1210 sh

Table 3 (continued)

Assignment	2NH ₃ · H ₂ O		2NH ₃ · D ₂ O		2ND ₃ · H ₂ O		2ND ₃ · D ₂ O	
	15 K	90 K	15 K	90 K	15 K	70 K	15 K	90 K
ν_4 [ND ₃ (I)]					~1200 sh	1195		
ν_2 (D ₂ O)			1195	~1195			1202	
ν_4 (ND ₃)(II)					1188	1182	1184 sh	1182
ν_4 (ND ₃)(III)					1180	~1170	1179	
NH ₃	1180 sh		1180 sh					
ND ₃ ?					~1166 sh			
$2\nu_R$ (D ₂ O)							1165	1160
H ₂ O?	1165 sh							
ν_2 [NH ₃ (I)]	1160	1156	1157	1152				
	~1110 sh		~1110 sh					
ν_2 [NH ₃ (II)]	1099	1092	1099	1095				
	1085	1083	1085	1084				
	891	~882			903			
ν_R (H ₂ O)	839				839	830		
	822	817			824	~817		
	775	767			759	755		
ν_2 [ND ₃ (I)]					878	894	890	884
							~860 sh	
ν_2 [ND ₃ (II)]					848	843	849	848
							840	838
v.w.					721			
			681	675			653	646
ν_R (D ₂ O)			619	608			622	
			~596				611	606
							566	560
	536(vw)		533(vw)					
ν_R (NH ₃)	493	489	474	470				
	441	441	~437					
			420	~416				

are two types of oxygen atoms (O_I and O_{II}) in the dihydrate structure; each nitrogen atom is surrounded by four oxygen atoms, O_{II} is bonded to three type I oxygen atoms and one nitrogen atom. The O_I is bonded to three type II oxygen atoms and three N–H...O bonds share its remaining lone pair electrons.

The infrared spectrum of the $NH_3 \cdot 2H_2O$ at 100 K is shown in Figure 14 and the assignments of the vibrational modes are given in Table 4.

6. Reactions in the Solid State and Deuterium Isotope Effects on Reaction Kinetics

A brief explanation of the definition of the rate constant in the solid state reactions and the deuterium isotope effect on the reaction kinetics is now discussed.

In the work on the kinetics of solid state reactions, the definition of the rate constant is different than that of gases and solutions. This is because in solid state reactions, the concept of concentration and order of reaction generally have no significance. Reaction rates in the solid state reactions are generally defined as the change of the thickness of the layer of product formed or weight of this layer. For instance, if the reaction rate is controlled by diffusion through the growing layer, the rate (diffusion) constant is given in units of cm^2/s . Furthermore, if the growing product is highly porous, the reaction rate is controlled by a phase boundary (reaction interface) process and the rate constant is expressed in units of cm/s .

Many solid state reactions can be classified depending on the rate controlling factor in the reaction;

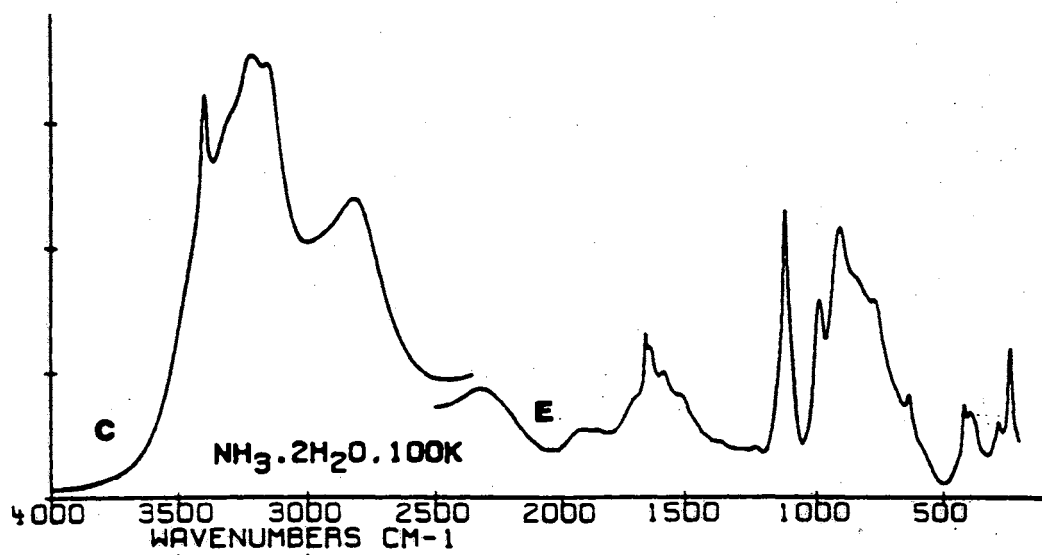


Figure 14. Infrared spectrum of $\text{NH}_3 \cdot 2\text{H}_2\text{O}$ at 100 K (adapted from reference 36).

Table 4

Infrared spectral features of $\text{NH}_3 \cdot 2\text{H}_2\text{O}$ at 100 K.

ν/cm^{-1} ^a	Intensity ^b	Assignment
5019.7(8)	w	$\nu_3(\text{NH}_3) + \nu_4(\text{NH}_3)$
~4950	vw.br	
~4830	vw.br	
4521.1(9)	w	$\nu_3(\text{NH}_3) + \nu_2(\text{NH}_3)$
~4424	vw.br	
~4375	vw.br	
3404.0(5)	vs	$\nu_3(\text{NH}_3)$
3396.3(4)	vs	
3391.2(9)	vs	
~3298	sh	$\nu_1(\text{NH}_3)/2\nu_4(\text{NH}_3)$
3207 (5)	vs	
3150 (4)	vs	$\nu_{\text{O-H}\cdots\text{N}}$
2803 (6)	s	$\nu_{\text{O-H}\cdots\text{N}}$
2319 (5)	w	$\text{H}_2\text{O comb}$
~2200	sh	
~2150	sh	
~2103	sh	
1898 (4)	w.br	
1840 (3)	w	
~1697	sh	$\nu_4(\text{NH}_3)$
1649.2(5)	s	
1631 (2)	sh	$\nu_2(\text{H}_2\text{O})$
1577 (2)	ms	
1505 (4)	ms	$2\nu_R(\text{H}_2\text{O})$
~1361	w	
~1279	w	
1231.3(6)	w	
1115.9(7)	vs	$\nu_2(\text{NH}_3)$
986 (2)	s	
900 (2)	vs	$\nu_R(\text{H}_2\text{O})$
~838	sh	
766 (3)	s	
684	st.	
633 (1)	ms	
614	w.sh	
~560	sh.br	$\nu_R(\text{NH}_3)$
415.7(6)	ms	
391 (2)	ms	
~373	sh	
297 (1)	m or sh	$\nu_7(\text{NH}_3)$
283 (1)	ms	
~239	sh	
235.0(15)	s	and $\nu_7(\text{H}_2\text{O})$

- a) Process limiting factor is rate of diffusion;
- b) Process limiting factor is rate of reaction at the phase boundary;
- c) Process limiting factor is rate of nucleus formation;³⁹⁻⁴¹

6.1. Deuterium Isotope Effects on Reaction Kinetics

When a hydrogen atom in a given reactant molecule is replaced by deuterium, the observable changes are called “deuterium isotope effects” (DIEs). DIEs have a variety of forms^{28,42}, such as the isotope frequency ratio (v_{AH}/v_{AD}), the thermodynamic isotope effect (K_H/K_D or $\Delta K_a = pK_a(AD) - pK_a(AH)$), the kinetic isotope effect (k_H/k_D), vapor pressure isotope effect (P_{AH}/P_{AD}). Since one interest of this study is to determine the kinetic isotope effect, it will be explained here in detail.

There are two factors that contribute to the generally lower reactivity of bonds to deuterium as compared to the corresponding bonds to hydrogen, namely, the difference in free energy and the effect of the difference in mass on the velocity of passage over the potential energy barrier.

The primary factor that contributes to the free energy difference is the difference in zero-point energy between a bond to deuterium and the corresponding bond to hydrogen. The theoretical explanation of isotope effects on the reaction rates are generally based upon Absolute Reaction Rate Theory (or Transition State Theory).⁴³

Figure 15 (modified from reference 44) shows the potential energy diagram and the zero-point energies for a given reaction of a molecule with H or

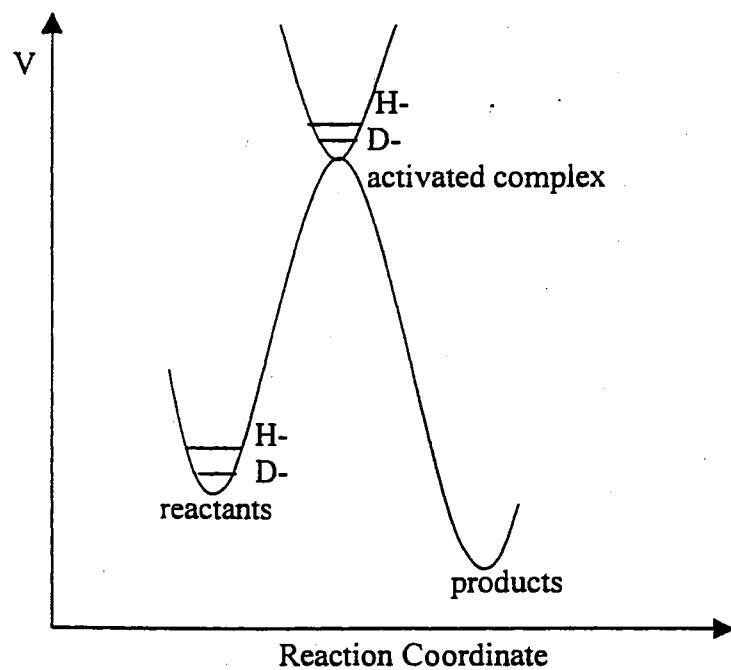


Figure 15. Potential energy diagram for a molecule with H and D.

D.⁴⁴ The Hooke's law expression is

$$\nu = (1/2\pi c) (\sqrt{k/\mu}),$$

where ν is the frequency, k is the force constant, μ is the reduced mass that is approximately equal to 1 and 2 for heavy molecules with H and with D, respectively.⁴⁴ The energy levels of the harmonic oscillator are given by $E_n = (1/2 + n) h\nu$, where n is the vibrational quantum number (0, 1, 2, ...), h is Planck's constant, and ν is the vibrational frequency. Putting $n = 0$ (because at room temperature or below, most of the molecules reside in the ground vibrational state) gives $E = h\nu/2$. Combination of the energy and frequency equations explains why the zero-point energy is different for the isotopic hydrogen. Since the molecule with deuterium has the lower zero-point energy, it is more stable than that with hydrogen due to the dissociation energy differences.⁴⁴

Moreover, when the reactant with hydrogen or deuterium reaches the activated complex point, the bonds between the atom and hydrogen or deuterium become weaker. Consequently, the force constants between the atom and hydrogen or deuterium become smaller (and the vibrational energy is directly proportional to the square root of the force constant). Thus, in the activated complex, the difference in the zero-point energy levels for the molecule with hydrogen and the molecule with deuterium becomes smaller. If one considers the rate process, this difference makes the activation energy for the molecule with deuterium higher than that for molecule with hydrogen. Simply put, the molecule with hydrogen reacts faster than that with deuterium.⁴⁴

The relation between the activation energies and the zero-point energies for the isotopic molecules was found by Bigeleisen.⁴⁵ He concluded that the difference in activation energies at low temperature resulted from the difference in the zero-point energies between the isotopic molecules and their activated complexes.

CHAPTER II

EXPERIMENTAL

1. Introduction

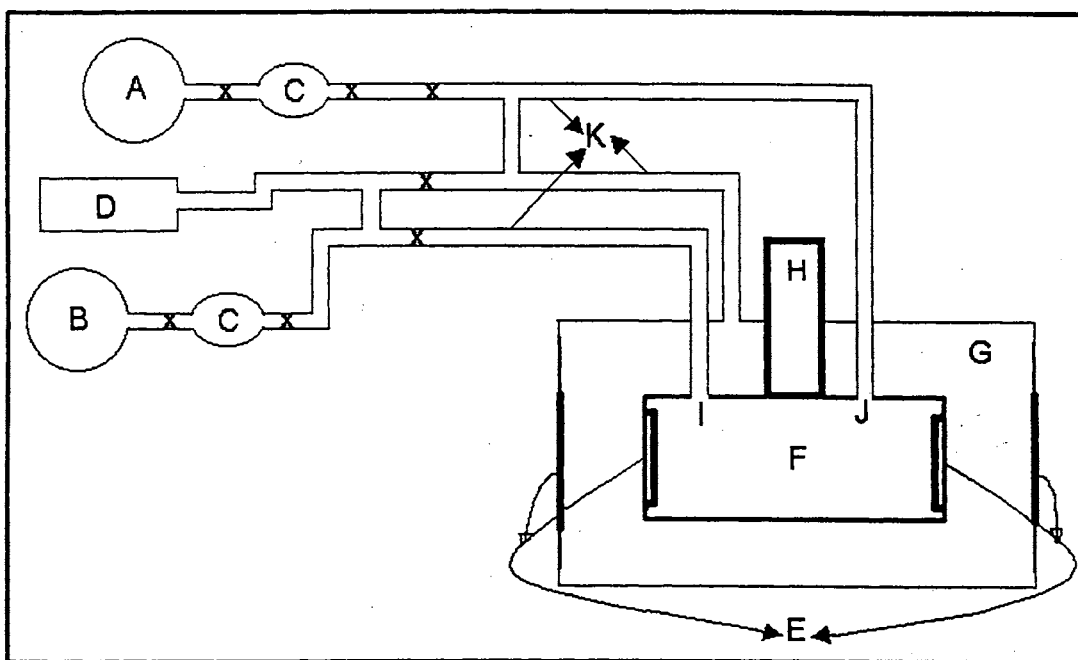
This research was performed to find the rates and mechanisms for the conversion of ice nanocrystals to nanoparticles of the hydrates of ammonia using FTIR. Two methods were used to prepare the FTIR samples: In the first method, the ice nanocrystals were deposited onto the windows of a cluster cell, then, they were exposed to NH_3 vapor near 120 K. In the second method, the ice nanocrystals were mixed with NH_3 nanocrystals on the windows of the cluster cell at somewhat lower temperatures. In both methods, the experimental equipment was the same, except in the first method the cluster cell had one loading port while, in the second method a second entry port was used.

2. Experimental Equipment

This section provides detailed information about the experimental apparatus, which mainly consists of a cryogenic system and a cryogenic cell, a vacuum system and the FTIR instrument. The components of the equipment are shown schematically in Figure 16.

2.1. Cryogenic System and Cryogenic Cell

The main component of the cryogenic system is an Air Products Model CS202 closed-cycle helium refrigerator. The minimum temperature capability



	Definition
A, B	Gaseous sample bulbs
C	1 L charging bulb
D	Vacuum system/manifold
E	IR transparent windows
F	Cryogenic cell
G	Outer evacuated can
H	Refrigerator
I, J	Entry ports
K	Vacuum lines

Figure 16. Main components of the experimental equipment.

was ~ 35 K depending on the thermal load. The other components of the cryogenic system are a Lake Shore or Air Products temperature control assembly and a hand-coiled 45 ohm resistance heater. These components of the cryogenic system are directly connected to the inner portion of the cell that is surrounded by the outer can which thermally isolates the inner portion of the cell (see Figure 16). The inner portion is a cylinder with dimensions of 15 cm length and 5 cm diameter. The ZnS infrared transparent windows, onto which the sample loading was done, seal the two ends of the inner cell. The temperature-measuring sensor is embedded in the cell wall near one window, so the temperature near the window will be cited throughout this discussion.

2.2. Vacuum System

A Welch Duo Seal vacuum pump model 1402 and an oil diffusion pump are used to evacuate the glass manifold. The manifold is connected to the outer portion and the inner portion of the infrared cell by vacuum lines (see Figure 16 K). The connection between the outer portion and the vacuum system provides a vacuum required to isolate the inner portion of the cell from thermal transport. The inner port connection is used for evacuation of the cell and admission of the gaseous samples into the cell. The pressure is measured with a Hastings Vacuum Gauge. The minimum pressure for this system is $\sim 10^{-5}$ torr. Loading of the gaseous samples is monitored using a dual channel Validyne Model AP10-32 or AP10-42 gauge with the measurable pressure ranges of 0.01 to 150 and 0.1 to 1000 torr, respectively.

2.3. FTIR Instrument

A Digilab FTS-40 model instrument is used to collect FTIR absorbance spectra that are monitored, stored and manipulated on a HP 486 PC. A background single-beam is collected using 400 co-added scans for each series of spectra. Sample spectra are collected at 4 cm^{-1} resolution.

3. Experimental Procedure

As noted before, two methods are used to prepare the FTIR samples. The methods differ in the introduction of ammonia to the cluster cell. Changing of the sampling method also changes the type of hydrate formed; ammonia monohydrate is produced with the first method and the ammonia hemihydrate is obtained with the second method.

Procedures for the preparation of the samples and methodology for the evaluation of the experimental results are different in both methods. For this reason, it is convenient to divide the description of the experimental procedure into two sections; namely, the procedure for the conversion of the ice nanocrystals to the monohydrate of ammonia and the procedure for the conversion of the ice nanocrystals to the hemihydrate of ammonia.

3.1. Procedure for the Conversion of the Ice Nanocrystals to the Monohydrate of Ammonia

3.1.1. Preparation of the Window Deposited Ice Nanocrystals

Procedures for this method are as follows; H₂O (D₂O) vapor and carrier gas (N₂ (g)) are first loaded into the sample bulb (Figure 16 A) so that their molar ratio is 1/100 (H₂O/N₂). After that, this gas mixture is loaded into the precooled cell with ~300 torr of the gaseous mixture from the one-liter sample bulb (Figure 16 C) expanded into the cell during each loading stage. A load-evacuation cycle is repeated ~30 times to complete formation of an assembly of the nanocrystals. The temperature for the loading can be varied from 70 K to 145 K (the loading temperatures used in this study are 70, 135, 140 and 145 K) and the loading temperature is held constant during the load-evacuation cycles.

When the gas mixture expands into the cold inner cell, the water vapor in the ~1% gas mixture becomes liquid droplets. On a short time scale, these liquid droplets crystallize and some of the nanocrystals whose amount depends on temperature become attached to the windows of the cell. The thickness of the resulting network increases with the number of loads, as observed with FTIR spectroscopy as increasing peak intensities. When the loading is done at 70 K, the sample is subsequently annealed. During the annealing process, small particles become larger by Ostwald ripening. The annealing temperature is chosen roughly 20 K higher than the planned reaction temperature so that the particle size remains stable during the reaction. The samples loaded at 135, 140 and 145 K are not further annealed.

3.1.2. Adding NH₃ (ND₃) and Collecting FTIR Spectra

After the ice nanocrystals are annealed, the temperature is decreased to the reaction temperature. Before adding NH₃ (ND₃), the bare ice spectrum is taken. Since the guideline for production of the monohydrate of ammonia is a one to one mole ratio of ammonia and ice, the same amount of ammonia as water in the nanocrystals is admitted. After NH₃ (ND₃) is added, the spectra of the ice nanocrystals were taken as a function of time. All spectra are collected by co-adding 50 to 400 scans at a nominal 4.0 cm⁻¹ resolution.

3.1.3. Evaluation of the Data

To evaluate the rate data, the best ammonia monohydrate spectra are chosen as standard spectra for NH₃.H₂O, NH₃.D₂O and ND₃.D₂O. The standard spectra are obtained from samples following complete reaction after several hours. In Figure 17, the standard spectra are shown for each monohydrate form. All data were evaluated according to these standard spectra as follows; two characteristic peak intensities for peaks marked * are measured from the standard spectrum of each monohydrate and the ratio of these two peak intensities is found. Then, the bare ice spectrum is subtracted from spectra of partially reacted ice that are collected as a function of time until the same peak ratios are obtained. In Figure 18, one example of data evaluation is shown to help visualize the procedure. In this figure, the top spectrum is the bare D₂O ice spectrum and the middle one is the partially reacted ice spectrum that taken after

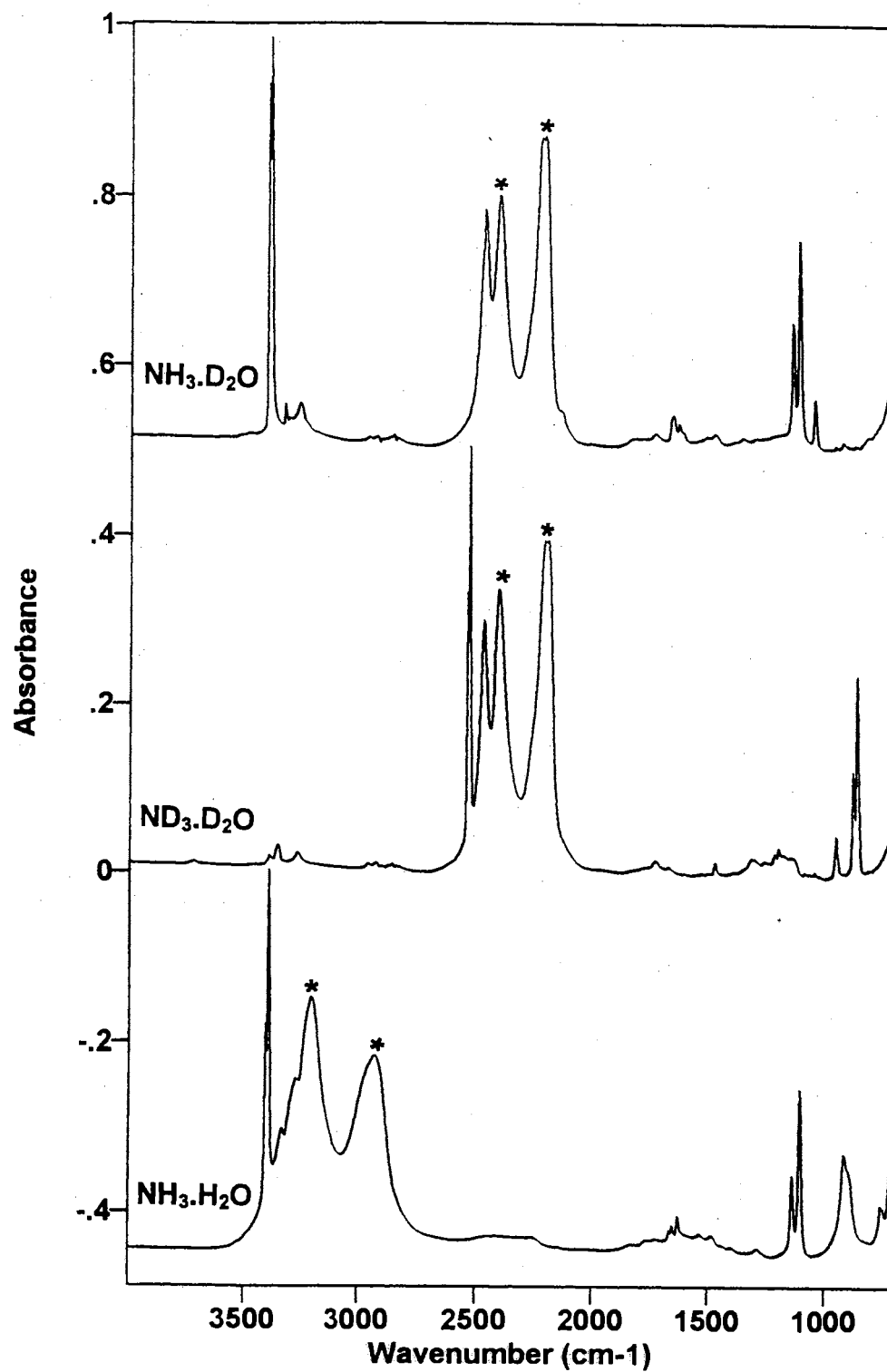


Figure 17. Standard spectra of $\text{NH}_3 \cdot \text{D}_2\text{O}$, $\text{ND}_3 \cdot \text{D}_2\text{O}$ and $\text{NH}_3 \cdot \text{H}_2\text{O}$.

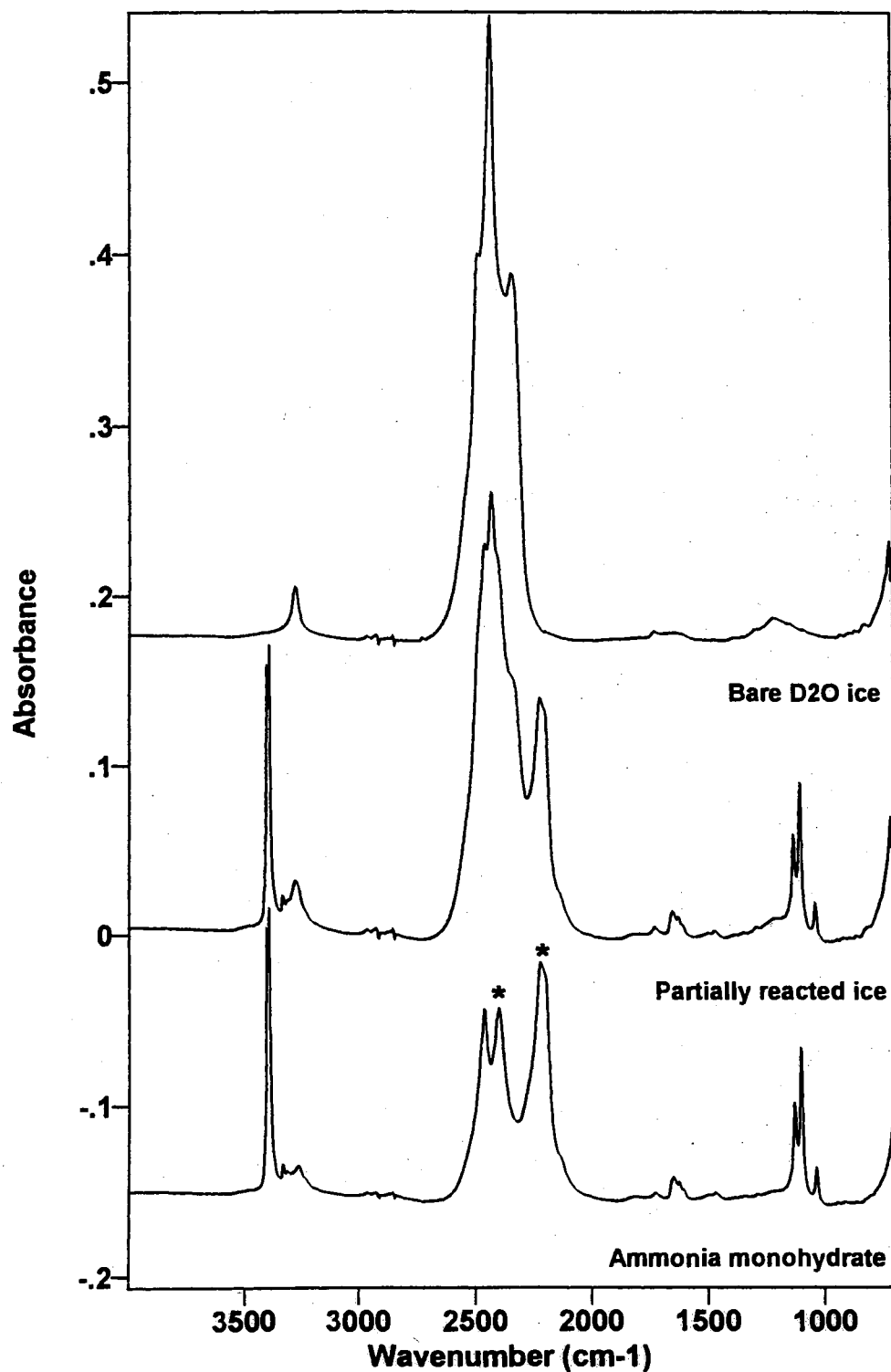


Figure 18. Finding one datum for extent of formation of $\text{NH}_3 \cdot \text{D}_2\text{O}$: top; the bare D_2O ice spectrum, middle; the partially NH_3 reacted ice spectrum (monohydrate spectrum + unreacted ice spectrum) and bottom; the subtracted spectrum (partially reacted ice spectrum - bare ice spectrum) with * peak ratios of standard value for $\text{NH}_3 \cdot \text{D}_2\text{O}$.

8 hours of exposure to ammonia. From the standard spectrum of $\text{NH}_3 \cdot \text{D}_2\text{O}$, the ratio of 2200 and 2400 cm^{-1} peak intensities is known. When the bare D_2O ice spectrum is subtracted from the partially reacted spectrum, the subtracted spectrum, which is the bottom one, is obtained as the monohydrate spectrum whose 2200 and 2400 cm^{-1} peak intensity ratio is equal to that ratio for the standard spectrum of $\text{NH}_3 \cdot \text{D}_2\text{O}$.

For kinetic analysis, the subtraction factors are the basic data. Since the subtraction factor equals the fraction of the unreacted ice, one minus the subtraction factor gives the reacted ice portion for a specific reaction time. Using these values, the reacted ice fractions could be plotted as a function of the reaction time.

3.2. Procedure for the Conversion of the Ice Nanocrystals to the Hemihydrate of Ammonia

3.2.1. Alternating Layers

The same procedure described in the previous method is used to prepare the network of ice nanocrystals. In this method, the ammonia also is loaded with a carrier gas, using a separate loading port, with alternate loading of ammonia particles with pure ice particles. For this reason, 3% ammonia in $\text{N}_2(\text{g})$ was prepared as a separate sample bulb (see Figure 16 B). These mixtures are loaded into the precooled cell (~ 90 K) from the one liter sample bulbs (see Figure 16 C) expanded into the cell during each loading, giving a load pressure of ~ 300 Torr. After each pumping stage of NH_3 or H_2O , there is a delay. This is to

minimize NH_3 or H_2O vapor deposited near the entry port at which the temperature is above that of the cell.

When the gas mixture enters the cold inner cell, the water or ammonia vapors become liquid droplets. On a short time scale, these liquid droplets crystallize and the nanocrystals of H_2O or NH_3 become attached to the windows of the cell. The thickness of the resulting network increases with the number of loadings, as observed with FTIR spectroscopy, as increasing peak intensities.

The spectrum of a network of NH_3 and H_2O particles obtained from this second method at 90 K is shown in Figure 19 (top spectrum). As seen from this figure, the spectrum is just the combination of the spectrum of NH_3 and H_2O (the overlaid spectra of NH_3 and H_2O are shown at the bottom of this figure).

The spectra of the other isotopomer pairs of ammonia and water, $\text{ND}_3 + \text{D}_2\text{O}$ and $\text{NH}_3 + \text{D}_2\text{O}$, are shown in Figures 20 and 21, respectively.

3.2.2 Collecting Data

The sample is prepared at 90 K after which the temperature is raised to the reaction temperature. As soon as it reached this point, the collection of data is initiated. All spectra are taken as a function of time. Depending on the reaction temperature, the spectra are collected by co-adding 50 to 400 scans at a nominal 4.0 cm^{-1} resolution, in a manner such that the extent of reaction during a scan was minimal.

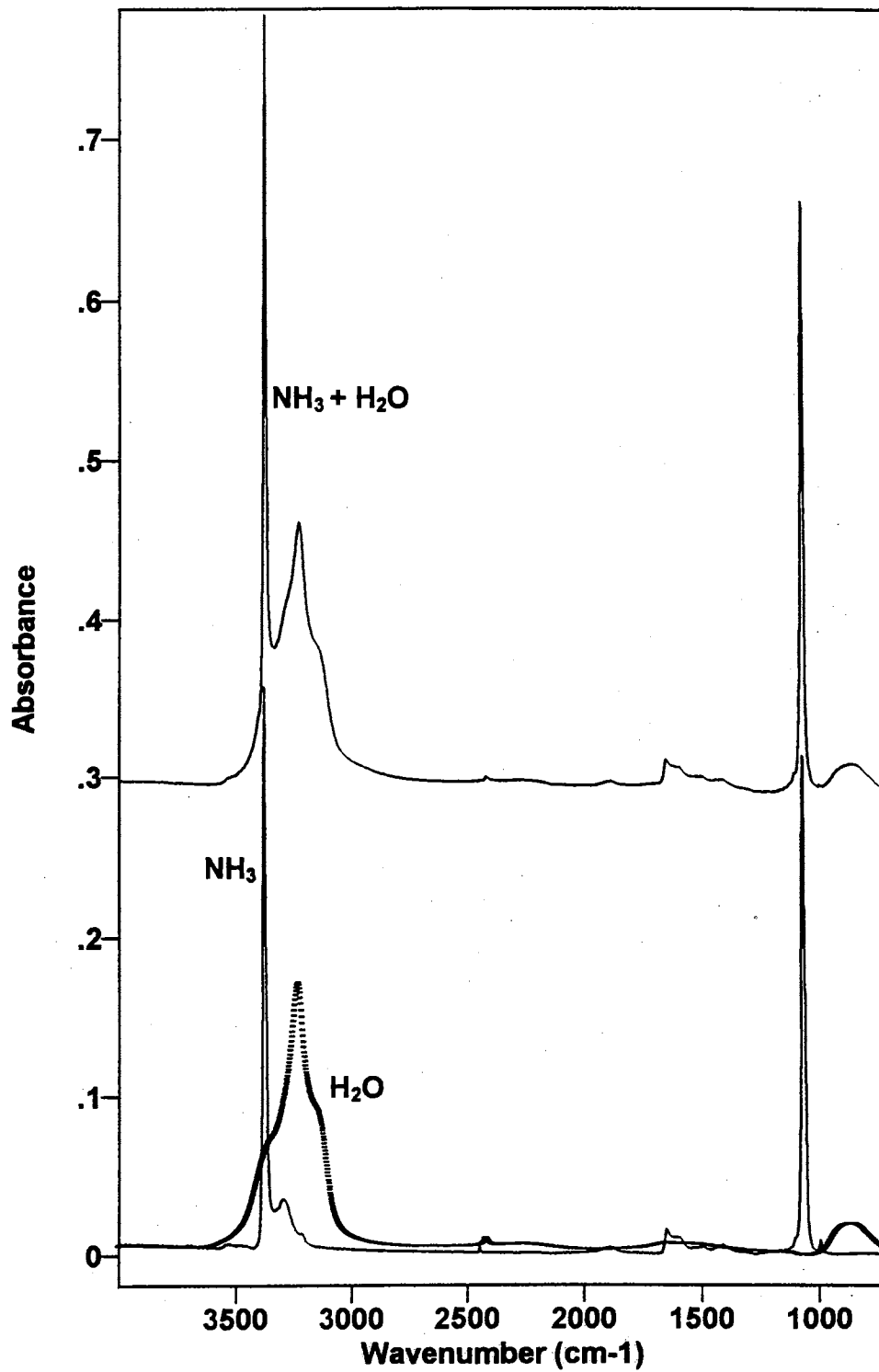


Figure 19. Top; the spectrum of a network of NH₃ + H₂O particles at 90 K: bottom; the dotted line spectrum is the bare H₂O ice spectrum and the connected line spectrum is the NH₃ spectrum.

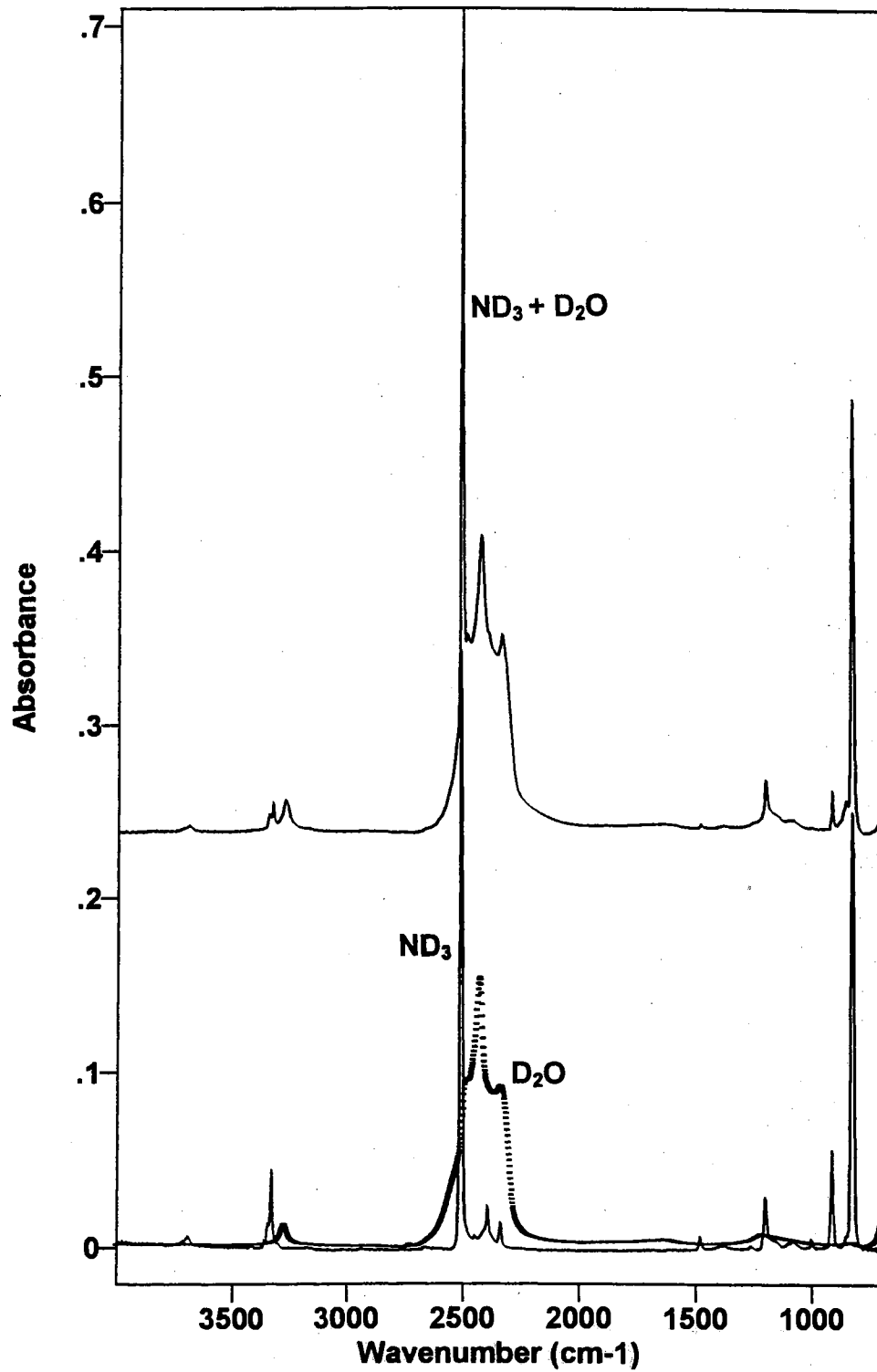


Figure 20. Top; the spectrum of a network of ND₃ + D₂O particles at 90 K; bottom; the dotted line spectrum is the bare D₂O ice spectrum and the connected line spectrum is the ND₃ spectrum.

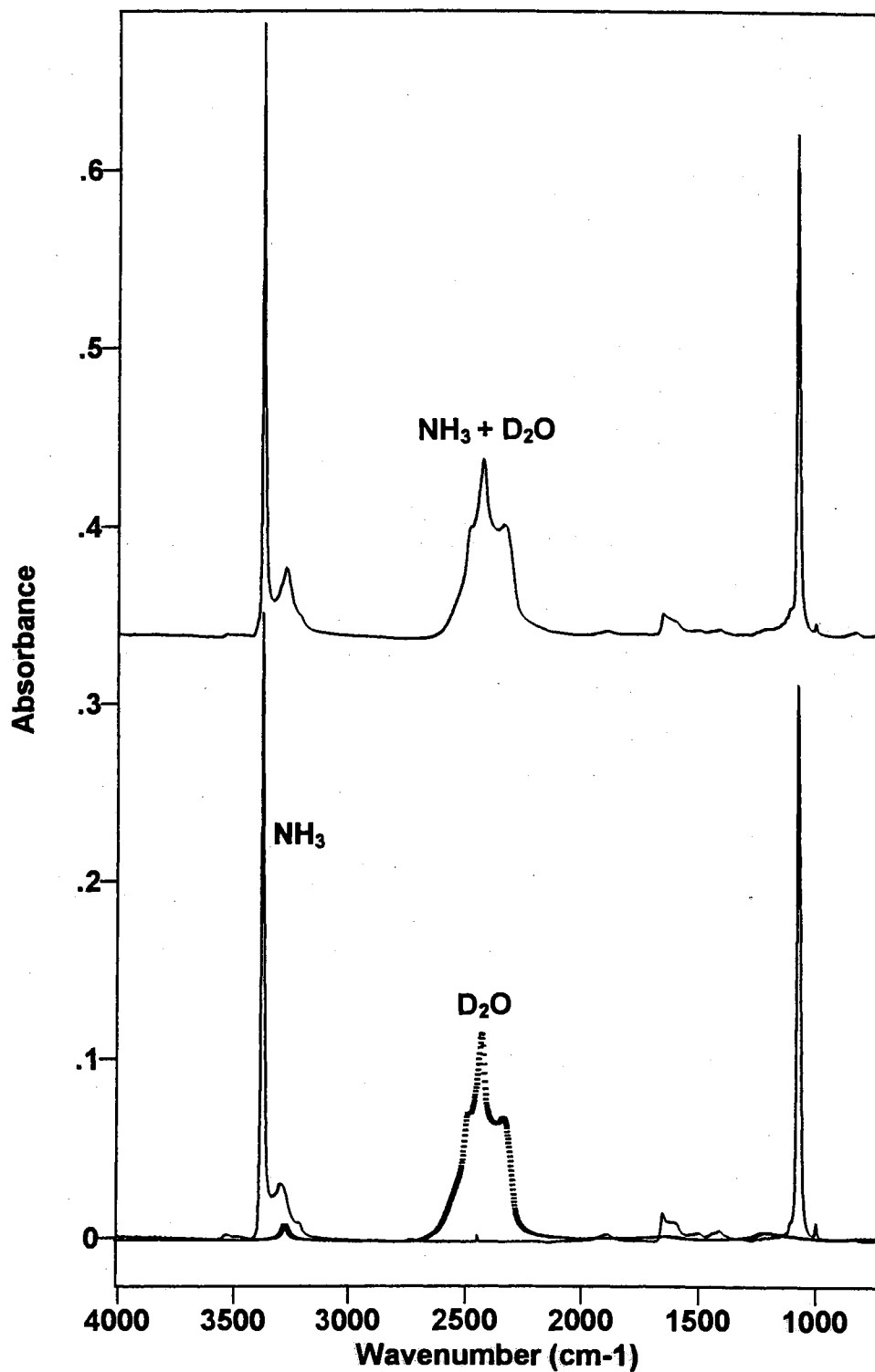


Figure 21. Top; the spectrum of a network of NH₃ + D₂O particles at 90 K: bottom; the dotted line spectrum is the bare D₂O ice spectrum and the connected line spectrum is the NH₃ spectrum.

3.2.3. Methodology for Evaluation of Experimental Results for Conversion of Ice Nanocrystals to the Hemihydrate of Ammonia

Evaluation of results in this part of the study is not as direct as in the monohydrate section. This is because the data obtained on a laboratory time scale at the lower reaction temperature is mostly for the amorphous hemihydrate. For this reason, the method described in the previous section is not useful in this part of the study.

The first step in the evaluation of the experimental results can be represented by mathematical expressions as follows;

Fraction of reacted ice at the specific reaction time = $1 - (\text{subtraction factor for: partially reacted ice band intensity} - \text{zero-time ice band intensity})$
(1)

Fraction of reacted ice consumed during the warming process = $1 - (\text{subtraction factor for: zero time at time zero ice intensity} - \text{the bare ice intensity})$
(2)

The total fraction of reacted ice = fraction of reacted ice during the reaction + fraction of reacted ice consumed during the warming process (3)

Consequently, the kinetic data is plotted as the total fraction of reacted ice versus time for the given conditions (i.e. temperature, isotope). Each formula is discussed in detail in the following sections.

Fraction of reacted ice at the specific reaction time = $1 - (\text{subtraction factor for: partially reacted ice intensity} - \text{zero-time ice intensity})$ (equation 1)

The zero-time ice spectrum is taken as soon as the temperature reaches

the chosen reaction temperature and then each partially reacted ice spectrum is collected at the specific reaction time. The unreacted ice amount is directly obtained from the subtraction factor for the difference spectra between the partially reacted ice and zero-time ice. Since the total fraction of ice is one, one minus subtraction factor gives the fraction of reacted ice with respect to zero-time ice (left side of equation 1).

The zero-time ice spectrum is used here as a reference spectrum instead of the bare ice spectrum. The reason for this choice is that since NH_3 (or ND_3) samples were contaminated with NH_2D (or ND_2H and NDH_2) species their spectra interfered in the ice region. The spectra for NH_3 and ND_3 are shown in Figure 22. Although, the absorbance intensity of these species is not strong, due to the small amount of exchange, these interfered with the subtracted spectrum. However, when the zero-time ice spectrum is used as a reference spectrum, most of the peak is cancelled during the subtraction and the net result gives the relative fraction of reacted ice with respect to zero-time ice.

In Figure 23, the evaluation of one datum at 102 K for the sample of NH_3 and D_2O is shown. The dotted line spectrum, at the top of Figure 23, is the zero-time ice spectrum (hemihydrate spectrum + unreacted ice spectrum) and the connected line (at the top of this figure) is the spectrum (hemihydrate spectrum + unreacted ice spectrum) that is taken after ~5.3 hours. The zero-time ice spectrum is subtracted until the peak marked * (that is, the main ice band) vanishes. That is, when the zero-time ice spectrum is subtracted from the partially reacted ice spectrum beyond this point, the spectrum A in Figure 24 is

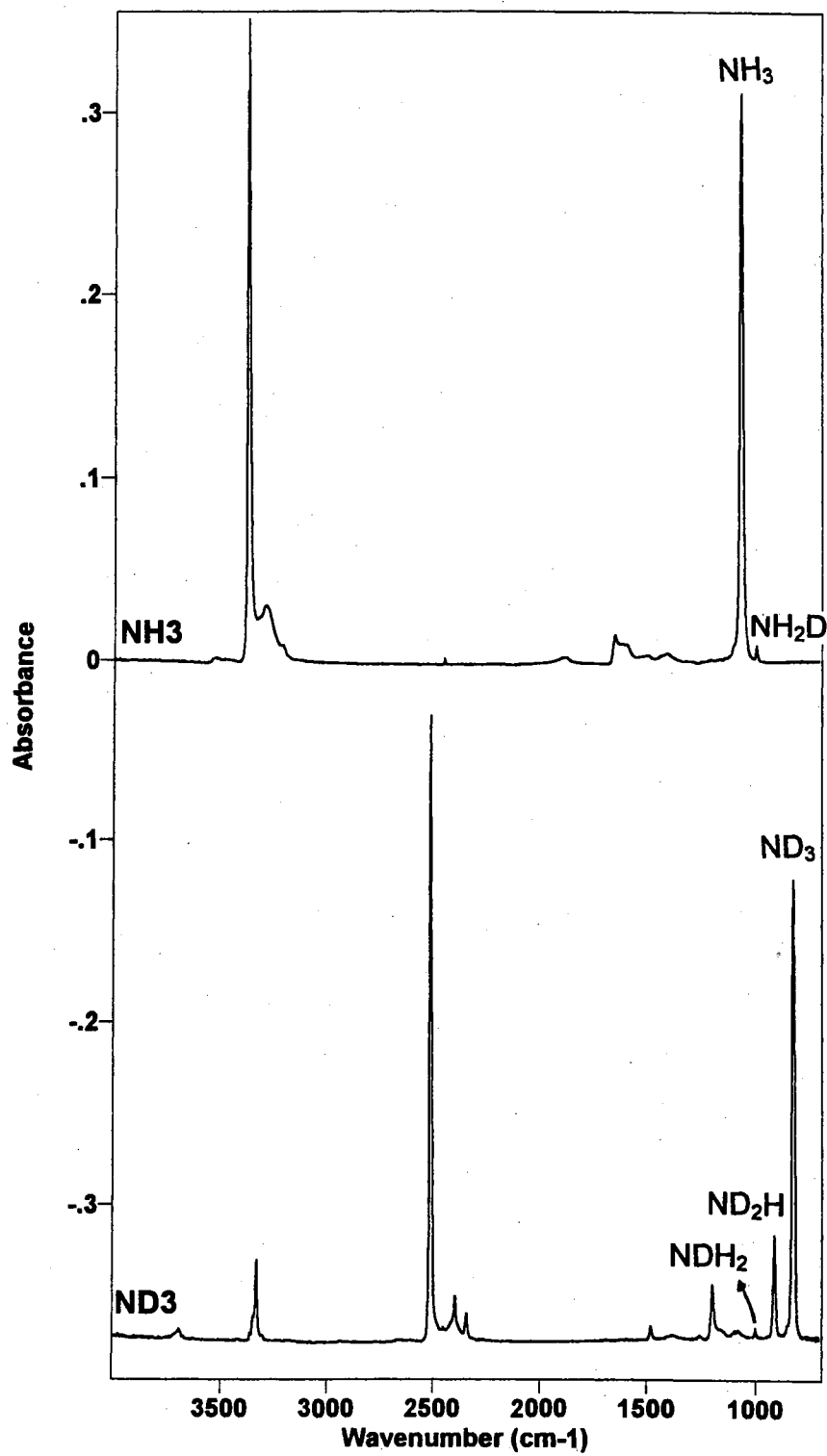


Figure 22. Top; spectrum of NH₃ with NH₂D: Bottom; spectrum of ND₃ with ND₂H and NDH₂.

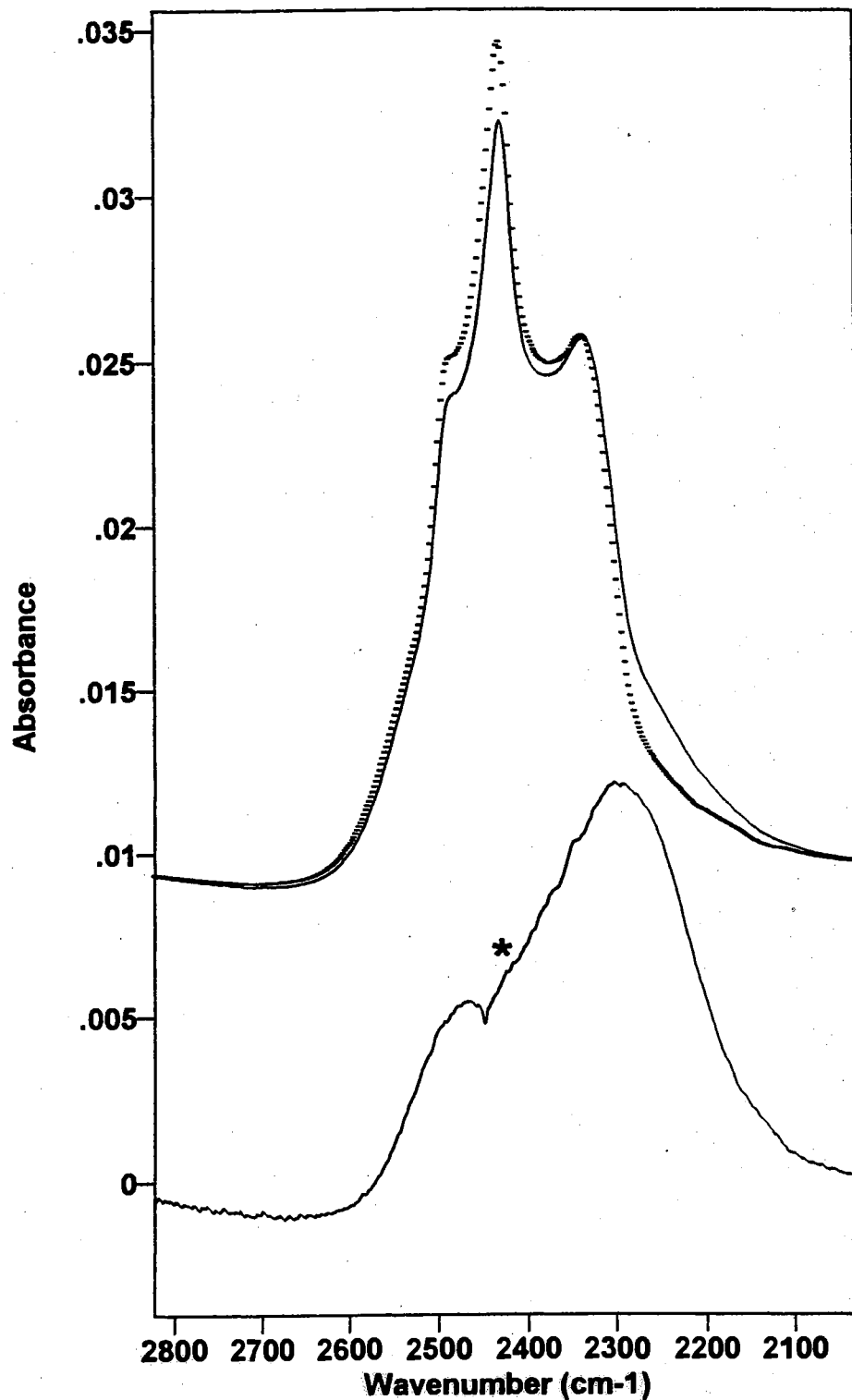


Figure 23. Finding one datum for extent of formation of amorphous $2\text{NH}_3 \cdot \text{D}_2\text{O}$ at 102 K: Top; dotted line is spectrum of zero-time ice and connected line is spectrum of partially reacted ice taken after 5.3 h., bottom; subtracted spectrum (partially reacted ice spectrum - zero-time ice spectrum).

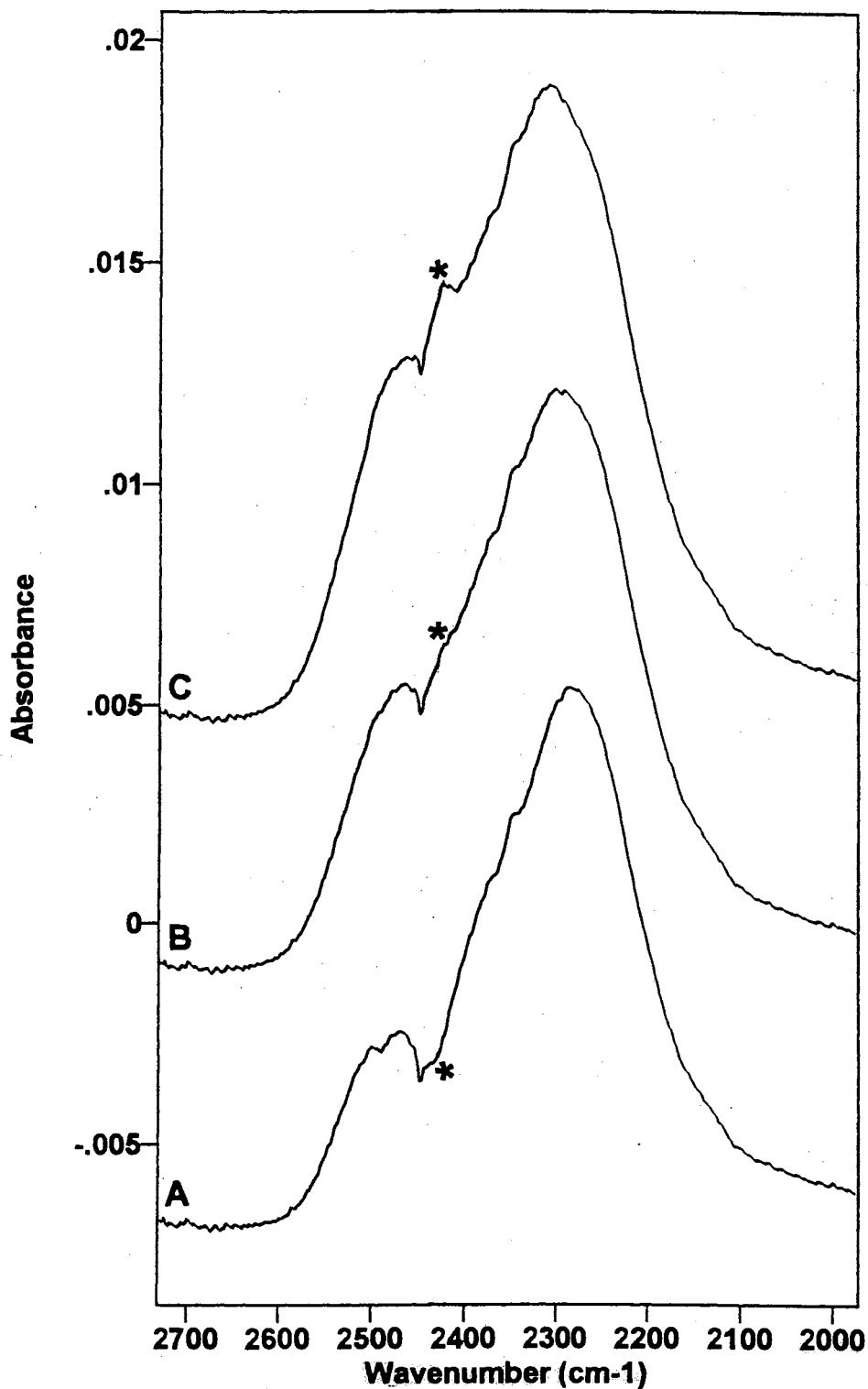


Figure 24. Subtracted spectra between zero-time ice and partially reacted ice spectra shown in Figure 23: **B** - is the same spectrum with the spectrum shown in Figure 23 (the subtraction factor = ~ 0.85), **A** - subtracted spectrum with the subtraction factor ~ 0.9 , **C** - subtracted spectrum with the subtraction factor ~ 0.7 .

obtained. The spectrum B in Figure 24 is the same spectrum shown in Figure 23. As seen the A and B spectra, the negative band corresponding to the main ice band, starts to appear in B. If less ice intensity is subtracted than, in Figure 24B, the spectrum C in Figure 24 is observed with the positive ice band apparent.

The fraction of reacted ice consumed during warming = 1 – (subtraction factor for: partially reacted ice intensity – the bare ice intensity) (equation 2)

Since some of the ice reacted with ammonia during the warming of the sample to the chosen reaction temperature, the zero-time ice spectrum contains some hydrate spectrum that should be included in equation 1 to find the total fraction of reacted ice. For this reason, the fraction of reacted ice in the zero-time ice spectrum is found by using the bare ice spectrum. The zero-time ice spectrum ($\text{NH}_3 + \text{D}_2\text{O}$) with the bare D_2O ice spectrum are shown in Figure 25 for the reaction temperatures of 100 (A), 102 (B), 105 (C), 107 (D) and 110 (D) K. As seen from the figure, the extent of the reaction in the zero-time ice spectrum becomes larger as the reaction temperatures increase (from bottom to top).

One drawback of the alternating layer method of sampling is that we do not have a bare ice spectrum for any sample so that the results are not analyzed directly from them (i.e., as we did in the case of the monohydrate). However, since the spectrum of ice nanocrystals is reproducible, the bare ice spectrum can be achieved for pure ice samples and used to calculate the fraction of the reacted ice in the zero-time ice spectrum. Nevertheless, because the ice spectrum is temperature dependent, the bare ice spectrum must be collected for

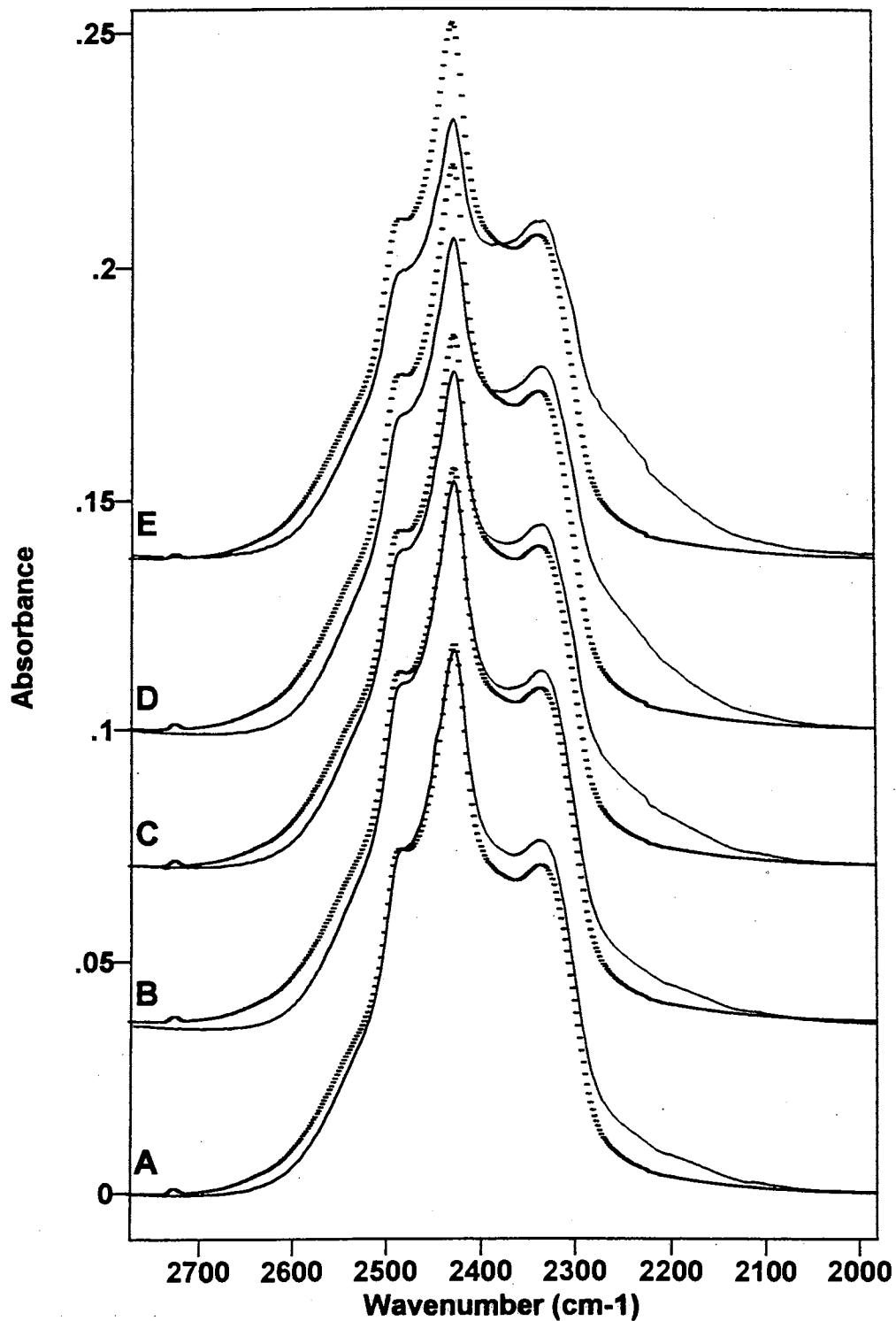


Figure 25. Shows extent of reaction in the zero-time ice spectrum of $\text{NH}_3 + \text{D}_2\text{O}$ (connected line) comparing with the bare D_2O ice spectrum (dotted line) at different reaction temperatures: A – 100 K, B – 102 K, C – 105 K, D – 107 K, and E – 110 K.

each reaction temperature.

The total ice amount for a given alternating particle sample is found by assuming that the ice spectrum at 90 K (sample preparation temperature) corresponds to the bare ice spectrum, since most of the ammonia molecules are in the adsorbed phase on the surface of the ice particles so ice has not been lost to hydrate formation. The spectra of the network of $\text{NH}_3 + \text{D}_2\text{O}$ for the different samples and the bare D_2O ice spectrum (shown by dotted line) at 90 K are shown in Figure 26A. In Figure 26B, the spectra are expanded along both axes. Because of the band intensity near 2240 cm^{-1} for these samples, the need for a truly bare ice reference spectrum is apparent.

Once the intensity of ice at 90 K was known, the intensity of ice at the reaction temperature could be calculated as follows: If the intensity of bare ice at 90 K and, for instance, at 100 K represented by I_{B90} and I_{B100} , respectively, and the intensity of one of the spectra of the network of $\text{NH}_3 + \text{D}_2\text{O}$ samples at 90 K shown in Figure 26 were known, the intensity of ice (I_{A100}) in the network of $\text{NH}_3 + \text{D}_2\text{O}$ at 100 K was calculated from;

$$I_{A100} = (I_{A90}/I_{B90}) \times I_{B100}$$

The completely bare ice spectrum corresponding to the intensity I_{A100} , then, was obtained from the bare ice spectrum with the intensity I_{B100} by subtracting the same ice sample from itself using a subtraction factor calculated from the following relation;

Result = Original – (Subtrahend * Factor).

In other words, the intensity (I_{A100}) and the intensities of the original and

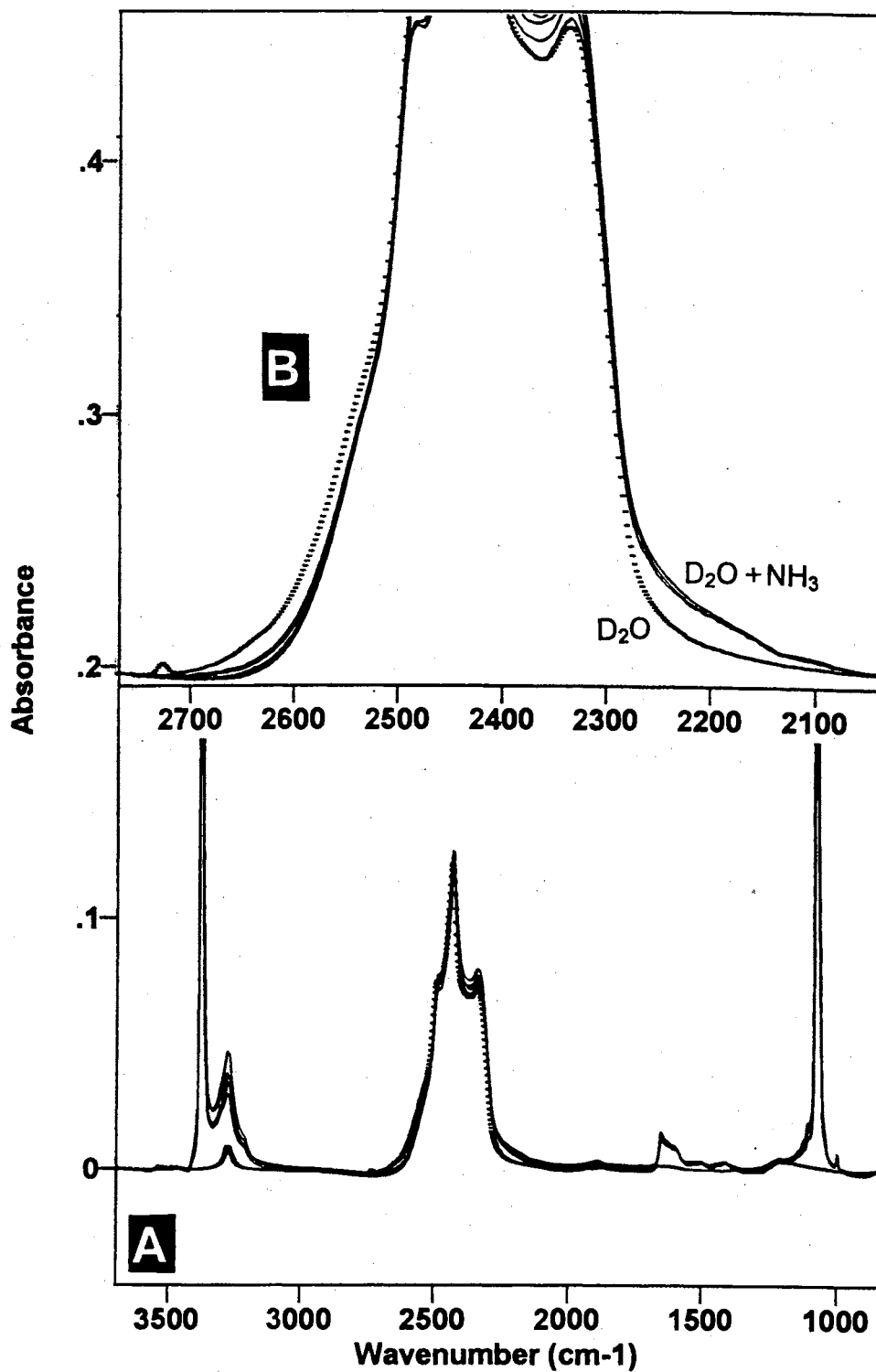


Figure 26. **A** – spectra of the network of NH₃ + D₂O for the different samples (connected lines) and the dotted line is the spectrum of bare D₂O ice. **B** – the spectra are expanded along both axes. All spectra were taken at 90 K.

subtrahend (I_{B100}) were placed in the formula and the factor is obtained. This subtraction is shown in Figure 27 and as seen from that figure, $I_{B100} = 0.3$ (the bare ice intensity) and $I_{A100} = 0.12$ (calculated from $(I_{A90}/I_{B90}) \times I_{B100}$) as the subtraction factor is 0.6.

Once the bare ice spectrum at the reaction temperature is found, the fraction of reacted ice in the zero-time ice is obtained by using the difference spectra as following: in Figure 28, evaluation of one datum at 107 K for the sample of $\text{NH}_3 + \text{D}_2\text{O}$ is shown. The dotted line spectrum, at top of Figure 28, is the bare ice spectrum and the connected line spectrum is the zero-time ice spectrum. The bare ice spectrum is subtracted until the peak marked *, the main ice band, (at the bottom of Figure 28) vanishes. The subtraction factor found from this process is then placed in the equation 3 to calculate the total fraction of reacted ice.

Total fraction of Reacted ice = fraction of reacted ice during the reaction + fraction of reacted ice consumed during the warming process (equation 3)

The total fraction of reacted ice is calculated simply by adding the results obtained from the equation 1 and equation 2.

Hereafter, the total fraction of reacted ice will be cited as the fraction of reacted ice.

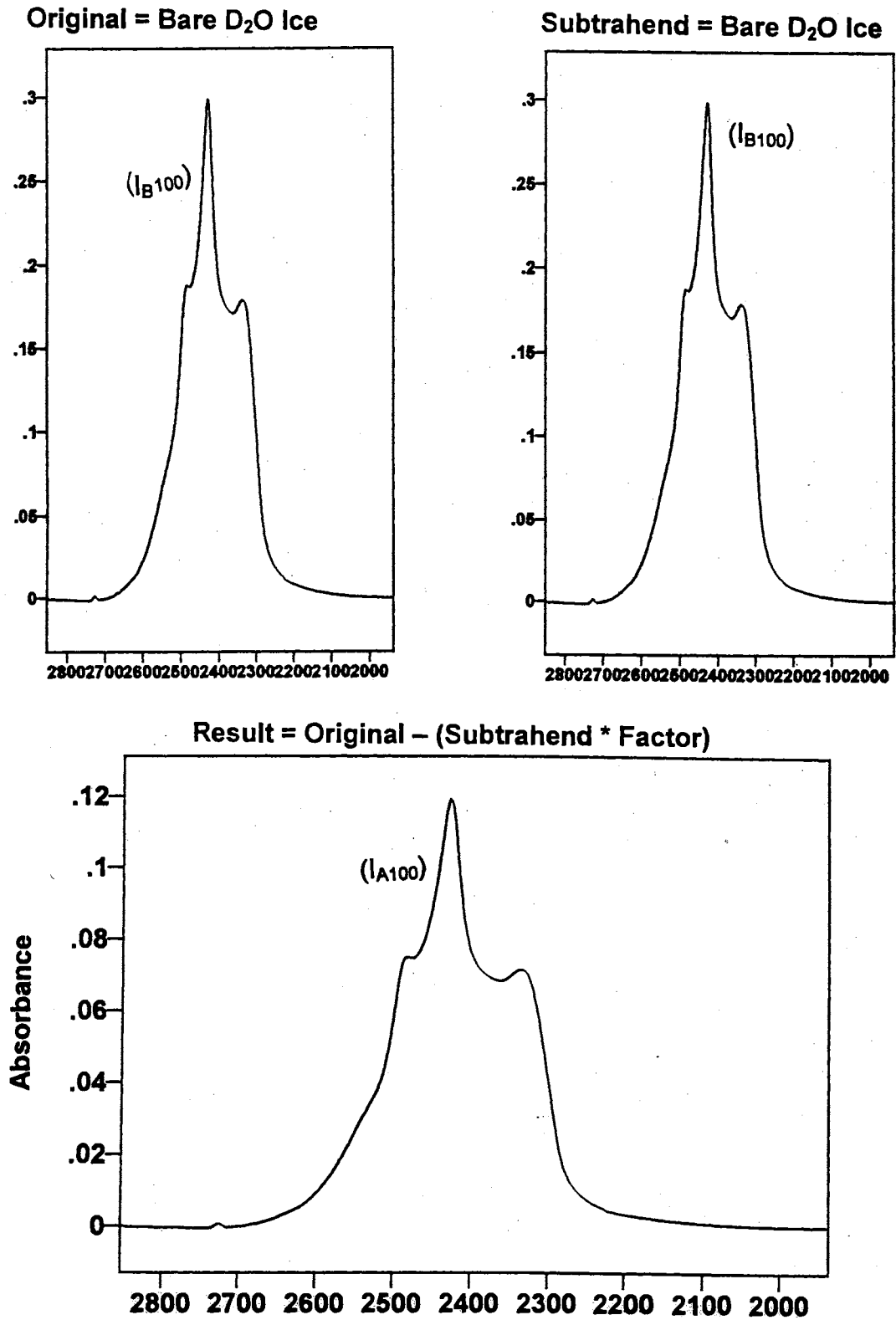


Figure 27. Subtraction of the bare D₂O ice spectrum with intensity of I_{B100} from itself; result: the subtracted bare ice spectrum with intensity of I_{A100}.

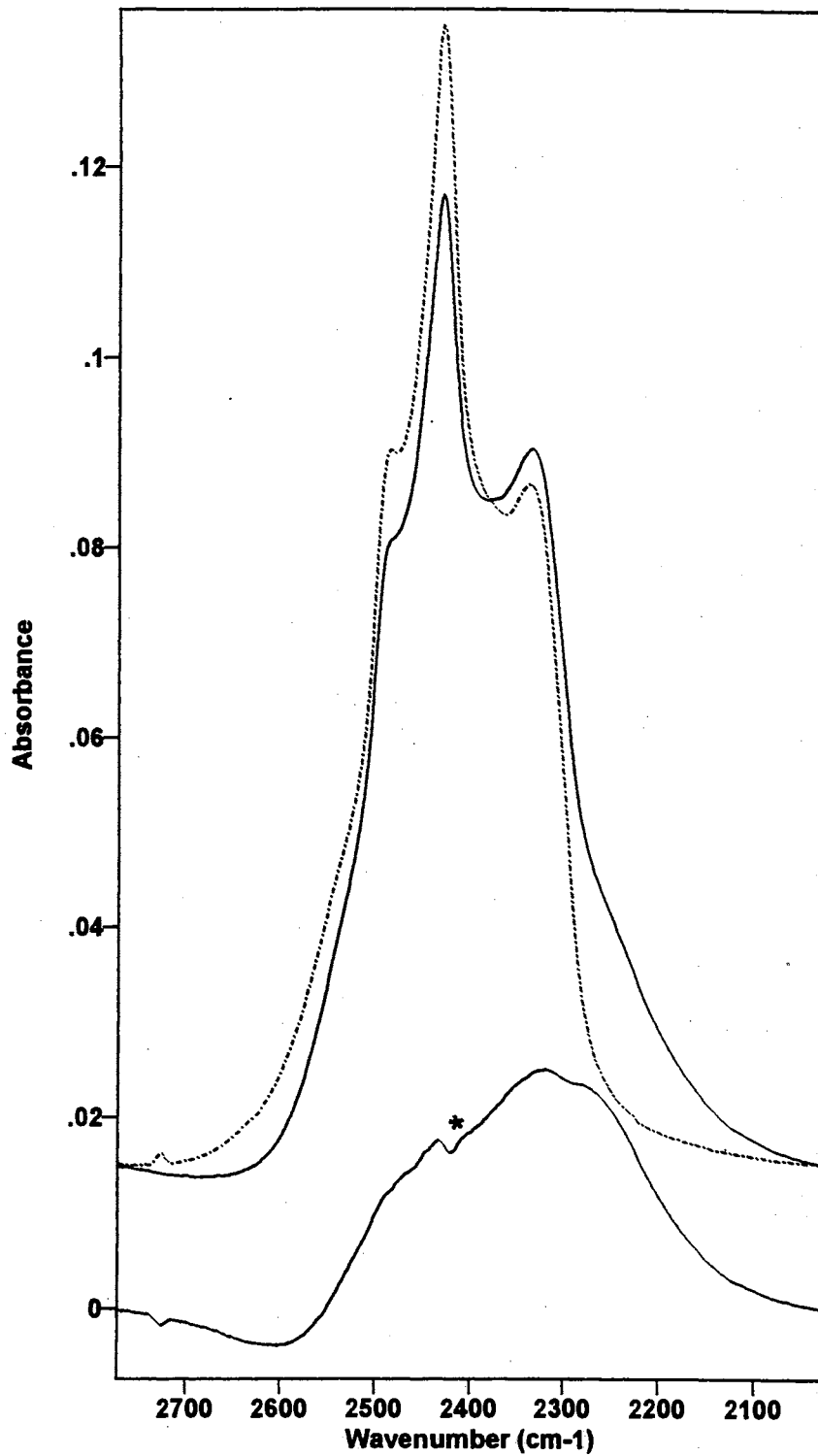


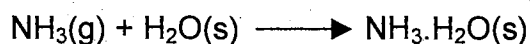
Figure 28. Finding one datum for extent of formation of amorphous $2\text{NH}_3 \cdot \text{D}_2\text{O}$: top; the bare ice spectrum (dotted line) and the sample spectrum (connected line), bottom; the subtracted spectrum (sample spectrum - bare ice spectrum), which shows the amorphous $2\text{NH}_3 \cdot \text{D}_2\text{O}$ spectrum.

CHAPTER III

CONVERSION OF ICE NANOCRYSTALS TO THE MONOHYDRATE OF AMMONIA

1. Introduction

The conversion of ice nanocrystals to the monohydrate of ammonia is a heterogeneous gas-solid process, represented as;

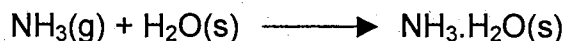


As described in the experimental part, the ammonia vapor was introduced into the system at the chosen reaction temperature and it condenses near the entry port of the cell. For the reaction given above, the cell temperature needs to be appropriate for a significant equilibrium vapor pressure of ammonia. On the other hand, the reaction temperature should be chosen as suitable for the reaction to be followed by FTIR spectroscopy.

The plan of this chapter is as follows: the kinetics for the conversion of the ice nanocrystals to the monohydrate of ammonia will be considered first for the $\text{NH}_3\text{-D}_2\text{O}$ system at various reaction temperatures and then the deuterium isotope effect on the reaction kinetics will be examined for the $\text{NH}_3\text{-H}_2\text{O}$ and $\text{ND}_3\text{-D}_2\text{O}$ systems. Moreover, the effect on kinetics of this conversion from changing the thickness of network of ice and the size of the ice nanocrystals, prepared under different experimental conditions, will be discussed.

2. Mechanism for the conversion of Ice Nanocrystals to the Monohydrate of Ammonia

The conversion of the ice nanocrystals to the monohydrate of ammonia proceeds via a molecular mechanism as follows;



The evidence for the molecular mechanism was that no O-H band in the $\text{NH}_3 \cdot \text{D}_2\text{O}$ spectrum (see Figure 17) was observed. If this reaction had proceeded via an ionic mechanism based upon formation of NH_3D^+ and OD^- , isotopic hydrogen exchange would have been observed between the NH_3 and D_2O molecules of the reacting ice, with HOD produced.

3. Kinetics of Conversion of Ice Nanocrystals to the Ammonia Monohydrate

3.1. Introduction

Before presenting experimental results, it is appropriate to describe the kinetic picture for this conversion, which contains;

1. Vaporization and transport of ammonia to the network of ice nanocrystals at the chosen reaction temperatures: When NH_3 is expanded into the cold cell, it condenses at the cold entry port of the cell, which is warmer than other parts of the cell (see Figure 29). Then, it starts to vaporize and moves to the wall of inner cell (the coldest part of the cell) containing also ice particles. First, a tight adsorbate monolayer forms on the ice. After that, as a multilayer of NH_3 forms, the vapor pressure becomes significant so the NH_3 begins to move through the network of ice nanocrystals deposited on the window.

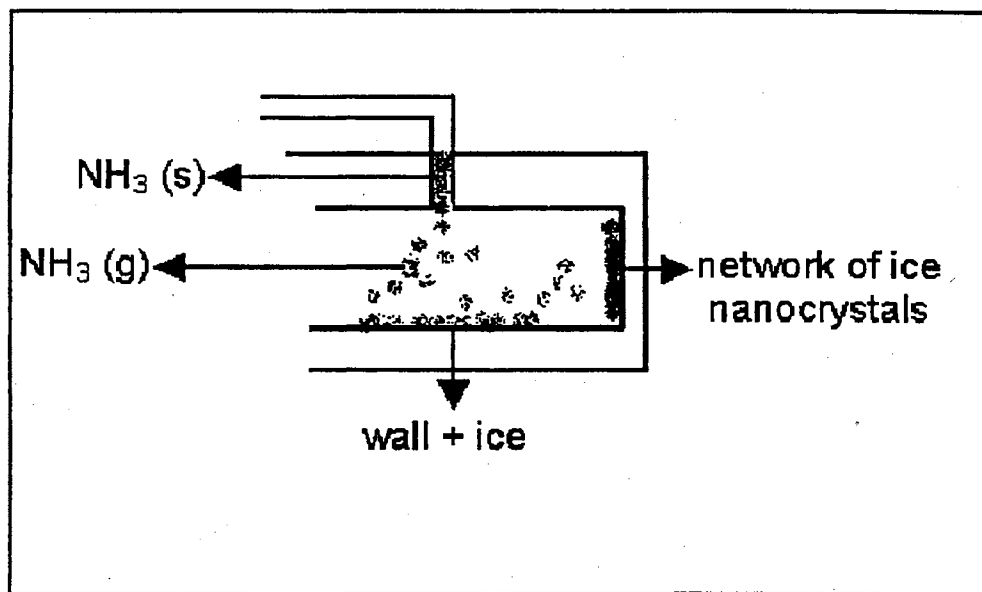


Figure 29. A simple picture of the mechanism of the transport of NH_3 to the ice nanocrystals.

2. Adsorption and penetration/conversion of ammonia to the hydrate: the mechanism for these stages, particularly penetration/conversion of ammonia to the hydrate, will be given in Chapter IV.2.

3.2. Conversion of D₂O Ice Nanocrystals to NH₃.D₂O at Different Reaction Temperatures

Five different reaction temperatures were used for these isotopomers of water and ammonia; namely 115, 117, 119, 121 and 123 K.

As noted in the experimental part, the scaled difference spectrum between the spectra of partially NH₃ reacted ice and the spectra of the bare ice was used to obtain the rate for the conversion of ice nanocrystals to the monohydrate of ammonia. Figure 30A (in 4000-800 cm⁻¹ region) shows the formation of NH₃.D₂O as a function of time at 115 K. In Figure 30B, C, and D, the spectra are expanded along both axes. In these figures, each spectrum taken at the specific reaction time has a subtraction factor equal to the fraction of unreacted ice. Since the total fraction of ice is one, one minus the subtraction factor gives the fraction of reacted ice.

Plots of these values with corresponding reaction time are shown in Figure 31 for the conversion of D₂O ice nanocrystals to NH₃.D₂O at the different reaction temperatures. Since the amorphous structures of the monohydrate were the dominant product at the beginning of the reaction, the resolution of the spectra into ice and hydrate components using the standard monohydrate spectra was not possible. Therefore, we do not report any value in Figure 31 until a certain time, depending on the reaction temperatures.

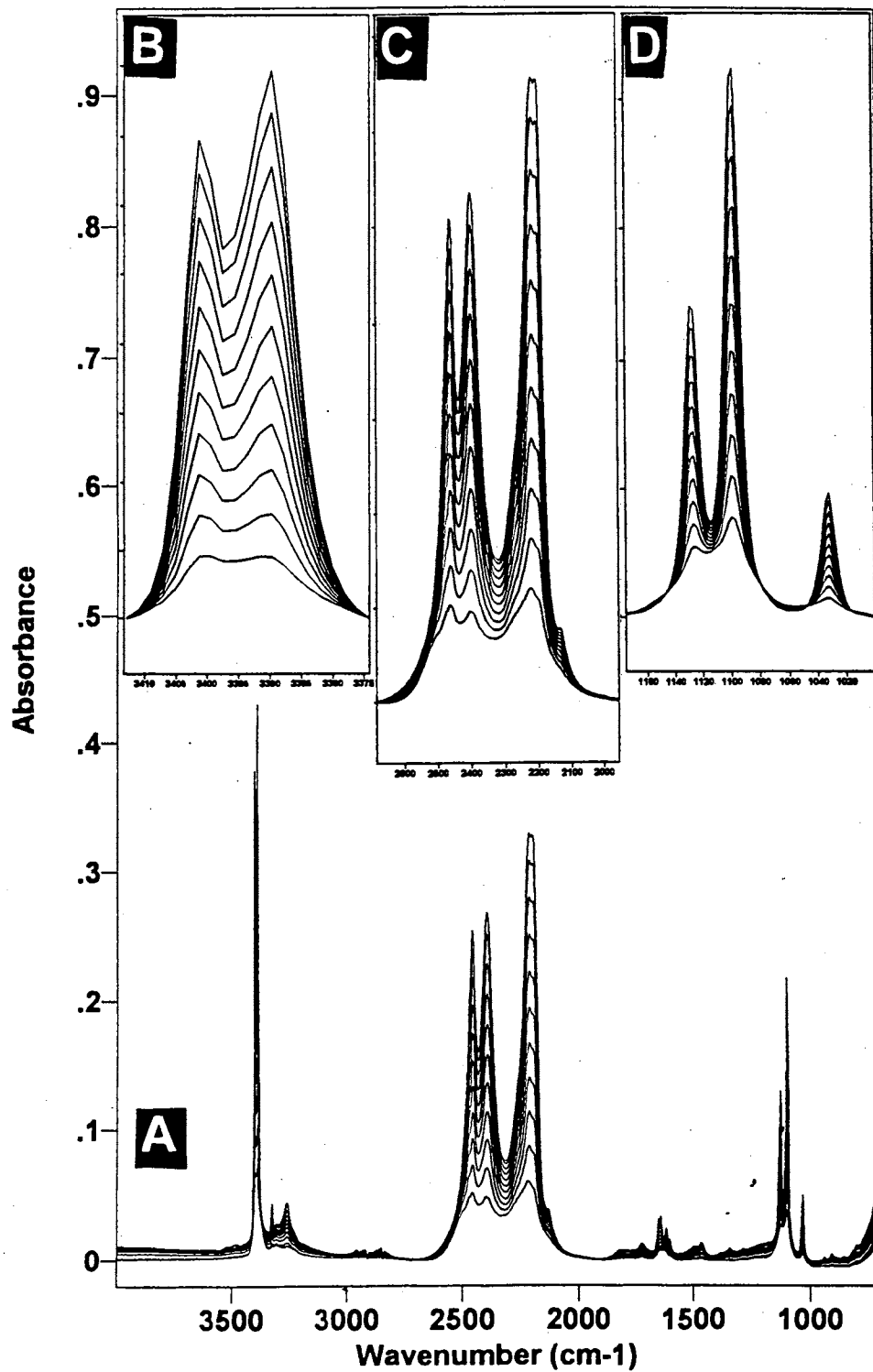


Figure 30. A – The monohydrate of ammonia ($\text{NH}_3\text{D}_2\text{O}$) at 115 K obtained by subtracting the bare ice spectrum from the partially NH_3 reacted ice spectrum as a function of time. B, C, and D – the spectra are expanded along both axes.

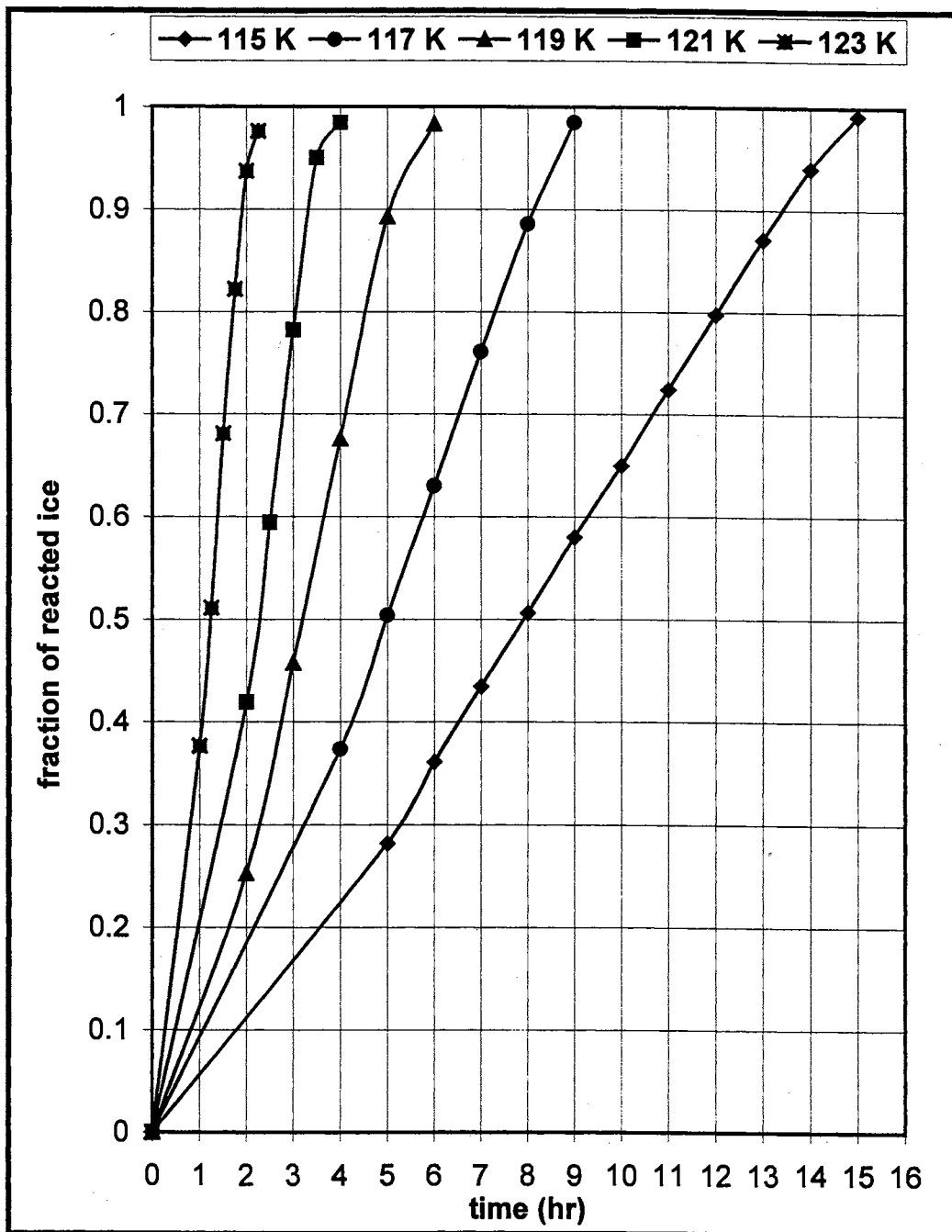


Figure 31. Plots of the fraction of reacted ice versus time (h) for the conversion of D_2O ice nanocrystals to $NH_3 \cdot D_2O$ at the different reaction temperature.

As seen from Figure 31, the lines became curved after some point, matching the onset of the formation of hemihydrate. The reason for the hemihydrate formation will be discussed in the later part of this chapter.

3.2.1. Temperature Dependence of the Reaction Rates

The variation of the rate of the reaction with temperature is generally expressed by the Arrhenius equation

$$\ln k = \ln A - E_a/RT.$$

where k is the rate constant, E_a is the activation energy, A is the frequency factor, T is temperature and R is the gas constant. Therefore, the activation energy is calculated from a plot of $\ln k$ versus $1/T$ with the slope of the curve equal to $-E_a/R$.

Taking the slopes of the straight lines of plots of $\ln k$ versus $1/T$ (see Figure 32) for the formation of $\text{NH}_3 \cdot \text{D}_2\text{O}$, the activation energy is calculated as 6.54 kcal/mol with $A = 1.83 \times 10^{11} \text{ s}^{-1}$.

4. Isotope Effects on Reaction Kinetics

4.1. D_2O versus H_2O

Five different reaction temperatures were used for the $\text{NH}_3 + \text{H}_2\text{O}$ system; namely 115, 117, 119, 121 and 123 K. The spectra for the conversion of H_2O ice nanocrystals to $\text{NH}_3 \cdot \text{H}_2\text{O}$ at 115 K is shown as a function of time in Figure 33A in 4000-800 cm^{-1} region. In Figure 33B, C and D, the spectra are expanded along both axes.

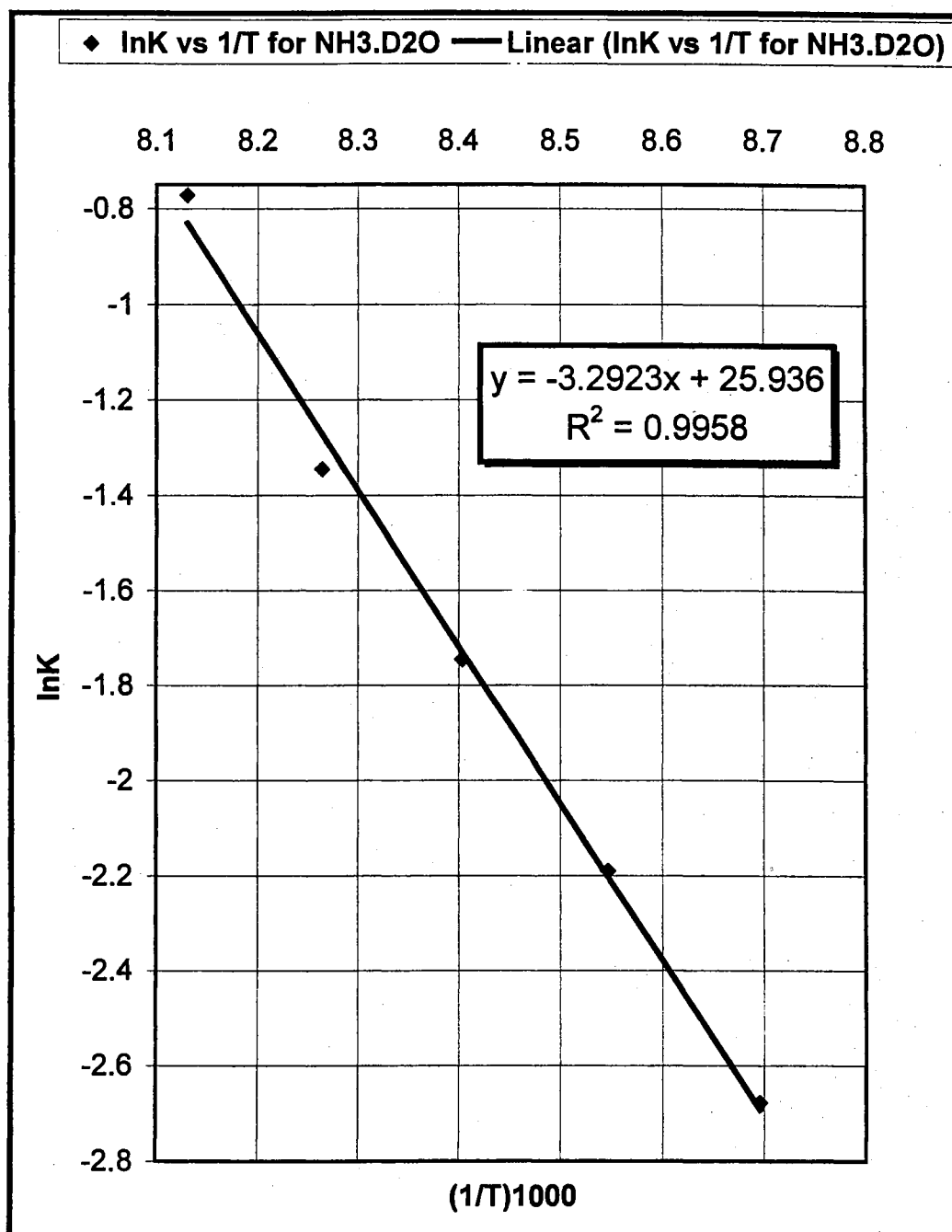


Figure 32. Arrhenius plot of the rate constant (k) of conversion of D₂O ice nanocrystals to NH₃.D₂O.

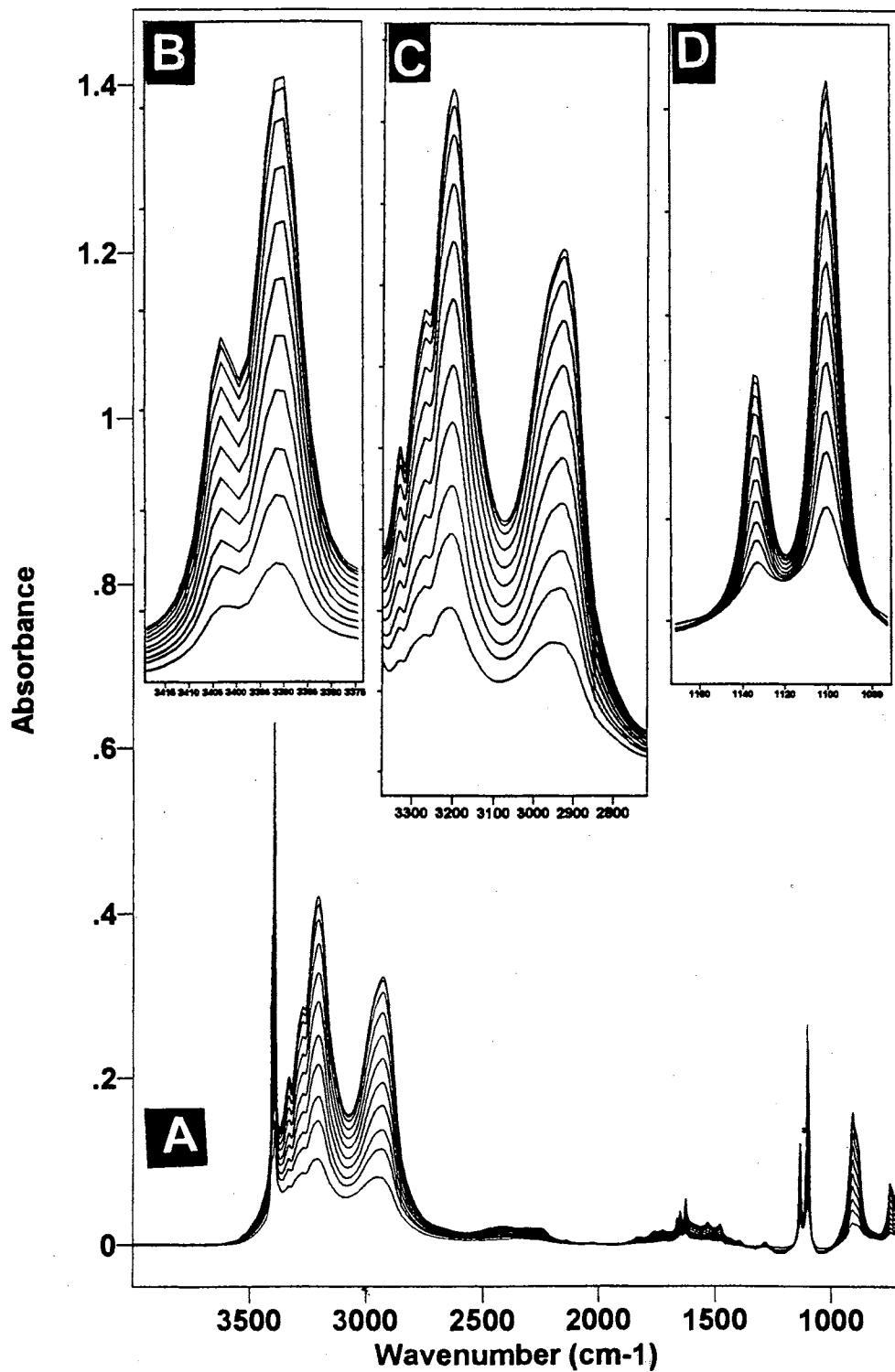


Figure 33. A – The monohydrate of ammonia ($\text{NH}_3 \cdot \text{H}_2\text{O}$) at 115 K obtained by subtracting the bare ice spectrum from the partially NH_3 reacted ice spectrum as a function of time. B, C, and D – the spectra are expanded along both axes.

The plot of fraction of reacted ice versus time for the different reaction temperatures is in Figure 34. At the beginning of the reaction, the product is again the amorphous monohydrate.

The plots of fraction of reacted ice versus time for the D₂O and H₂O ice at three different temperatures are shown in Figure 35 and as seen from that figure, within the experimental errors, there is almost no deuterium isotope effect for H₂O versus D₂O.

The plot of $\ln k$ versus $1/T$ is given in Figure 36 and the activation energy is calculated as 5.76 kcal/mol. The difference of the activation energies between the formation of NH₃.D₂O and NH₃.H₂O is 0.81 kcal/mol.

4.2. NH₃ versus ND₃

Four different reaction temperatures were used for the ND₃ + D₂O system; namely, 117, 119, 121 and 123 K. The spectra of the conversion of D₂O ice nanocrystals to ND₃.D₂O as a function of time at 117 K is shown in Figure 37.

The plots of fraction of reacted ice versus time (hr) for the conversion of D₂O ice nanocrystals to ND₃.D₂O at different reaction temperatures are shown in Figure 38.

In Figure 39, the plots of the fraction of reacted ice versus time for the formation of NH₃.D₂O and ND₃.D₂O at 117 and 119 K are given. There is a deuterium isotope effect for NH₃ versus ND₃ that will be discussed in the later part of this chapter.

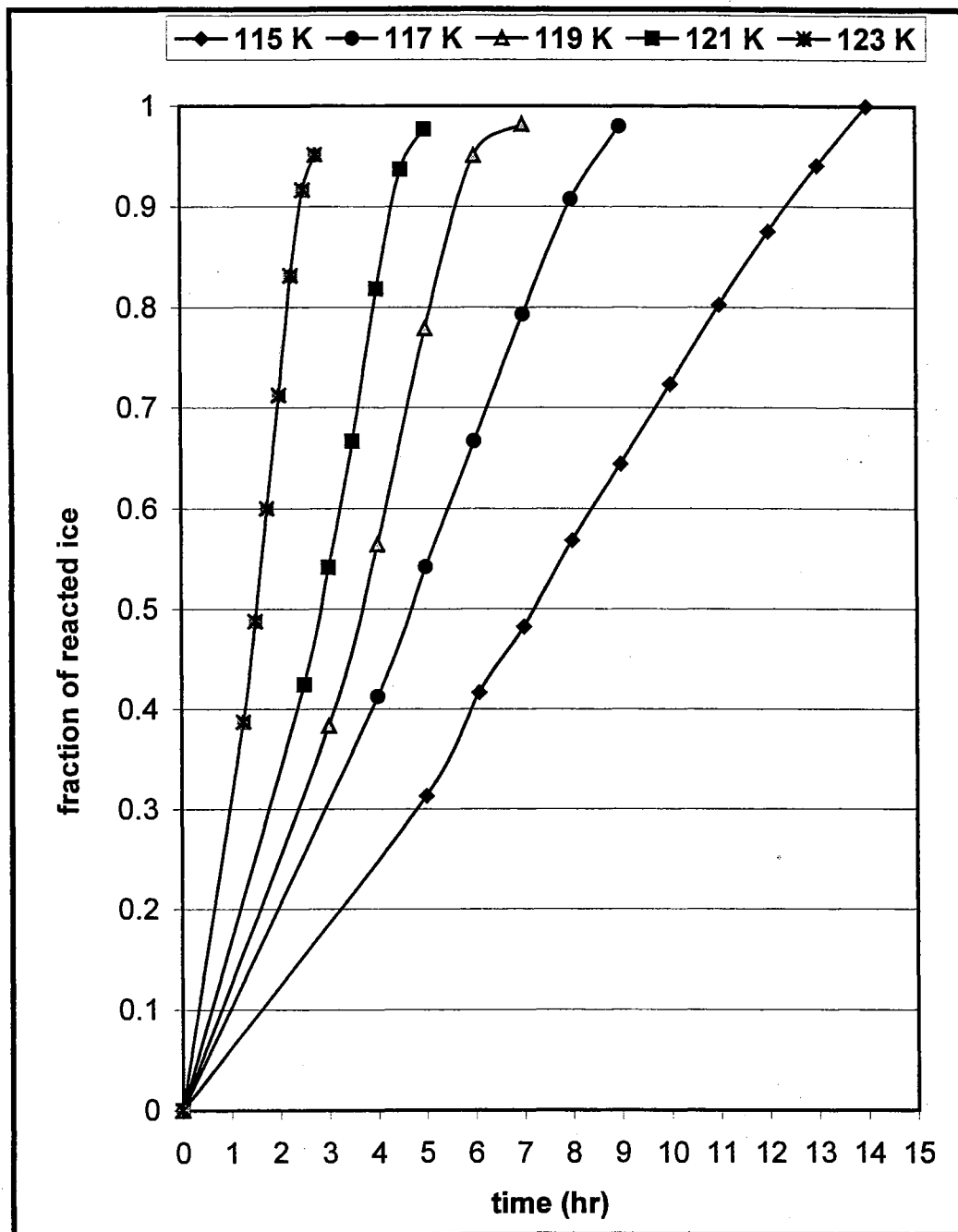


Figure 34. Plots of the fraction of reacted ice versus time (h) for the conversion of H_2O ice nanocrystals to $\text{NH}_3 \cdot \text{H}_2\text{O}$ at the different reaction temperature.

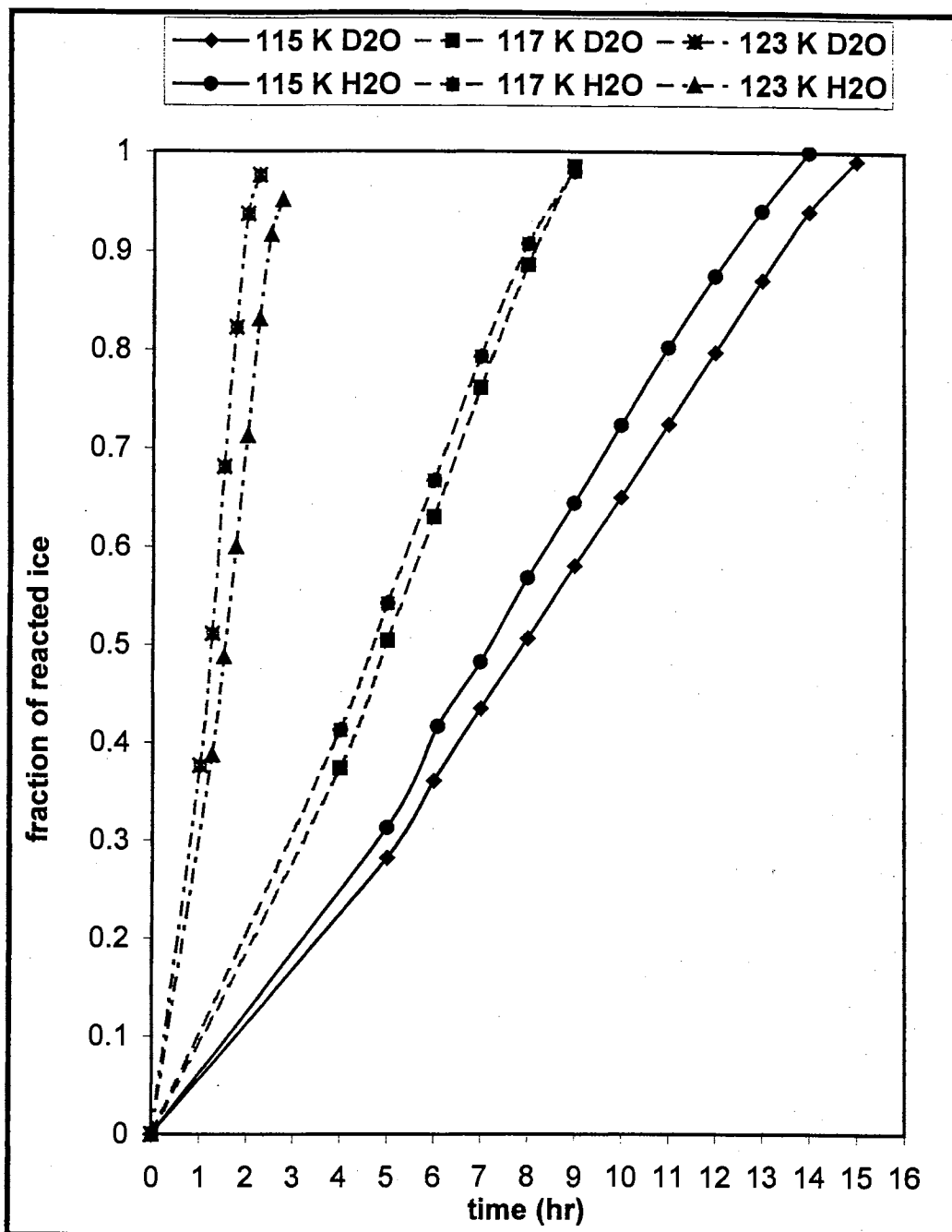


Figure 35. Comparison of the formation rates for $\text{NH}_3 \cdot \text{D}_2\text{O}$ versus $\text{NH}_3 \cdot \text{H}_2\text{O}$ at 115, 117 and 123 K.

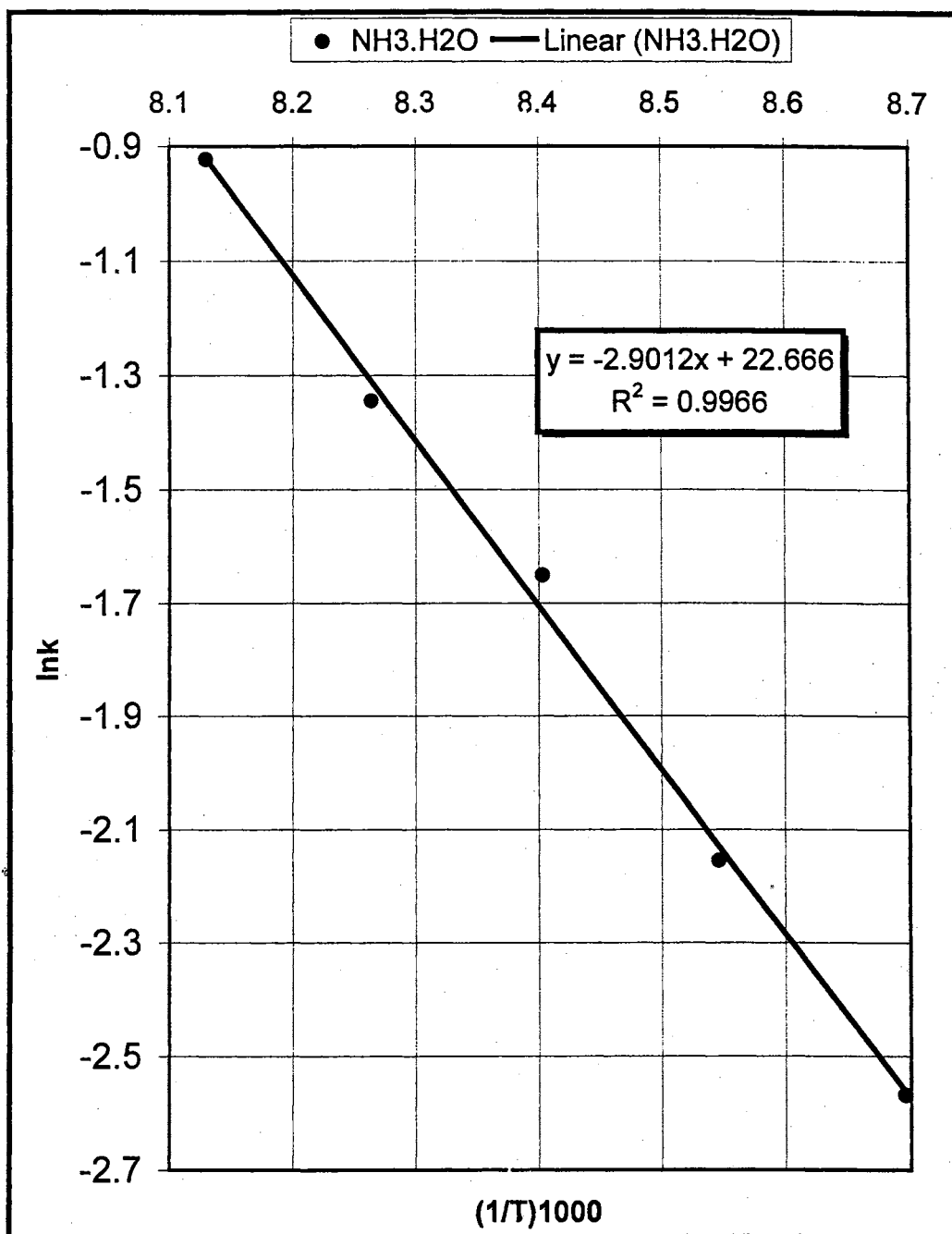


Figure 36. Arrhenius plot of the rate constant (k) of conversion of H₂O ice nanocrystals to NH₃.H₂O.

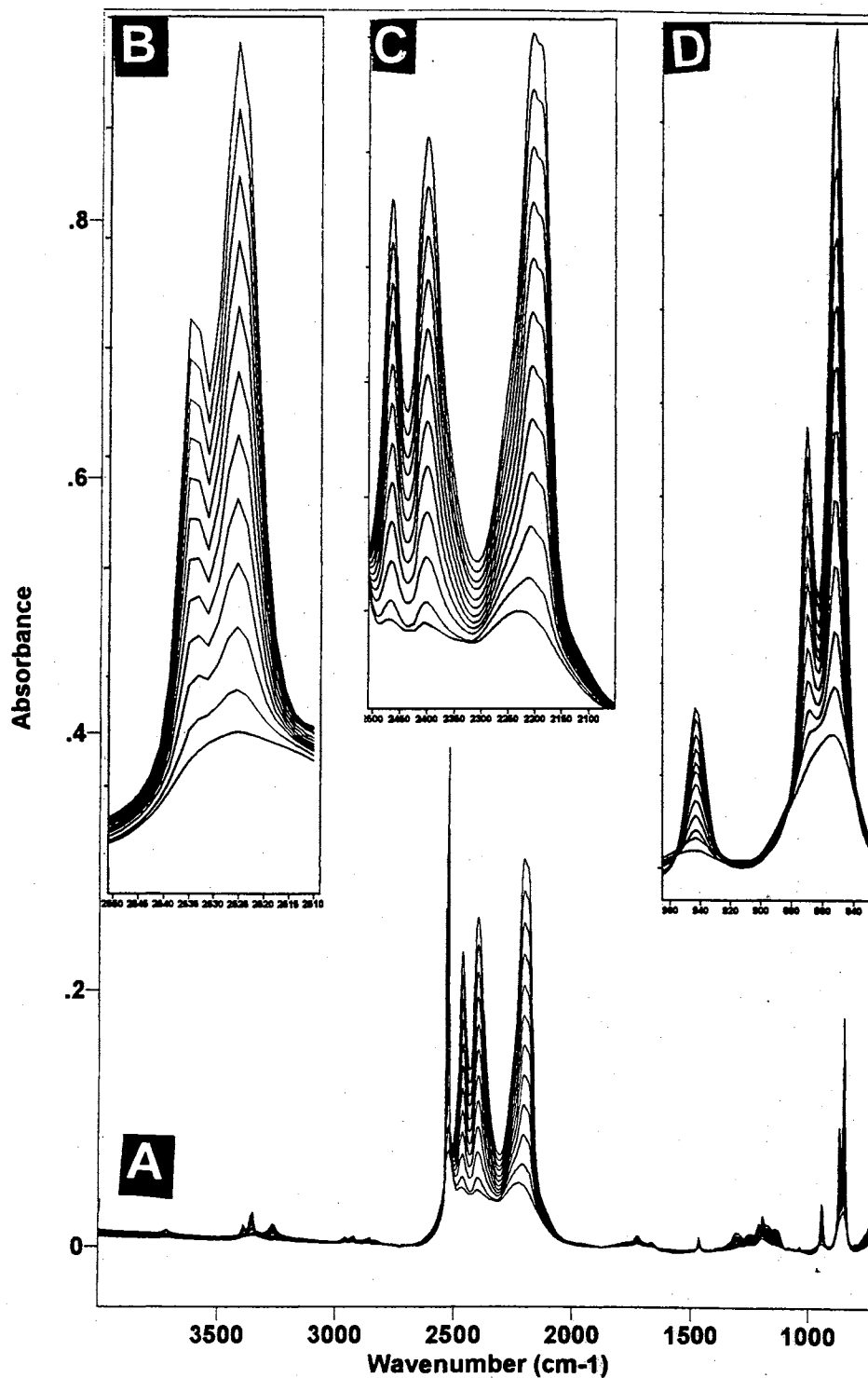


Figure 37. A – The monohydrate of ammonia ($\text{ND}_3 \cdot \text{D}_2\text{O}$) at 117 K obtained by subtracting the bare ice spectrum from the partially ND_3 reacted ice spectrum as a function of time. B, C, and D – the spectra are expanded along both axes.

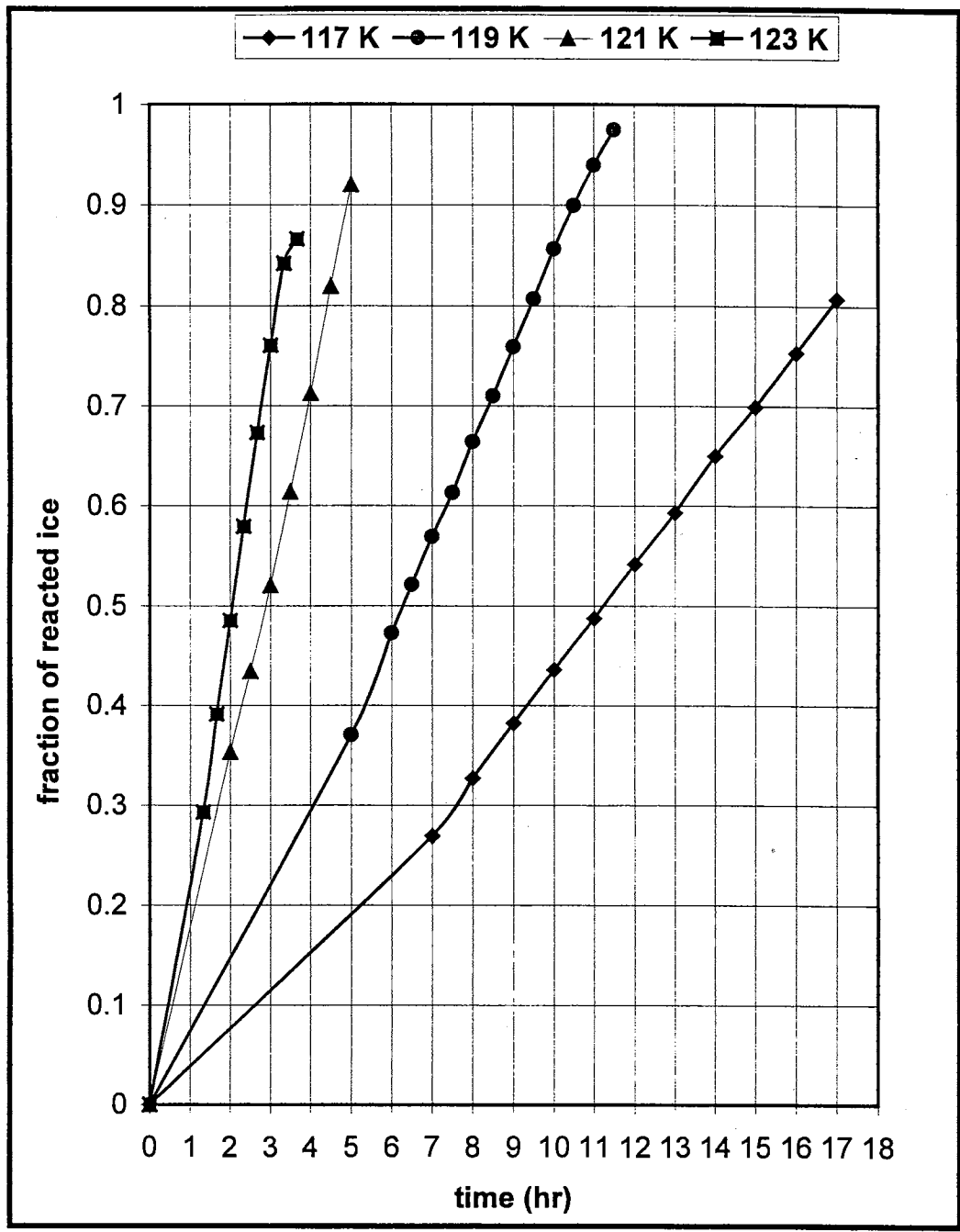


Figure 38. Plots of the fraction of reacted ice versus time (hrs) for the conversion of D₂O ice nanocrystals to ND₃.D₂O at the different reaction temperature.

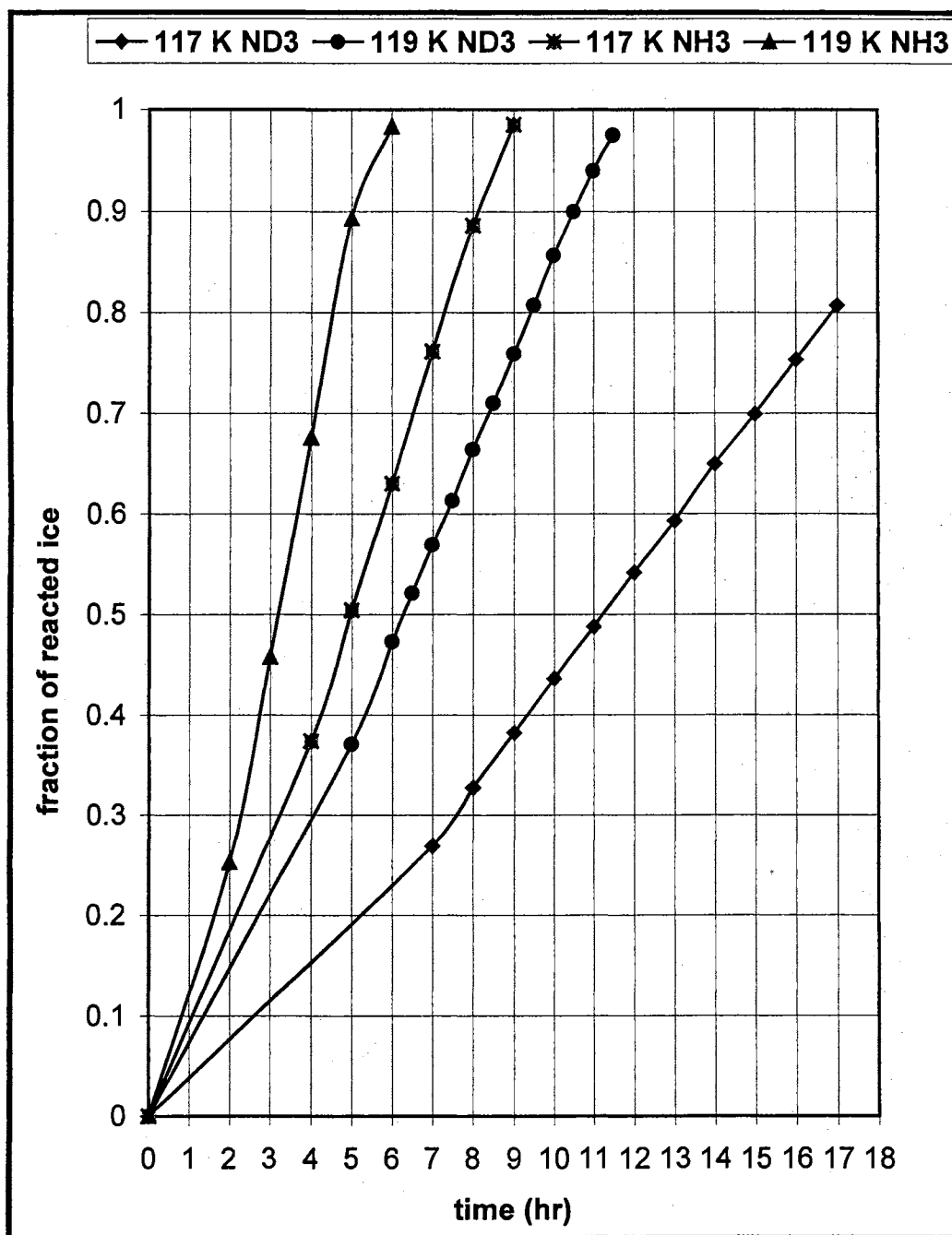


Figure 39. Comparison of the formation rates for $\text{NH}_3 \cdot \text{D}_2\text{O}$ versus $\text{ND}_3 \cdot \text{D}_2\text{O}$ at 117 and 119 K.

From the same procedure that was followed for the other isotopomers, the plot of $\ln k$ versus $1/T$ is given in Figure 40 and the activation energy is calculated as 7.75 kcal/mol.

5. Effect of Size of the Ice Nanocrystals on the Reaction Kinetics

Either using Ostwald ripening or preparing the particle at high temperature, i.e. 140 or 145 K, can change the size of the ice nanocrystals. The spectroscopic evidence of the change of the size is obtained from the relative intensity of the d-H band, as will be seen later. We used the $\text{NH}_3+\text{D}_2\text{O}$ system at 115 K to examine these experimental conditions.

5.1. Changing Particle Size by Ostwald Ripening

All results presented above were obtained from samples prepared at 63 K and then annealed at 133 K. In this part of the study, the particles were also prepared at 63 K, but they were annealed to 140 and 145 K.

As noted in the first chapter, when the ice nanocrystals are annealed, the size of the particles becomes larger by the Ostwald ripening process. During this process, the small particles vaporize and the vapor is added to the surface of the larger ones. Further, one can arrange the average particle size depending on the annealing temperature, as the size changes between 110-150 K. Consequently, after the annealing process, some of the surface and subsurface molecule absorption is lost due to this conversion. This can be followed by FTIR difference spectroscopy as decreasing peak intensities of the surface molecules. Although,

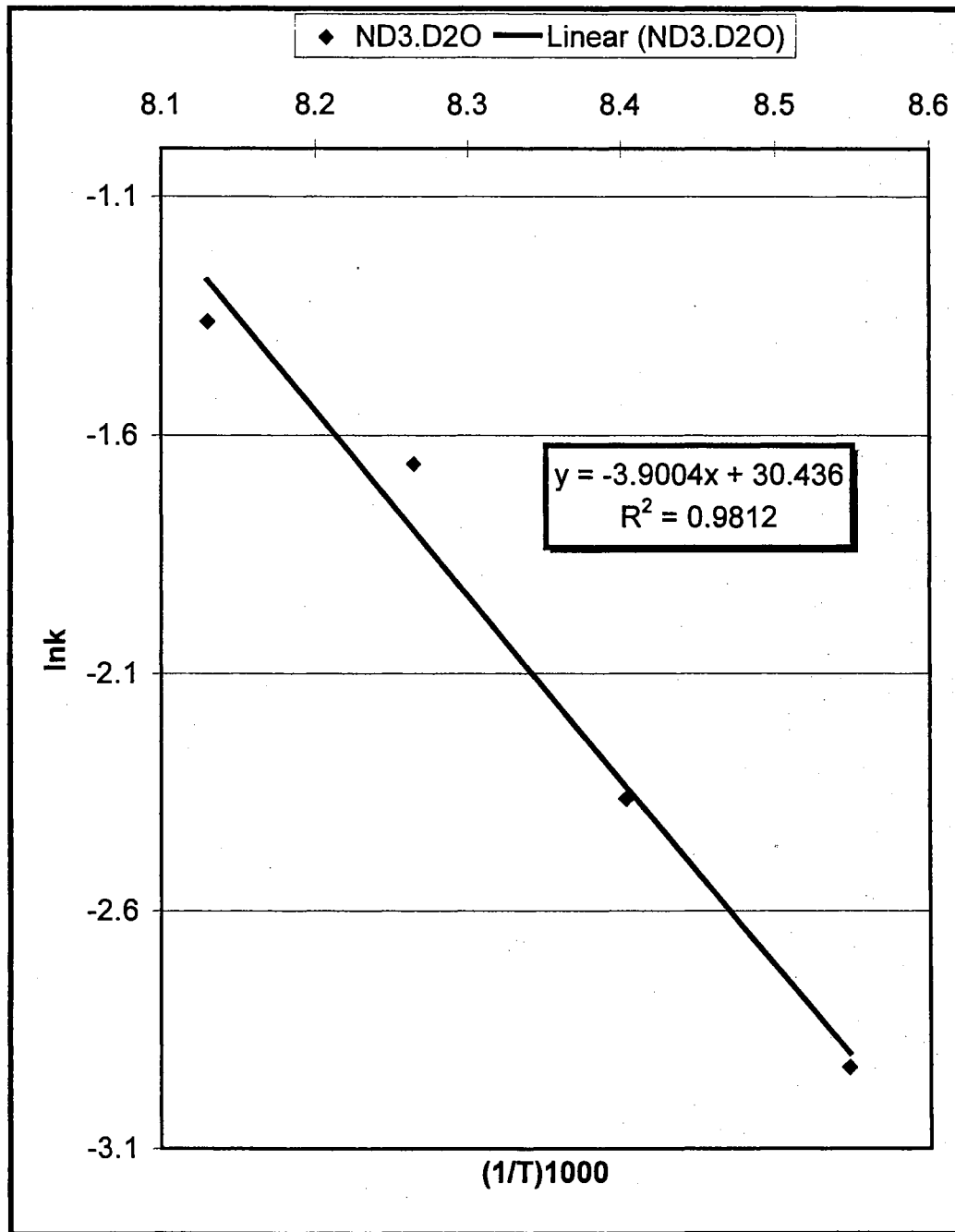


Figure 40. Arrhenius plot of the rate constant (k) of conversion of D₂O ice nanocrystals to ND₃.D₂O.

the total amount of ice does not change, different relative amounts of surface and interior absorption are obtained from the annealed and unannealed ice sample spectra that are taken at the same temperature.¹⁷

This means that, when the different ice samples having the same amount of surface-to-volume ratio are annealed, the surface-to-volume ratio decreases as the annealing temperature increases. Three ice samples having a similar amount of D₂O ice band intensity were annealed to 133, 140 and 145 and as shown in Figure 41, the intensity of the d-D band was decreased from top (low annealing temperature) to bottom (high annealing temperature).

The same ice samples, having different surface areas shown in Figure 41, were exposed to the same amount of ammonia at 115 K and the spectra obtained within 5 minutes after NH₃ was added, are shown in Figure 42 as difference spectra between the partially NH₃ coated ice spectrum and the bare D₂O ice spectrum with the subtraction factor one. In these spectra, the negative bands correspond to the surface modes (d-D, d-O, and s-4) and the positive bands are the adsorbate (NH₃) and adsorbate induced-shifted surface bands.²³ As seen from the figure, the extent of the initial uptake of ammonia on the ice surface becomes larger when the surface area is small, i.e. the surface was fully saturated by the ammonia for the sample of the top spectrum.

Although the particles having the small surface area were saturated fastest, the reaction rates, under the same experimental conditions, followed the similar straight line, as shown in Figure 43 at 115 K. However, one should notice that as the particle size increases, the curvature of the plots due to the

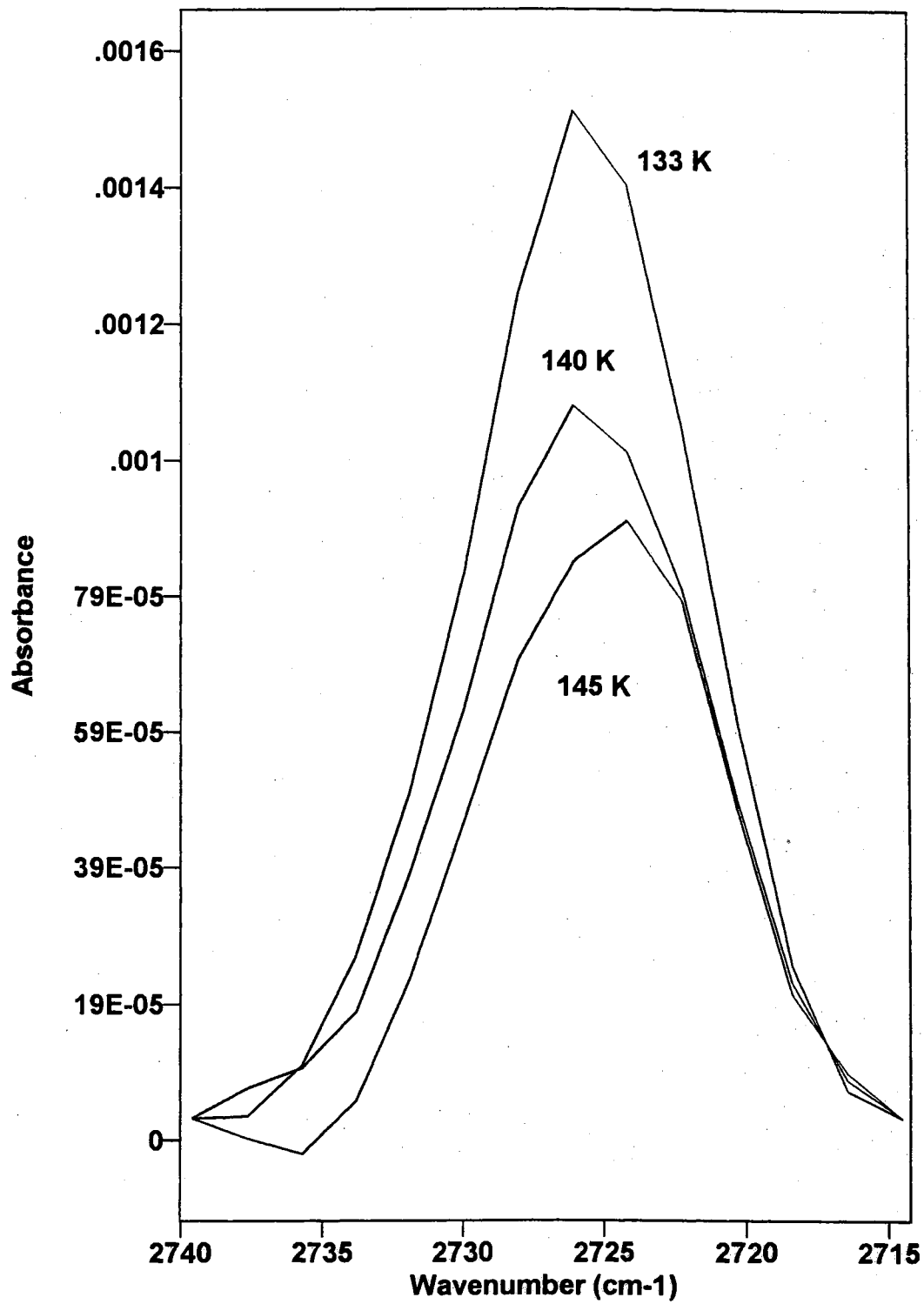


Figure 41. Shows decreasing d-D (dangling-deuterium) intensity with increasing annealing temperature for three different samples having similar amount of interior ice intensity.

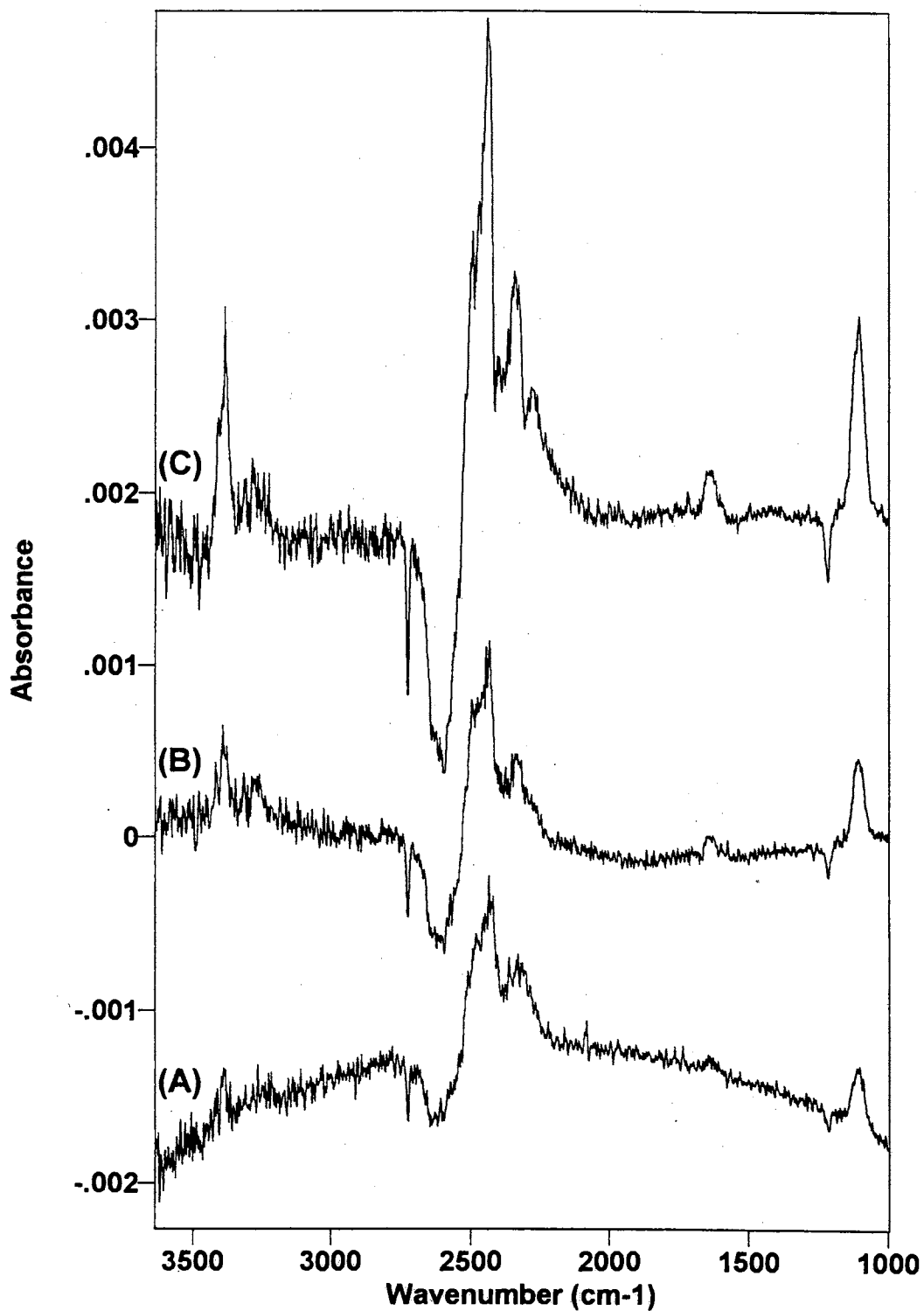


Figure 42. Difference spectra obtained by subtracting the spectrum of the bare ice nanocrystals from the spectra of NH_3 -coated ice nanocrystals (taken within 5 minutes after NH_3 was added to cell), using a subtracting factor of 1.0: all loading temperatures were 63 K, the reaction temperatures were 115 K and annealing temperature was: (A) 133 K, (B) 140 K and (C) 145 K.

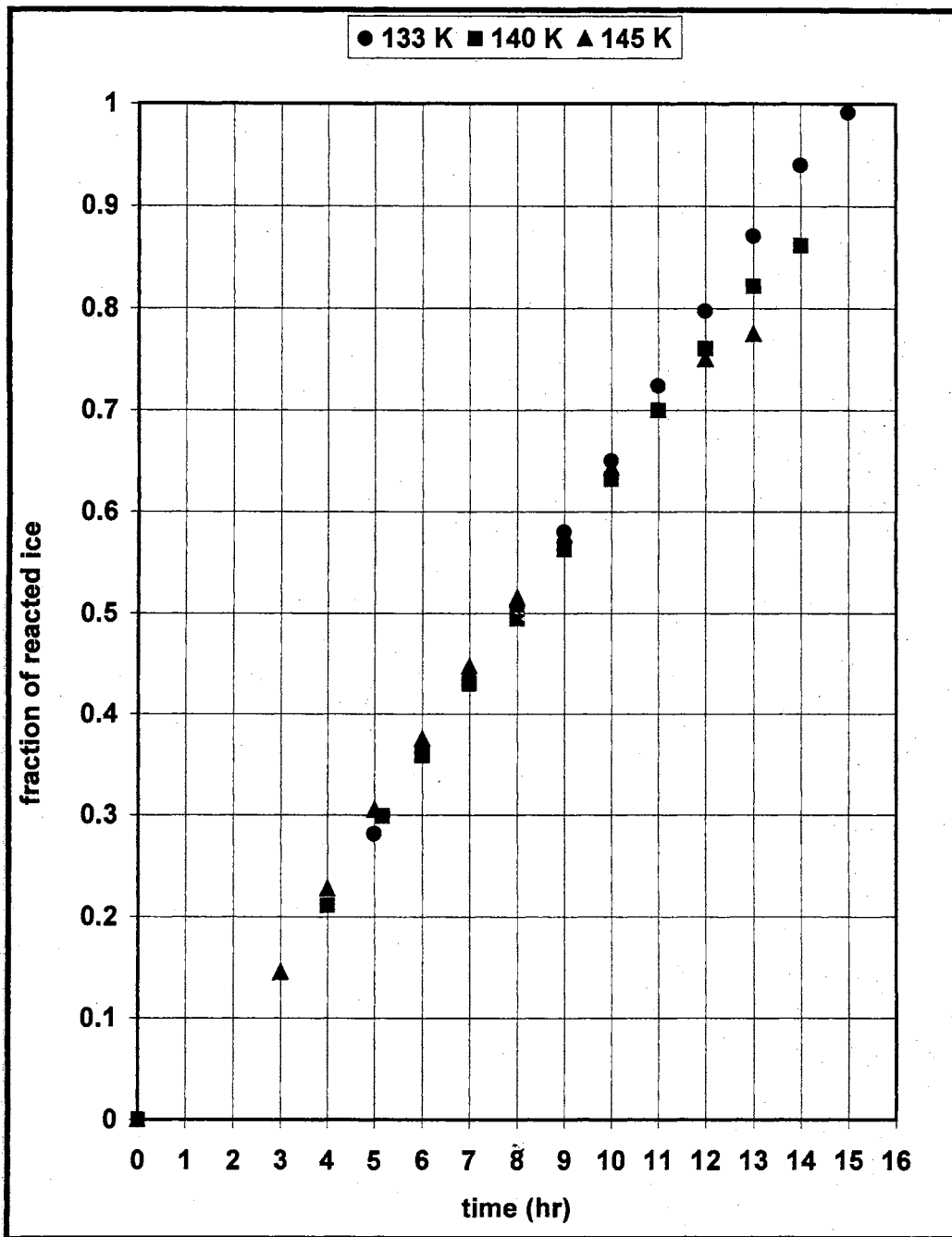


Figure 43. Effect of the ice particle size on the reaction kinetics: all loading temperatures are 63 K, reaction temperatures are 115 K, and annealing temperature is 133, 140, and 145 K.

hemihydrate formation onsets more quickly, as observed for the high reaction temperatures shown in Figure 31. This may indicate that the diffusion of ammonia through the hydrate, which has formed at the outer surface of the ice particles, becomes a governing factor of the rate for larger particles. In other words, before it may react with ice on the hydrate/ice interface, the ammonia molecules must pass through the hydrate crust, which is thicker for the large particles for the same fraction of reacted ice. Since the diffusion of ammonia through the hydrate may become a rate-limiting factor, ammonia may accumulate on the hydrate surface at the concentration required to start to convert the monohydrate to the hemihydrate of ammonia. The spectroscopic evidence for this conversion was that when the formation of ammonia hemihydrate starts, the loss of ice almost stops. This conversion to hemihydrate may start, particularly, on the vacuum/hydrate interface, where the ammonia vapor first encounters the network.

The mechanism for the conversion of ice nanocrystals to the monohydrate of ammonia or for the conversion of monohydrate to the hemihydrate of ammonia will be discussed in the following chapter. However, it should be noted here the formation of hemihydrate requires some certain level of the ammonia concentration on the surface of the monohydrate, as observed in the high temperature results and in the results for the different sizes of ice particles.

5.2. Changing the Particle Size by Preparing Particles at 140 and 145 K

Instead of annealing particles to the high temperatures to obtain large

particles, they can be prepared at high temperature. For this purpose, we prepared the ice particles at 140 and 145 and the reaction rates were measured at 115 K.

The difference spectra between the ammonia coated D₂O ice and the bare D₂O ice are shown in Figure 44. In this figure, the bottom spectrum (A) is the same spectrum shown in Figure 42 (B), i.e., sample prepared at 63 K and annealed to 140 K, and the top spectrum was taken from the sample that was prepared at 140 K (both samples were exposed to ammonia at 115 K). As seen from the figure, although the samples have a similar surface area, only the sample prepared at 140 K had almost all of the surface coated with ammonia as well as the negative band below 2500 cm⁻¹ corresponding to the loss of interior ice. This rapid access of ammonia to the surface clearly shows that making particles at high temperature creates gaps between the particles. By contrast, when the particles are annealed, the particles come close to each other so that the path of NH₃ (g) through the assembly of particles is obstructed.

The plots of the fraction of reacted ice versus time are shown in Figure 45. As seen from the figure, within the experimental error, the rates of both reactions follow the same linear plot.

The thickness of ice also was changed to examine the kinetics of this conversion. The regular ice samples discussed until here had generally 0.4 peak absorbance unit intensity. In this part, a sample with 0.2 absorbance unit intensity was prepared at 140 K. The plots of fraction of reacted ice versus time are shown in Figure 46. The data represented with squares are normalized

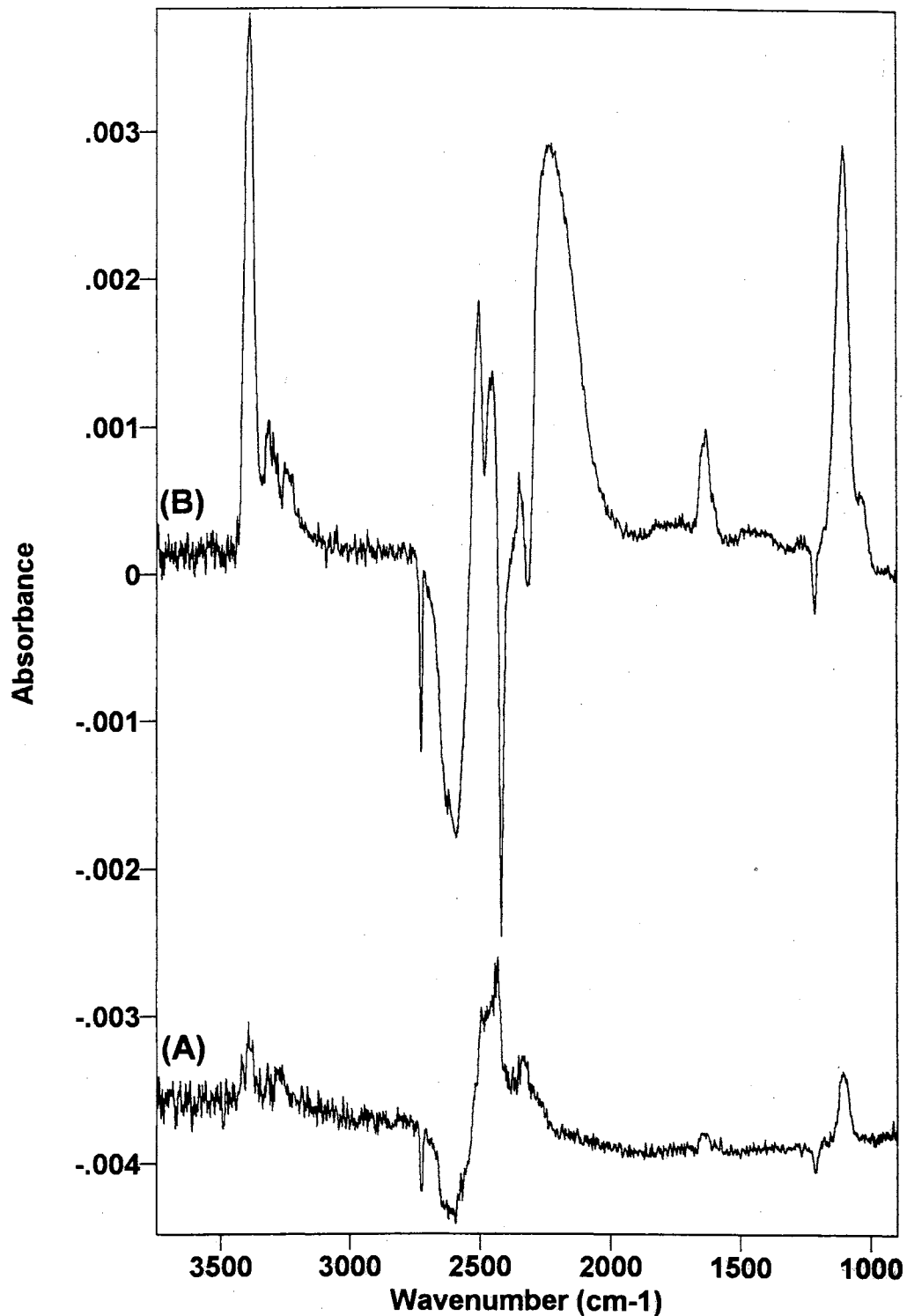


Figure 44. Difference spectra obtained by subtracting the spectrum of the bare ice nanocrystals from the spectra of NH_3 -coated ice nanocrystals (taken within 5 minutes after NH_3 was added to the cell), using a subtracting factor of 1.0: all reaction temperatures were 115 K: (A) loading temperature was 63 K and annealing temperature was 140 K and (B) loading temperature was 140 K.

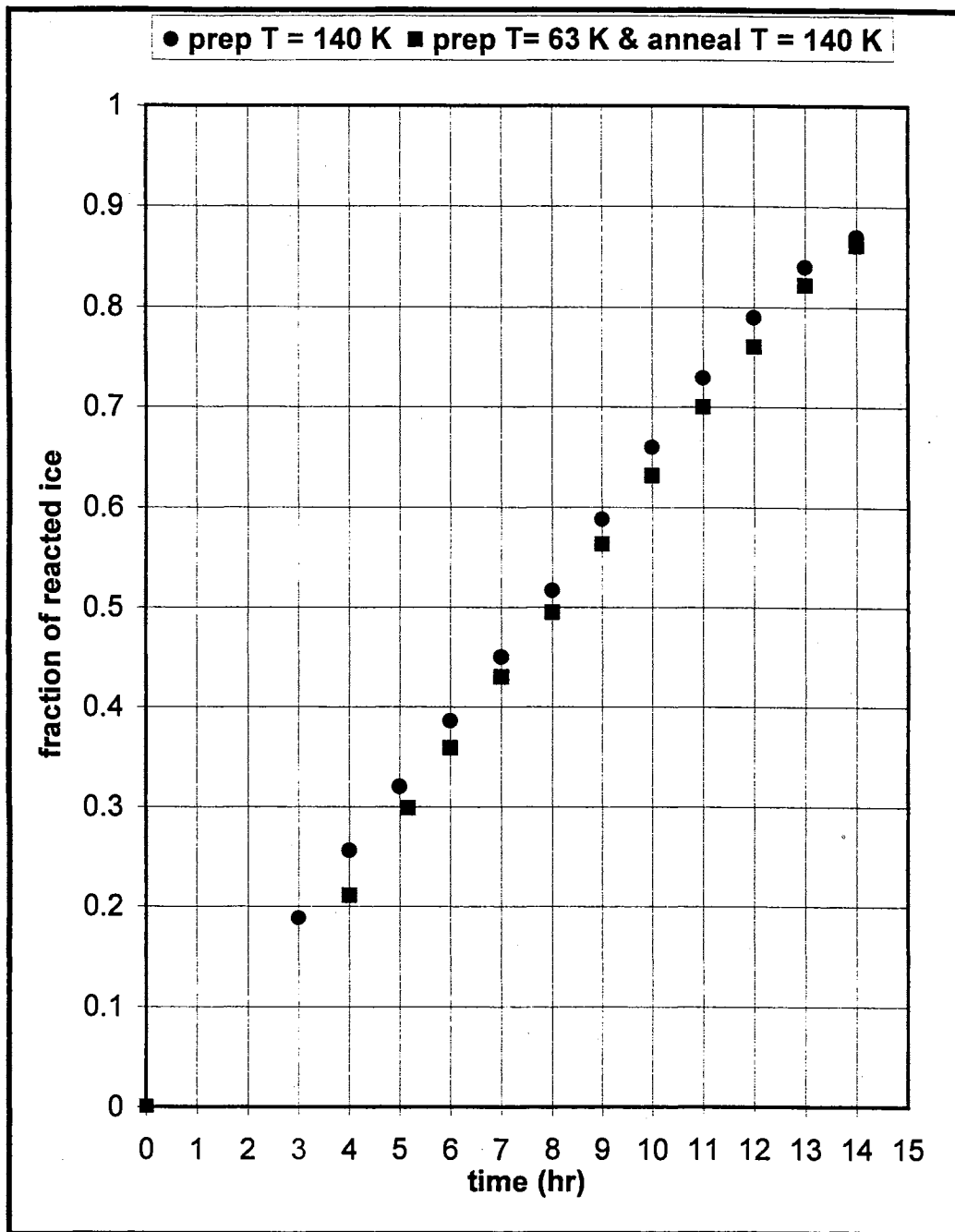


Figure 45. Plots of fraction of reacted ice versus time (hr) for the samples having the similar amount surface areas; ● is for the sample prepared at 140 K and ■ is for the sample prepared at 63 K and annealed to 140 K.

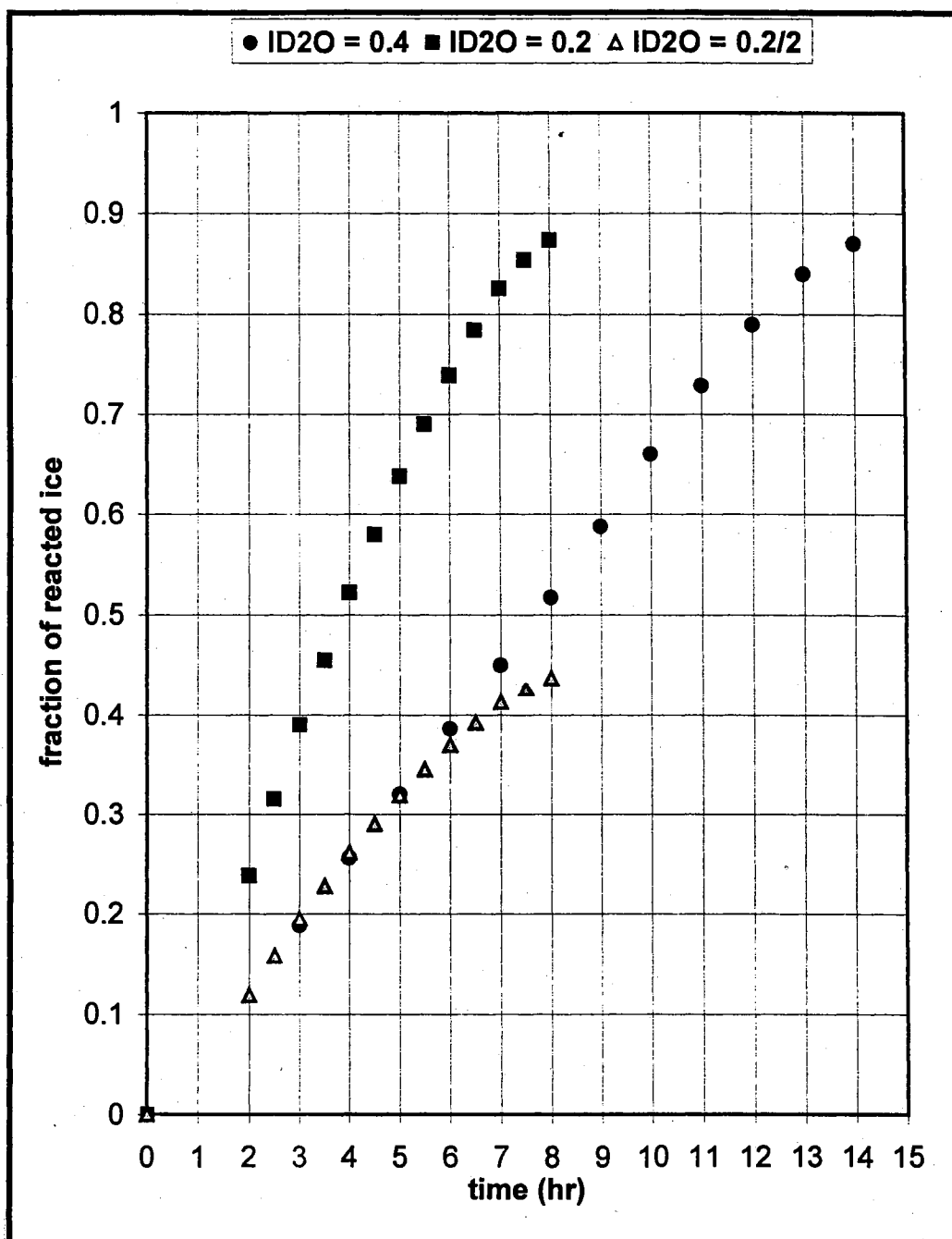


Figure 46. Plots of fraction of reacted ice versus time (hr) for the samples having the different thickness of ice network; ● is for the sample having a 0.4 absorbance unit intensity, ■ is for the sample having a 0.2 absorbance unit intensity and ▲ is for the same sample as ■, but the fraction of reacted ice values shown with ■ are divided by two. All loading temperatures are 140 K and reaction temperatures are 115 K.

by dividing the fraction of reacted ice by two and the resulting values are shown by triangle. Again, the rate did not change as seen from that figure and this clearly shows that diffusion of ammonia vapor through the network is not a rate-limiting factor.

6. What is the Rate Determining Step for the Conversion of Ice Nanocrystals to the Monohydrate of Ammonia?

For a given (fixed) reaction temperature and isotopomer of water and ammonia (i.e., $\text{NH}_3+\text{D}_2\text{O}$ or $\text{ND}_3+\text{D}_2\text{O}$), the reaction kinetics may depend on the following; vapor pressure of ammonia, the size of the ice nanoparticles (or the surface area), the thickness of the network of the ice nanocrystals, diffusion time of ammonia through the crust of the hydrate that has formed.

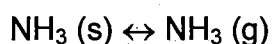
As shown in Figures 31, 34 and 38, the reaction between the ice and ammonia followed the linear plots for several hours of reaction. A linear plot indicates that the reaction is of (pseudo) zeroth order. If the reaction proceeds with zero order kinetics, the reaction rate must be controlled by a factor that is constant during the reaction.

If one looks at the possibilities on which the reaction kinetics depended, the diffusion time of ammonia through the crust of the hydrate that has formed is not rate limiting since the diffusion length becomes larger as the reaction proceeds. Moreover, if this were rate limiting, we would have observed different reaction kinetics when the size of the particles was changed.

As examined, the thickness of the network did not change the reaction rate; neither did the gap between the particles, although the rate for the

saturation of the surface of the ice was faster for the large particles prepared at the high temperature.

The possibility that the vapor pressure of ammonia is the rate-determining factor satisfies the condition that the rate must be controlled by a constant during the reaction. Since there is an equilibrium (shown below) between the solid and gas phase of ammonia, the vapor pressure of ammonia can be considered as a constant (see section 3.1, also).



If the ammonia vapor pressure is rate controlling, then the activation energy for the hydrate formation should equal the ammonia sublimation energy at the reaction temperatures. The heat of vaporization of $\text{NH}_3 (\text{s})$, can be calculated using a modified version of the Clausius-Clapeyron equation as follows;⁴⁵

$$\ln(P^2/P^1) = -(\Delta H_{\text{sub}} / R) [(1/T_2) - (1/T_1)]$$

where P^1 and P^2 are the vapor pressures of ammonia at T_1 and T_2 , respectively. ΔH_{sub} is the heat of sublimation and R is the gas constant. The vapor pressure of $\text{NH}_3 (\text{s})$ for a given temperature is calculated from;⁴⁶

$$\log P_{\text{NH}_3} = -(1630.700/T) + 9.00593$$

where P_{NH_3} is the vapor pressure of $\text{NH}_3 (\text{s})$ (in units of cm of Hg) at the temperature T . The vapor pressures are;

$$P^1_{\text{NH}_3} = 6.6977 \times 10^{-6} \text{ cm-Hg at } 115 \text{ K}$$

$$P^2_{\text{NH}_3} = 5.6002 \times 10^{-5} \text{ cm-Hg at } 123 \text{ K.}$$

Therefore, the heat of sublimation is calculated as 7.46 kcal/mol, which is

greater than the average activation energy of 6.7 kcal/mol that has been found above. There may be reasons for this difference in the activation energy and the heat of sublimation, they will be discussed at the end of this chapter.

The vapor pressure of ammonia as the rate-limiting factor also explains the deuterium isotope effect NH_3 versus ND_3 , since it is known that the vapor pressure of a substance containing D is generally lower than that containing H. For example, there is an equation that gives the relation between the vapor pressures of NH_3 and ND_3 at temperature T as follows;

$$\log(P_{\text{NH}_3}/P_{\text{ND}_3}) = (49.69/T) - 0.1305.$$

7. Major sources of Errors in Determination of the Reaction Rates

The significant factor that contributes to source of error is the spectroscopic measurements discussed as follows: for each reaction temperature, a standard monohydrate spectrum was taken from the same sample following the complete reaction after several hours, since the monohydrate spectrum is temperature dependent. As noted before, above the 117 K reaction temperature, before completing the reaction, the formation of the hemihydrate started. The standard monohydrate spectrum was derived by subtracting the hemihydrate spectrum from the monohydrate spectrum or by annealing the low reaction temperature samples at the desired reaction temperatures. Therefore, some error may come from the standard spectra.

In addition to this, the intensities of the peaks were used to evaluate the data, as noted in the experimental part. Although the base line corrections were

made to measure accurately these peak intensities, since these were broad peaks, the measurement of these peak intensities caused some errors.

The other source of the error may be the pressure of residual noncondensable gasses (the components of air, such as nitrogen, oxygen, carbon dioxide, argon and so on) in the reaction system. Since the presence of the residual gasses reduces the vapor transport of ammonia, the reaction rate could be influenced. We cannot say anything about the magnitude of this error. However, it must be noted here as a potential error source.

CHAPTER IV

CONVERSION OF ICE NANOCRYSTALS TO THE AMMONIA HEMIHYDRATE

1. Introduction

The main objective of this research is to advance the understanding of the interaction between ammonia and ice within a mechanistic and kinetic perspective. Furthermore, as discussed before, this research will be a basis of the computer simulation for the molecular level investigation of this interaction. Particularly, the computer simulation technique will be developed to understand initial steps of NH_3 adsorption, penetration and hydrate formation.

However, it was shown in the previous part that the conversion of the ice nanocrystals to the monohydrate of ammonia was controlled by the vapor pressure of ammonia and it is difficult to get useful reaction kinetic data under these conditions.

The question arises then, if the vapor of ammonia is supplied to the ice-hydrate interface in abundance, how does the reaction proceed and what is the reaction kinetics? To answer these questions, an alternating-layer method has been developed and applied to NH_3 and ice. In this method, the ice particles were mixed with ammonia particles at cryogenic temperatures so that the ammonia was more uniformly distributed within the network of the ice particles. Moreover, even at 100 K, the rate of thermal vaporization of ammonia was enough to allow measurement of the kinetics for conversion of ice nanocrystals to the hydrate of ammonia by monitoring the FTIR spectra as a function of time.

In contrast to the first reaction method that resulted in monohydrate formation, the alternating particle method ended with the formation of hemihydrate (not the monohydrate or dihydrate). The reasons why we observed monohydrate in one case and hemihydrate in the other are discussed in the following section. After that, the kinetics for the conversion of the ice nanocrystals to the hemihydrate of ammonia are considered for the $\text{NH}_3\text{-D}_2\text{O}$ system, at different reaction temperatures; and the deuterium isotope effect on the reaction kinetics is examined for the $\text{NH}_3\text{-H}_2\text{O}$ and $\text{ND}_3\text{-D}_2\text{O}$ systems.

2. Mechanism for Conversion of Ice Nanocrystals to the Hemihydrate of Ammonia

Before proceeding with kinetic information, this is an appropriate point to introduce discussion of the interplay of processes of the penetrating adsorbate on the surface of the ice; namely, adsorption, penetration and conversion of ice to hydrates of NH_3 . When considering the kinetics of heterogeneous reactions, these stages should be properly understood. As discussed in the first chapter, the penetrating adsorbates, i.e. NH_3 , HCl , HNO_3 , small ethers, and methanol, have the capability to break the water-water bonding in the ice structure due to the comparable strength of the adsorbate-water bonds. In recent years, intensive work has been done to understand physical and chemical properties of the resulting hydrates. Among them, particularly extensive data have been determined for the hydrates of HCl and HNO_3 , due to the discovery that their heterogeneous reactions within ice clouds play an important role in stratospheric ozone depletion.

2.1. NH₃ on the Ice Surface

The behavior of NH₃ on the ice surface has been discussed in the first chapter. As a summary, exposure of the ice nanocrystals to ammonia at levels less than a monolayer resulted in strong hydrogen bonding of the ammonia to the dangling-hydrogen sites (saturation of d-H) while limited uptake was observed for the d-O and s-4 surface sites. This is not a surprising phenomenon since ammonia is known as a good proton acceptor. The complete monolayer coating of the ice surface with ammonia causes, through crowding, a gain in linearity and strength of the hydrogen-bonded structures at the d-H sites. However, the interactions of NH₃ with the sites of d-O and s-4 are not as favorable as that with the d-H site, since NH₃ is a weak proton donor molecule. Therefore, an equilibrium between the gas phase NH₃ and the adsorbate phase of NH₃ on the d-O and s-4 sites may be established for the complete monolayer coating of the ice surface with ammonia, such as the following,²³



Furthermore, the saturation process, which occurs on the d-H, d-O and s-4 sites, does not require an activation energy since it takes place on the available sites of the surface of the ice. It was shown that the surface of the ice nanocrystals could be held saturated, at 120 K for long periods of time, without forming the hydrate.

2.2. Penetration/Conversion to the Hydrates

Keeping all this in mind, the hydrate formation mechanism is proposed

based on the works of Devlin *et al.*²⁵ and Davidovits *et al.*³³

Once the surface of the ice is saturated, the incoming ammonia interacts (physically) very weakly with the surface sites, i.e., with previously chemisorbed NH_3 or/and D_2O within the first layer of the ice surface. Therefore, the above equilibrium may become irreversible as follows: when the free energy of weakly interacting ammonia exceeds some certain level, it may penetrate the ice, form "critical hydrate clusters" and begin to convert the ice to the hydrate. The free energy of NH_3 molecules, interacting weakly with the surface species, should be only slightly less than ammonia in the vapor phase but greater than chemisorbed NH_3 . Figure 47 is proposed to represent this process. If the ammonia-water clusters do not reach a certain size (D), i.e., surmount the free energy barrier, the process is reversed. At that stage, there would still be an equilibrium between the weakly bound ammonia (C) and vapor ammonia, as the NH_3 free energy is too low to form the critical nucleating clusters (D) required for the hydrate formation.

To the author's knowledge, an appropriate terminology used to explain this process is not available in the literature for the gas/solid interface except in the work of Devlin *et al.* in which it was identified as a "nucleation" process. Here, the terminology of nucleation refers to the start of any kind of phase transition (in our case, the start of the hydrate phase). In nucleation theory, the formation of a critical cluster is explained by the free energy relationship to cluster size with the equilibrium density of clusters proportional to $\exp(-\Delta G_N/RT)$, where ΔG_N is the molar Gibbs energy relative to separate molecules, for the formation of clusters with N molecules. According to the nucleation theory, ΔG_N initially increases with

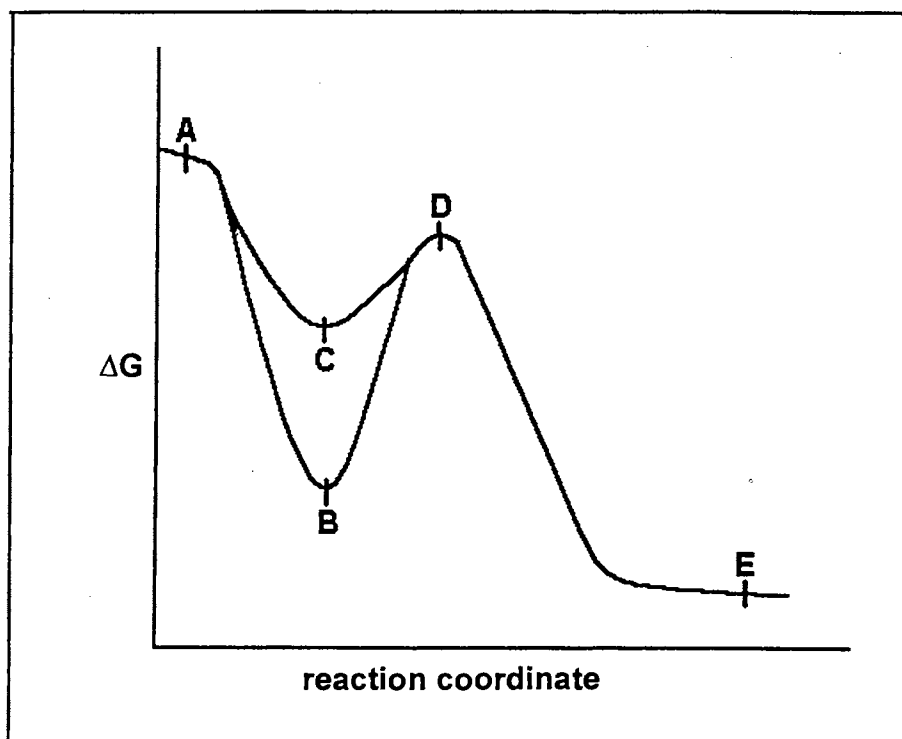


Figure 47. Proposed free energy diagram; A – NH_3 (g); B – NH_3 on the d-H; C – NH_3 on the d-O and s-4; D – NH_3 in the hydrate nucleus (critical $\text{NH}_3 - \text{D}_2\text{O}$ clusters); E – hydrate.

increasing cluster size, comes to a maximum at the critical cluster size and then decreases. In fact, the nucleation process is a complex problem that can be explained by a mathematical representation.

If the proposed mechanism is correct for the hydrate formation on the ice surface, it should be valid at the temperatures less than 140 K. Above this temperature, the water molecules near the ice surface have a sufficient volatility for the ice particles to grow without a limit, so the reaction mechanism may change.

The same sequence was suggested in the case of hydrate formation of HCl, HBr and HNO₃, which are also in the classification of penetrating adsorbates.²⁵ The same terminology was also used for the gas/liquid interface in the work of Davidovits *et al.*³³ In their work, they proposed a new model based on nucleation theory for the incorporation of the incoming gas molecule at a liquid surface.

The question may come up “if the hydrate formation starts with a nucleation process, why do two kinds of hydrate (monohydrate and hemihydrate) form?” As discussed above, the hydrate formation requires a certain level of adsorbate free energy with respect to that of the critical nucleus. The nucleation of these two kinds of hydrate must be related to the number of ammonia (or concentration) in the critical clusters. That concentration will depend on the population of NH₃ molecules of high free energy at the surface (C in Figure 47). Therefore, the rate at which ammonia comes to the surface and at which the surface sites accommodate the ammonia molecules into the weakly bound state

is important in this process. If the ammonia vapor concentration is high, so will the concentration be high in the nucleus; then the hemihydrate is nucleated. In contrast, if the concentration is low, then monohydrate is formed.

The conversion of ice nanocrystals to the hemihydrate of ammonia proceeds via a molecular mechanism, like in the case of the monohydrate formation; with the spectroscopic evidence for the monohydrate formation valid for this hydrate, as well.

3. Kinetics of Conversion of Ice Nanocrystals to the Ammonia Hemihydrate

3.1. Introduction

A simple description for the conversion of ice nanocrystals to the hemihydrate of ammonia is the heterogeneous reaction of NH_3 with spherical ice particles (see Figure 48) based on the following reaction;

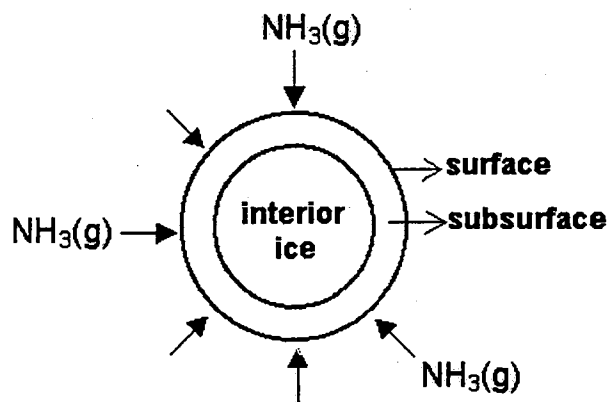


Figure 48. The heterogeneous reaction of NH_3 with spherical ice particles.

Before presenting the results generated from the experiments conducted in our laboratory, one should clearly discuss the kinetic scheme for this conversion, which involves:

(1) Vaporization of the ammonia particles [$\text{NH}_3(\text{s}) \rightleftharpoons \text{NH}_3(\text{g})$] at the chosen reaction temperature: This equilibrium occurs at the surface of the ammonia nanoparticles, since NH_3 also forms particles, like the ice nanocrystals. The vapor pressure of $\text{NH}_3(\text{s})$ at the chosen temperature can be calculated approximately from the modified version of Clausius-Clapeyron equation given as;⁴⁶

$$\log P_{\text{NH}_3} = -(1630.700 / T) + 9.00593$$

and the vapor pressure of ND_3 can be found from

$$\log (P_{\text{NH}_3}/P_{\text{ND}_3}) = (49.69 / T) - 0.1305.$$

(2) Collision-adsorption steps: After vaporization of ammonia particles, the $\text{NH}_3(\text{g})$ molecules move through the ice network with many collision/adsorption steps prior to reaction. Most of the adsorbed ammonia escape from the surface and follow, again, collision/adsorption steps or leave to the cold walls of the cell. This was observed as the large amount of the loss of ammonia with respect to gain of the product band in the spectrum.

Actually, the collision/adsorption steps occur on the hydrate surface, which has formed on the ice surface. When the data collection was started, the hydrate formation had already begun (see Figure 49). Furthermore, during the reaction, NH_3 reacts with the ice sphere and leaves the hydrate product as an outer spherical crust.

(3) Diffusion of ammonia through the hydrate and reaction with ice most probably at the hydrate/ice interface.

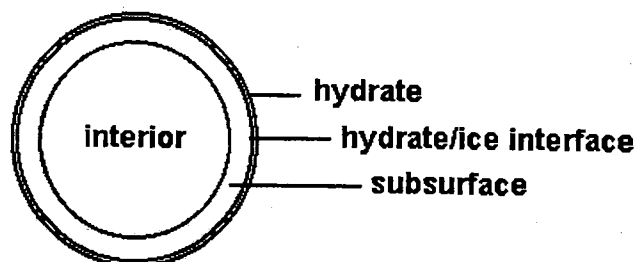


Figure 49. Starting point of the reaction.

3.2. Conversion of D_2O Ice to $2NH_3 \cdot D_2O$ at Different Reaction Temperatures

Six different reaction temperatures were used for these isotopomers of water and ammonia; namely 100, 102, 105, 107, 110 and 112 K. In the monohydrate case, it was shown that the crystalline hydrate was the dominant product only after ~20-25% conversion of the ice. In this part of the study, the initial product is also the amorphous hemihydrate, but particularly for the reaction temperatures of 100 and 102 K, the data were taken exclusively for the formation of the amorphous hemihydrate, since only ~25-30% conversion was achieved on a laboratory time scale. The amorphous nature of the product was seen from the IR data (by comparing to that of the crystalline hemihydrate). The amorphous hemihydrate data have a specific added value since, as discussed in the introduction, one of the aims of this research is to provide a basis for the computer simulation. That study is expected to more readily aid the

understanding of the formation of the first few layers of ammonia hemihydrate if the product is amorphous.

The difference spectra between the zero-time ice spectrum and partially reacted ice spectra measured at 100 K as a function of time are shown in Figure 50A in the region of 4000-800 cm^{-1} . In Figure 50B, the spectra are expanded along both axes to show the growth of the intensity of the amorphous hemihydrate spectra as a function of time.

In Figure 50A, the intense negative bands around 3375 and 1060 cm^{-1} correspond to lost of ammonia, from the $\text{NH}_3(\text{s})$ particles that were also deposited with the ice on the windows. It should be noted here again that most of the lost ammonia is not consumed during the reaction. As described before, since the IR cell used in this study has a section colder than the windows, most of the ammonia from the particle network, particularly at the network/vacuum interface, was cryopumped to the cold part. However, even though most of the ammonia molecules were lost due to the above mentioned process, there is surplus ammonia for the reaction.

Since the ammonia sample contained contaminant NH_2D , the negative band around 2450 cm^{-1} corresponds to NH_2D species, which also reacts with ice.

The plot of the fraction of reacted ice versus time, for the 100 K reaction temperature, is shown in Figure 51. The zero time is the time that the zero-time ice spectrum is taken. Since the zero-time ice spectrum ice contains some product (formed during the warming process), the y-axis corresponding to the fraction of reacted ice starts from that value (see Chapter II) instead of zero.

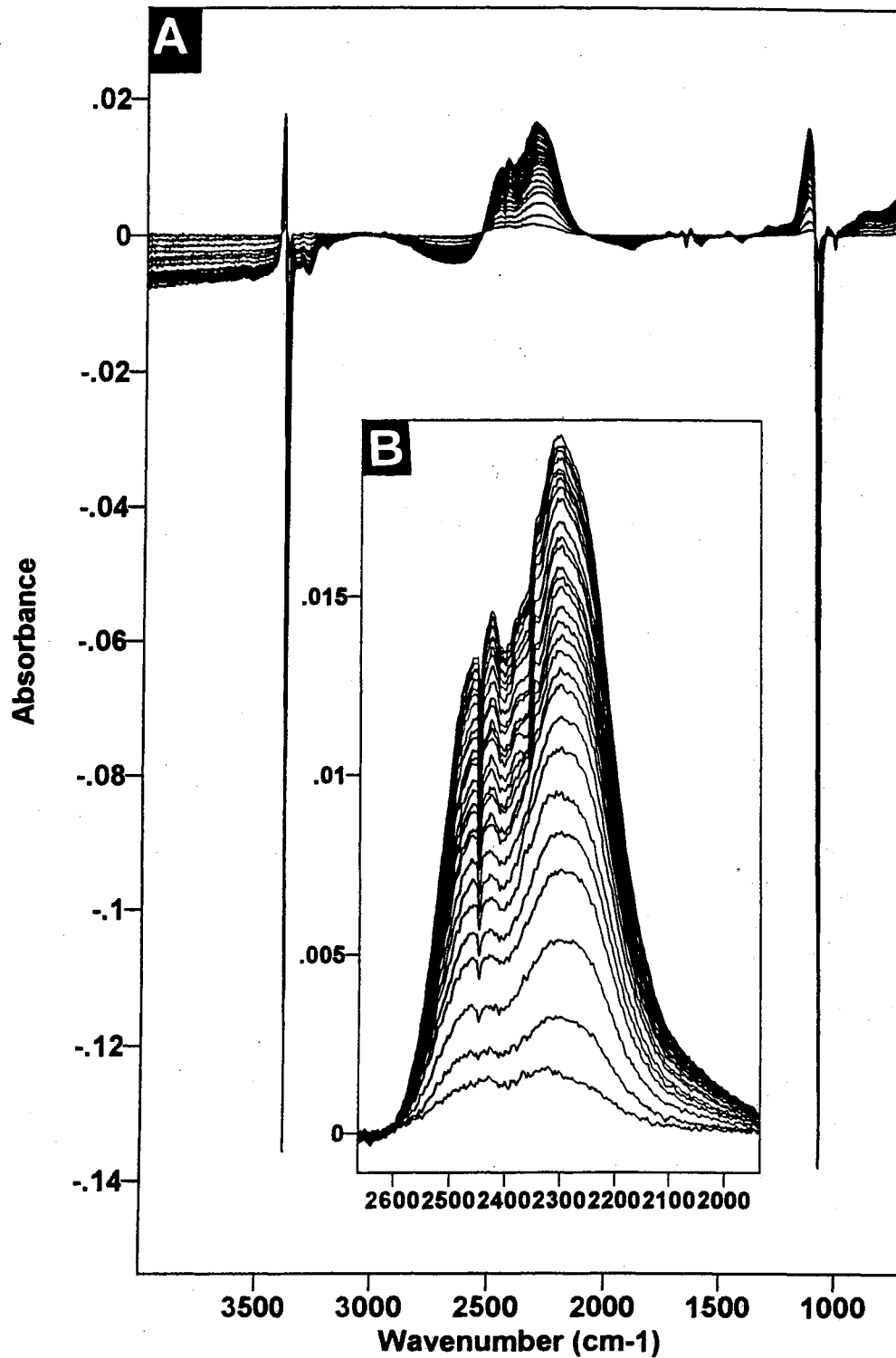


Figure 50. The product spectra, from the difference spectra between the zero-time ice and the partially reacted ice, as a function of time at 100 K; A – in the $4000 - 800 \text{ cm}^{-1}$ region; B – the spectra are expanded along both axes.

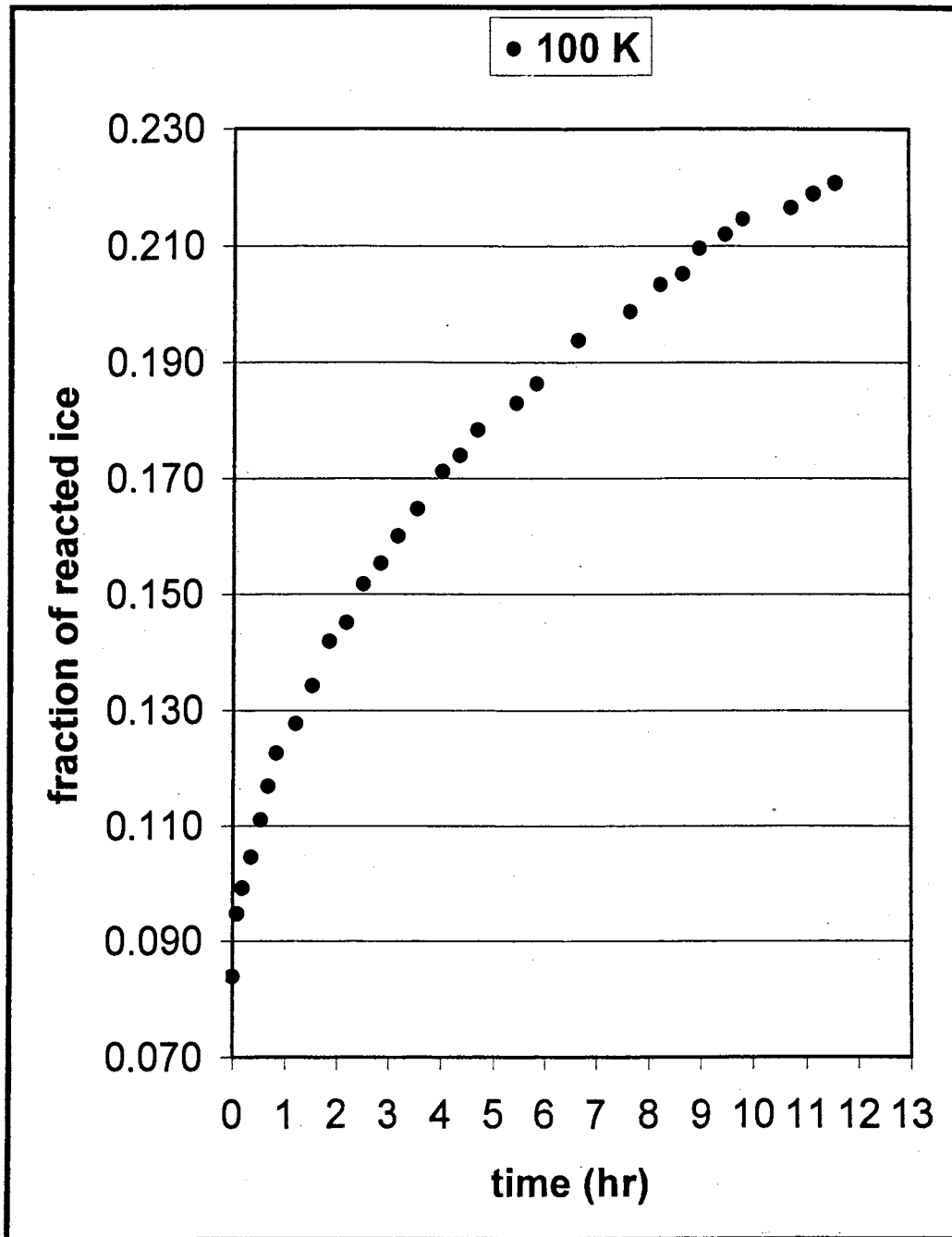


Figure 51. The plot for the conversion of D_2O ice nanocrystals to $2NH_3 \cdot D_2O$ at 100 K.

The plot for the conversion of ice to amorphous hydrate at 102 K is shown in Figure 52. As seen from the plot the initial fraction of reacted ice is a little larger than that at 100 K, due to the longer warming process to reach the higher reaction temperature. At 102 K, the product is again the amorphous hemihydrate and spectra of the product as a function of time are shown in Figure 53.

For the reaction temperatures 105, 107 and 110 K, initially the product was the amorphous hemihydrate of ammonia, but after ~25-30 % conversion, depending on the reaction temperature, crystalline hemihydrate becomes the dominant product. At 112 K, the product during the data collection was only the crystalline hemihydrate. Again, the evidence for the crystalline nature of the product can be observed within the IR spectra.

The difference spectra are shown in Figure 54 for the reaction temperature at 105 K and the plot of the fraction of reacted ice versus time at 105 K is given in Figure 55. As seen from the difference spectra, after 35% conversion crystallinity starts to appear, although the product has mostly an amorphous nature. However, at 107 K the crystalline character of the hydrate shown in Figure 56 as the difference spectra is much more apparent. The transformation from the amorphous to crystalline hydrate is found to correspond to the change in slope of the curve plotted in Figure 57. The same trend is observed for the reaction at 110 K and the plot of fraction of reacted ice versus time is shown in Figure 58. As seen from the difference spectra given in Figure 59, the product spectrum is that of the crystalline hemihydrate after an induction period elapsed.

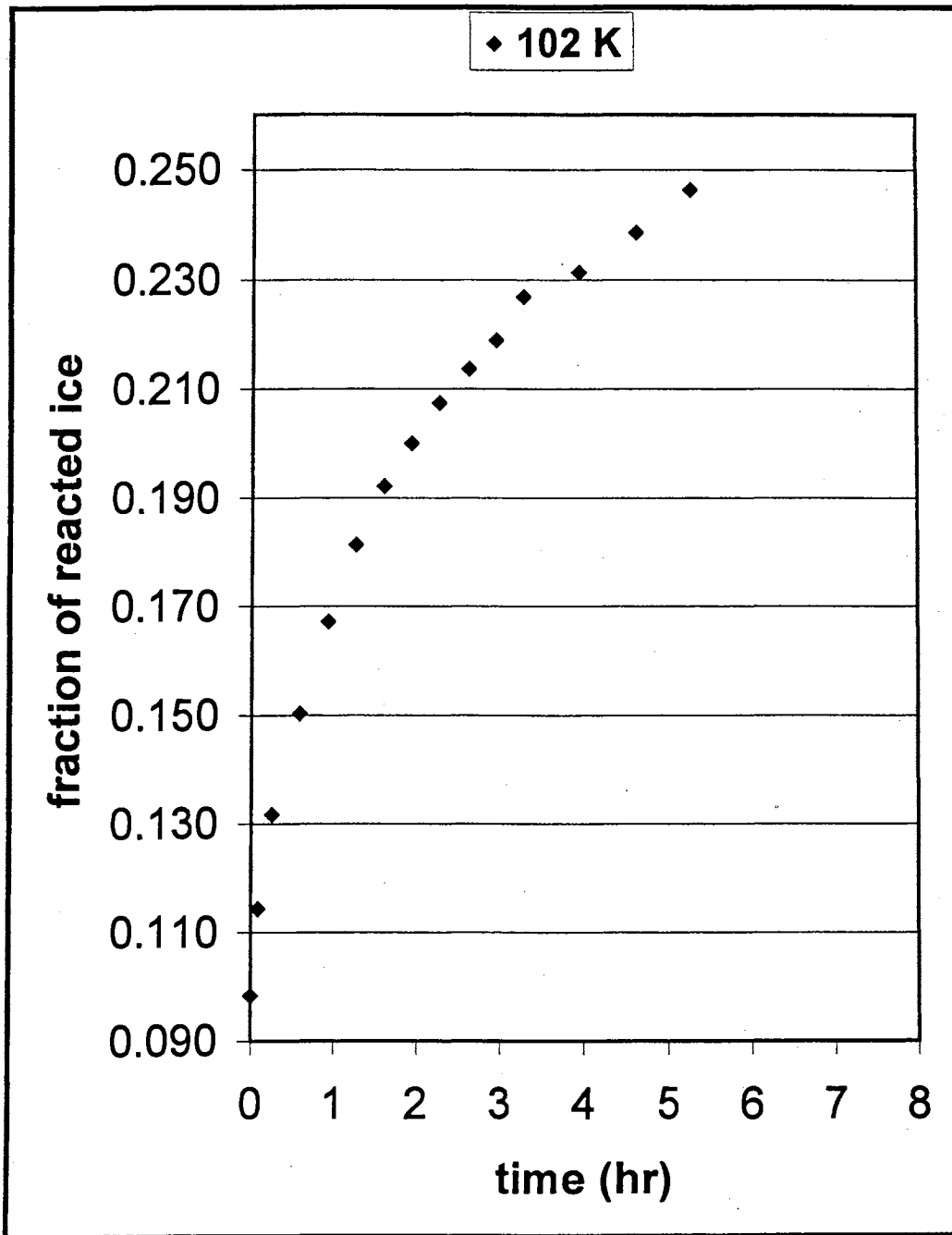


Figure 52. The plot for the conversion of D_2O ice nanocrystals to $2NH_3 \cdot D_2O$ at 102 K.

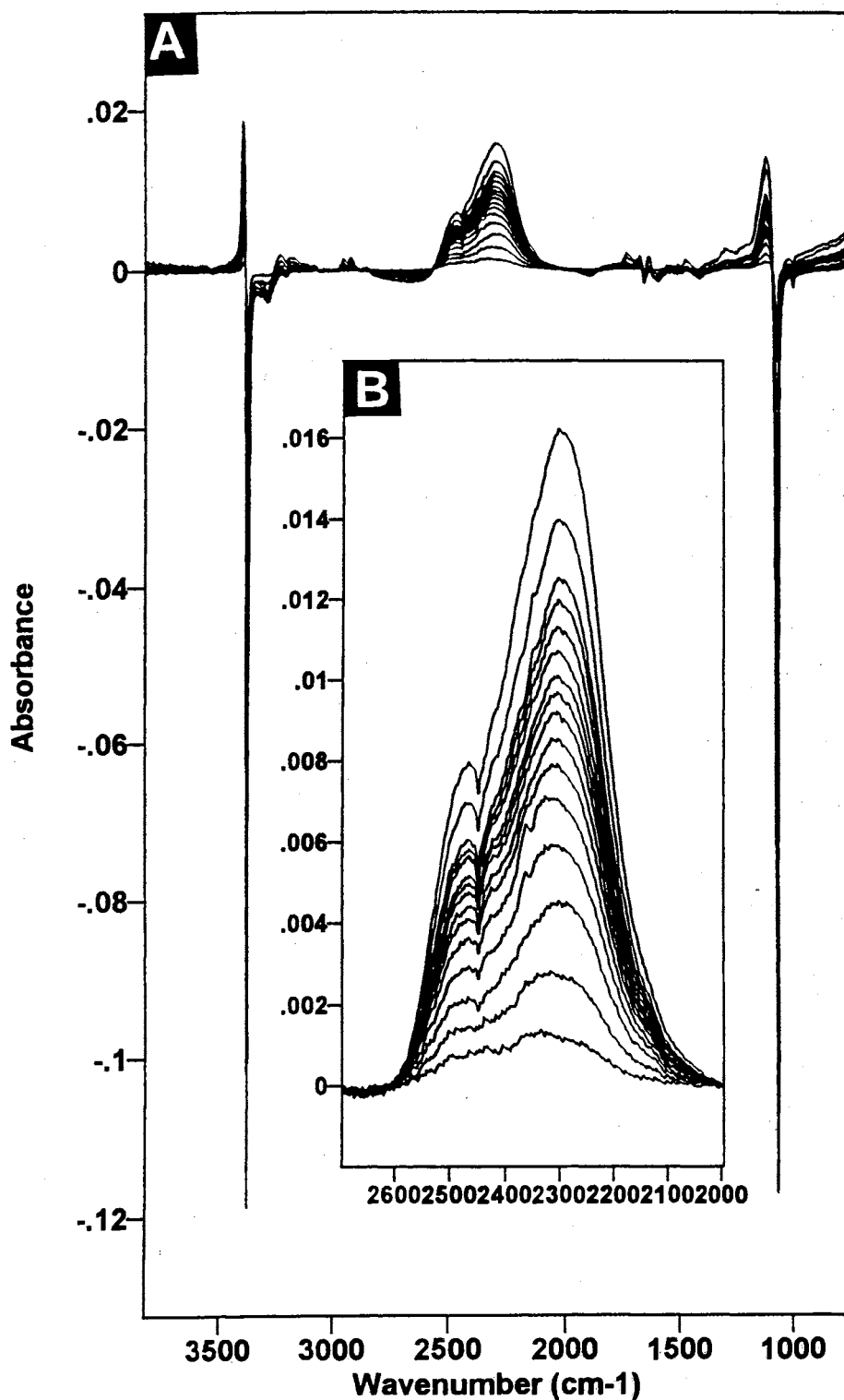


Figure 53. The product spectra, from the difference spectra between the zero-time ice and the partially reacted ice, as a function of time at 102 K; A – in the 4000 – 800 cm⁻¹ region; B – the spectra are expanded along both axes.

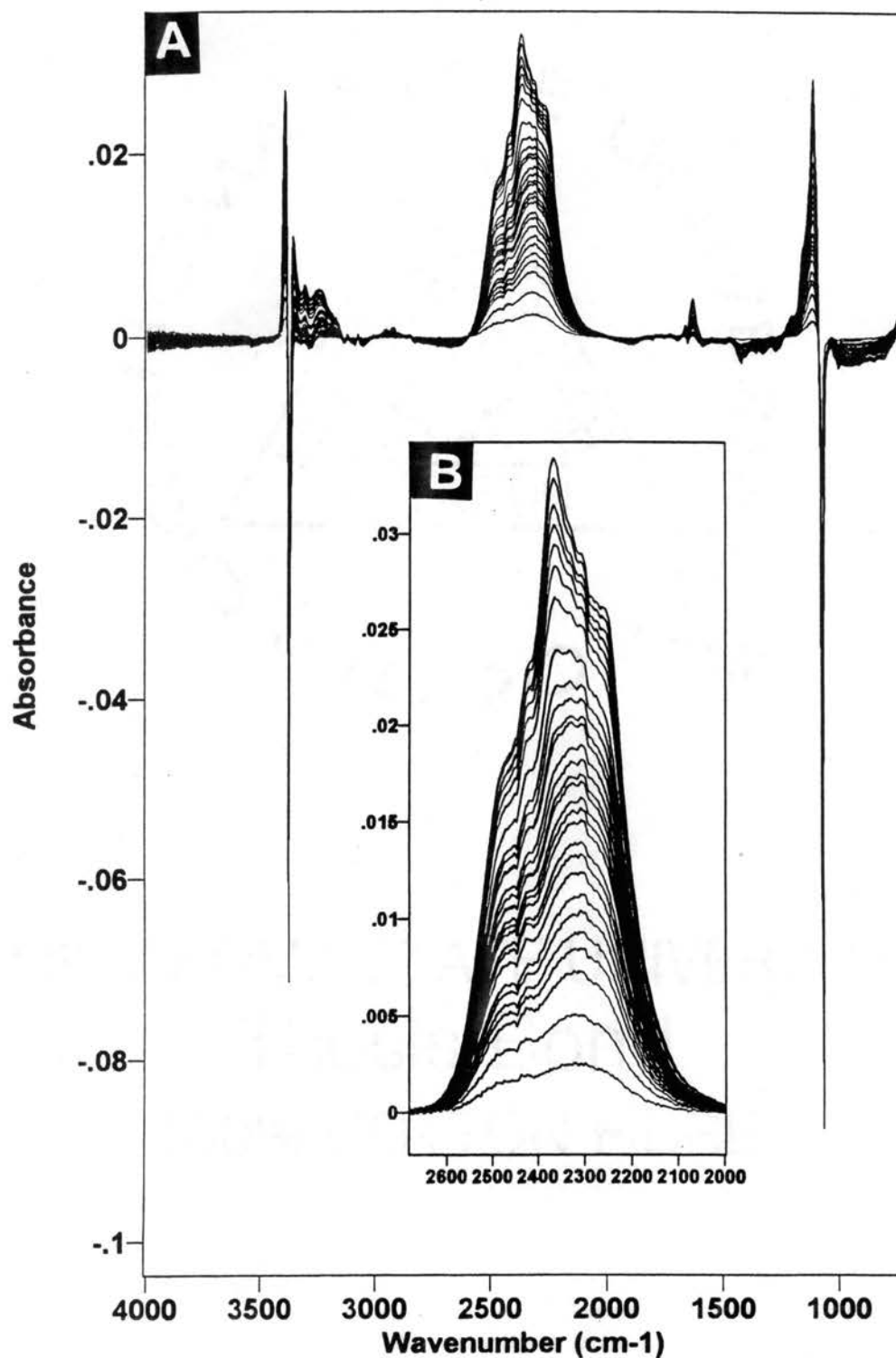


Figure 54. The product spectra, from the difference spectra between the zero-time ice and the partially reacted ice, as a function of time at 105 K; A – in the 4000 – 800 cm^{-1} region; B – the spectra are expanded along both axes.

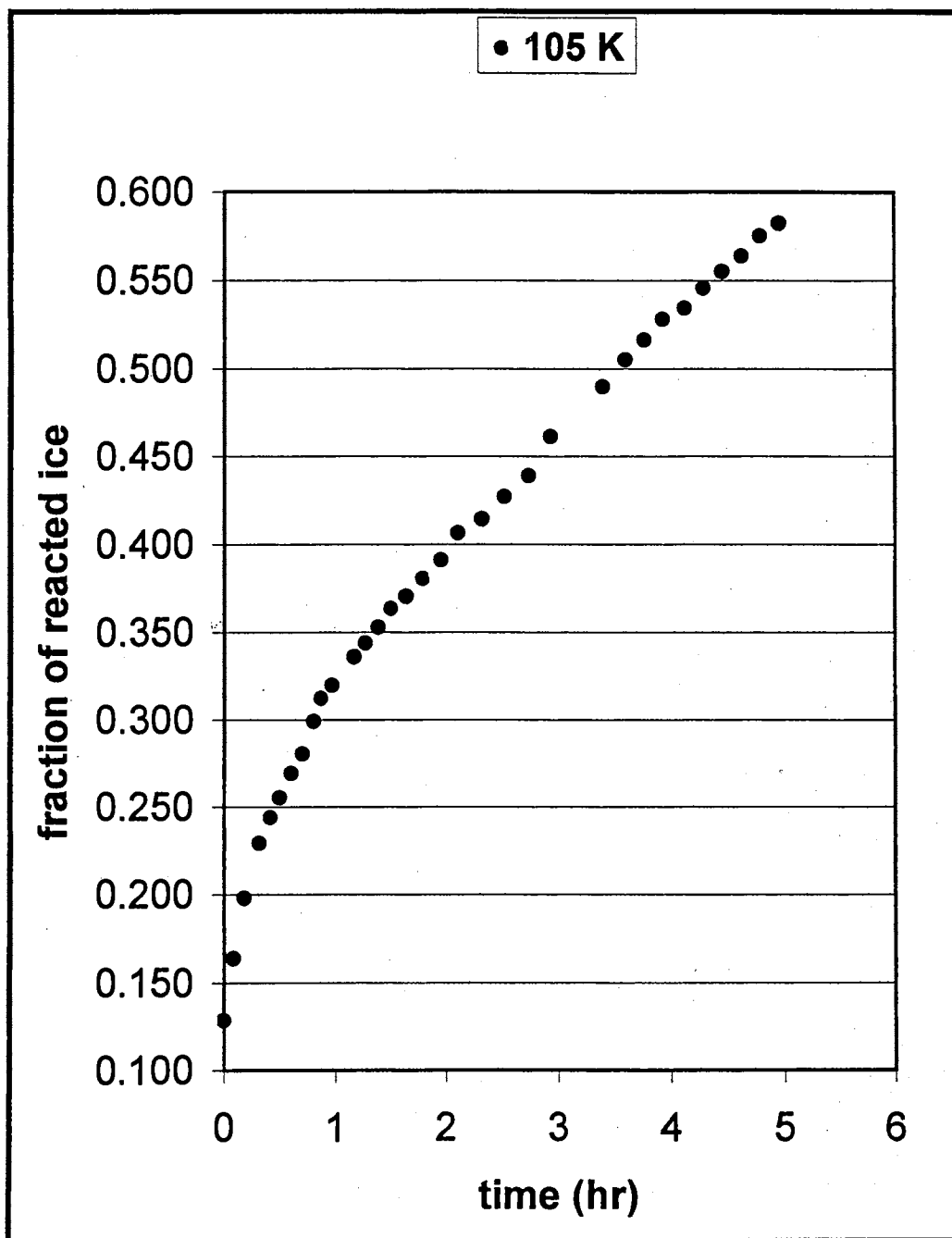


Figure 55. The plot for the conversion of D_2O ice nanocrystals to $2NH_3 \cdot D_2O$ at 105 K.

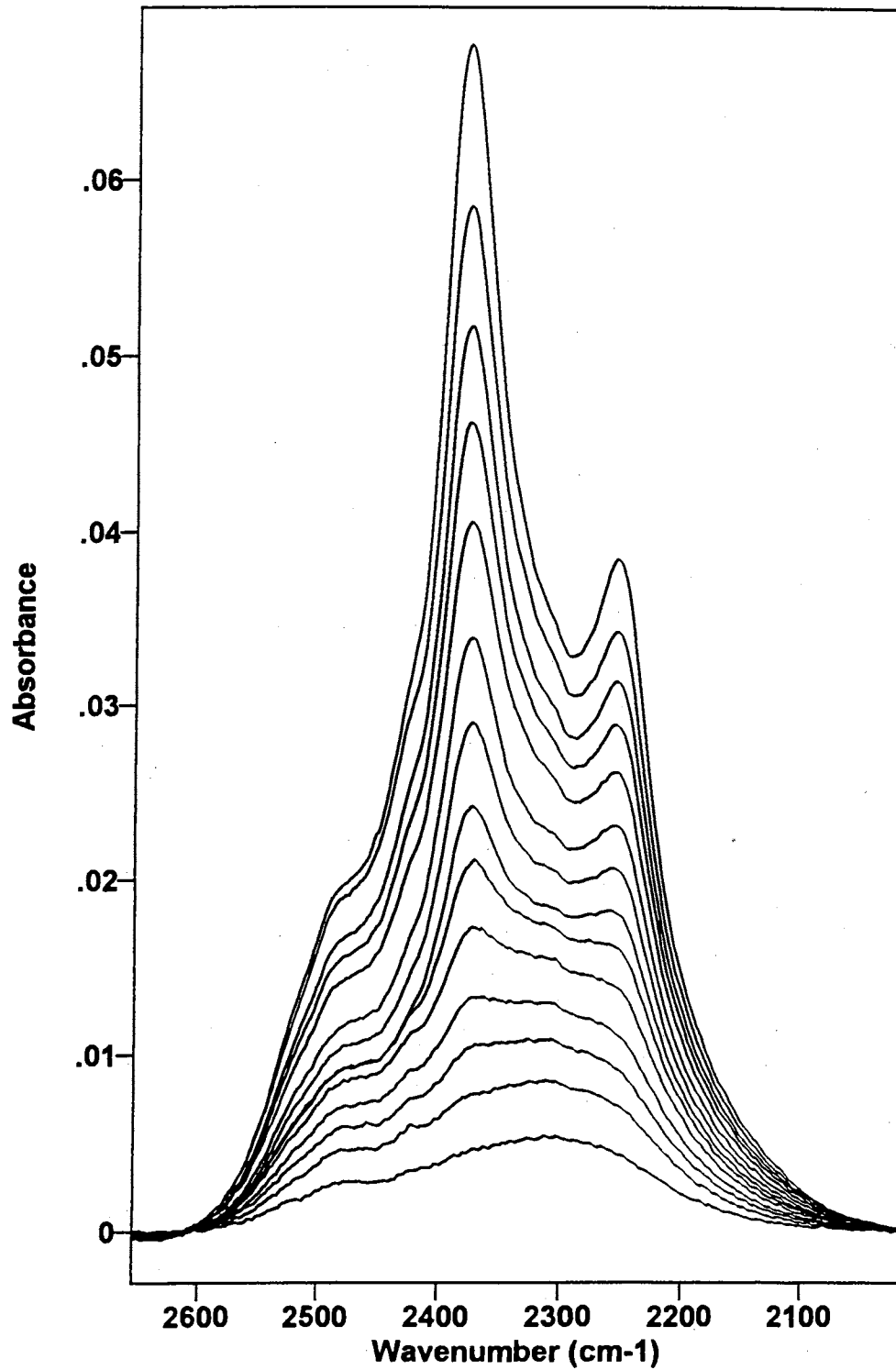


Figure 56. The product spectra, from the difference spectra between the zero-time ice and the partially reacted ice, as a function of time at 107 K

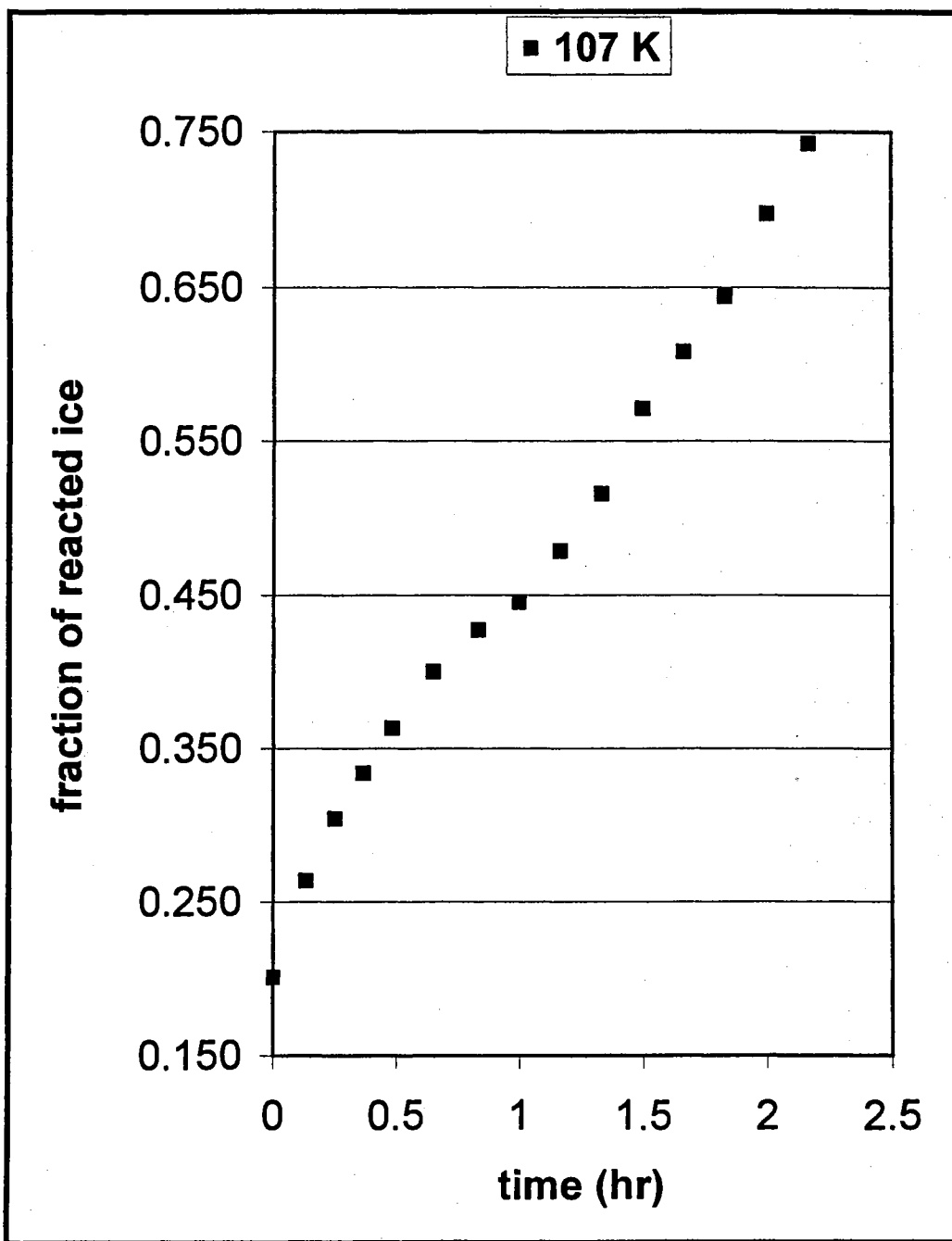


Figure 57. The plot for the conversion of D_2O ice nanocrystals to $2NH_3 \cdot D_2O$ at 107 K.

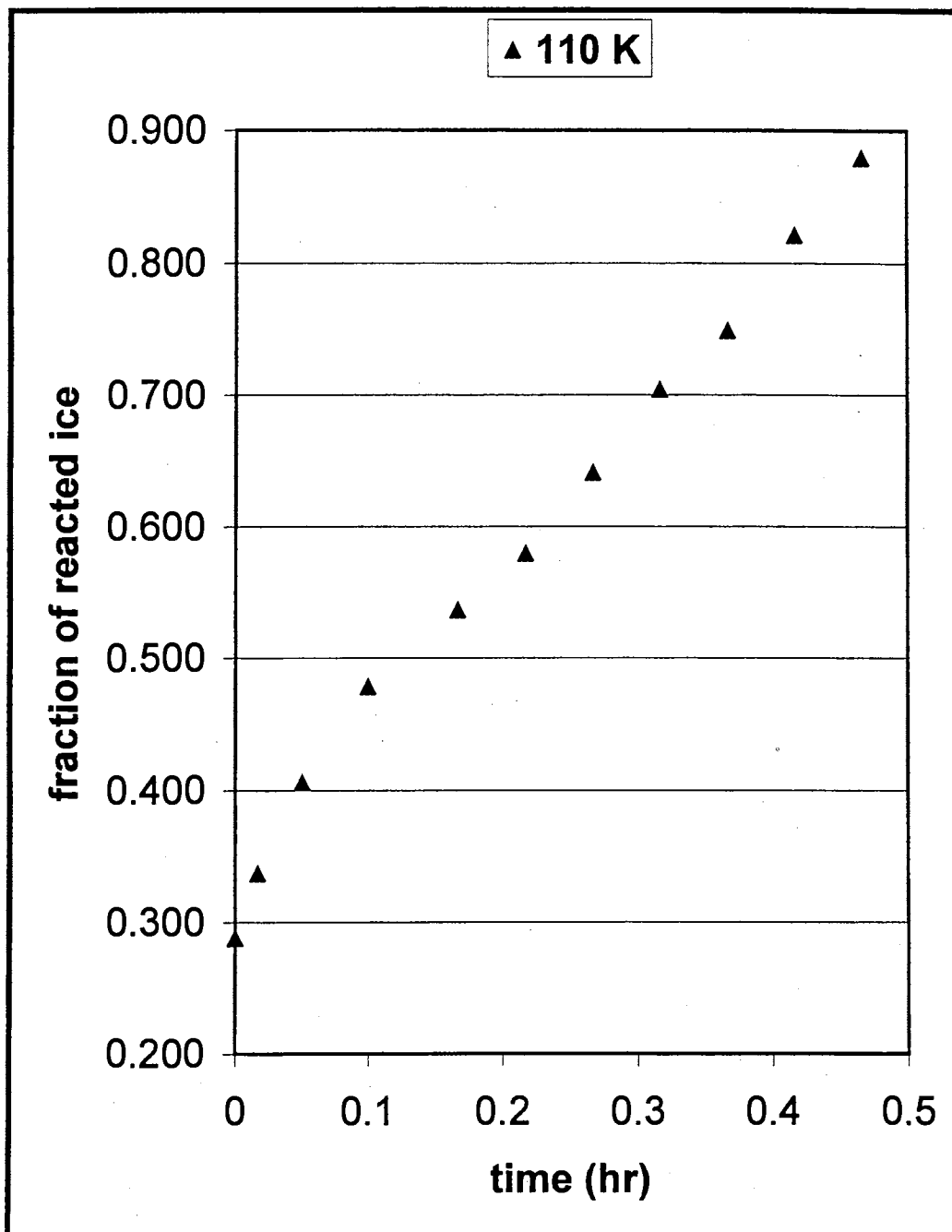


Figure 58. The plot for the conversion of D_2O ice nanocrystals to $2NH_3 \cdot D_2O$ at 110 K.

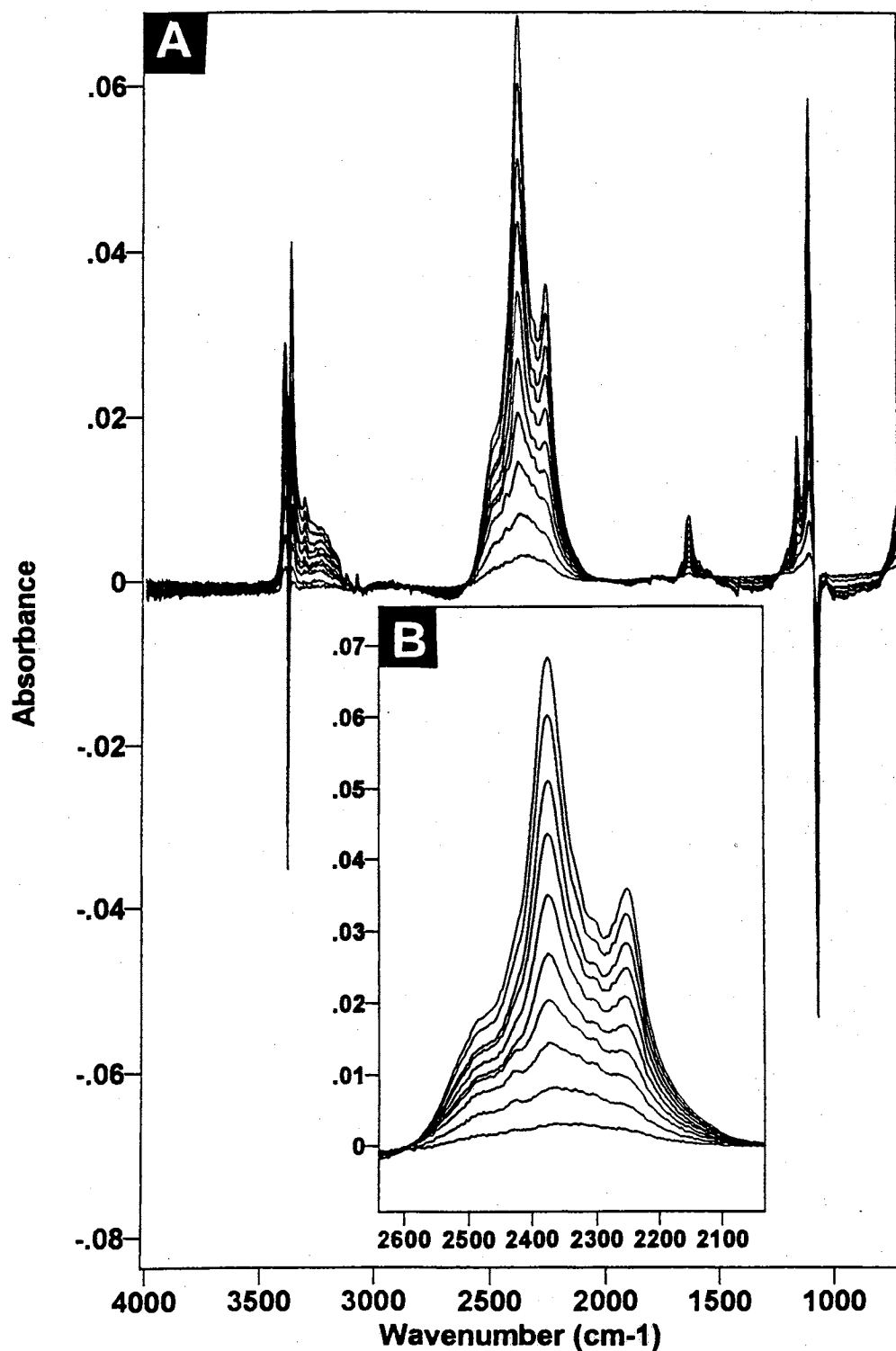


Figure 59. The product spectra, from the difference spectra between the zero-time ice and the partially reacted ice, as a function of time at 110 K; A – in the 4000 – 800 cm^{-1} region; B – the spectra are expanded along both axes.

At 112 K, the data were collected for the conversion of D₂O ice nanocrystals to the crystalline 2NH₃.D₂O and the spectra are shown in Figure 60 as a function of time. The crystalline nature of the hydrate can be seen from this figure by comparing with the published hemihydrate spectra (Devlin et al) shown in the first chapter. The plot at 112 K is shown in Figure 61.

As discussed before, the reaction between the ice and NH₃ is achieved from the diffusion of NH₃ molecules through the hydrate. Therefore, the change of the slope due to the crystalline hydrate formation is not surprising, if one presumes the reaction rate is controlled by the solid state diffusion and considers the differences between the diffusion through the amorphous and crystalline hydrates.

The similar changes of slope were obtained in the work of Jorgensen *et. al.*⁴⁸ due to the switch from the amorphous to a crystalline structure. In their work, the rate of oxidation of silicon carbide (SiC) was measured by using a thermogravimetric apparatus and was found to be diffusion controlled. At low temperatures, the reaction product, SiO₂, was the amorphous silica and the existence of the amorphous nature was studied by x-ray diffraction methods. At high temperatures, the amorphous silica was transformed to the crystalline phase and they observed that the transformation from the amorphous to crystalline product was associated with a change of the slope of the curves plotted of fraction reacted versus time.

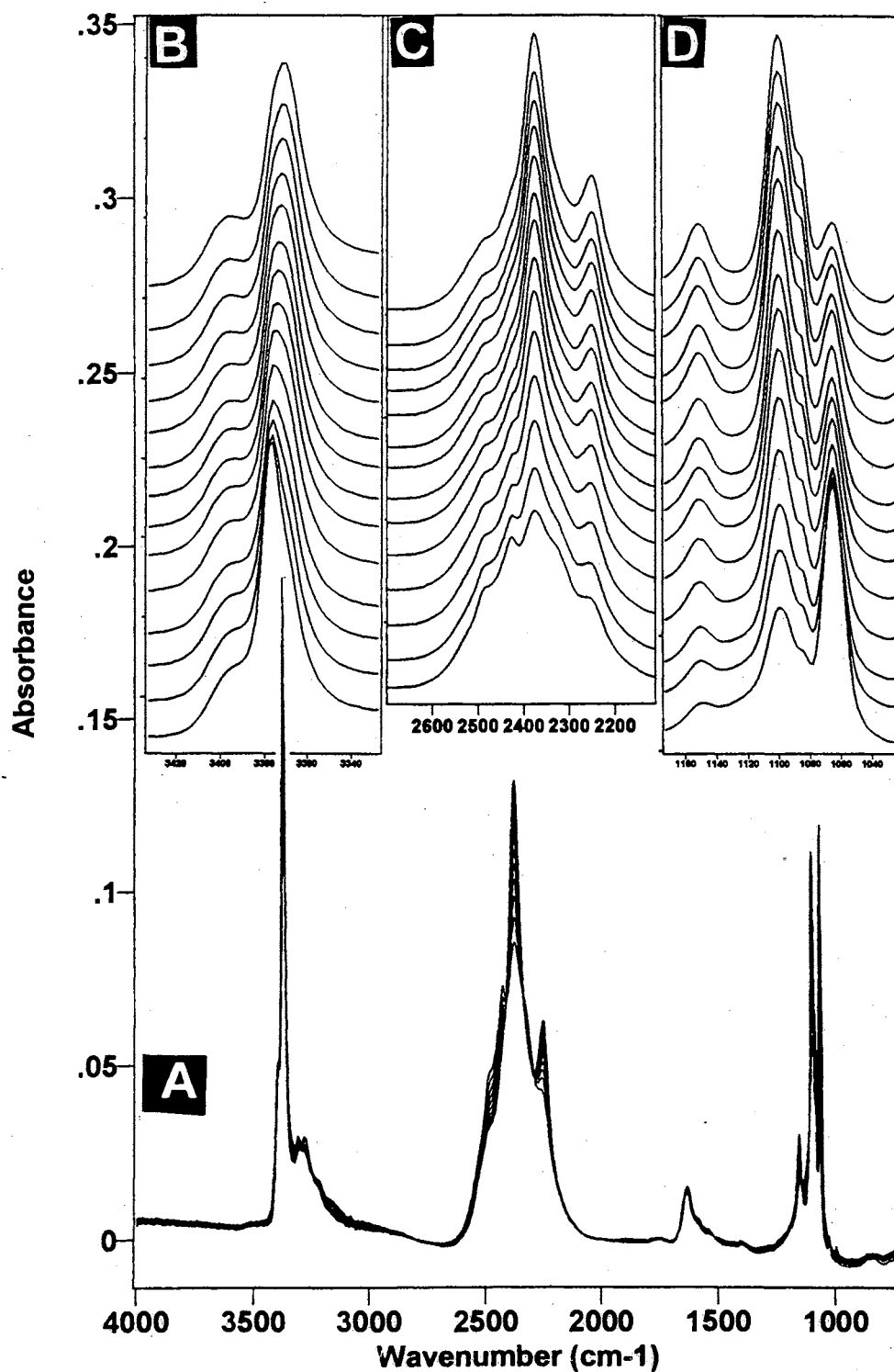


Figure 60. The sample spectra, after partial reaction, as a function of time at 112 K; A – in the 4000 – 800 cm^{-1} region; B, C, and D – the spectra are expanded along both axes.

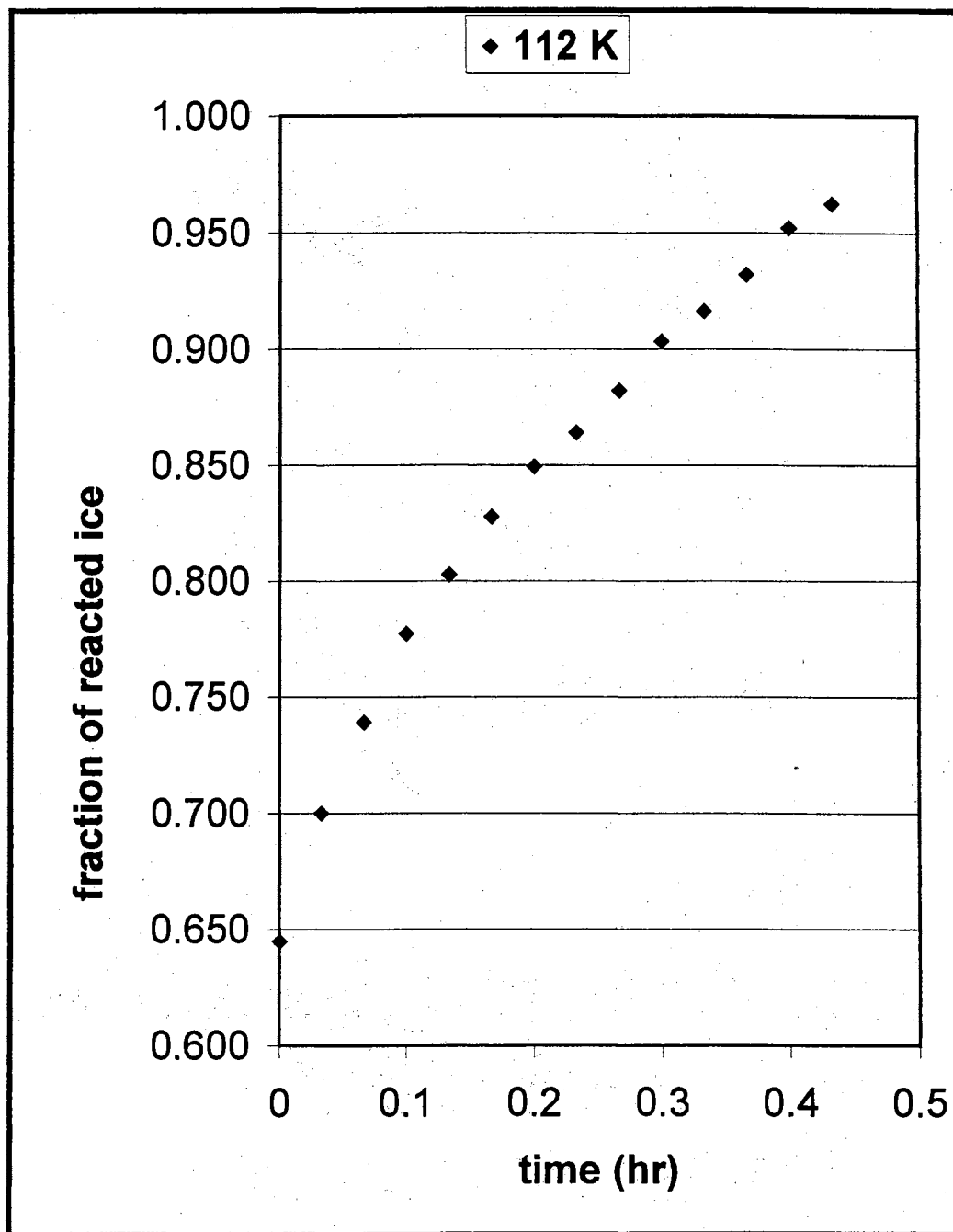


Figure 61. The plot for the conversion of D_2O ice nanocrystals to $2NH_3 \cdot D_2O$ at 112 K.

4. Relation of the Subsurface Spectrum to the Initial Fraction of Reacted Ice

As discussed earlier, the surface, subsurface and interior of the ice nanocrystals have different distinct spectra. The band intensities of these spectra depend on the numbers of water molecules of the surface, subsurface and interior; which are related to the surface-to-volume ratio. The average diameter of the ice nanocrystals, prepared under conditions that have been described in the experimental part, was estimated as 25 nm.⁴⁷

Furthermore, it was shown that ~10 % of the water molecules are on the surface; that is, the conversion of the surface to interior ice by Ostwald ripening increases the interior ice intensity by ~10 %. This corresponds to one bilayer intensity.⁴⁷

The subsurface is the transition region that connects the highly disordered surface to the crystalline core and it is not as disordered as the surface. As discussed in the first chapter, some of the adsorbates cause a subsurface relaxation to interior ice structure and, also, when the particles are annealed, some subsurface of the enlarged particles relaxes to the interior. That means that the existence of the subsurface, spectroscopically, can be observed from two independent processes and the spectrum of the subsurface obtained from these processes are very similar.^{19, 21}

It is believed from the spectroscopic evidence that the subsurface contains two bilayers of water molecules that corresponds to ~20% of the ice intensity for the 25 nm particles. Consequently, ~30% ice band intensity comes from the three bilayers of surface and subsurface. If one looks at the first fraction of

reacted ice (see Table 6 of the Appendix), these values approximately correspond to the surface plus subsurface amounts. However, the fraction of reacted ice versus the zero-time ice was evaluated by using the main ice band (at 2424 cm^{-1}) which has sharper and stronger band components than the subsurface. For this reason, the fraction of reacted ice should be greater than what was determined as lost interior ice. Therefore, another method of data analysis was tried that will be discussed in the following section.

5. Evaluation of the kinetic results by using the product band intensities

The explanation of this method is that the intensity of the growing product band was measured versus the original sample spectrum at each reaction time. Then, the fraction of reacted ice producing this product band intensity was calculated by using the difference spectra, in the manner explained in the experimental chapter. The spectra of ice and hydrate samples are shown as a function of time in Figure 62A for the conversion of D_2O ice to the hemihydrate of ammonia at 102 K. The intensities (absorbance at 2240 cm^{-1}) of the product (shown by * in Figure 62B) as a function of time is given in Table 5. To calculate how much ice corresponds to these product intensities, one of the partially reacted ice spectra, for which the product intensity is known, is chosen (in this calculation, it is 0.02958 at 2260 cm^{-1}). The difference spectrum between this partially reacted ice and bare ice is found using the criteria presented in the experimental section. The fraction of reacted ice is ~ 0.29 for this subtraction. The other fractions of reacted ice for each spectrum can be calculated from the

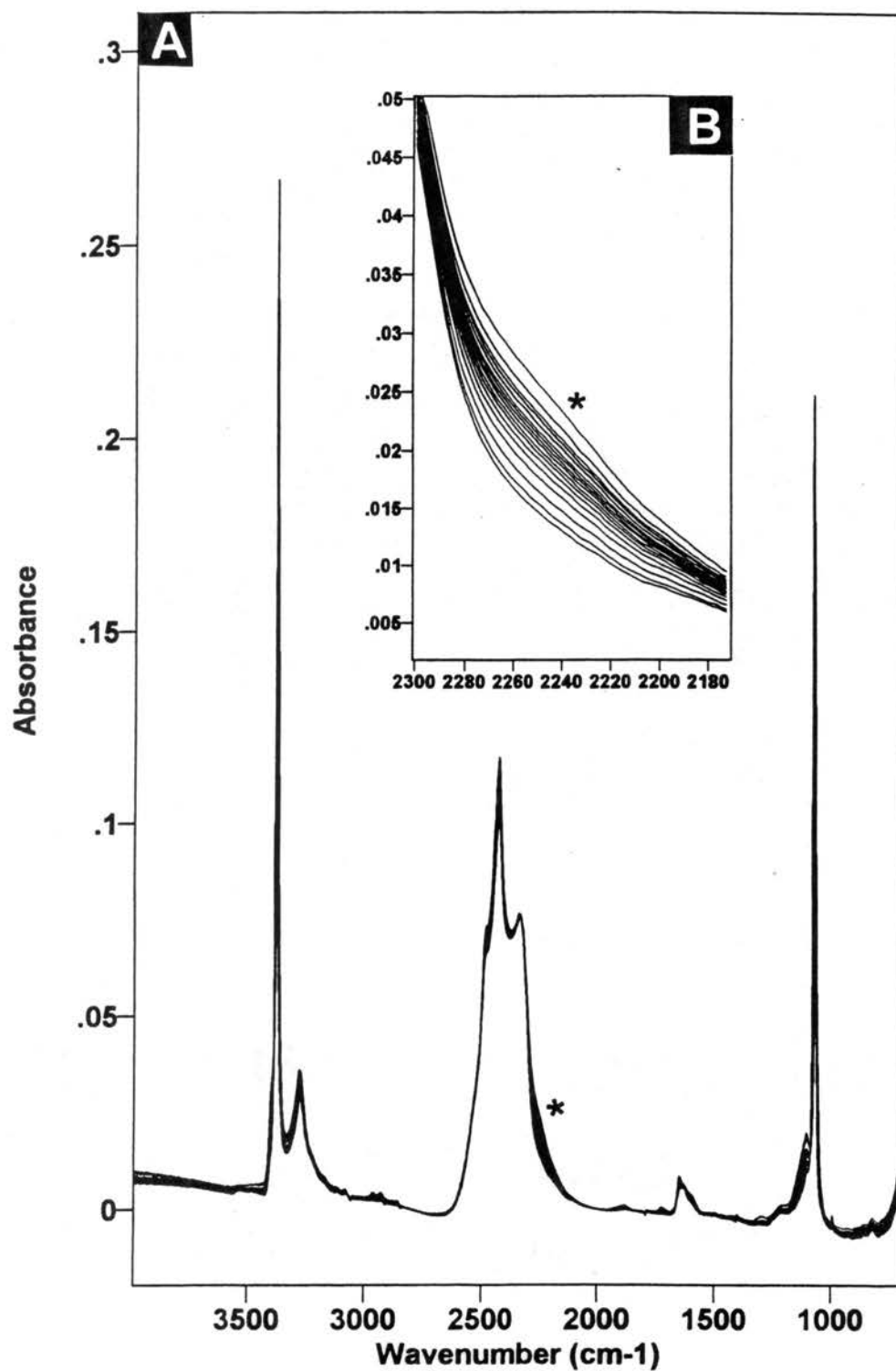


Figure 62. The sample spectra, after partial reaction, as a function of time at 102 K; A – in the 4000 – 800 cm⁻¹ region; B – the spectra are expanded along both axes.

Table 5.

 $2\text{NH}_3 \cdot \text{D}_2\text{O}$ at 102 K from the second method.

time	intensity	A	B	C	$(A+B+C)/3$
0	0.017	0.176	0.175	0.168	0.173
0.083	0.018	0.182	0.180	0.174	0.179
0.25	0.019	0.193	0.192	0.185	0.190
0.583	0.021	0.209	0.207	0.200	0.205
0.933	0.021	0.215	0.213	0.206	0.211
1.266	0.022	0.222	0.220	0.213	0.218
1.6	0.023	0.230	0.229	0.221	0.226
1.933	0.023	0.234	0.232	0.224	0.230
2.266	0.024	0.238	0.237	0.228	0.234
2.616	0.024	0.240	0.238	0.230	0.236
2.95	0.025	0.246	0.244	0.236	0.242
3.283	0.025	0.247	0.245	0.237	0.243
3.95	0.026	0.254	0.253	0.244	0.250
4.616	0.026	0.259	0.257	0.248	0.255
5.283	0.026	0.264	0.262	0.253	0.260
7	0.027	0.274	0.272	0.263	0.269

following equation;

$$\text{Fraction of reacted ice} = (\text{intensity of product} / 0.02958) * 0.29$$

The results are shown in the third column of Table 5. The same calculations were made by using two additional samples and the results are shown in the fourth and fifth column of Table 5. The sixth column is the average of the third, fourth and fifth columns (hereafter, all the results for the other temperatures are given in the appendix. It contains only the time and the average values of the fraction of reacted ice calculated in the manner discussed here). The spectrum that is chosen for the calculation of fraction of reacted ice is generally picked from the later reaction spectrum so that the subsurface spectrum does not create a major problem.

The plot obtained from this method for the conversion of D_2O to $2\text{NH}_3 \cdot \text{D}_2\text{O}$ at 102 K is shown in Figure 63. As seen from the figure, the initial fraction of reacted ice is changed with respect to the first method (hereafter, the method explained in the experimental part will be called the first method and the method using the product band intensities will be called the second method).

Nevertheless, if we accept the procedure of the second method, we cannot evaluate the kinetic data taken at 100 K. After 14 hours reaction time, the fraction of reacted ice is still only ~30% so only surface + subsurface ice has reacted. In the cases of 105 and 107 K reaction temperatures, only the part of the reaction that produces amorphous product may be used for the kinetic data of the second method since the crystallinity changes the hydrate IR bands. For the reaction temperatures at 107, 110 and 112 K, second method the data can

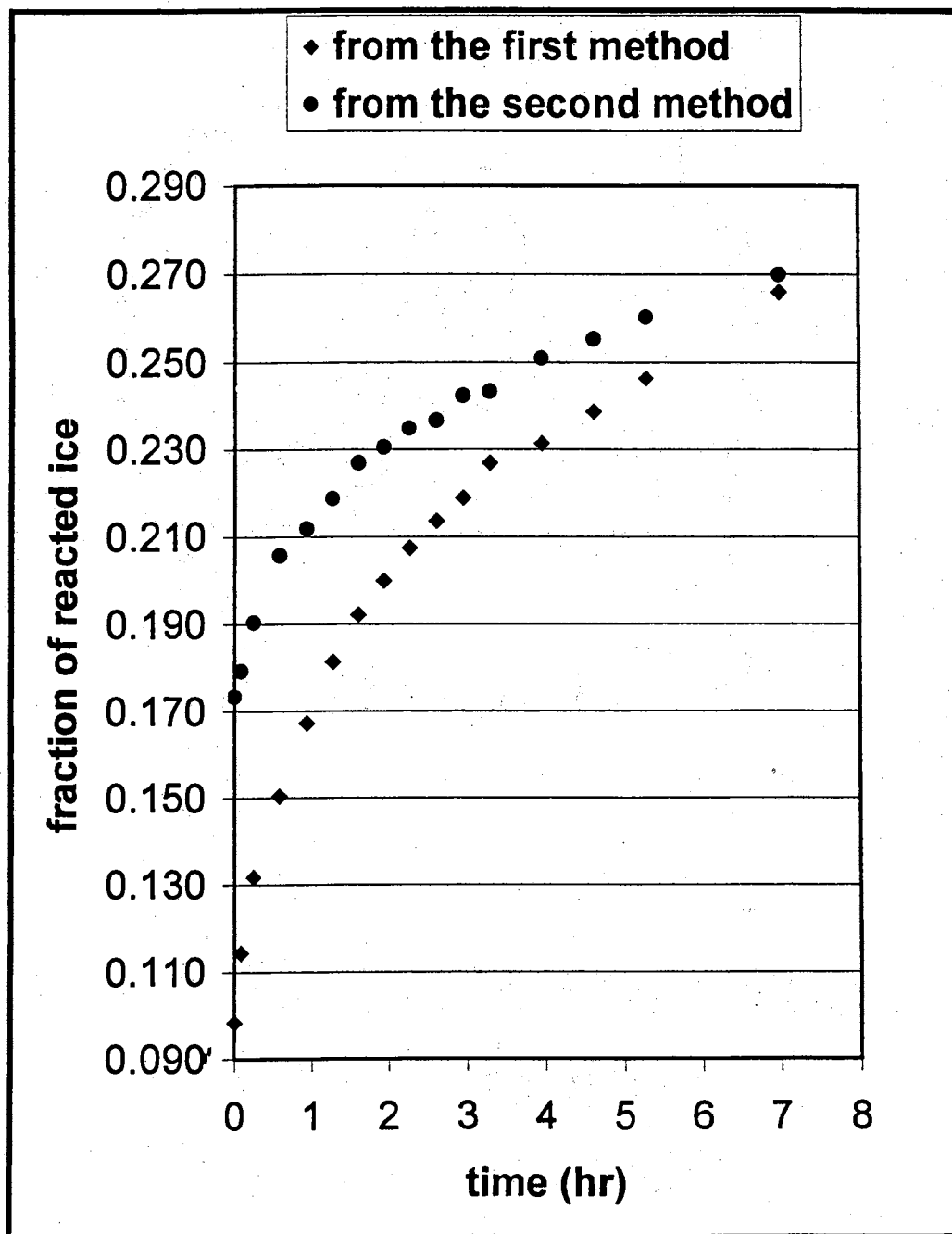


Figure 63. The plot obtained from two methods (see text) for the conversion of D_2O ice nanocrystals to $2NH_3 \cdot D_2O$ at 102 K.

be analyzed for the conversion of D_2O ice nanocrystals to the crystal $2NH_3 \cdot D_2O$. Therefore, we can divide the experimental results into two sections, namely, conversion of ice nanocrystals to the amorphous and to the crystalline hemihydrate.

We have already discussed the amorphous hydrate formation at 102 K. At 105 and 107 K, that formation was also taken into account and the spectra of partially reacted ice as a function of time are given in Figure 64 for 105 K and in Figure 65 for 107 K. The plot of fraction of reacted ice versus time for the reaction temperatures at 105 and 107 K is shown in Figure 66.

For the formation of the crystalline hydrates, the partially reacted ice spectra containing crystalline hydrate product are used. These can be found from the difference spectra between the partially reacted ice and bare ice (or, the zero-time ice, shown in previous evaluations). The partially reacted ice spectra as a function of time are given in Figure 67 at 110 K (at 112 K, see Figure 60) and the resulting plots for 107, 110 and 112 K are shown in Figure 68.

6. Isotopic effects on Reaction Kinetics

6.1 D_2O versus H_2O

To help understand the nature of this ice-to-hydrate conversion and to find the deuterium isotope effect on reaction kinetics, D_2O ice was exchanged with H_2O ice. For this purpose, three reaction temperatures were studied; namely 100, 102 and 105 K, for the conversion of H_2O ice nanocrystals to $2NH_3 \cdot H_2O$. The hydrate formed at these temperatures was the amorphous hydrate and, again,

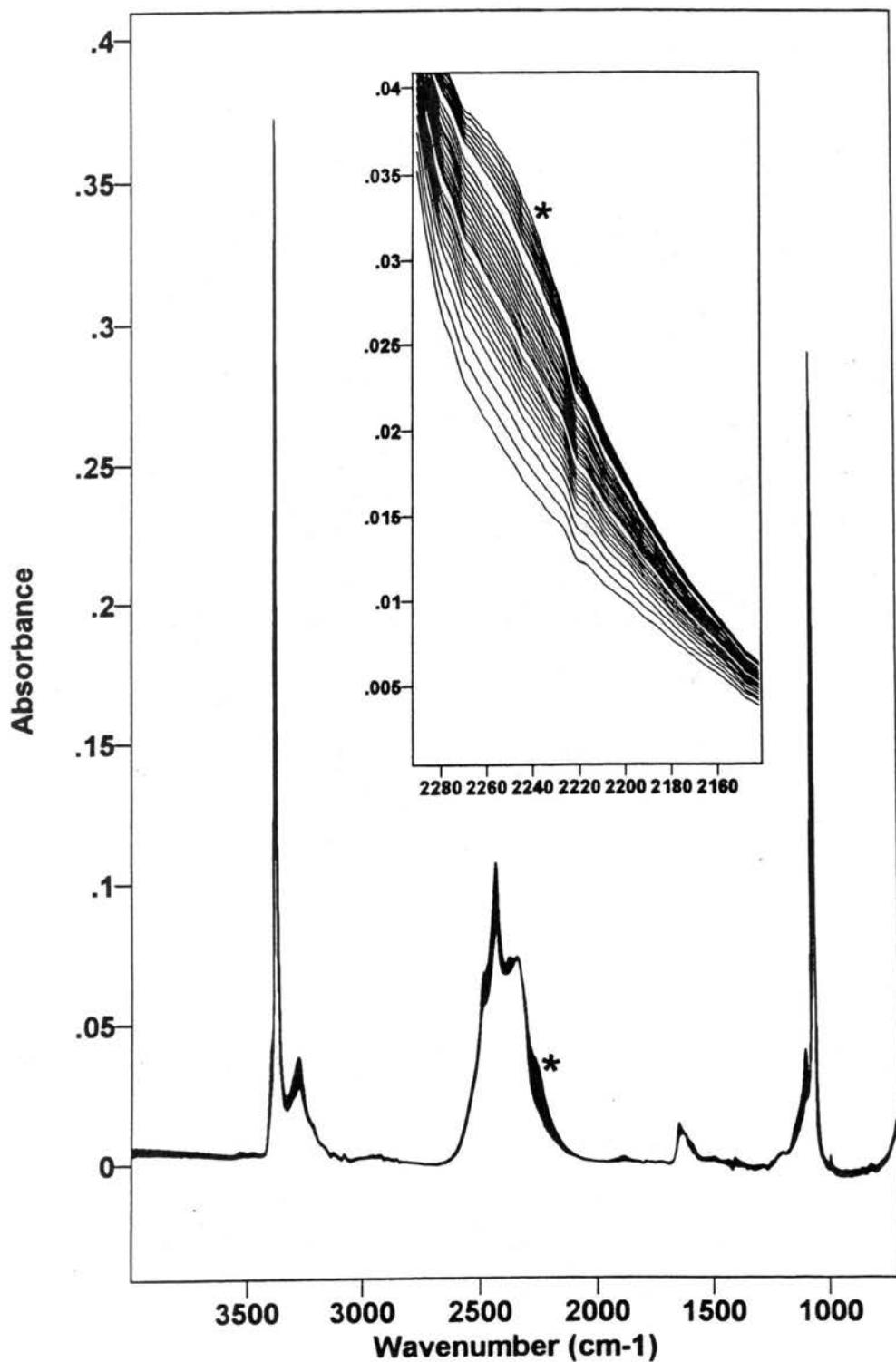


Figure 64. The sample spectra, after partial reaction, as a function of time at 105 K; A – in the 4000 – 800 cm⁻¹ region; B – the spectra are expanded along both axes.

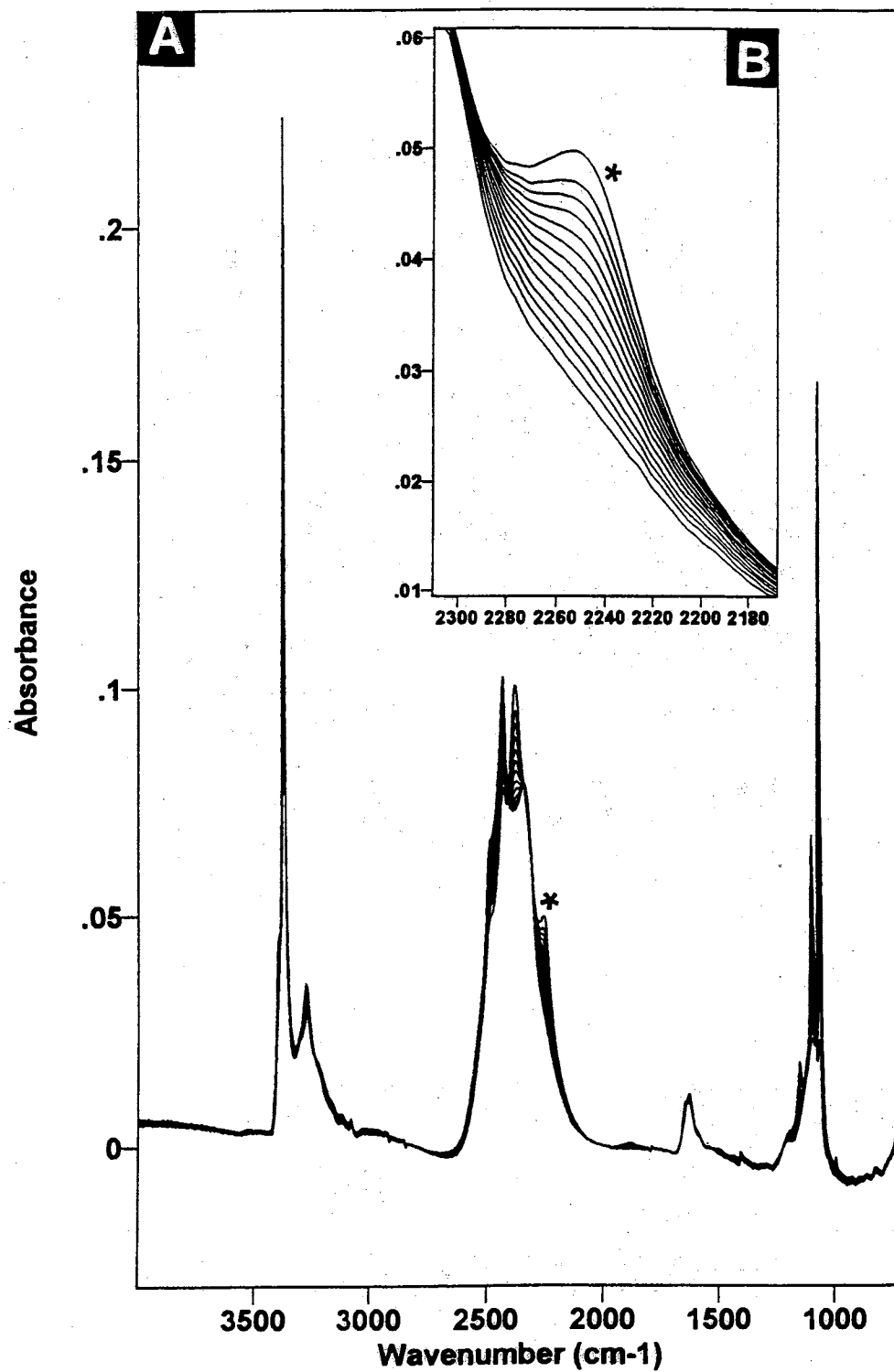


Figure 65. The sample spectra, after partial reaction, as a function of time at 107 K; A – in the 4000 – 800 cm^{-1} region; B – the spectra are expanded along both axes.

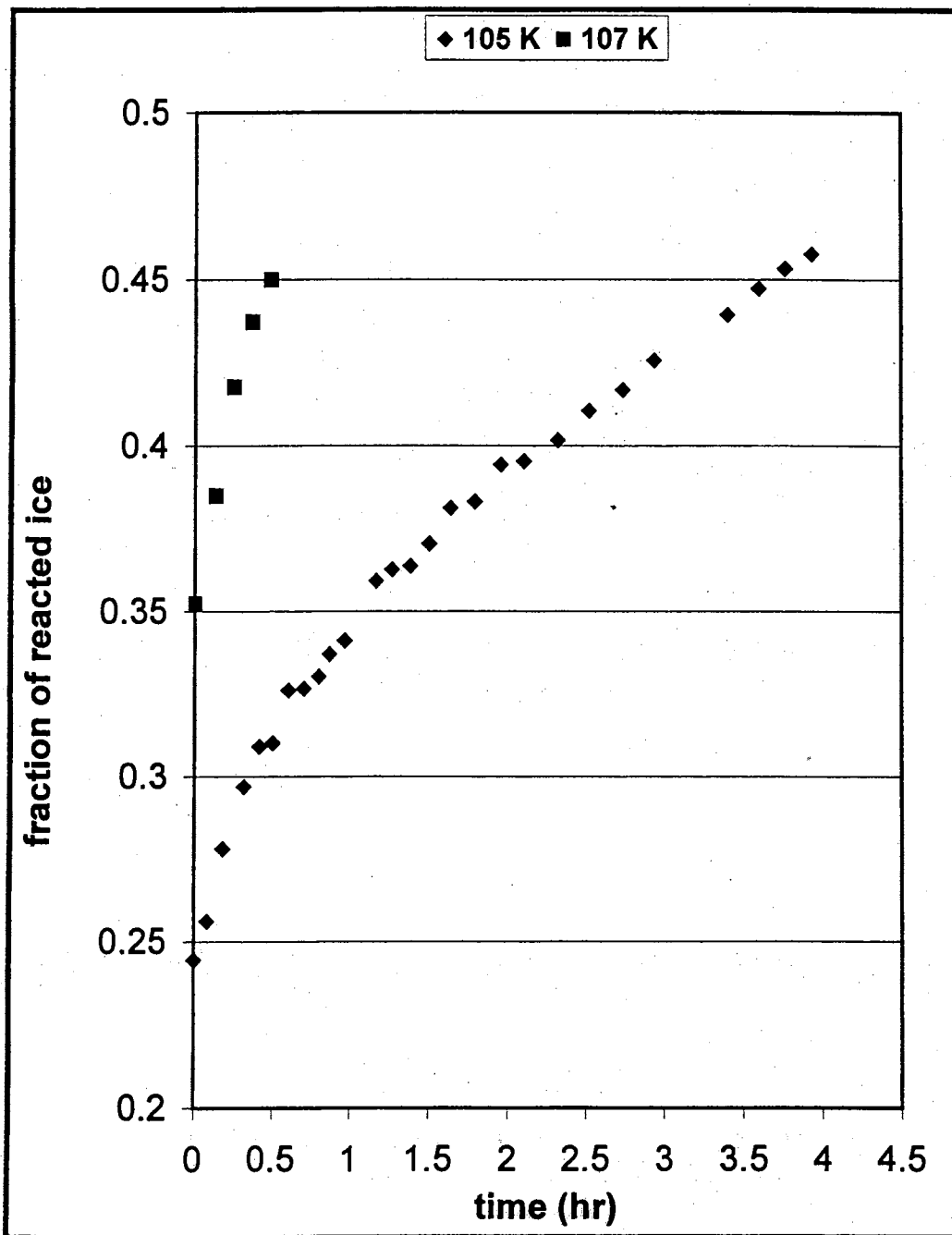


Figure 66. The plot for the conversion of D_2O ice nanocrystals to amorphous $2NH_3 \cdot D_2O$ at 105 and 107 K.

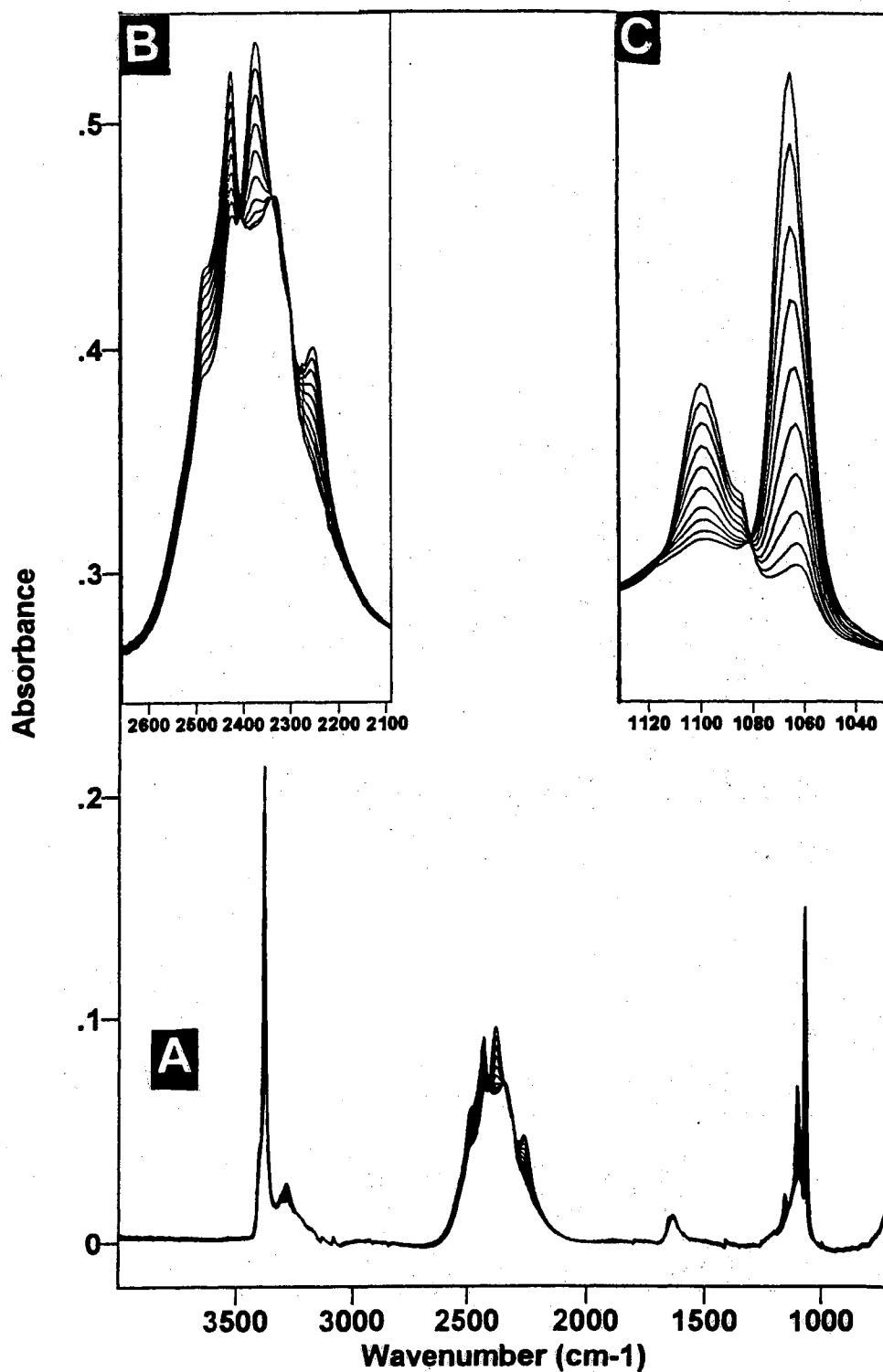


Figure 67. The sample spectra, after partial reaction, as a function of time at 110 K; A – in the 4000 – 800 cm^{-1} region; B and C – the spectra are expanded along both axes.

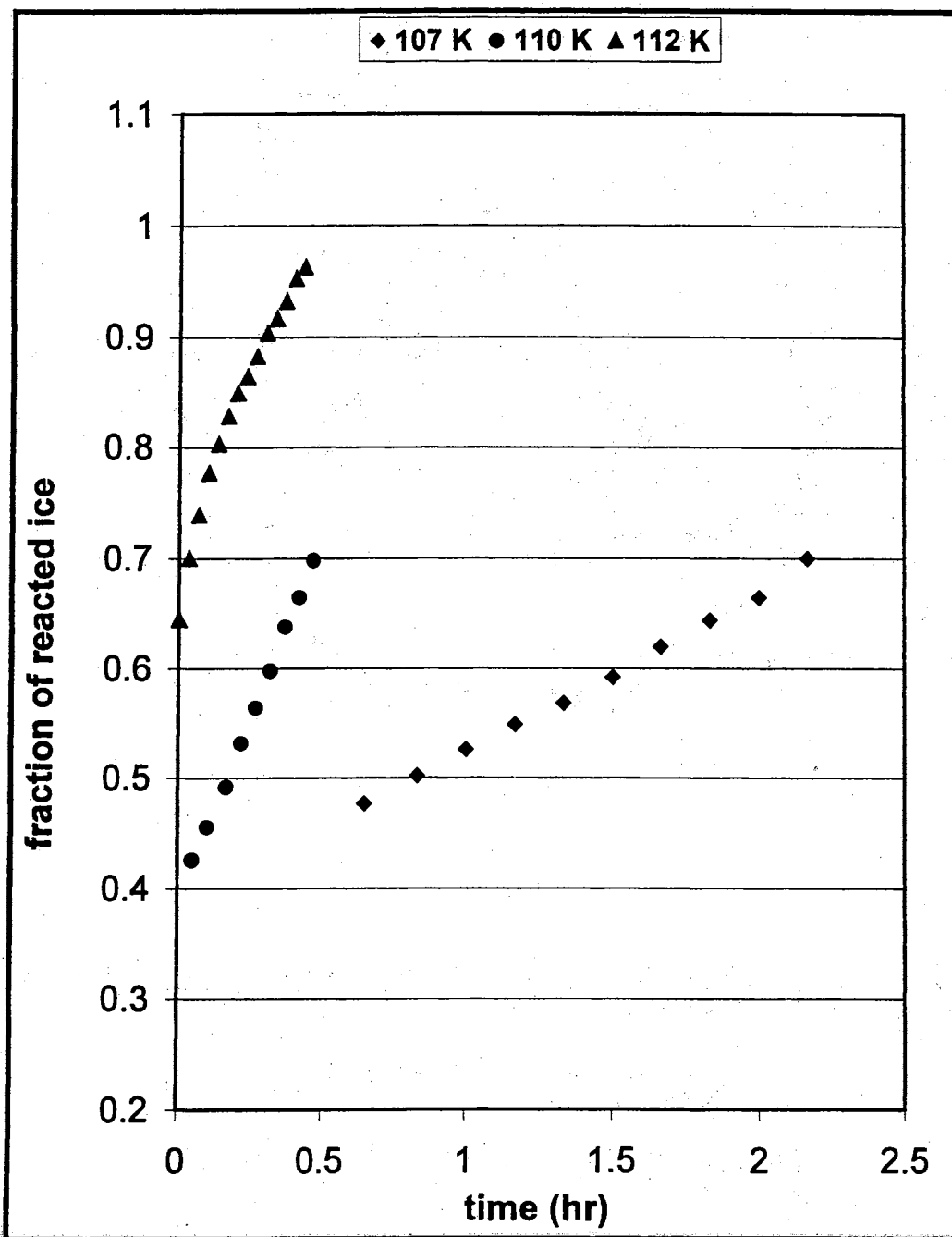


Figure 68. The plot for the conversion of D_2O ice nanocrystals to crystalline $2NH_3 \cdot D_2O$ at 107, 110 and 112 K.

the amorphous nature of this product can be seen from the difference spectra between the partially reacted ice and the bare ice, using subtraction method described in the experimental part.

The plot of the fraction of reacted ice versus time for the conversion of H₂O and D₂O ice nanocrystals to the 2NH₃.H₂O and 2NH₃.D₂O, respectively, is shown in Figure 69A at 102 K and in Figure 69B at 105 K. The spectra of partially reacted ice at 102 and 105 K are shown in Figure 70 and Figure 71, respectively.

There is no doubt about the existence of small differences in the measured reaction kinetics of D₂O and H₂O. However, the question is whether these differences correspond to a D-isotope effect or is there another parameter that effects the observed reaction kinetics. If the reaction rate is controlled by the diffusion of ammonia through the hydrate, there may be an association of ammonia with the D₂O or H₂O part of hemihydrate when it is passing through the hydrate layer. However, the observed rate difference between D₂O and H₂O is very small. The parameters that affect the reaction kinetics will be discussed in the next chapter.

6.2. NH₃ versus ND₃

Four different reaction temperatures were used to observe the reaction kinetics of the ND₃-D₂O system, namely 102, 105, 107 and 110 K. At the two former reaction temperatures, the product was again the amorphous hemihydrate for the laboratory time scale.

The partially reacted ice spectra as a function of time for ND₃ at 102 K is

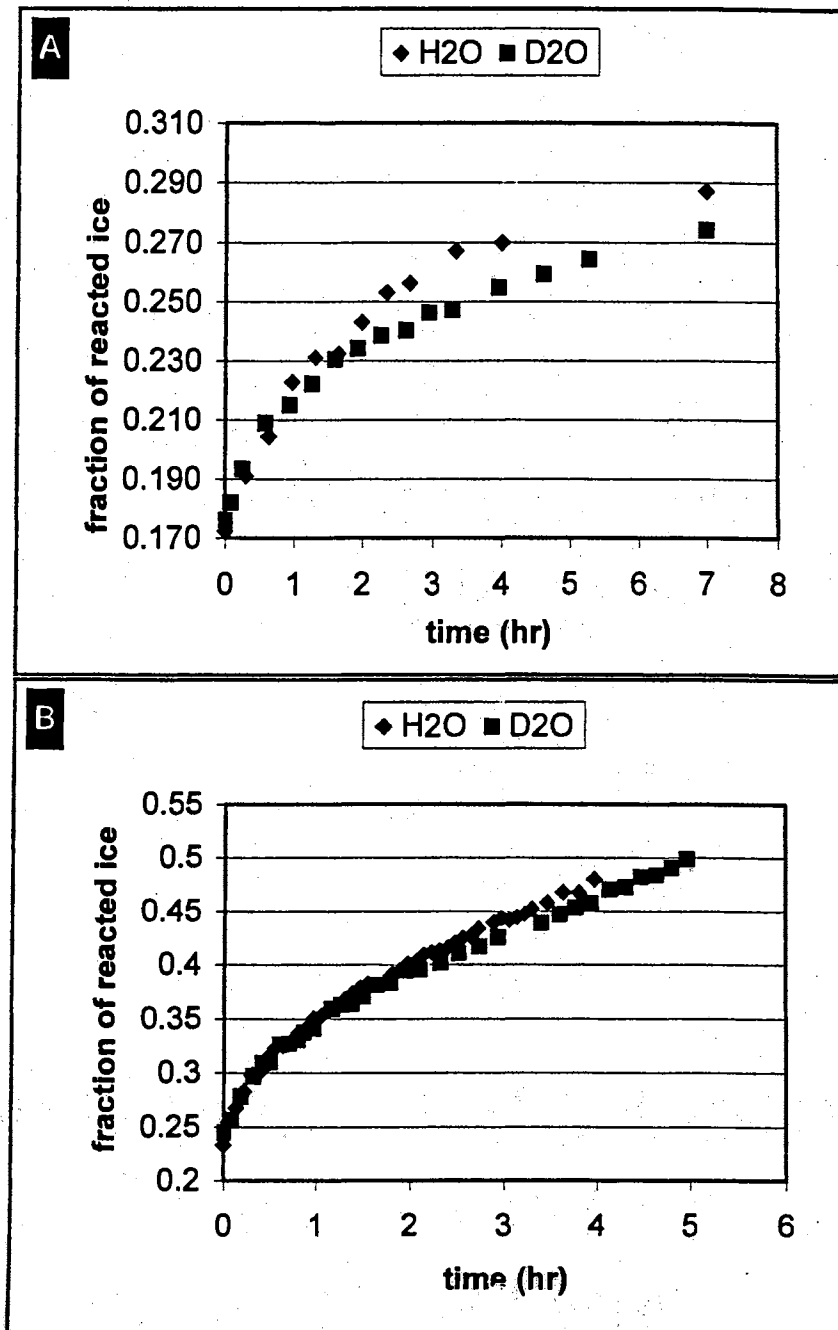


Figure 69. The plot for the conversion of H₂O and D₂O ice nanocrystals; A – 102 K and B – 105 K.

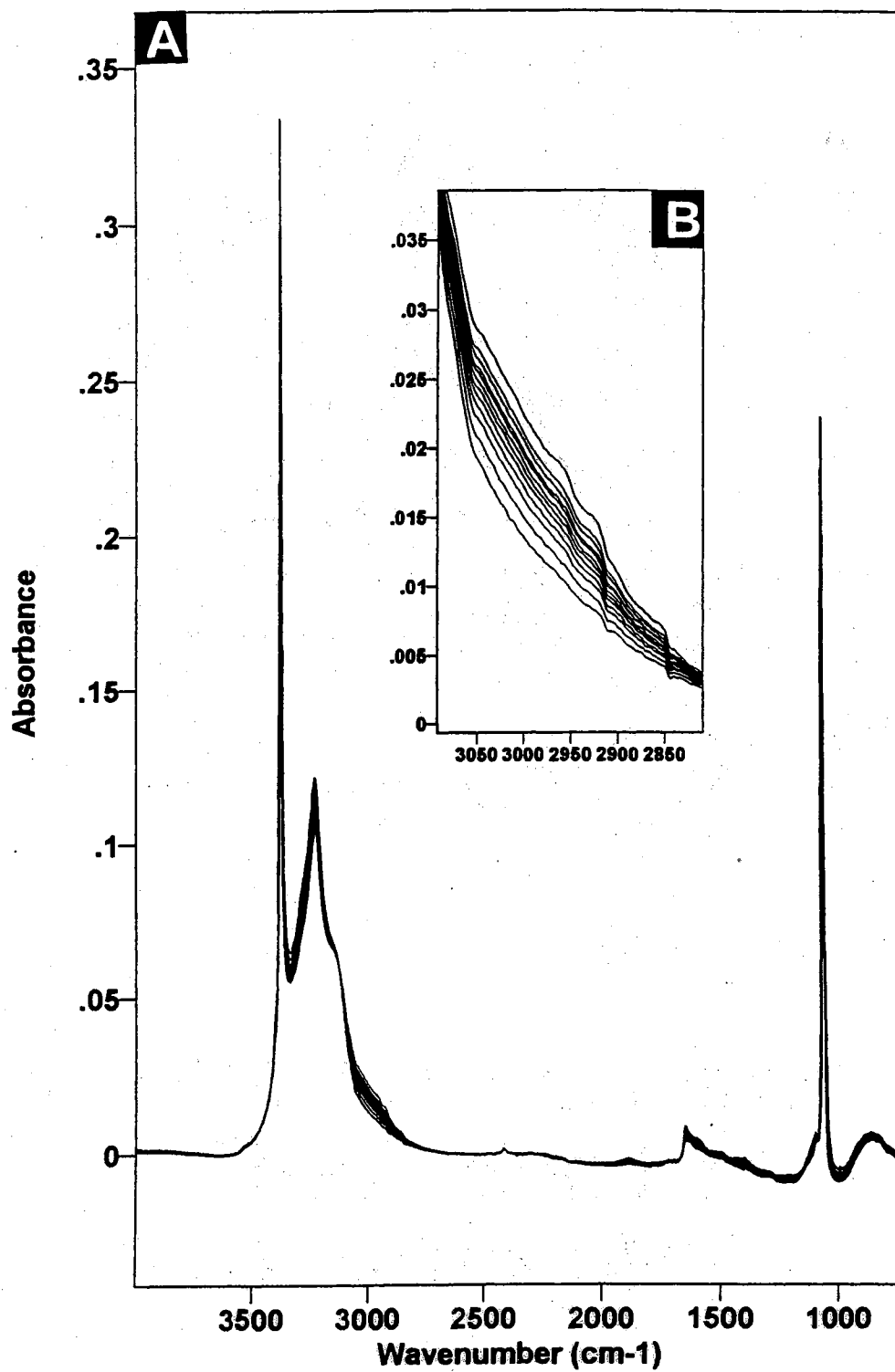


Figure 70. The sample spectra, after partial reaction, as a function of time at 102 K; A – in the 4000 – 800 cm^{-1} region; B – the spectra are expanded along both axes.

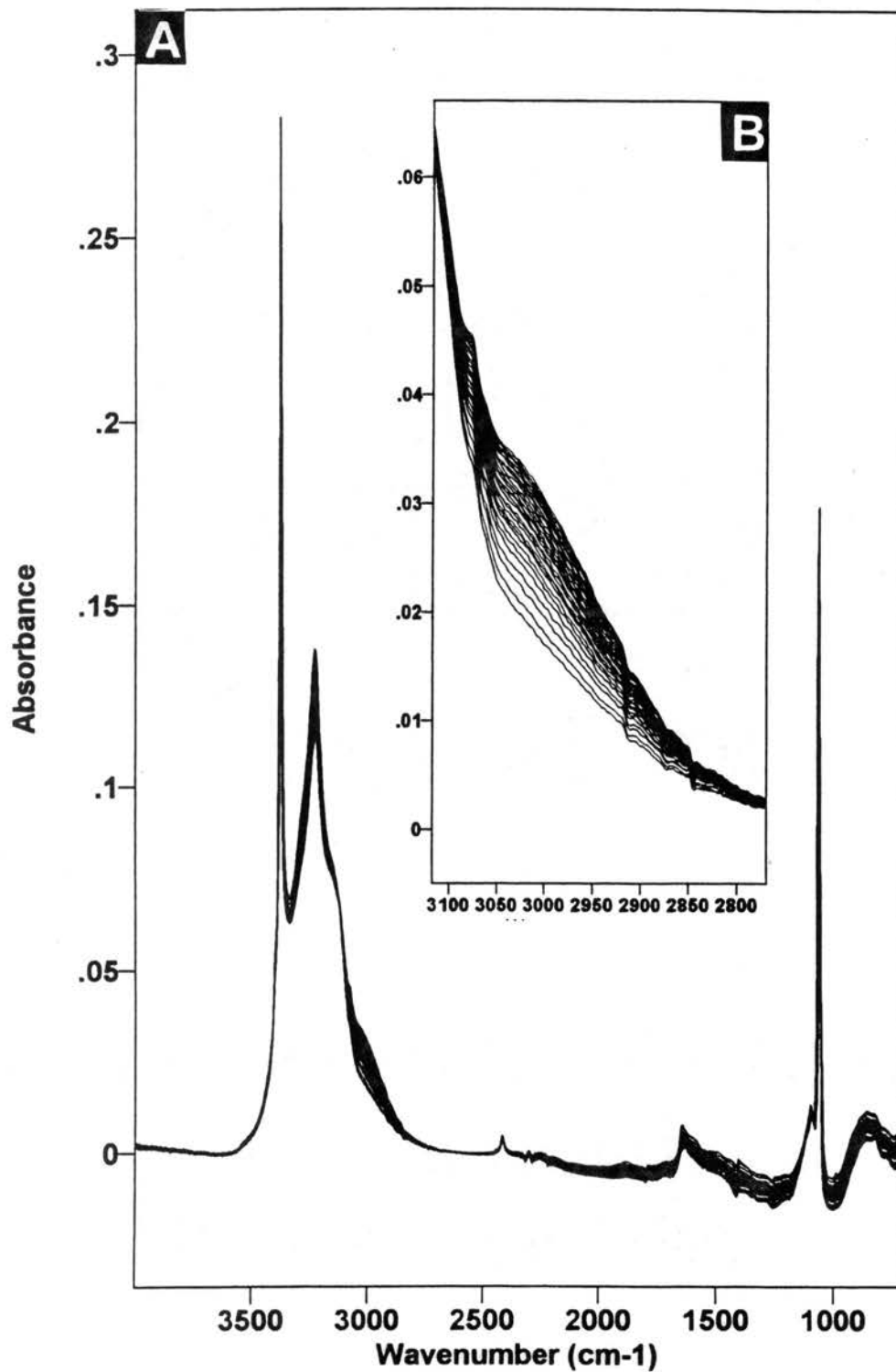


Figure 71. The sample spectra, after partial reaction, as a function of time at 105 K; A – in the $4000 - 800 \text{ cm}^{-1}$ region; B – the spectra are expanded along both axes.

shown in Figure 72 and the rate plot of this conversion is given in Figure 73A along with the analogue plot for NH_3 . For 105 K, the plot is shown in Figure 73B. As seen from the figures, as the fraction of reacted ice increases (increasing reaction temperature), the plots of NH_3 and ND_3 diverge. One should notice, from the Figure 73A and B, that the amounts of the initially reacted ice of NH_3 and ND_3 are very close to each other at the same temperature.

In the case of crystalline hemihydrate formation, a separation of the rate plots is more obvious as shown in Figure 74 for the reaction temperatures at 107 and 110 K. As seen from the figure, the plot for the ND_3 at 110 K matches with that for the NH_3 at 107 K.

Is this isotopic rate difference a vapor pressure effect? As shown and calculated in Chapter III, there is a vapor pressure effect between the NH_3 and its deuterium isotopomers. However, if this reflects the vapor pressure deuterium isotope effect, then the initial reaction amount should not be so close. The similarities of extent of the initial reaction and the divergence after some point offer a clear picture if one accepts the reaction rate is controlled by solid state diffusion.

As discussed in the first chapter, there are two factors that contribute to the generally lower reactivity of bonds to deuterium as compared to the corresponding bonds to hydrogen; namely, the difference in free energy (the difference in the zero point energy makes an important contribution to the free energy difference) and the effect of the difference in mass. These factors may explain the deuterium isotope effect for these conversions.

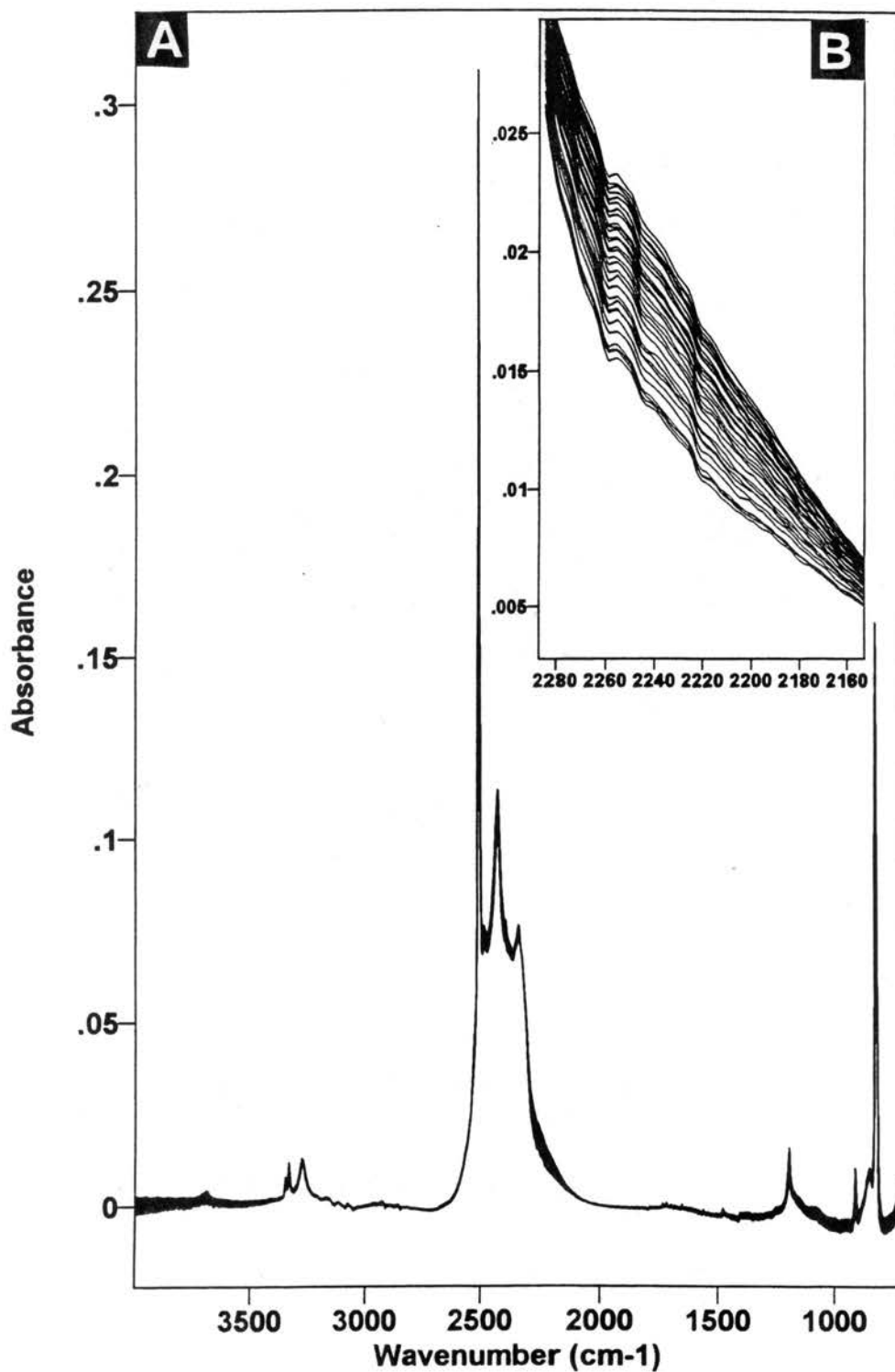


Figure 72. The sample spectra, after partial reaction, as a function of time at 102 K; A – in the 4000 – 800 cm⁻¹ region; B – the spectra are expanded along both axes.

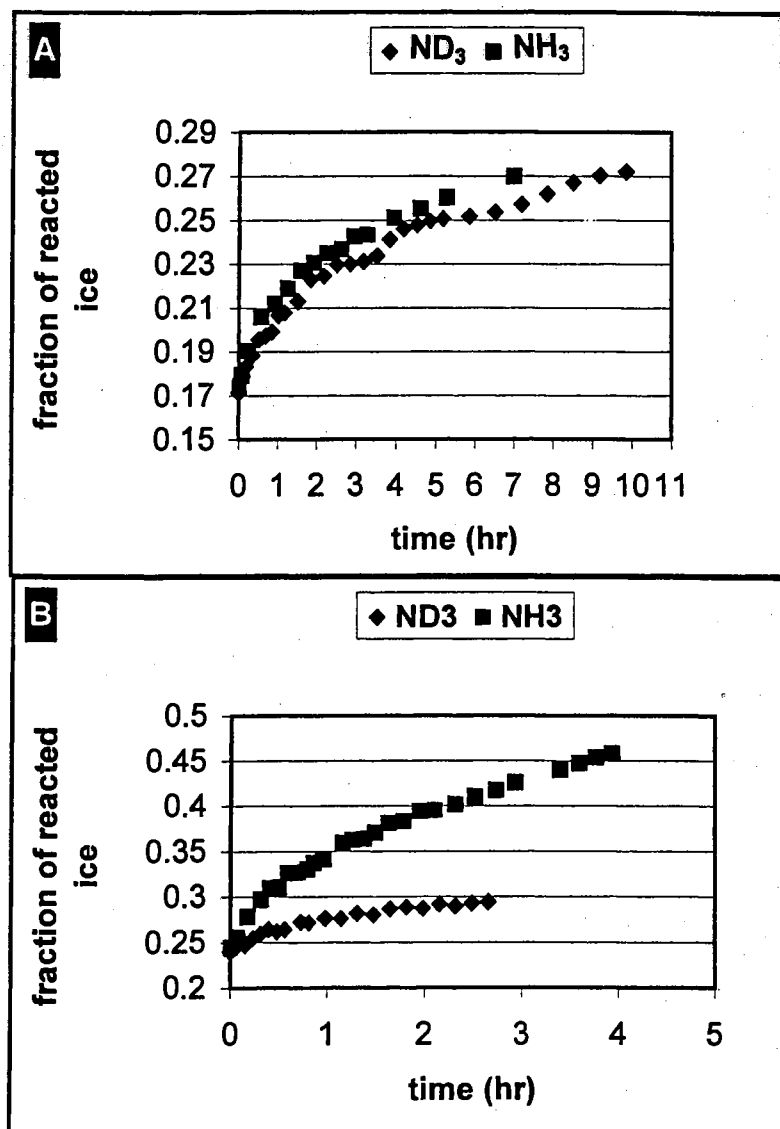


Figure 73. The plot for the reaction of NH₃ and ND₃ with the D₂O ice nanocrystals; A – 102 K and B – 105 K.

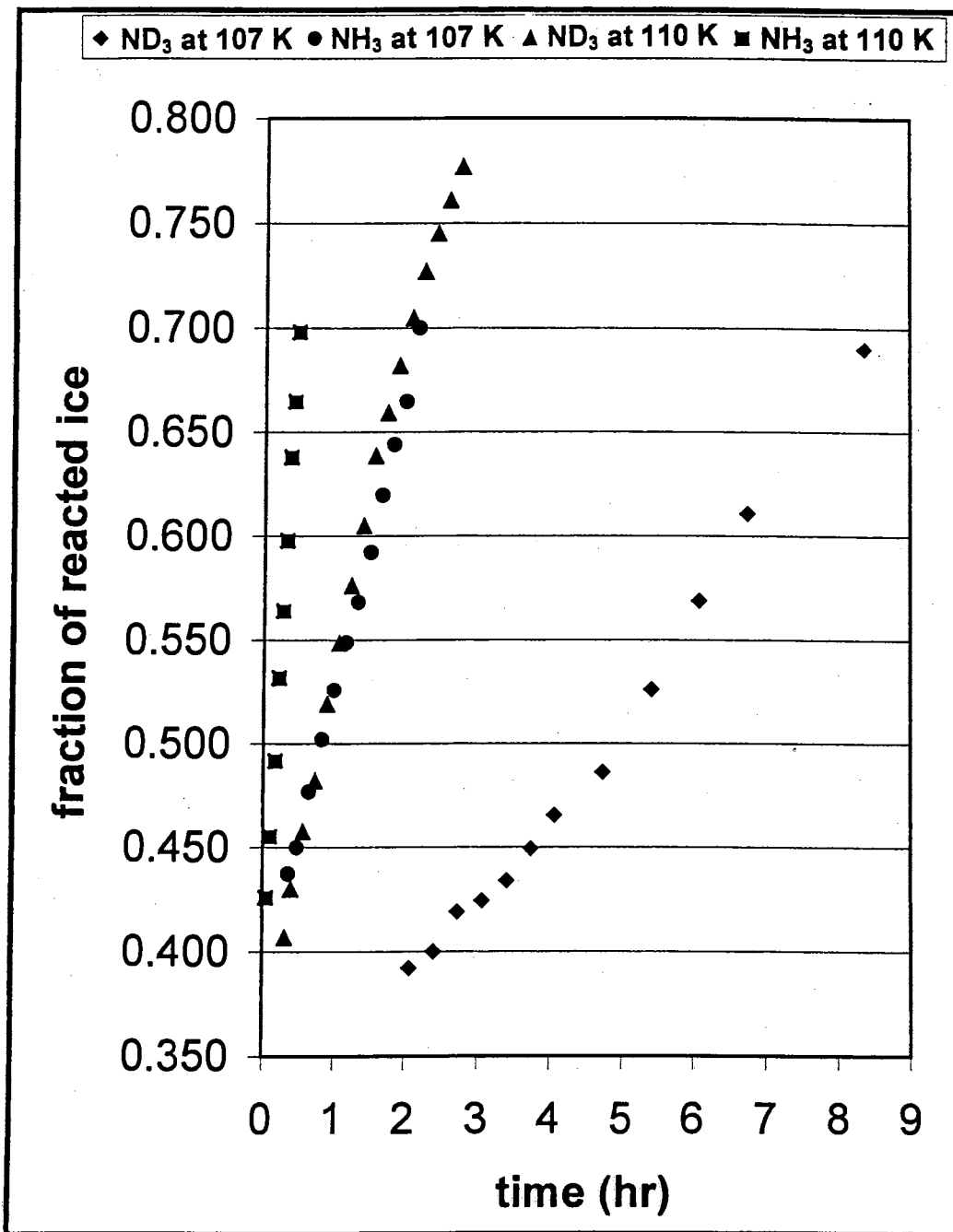


Figure 74. The plot for the reaction of NH₃ and ND₃ with the D₂O ice nanocrystals; A – 107 K and B – 110 K.

When the ammonia molecules are diffusing through the hydrate layer, they may associate with the ammonia and water molecules of the hydrate. This process may be the explanation of the temperature dependence of the reaction kinetics. Since the hemihydrate has a rich ammonia concentration, this association may be mostly with the ammonia molecules of the hydrate (as shown by little rate change for H₂O versus D₂O).

Bigeleisen⁴⁵ showed that when the molecules in reacting isotopomeric species contain different isotopic atoms that change their chemical bonding, the rate constants of the light molecules are generally greater than of the heavy molecules. Furthermore, he theorized that the largest ratio in the rates takes place when the isotopic atoms are particularly free in the activated complex.

These theories may explain the separation in the rate plots; but, why are the initial rates more or less similar? If the rate is controlled by the diffusion of ammonia through the hydrate, the initial rates will be expected to be similar for NH₃ and ND₃. Since the initial reaction is very near the particle surface, the factors that cause the D-isotope effect become significant only when the diffusion path becomes larger.

In the next chapter, the mathematical analysis of the experimental results will be explained.

CHAPTER V

KINETIC MODEL FOR THE CONVERSION OF ICE NANOCRYSTALS TO THE HEMIHYDRATE OF AMMONIA

1. Introduction

This chapter treats the kinetics for the conversion of the ice nanocrystals to the hemihydrate of ammonia. As noted in the previous chapter, the diffusion of ammonia through the solid hydrate product is apparently rate limiting for the conversion of the ice nanocrystals to the hemihydrate of ammonia under the chosen conditions. Furthermore, one of the critical aspects of this research was evidence that the formation of hemihydrate requires some minimum level of ammonia concentration at the surface. Further, exceeding of a certain concentration level is thought not to change the rate of this conversion and the rate measurements are made above this level.

In this chapter, the kinetic data obtained from this research is analyzed by a conceptual picture or a model from which the heterogeneous reaction kinetics in the spherical particles can be explained. We use models proposed in the literature that correspond closely to what takes place in our experimental method. Three models that correlate with our experimental data were found. As seen later, the experimental results are found to correlate successfully with these models.

In fact, the three models give the same result. Two of them were proposed independently during the 1950's and the third one was proposed around 1960.

2. Diffusion Equations

As known very well, the Fick's law of diffusion has two differential forms, namely;⁴¹

$$P = -\mathcal{D} (\partial C/\partial x) \quad (1)$$

and

$$\partial C/\partial t = \mathcal{D} (\partial^2 C/\partial x^2) \quad (2)$$

Equation 1 gives the rate of permeation, in the steady state of flow, in terms of the concentration gradient across the medium, with the constant \mathcal{D} known as the diffusion constant. In the steady state, there is no change of concentration with time ($\partial C/\partial t = 0$). Equation 2 refers to a non-stationary state of flow and describes the accumulation of matter at a given point in a medium as a function of time. In three dimensions of isotropic matter, the second equation becomes

$$\partial C/\partial t = \mathcal{D} (\partial^2 C/\partial x^2) + \mathcal{D} (\partial^2 C/\partial y^2) + \mathcal{D} (\partial^2 C/\partial z^2) \quad (3)$$

Equation 3 may be expressed in spherical polar coordinates r , θ , and ϕ using the transformation equations

$$\left. \begin{aligned} x &= r \sin \theta \cos \phi \\ y &= r \sin \theta \sin \phi \\ z &= r \cos \theta \end{aligned} \right\} \quad (4)$$

Equation 3 becomes

$$\partial C/\partial t = (\mathcal{D}/r^2) [(r \partial/\partial r)(r^2 \partial C/\partial r) + (1/\sin \theta)(\partial/\partial \theta)(\sin \theta \partial C/\partial \theta) + (1/\sin^2 \theta)(\partial^2 C/\partial \phi^2)] \quad (5)$$

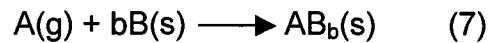
The last equation, for a spherically symmetric diffusion ($\partial C/\partial \theta = 0$ and $\partial^2 C/\partial \phi^2 = 0$),

reduces to

$$\partial C/\partial t = \mathcal{D} [(\partial^2 C/\partial r^2) + (2/r)(\partial C/\partial r)] \quad (6)$$

2.1. Shrinking (Unreacted) Core Model for Spherical Particles

This model was developed by Yagi and Kunii (1955).⁴⁹ The derivation based on the partially reacted particle as shown in Figure 75 requires a two-step analysis; first consider a spherical partially reacted particle by writing the flux relationship for this condition; then the second step gives the dependence of the first step result on the particle diameter. This model contains three successive steps, which are modified for our purposes, as explained in the following;



1. Transport of the gaseous reactant to the surface of the solid hydrate product.
2. Penetration and diffusion of the gaseous reactant (A) through the layer of (AB_b) product to the surface of the solid (B).
3. Reaction of the gaseous reactant with solid at this reaction surface.

From the stoichiometry of the equation 7,

$$dN_B = bdN_A \quad (8).$$

According to this model, both reactant A and the boundary of the unreacted core move inward toward the center of the particle but the shrinkage of the unreacted core is much slower than the flow rate of A toward the unreacted core. The unreacted core is, thus, considered stationary when evaluating the concentration gradient of A in the hydrate layer at any time. Then, the rate of

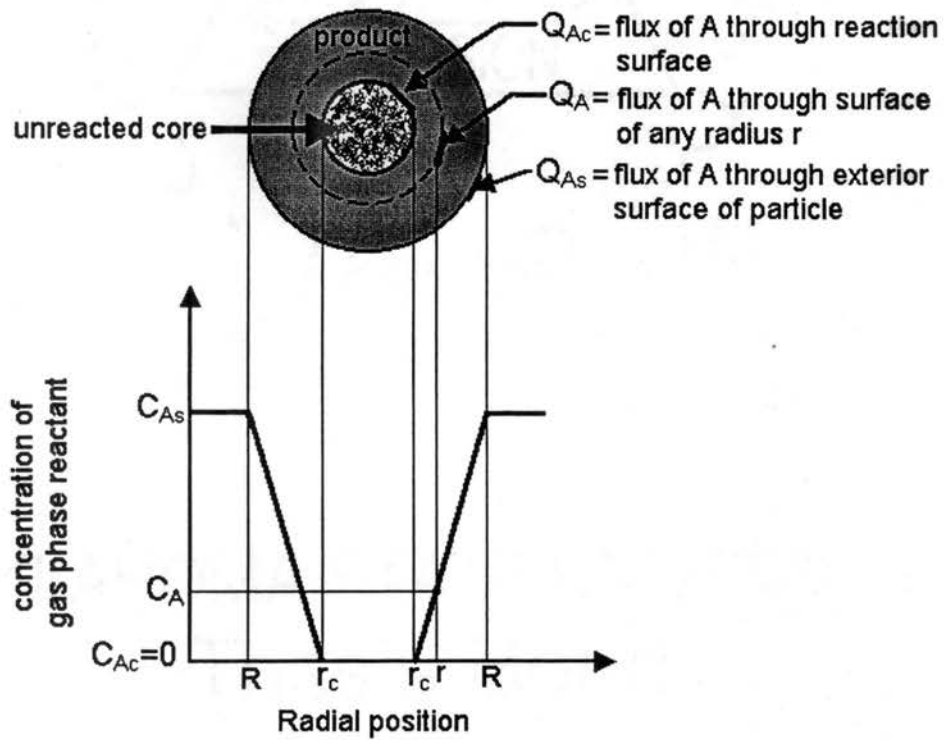


Figure 75. A representation of a partially reacted particle and the plot shows the dependence of the concentration of gas-phase reactant on the radial position (adapted from reference 49).

reaction of A at any instant is given by its rate of diffusion to the reaction surface

$$-(dN_A/dt) = 4\pi r^2 Q_A = 4\pi R^2 Q_{A_s} = 4\pi r_c^2 Q_{A_c} = \text{constant} \quad (9)$$

where Q_{A_s} is the flux of A through the exterior surface of the particle. The flux of A through surface of radius r_c , Q_{A_c} is the flux of A through the reaction surface. This means that for a given size of the unreacted core, dN_A/dt is a constant.

The flux of A within the product (hydrate) layer can be expressed by Fick's law as follows;

$$Q_A = \mathcal{D}_e (dC_A/dr) \quad (10)$$

where \mathcal{D}_e is the effective diffusion coefficient of gaseous reactant in the product layer. Combining equations 9 and 10, it is obtained for any r

$$-(dN_A/dt) = 4\pi r^2 \mathcal{D}_e (dC_A/dr) = \text{constant} \quad (11).$$

Integrating from R to r_c

$$-(dN_A/dt) \int_R^{r_c} dr/r^2 = 4\pi \mathcal{D}_e \int_{C_{A_g}=C_{A_s}}^{C_{A_c}=0} dC_A \quad (12)$$

gives

$$-(dN_A/dt) [(1/r_c) - (1/R)] = 4\pi \mathcal{D}_e C_{A_g} \quad (13).$$

This expression represents the condition of a reacting particle of radius r_c at any time.

If ρ_B is the molar density of B in the solid and V is the volume of a particle, the amount of B present in a particle is

$$N_B = \rho_B V = (\text{moles B/cm}^3 \text{ solid})(\text{cm}^3 \text{ solid}) \quad (14).$$

The decrease in volume or radius of unreacted core accompanying the disappearance of dN_B moles of solid reactant or bdN_A moles of gas is then given by

$$-dN_B = -bdN_A = -\rho_B dV = -\rho_B d[(4/3)\pi r_c^3] = -4\pi\rho_B r_c^2 dr_c \quad (15)$$

Replacing dN_A in equation 13, separating variables and integrating over the time and radius (here, the size of the unreacted core is let to change with time).

$$-\rho_B \int_{r_c=R}^{r_c} [(1/r_c)-(1/R)] r_c^2 dr_c = b\mathcal{D}_e C_{Ag} \int_0^t dt \quad (16)$$

or

$$t = (\rho_B R^2 / 6b\mathcal{D}_e C_{Ag}) [1 - 3(r_c/R)^2 + 2(r_c/R)^3] \quad (17)$$

For complete conversion of a particle, $r_c=0$, and the time required is

$$\tau = (\rho_B R^2 / 6b\mathcal{D}_e C_{Ag}) \quad (17a)$$

The progression of reaction in terms of the time required for complete conversion is found by dividing equation 17 by 17a, or

$$t / \tau = [1 - 3(r_c/R)^2 + 2(r_c/R)^3] \quad (17b)$$

Then, equation 17b can be written in terms of fractional conversion by noting that

$$\begin{aligned} 1 - X_B &= (\text{volume of unreacted core} / \text{total volume of particle}) \\ &= (4/3)\pi r_c^3 / (4/3)\pi R^3 \quad (18) \end{aligned}$$

$$1-X_B = (r_c/R)^3 \quad (19).$$

Therefore,

$$t / \tau = [1-3(1-X_B)^{2/3} + 2(1-X_B)] \quad (20)$$

The plot of $[1-3(1-X_B)^{2/3} + 2(1-X_B)]$ versus t should give a straight line with the slope of the line equal to $1/\tau$ which is $(6bD_eC_{A0} / \rho_B R^2)$.

2.2. The Diffusion Kinetics of Reactions in Spherical Particles: Ginstling and Brounshtein's Derivation⁵⁰

This model was developed by Ginstling and Brounshtein (1950) and the derivation was pretty much the same as in 2.1. The substance A reacting with the substance B is forming a product AB. The thickness of the AB layer continuously increases during the course of reaction. The substance A diffuses to the surface of the substance B through a layer of product AB. The rate of diffusion of A is immeasurably less than the rate of the chemical reaction between A and B so that the diffusion process entirely determines the kinetics of this reaction.

Since the external resistance of the diffusion is much less than the diffusion resistance through the product AB, the concentration of the substance A at the surface separating it from the AB is virtually constant. In the surface dividing the solids AB and B, the concentration of A is zero due to the extremely high velocity of the chemical reaction between A and B (see Figure 76).

The definition of symbols for the unsteady state diffusion:

t = time

C = concentration of A in a layer of AB

C_0 = concentration of A at the boundary between A and AB

\mathcal{D} = diffusion coefficient of A

x = thickness of the layer of AB

$e = \rho\eta / \mu =$ proportionality coefficient (ρ being the specific weight and μ the molecular weight of AB; η the stoichiometric coefficient of the reaction, expressing the number of moles A reacting with one mole of B). This equation for (e) is true if C_0 is the molar concentration, but if C_0 is the concentration by weight then $\epsilon = \rho\eta_{ij} / \mu_2$, where μ_2 is the molecular weight of A.

Fick's law in the case of spherical symmetry was used (equation 6)

$$\partial C / \partial t = \mathcal{D} [(\partial^2 C / \partial r^2) + (2/r)(\partial C / \partial r)] \quad (21)$$

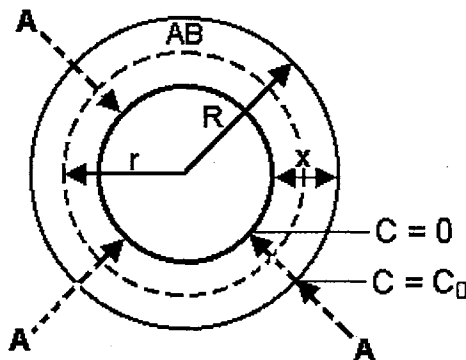


Figure 76. Diagram of the process (adapted from related paper).

The boundary conditions are;

$$\left. \begin{array}{l} C(r) = C_0 \\ r = R \\ t = 0 \end{array} \right\} \quad (22)$$

$$\left. \begin{array}{l} C(r) = 0 \\ r = R-x \end{array} \right\} \quad (23)$$

$$dx / dt = (D/e)(\partial C / \partial r)_{r=R-x} \quad (24)$$

$$\left. \begin{array}{l} x = 0 \\ t = 0 \end{array} \right\} \quad (25).$$

The equation 24 is obtained on the condition that

$$dx = dG/e$$

where $dG = -D(dC/dr)_{r=x} \dots dt$, and is the quantity of substance A diffusing through unit area of surface separating AB from B after time dt .

The amount of substance A diffusing in unit time through any cross sectional layer of product AB is denoted by $M(x)$; bearing in mind that $M(x)$ has different values for different x . For the stated distance x and the variable r , the relation can be written;

$$D(\partial C / \partial r)4\pi r^2 = M(x) = \text{constant}$$

hence,

$$dC/dr = (M(x) / 4\pi r^2 D) \quad (26).$$

Integrating equation 26 in the limits from $r=R-x$ to $r=R$ (with $C=0$ at $r=R-x$),

$$C_0 = -(M(x)/4\pi\mathcal{D})(1/r) \Big|_{R-x}^R = (M(x)/4\pi\mathcal{D})[x/(R(R-x))]$$

$$M(x) = C_0R(R-x)4\pi\mathcal{D}/x \quad (27).$$

Putting equation 27 into equation 26 gives

$$\partial C/\partial r = C_0R(R-x)/(xr^2) \quad (28)$$

and putting equation 28 into equation 24 gives

$$dx/dt = K_1R/[x(R-x)] \quad (29)$$

where $K_1 = \mathcal{D}C_0/\epsilon$ and equation 29 shows the rate of thickening of the layer of AB in the spherical particle.

Integrating equation 29, taking into account the initial condition 25,

$$x^2 [1 - (2x/3R)] = K't \quad (30)$$

where $K' = 2K_1$.

Instead of the thickness of the product layer (which is difficult to determine), the degree of conversion of material can be used

$$X_B = [(4\pi R^3/3) - (4\pi(R-x)^3/3)] / (4\pi R^3/3) = 1 - [(R-x)/R]^3 \quad (31)$$

where X_B is the degree of conversion of substance B. Writing x in equation 31 in terms of X_B and putting into equation 30 give

$$1 - 2X_B/3 - (1-X_B)^{2/3} = K't/R^2 \quad (32).$$

Equation 32 can also be written as;

$$t = (R^2/K') [1 - 3(1-X_B)^{2/3} + 2(1-X_B)] \quad (33)$$

which is identical with equation 20 except for the constants.

2.3. Kinetic Model for Solid-State Reactions; Carter's Derivation^{51,52}

The particle size in both analyses derived above for the reactions of the spherical particles were not changed. In Carter's derivation, the volume change was included in the analysis and when the Carter's derivation is repeated for the case of no volume change, the equation is identical with that of Ginstling and Brounshtein. Moreover, Carter showed that including the volume change barely changed the analysis of the experimental data for the nickel spheres reacting with oxygen and stated: "The analysis of Ginstling and Brounshtein is probably as accurate as any kinetic data can be analyzed." The Carter's analysis is explained here briefly and the results obtained from our experimental work will be compared with this analysis.

Definition of the symbols (see Figure 77);

r_0 = initial radius of B

r_1 = instantaneous radius of B

r_e = radius of product at $x = 1.0$ (complete reaction)

r_2 = instantaneous radius of unreacted B plus product

z = represents the volume of product formed per unit volume of component B consumed.

The volume Q_B of B present at any time t is

$$Q_B = (4/3)\pi r_1^3 \quad (34)$$

The rate of change of Q_B , equal to the flux of material diffusing through the spherical shell of thickness $r_2 - r_1$ is given by

$$dQ_B/dt = -4\pi k r_1 r_2 / (r_2 - r_1) \quad (35)$$

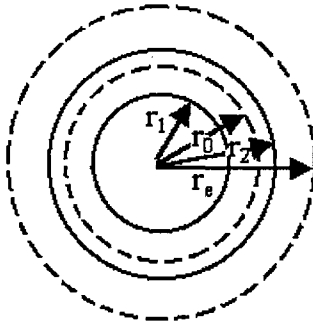


Figure 77. Model for the Carter's analysis (adapted from the related paper).

where k is the reaction rate constant in units of cm^2/sec .

The total volume of the sphere is made up of unreacted B plus the product layer;

$$r_2^3 = zr_0^3 + r_1^3(1-z) \quad (36).$$

Taking x as the fraction of reacted B, the radius of the unreacted core may be written as

$$r_1 = (1-x)^{1/3} r_0 \quad (37).$$

Differentiating equation 34 with respect to time gives

$$(dQ_B/dt) = 4\pi r_1^2 (dr_1/dt) \quad (38).$$

Equating equation 38 to the right-hand side of equation 35 gives

$$r_1 (dr_1/dt) = -kr_2 / (r_2 - r_1) \quad (39)$$

putting r_2 values from equation 36 into equation 39 gives

$$\{r_1 - (r_1^2 / [zr_0^3 + r_2^3(1-z)]^{1/3})\} dr_1 = -kdt \quad (40)$$

integrating equation 40 from r_0 to r_1 and substituting for r_1 from equation 37 gives

$$[1 + (z-1)x]^{2/3} + (z-1)(1-x)^{2/3} = z + 2(1-z)kt/r_0^2 \quad (41)$$

which is related to equation 33.

3. Analysis of $\text{NH}_3+\text{D}_2\text{O}$ Results Using Shrinking Core Model

3.1. Conversion of Ice Nanocrystals to the Amorphous Hemihydrate

The plot of the right-hand side of equation 20 versus time is given in Figure 78 for the conversion of the D_2O ice nanocrystals to amorphous $2\text{NH}_3.\text{D}_2\text{O}$ at 102, 105 and 107 K. The slope of these curves (should be converted to units of seconds, for this reason slope must be divided by 3600) equals $(6b\mathcal{D}_e C_{\text{Ag}}/\rho_B R^2)$, where ρ_B is the molar density of D_2O ice (cubic ice, I_c)¹ that is equal to 0.05191 mol/cm^3 at 140 K, R is the initial particle radius that is 25 nm ($25 \times 10^{-7} \text{ cm}$), b is the stoichiometric coefficient that is equal to $\frac{1}{2}$ for the ice and NH_3 reaction, \mathcal{D}_e is the diffusion coefficient (in units of cm^2/sec) that we are trying to determine, C_{Ag} is the ammonia concentration (mol/cm^3) at the surface.

The concentration of ammonia cannot be the amount of the vapor pressure since, as discussed in the previous chapter, there is a surplus of ammonia to keep the physically adsorbed ammonia on the hydrate surface above some concentration. Under our experimental conditions, we cannot detect what is the magnitude of this concentration. However, it reasonably corresponds to a monolayer coating of ammonia in which the ammonia molecules are physically bound to the hydrate surface.

Nevertheless, it is appropriate to talk about "maximum effective concentration of ammonia" on the hydrate surface, since some of the ammonia

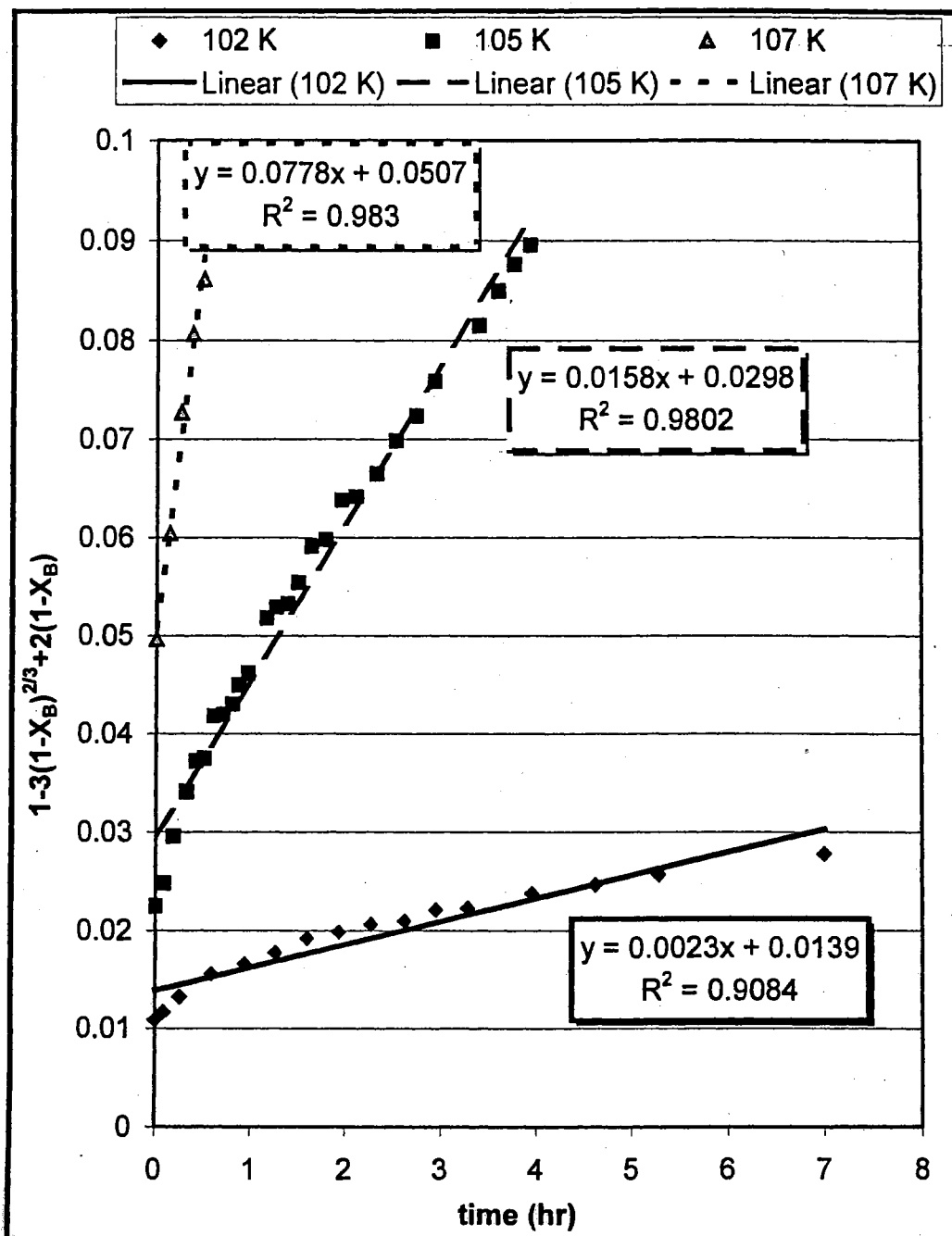


Figure 78. Plots of $[1-3(1-X_B)^{2/3}+2(1-X_B)]$ versus time for the conversion of D_2O ice nanocrystals to the amorphous $2NH_3 \cdot D_2O$.

may be chemisorbed by the surface hydroxyl groups and be inactive during the reaction. Although, there is no clear experiment with ammonia that shows this inactivation, this can be deduced from indirect evidence for THF on ice (unpublished result). It should be noticed that on the surface of the hemihydrate, the density of hydroxyl groups may be trivial since the hemihydrate contains more NH_3 than H_2O and the O-H groups bond tightly with the NH_3 .

Exposure of ice nanocrystals to THF causes the strong hydrogen bonding between the surface d-H sites and THF, like ammonia. However, subsequent exposure of the sample to SO_2 causes the formation of a "clathrate hydrate" (that is formed by the host water molecules assuming icelike lattice structure with tetrahedrally connected hydrogen bonds and with each (SO_2) guest molecule encaged in the host lattice, interacting with the host water molecules not through electrostatic attractive forces but through dispersion forces). During this SO_2 hydrate formation, THF stays on the d-H sites.

The maximum concentration for the adsorbed ammonia on the surface may be taken as the liquid ammonia density, which is $0.040164 \text{ mol/cm}^3$. Since the physically adsorbed NH_3 on the hydrate surface at levels of a monolayer or greater resembles more closely to the NH_3 in the liquid phase, the liquid density for the ammonia is used.

The slope of the 102 K curve given in the Figure 78 equals 6.3888×10^{-7} ($0.0023/3600$) and the diffusion coefficient can be found from;

$$6.3888 \times 10^{-7} = [6(1/2) D_e 0.040164] / [0.05191 (25 \times 10^{-7})^2]$$

$$D_e = 1.72 \times 10^{-18} \text{ cm}^2/\text{sec at 102 K.}$$

The same calculation can be made at 105 K

$$4.3888 \times 10^{-6} = [6(1/2) \mathcal{D}_e 0.040164] / [0.05191 (25 \times 10^{-7})^2]$$

$$\mathcal{D}_e = 1.18 \times 10^{-17} \text{ cm}^2/\text{sec at 105 K.}$$

For the reaction temperature at 107 K,

$$2.1611 \times 10^{-5} = [6(1/2) \mathcal{D}_e 0.040164] / [0.05191 (25 \times 10^{-7})^2]$$

$$\mathcal{D}_e = 5.82 \times 10^{-17} \text{ cm}^2/\text{sec at 107 K.}$$

Although there is no information available in the literature for the diffusion coefficient of NH_3 in the hydrate, the easiest way to check the diffusion coefficients obtained from the model is to calculate the effective distance (d) for the diffusion of NH_3 in a time t that is estimated approximately by $d = \sqrt{(\mathcal{D}_e t)}$.⁴¹

For the 102 K reaction, d is found as 2.08 nm (20.8 Å) for a time of 7 hr (=25200 sec). The N – O distance in the hemihydrate structure³⁶ is 2.85 Å, so dividing d by 2.85 gives ~7 layer of N – O. If one assumes that each layer of N – O bonds is formed using one monolayer of ice, then ~6 monolayers of ice was used. The fraction of reacted ice after 7 hour reaction time was ~27% (see Table 5) that corresponds to ~6 monolayer (~3 bilayer). Therefore, the calculated effective diffusion distance (d) is reasonable at 102 K reaction temperature, since each bilayer of ice has a thickness of ~3.6 Å.¹

3.1.1. The temperature Dependence of Reaction Rates

The temperature dependence of the diffusion coefficient can be calculated

from the equation $\mathcal{D}_e = Ae^{-E_a/RT}$.⁴¹ The plot of $\ln\mathcal{D}_e$ versus $1/T$ is shown in Figure 79 and the activation energy is calculated as $E_a = 15.13$ kcal/mol for the conversion of D_2O ice nanocrystals to the amorphous hemihydrate.

3.2. Conversion of Ice Nanocrystals to the Crystalline $2NH_3.D_2O$

The plot of $1-3(1-X_B)^{2/3}+2(1-X_B)$ in equation 20 versus time is shown in Figure 80 for the reaction temperatures at 107, 110 and 112 K. By following the procedure used above, the diffusion coefficients are found as;

$$\mathcal{D}_e = 6.89 \times 10^{-17} \text{ cm}^2/\text{sec at } 107 \text{ K}$$

$$\mathcal{D}_e = 3.21 \times 10^{-16} \text{ cm}^2/\text{sec at } 110 \text{ K}$$

$$\mathcal{D}_e = 8.81 \times 10^{-16} \text{ cm}^2/\text{sec at } 112 \text{ K}$$

The plot of $\ln\mathcal{D}_e$ versus $1/T$ is shown in Figure 81 and from it, the activation energy is calculated as 12.12 kcal/mol for the conversion of D_2O ice nanocrystals to the crystalline $2NH_3.D_2O$.

The difference between the diffusion through the amorphous and crystalline hydrates can be easily seen from, also, the difference between the activation energies (15.13 kcal/mol vs. 12.12 kcal/mol). Jorgensen⁴⁸ et. al. observed the similar trend for the activation energy of the formation of amorphous SiO_2 and crystalline SiO_2 from the oxidation of SiC . They calculated an activation energy of 20.2 kcal/mol for the amorphous product formation and 15.6 kcal/mol for the crystalline product formation.

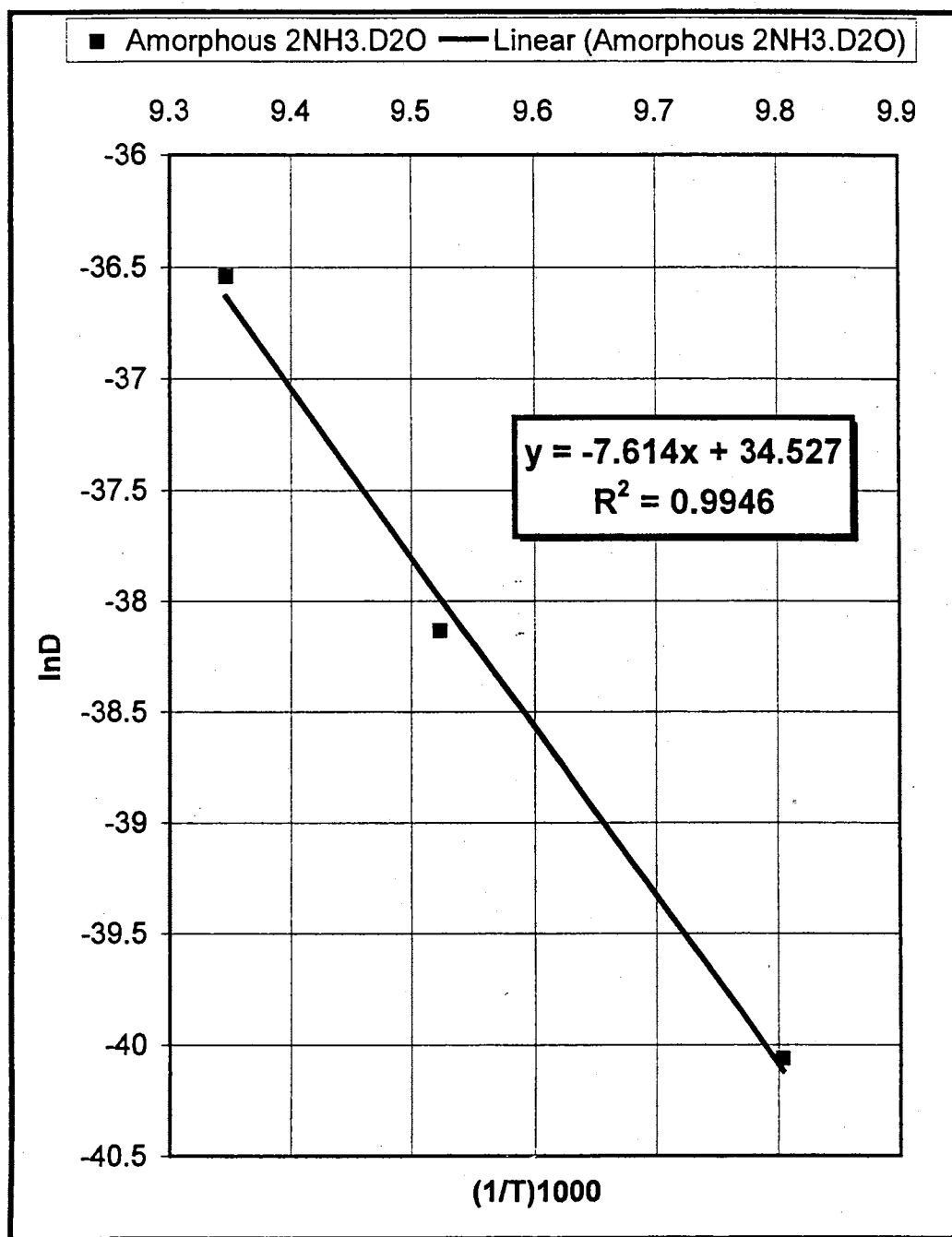


Figure 79. Plot of lnD versus 1/T for the conversion of D₂O ice nanocrystals to the amorphous 2NH₃.D₂O.

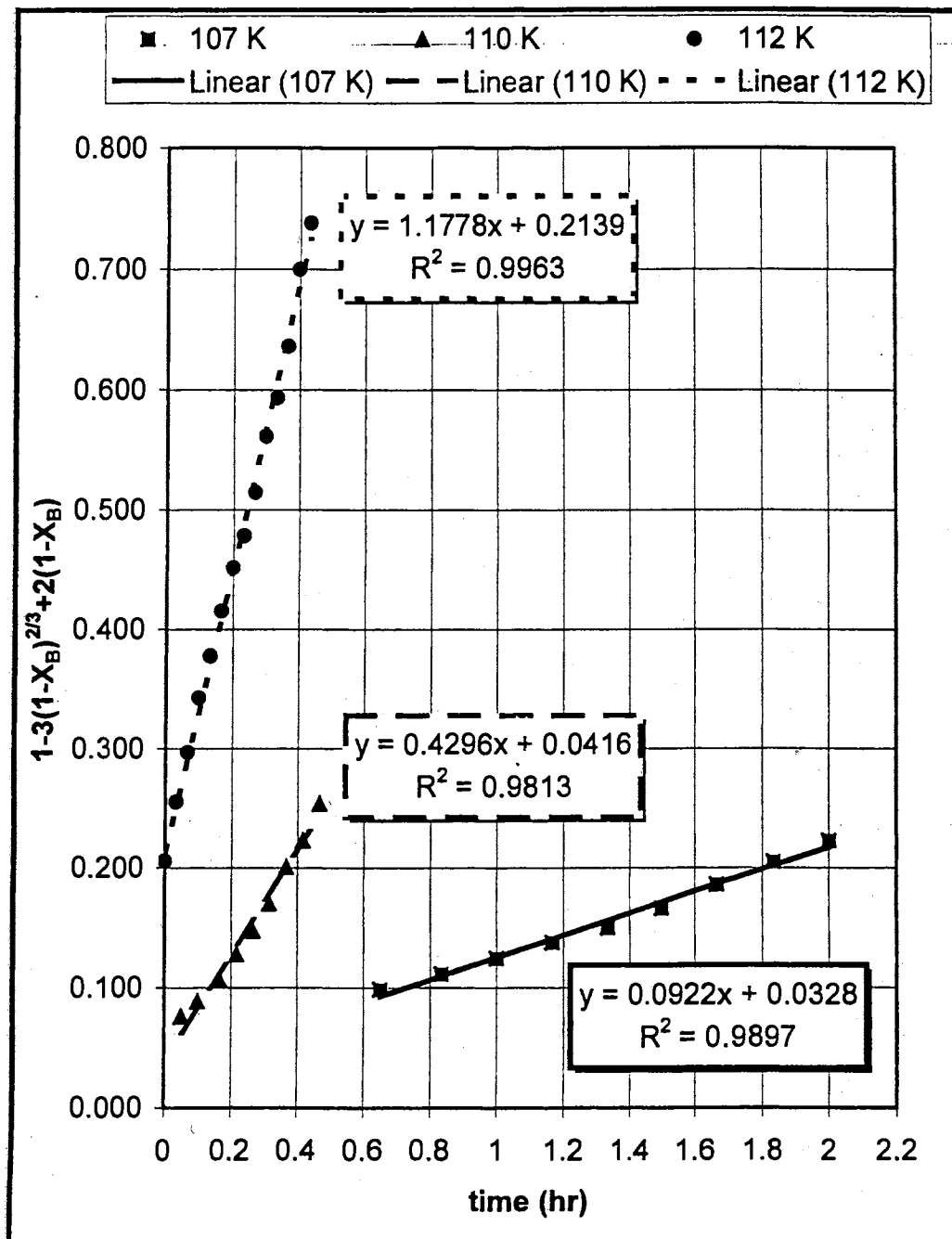


Figure 80. Plots of $[1-3(1-X_B)^{2/3}+2(1-X_B)]$ versus time for the conversion of D_2O ice nanocrystals to the crystalline $2NH_3 \cdot D_2O$.

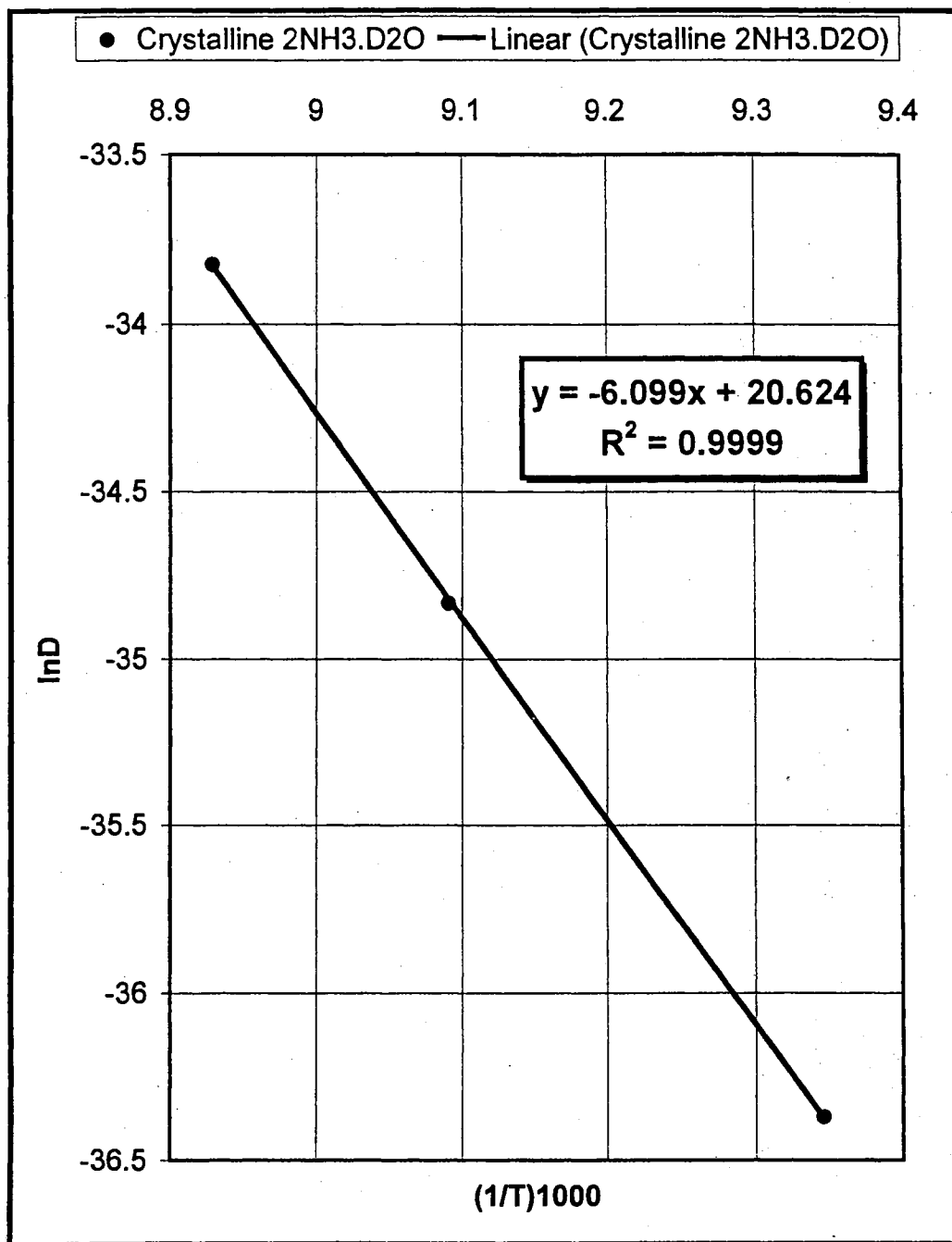


Figure 81. Plot of lnD versus 1/T for the conversion of D₂O ice nanocrystals to the crystalline 2NH₃.D₂O.

3.3. Gingstling's Equation

Comparing the shrinking core equation with Gingstling's gives

$$t = (\rho_B R^2 / 6bD_e C_{Ag}) [1 - 3(1-X_B)^{2/3} + 2(1-X_B)] \quad (20)$$

$$t = (n\rho R^2 / 2\mu DC_{Ag}) [1 - 3(1-X_B)^{2/3} + 2(1-X_B)] \quad (33).$$

If the equations 20 and 33 are equal to each other, the constants should be equal to each other. Substituting the constant values (diffusion coefficients, initial particle size and C_{Ag} are unchanged), we obtain

$$\rho / \mu = \rho_B / 3$$

where μ is the molecular weight of $2NH_3 \cdot D_2O$ (=54 g/mol), ρ is the density of $2NH_3 \cdot D_2O$ (g/cm³) and ρ_B is the molar density of D_2O ice (=0.05191 mol/cm³).

$$\rho = 0.93438 \text{ g/cm}^3.$$

Then, density of $2NH_3 \cdot H_2O$ (ρ)³⁶ is equal to 0.916 g/cm³ so this number is applicable.

The diffusion coefficient found from the Gingstling's equation is approximately the same with that from the shrinking core model's equation. This shows that using either the product density or the ice density in the equation does not change the result.

3.4. Carter's Equation

Carter equation including volume change effect is⁵¹

$$[1 + (z - 1)X_B]^{2/3} + (z - 1)(1 - X_B)^{2/3} = z + 2(1 - z)kt/r_0^2 \quad (41)$$

The Gingstling's equation can be written as⁵²

$$2X_B/3 + (1 - X_B)^{2/3} = 1 - (K'/r_0^2)t \quad (33)$$

As noted by Carter⁵², the influence of the volume change on the rate throughout the reaction can be found by plotting the left-hand side of equation 41 versus the left-hand side of equation 33. That means that the two functions of X_B (fraction of reacted ice) are plotted against one another for various values of z where z is volume change. If the effect of z on the rate is constant, straight lines are obtained.

As discussed before, we cannot detect the volume change. However, by taking different values of z (volume change), the comparative plot described above can be obtained. For this reason, low conversion (at 102 K) and high conversion (at 112 K) of ice values are chosen so that the influence of volume change can be seen for both cases.

The plot of $[1 + (z - 1)X_B]^{2/3} + (z - 1)(1 - X_B)^{2/3}$ versus $2X_B/3 + (1 - X_B)^{2/3}$ is shown in Figure 82 for $z = 1.25, 1.5, 1.75$ and 2 at 102 K. As seen from Figure 82, even if the volume change is increased by a factor of two, the influence is very small, seen from R^2 values.

In the case of high conversion (at 112 K), the plot of $[1+(z-1)X_B]^{2/3}+(z-1)(1-X_B)^{2/3}$ versus $2X_B/3 + (1-X_B)^{2/3}$ is shown in Figure 83. The linear fit of the curves with R^2 values is represented in the same figure and as seen from the R^2 values, the influence of the volume change on the rate is not too much.

Consequently, including the volume change in the rate equations for our case is not necessary.

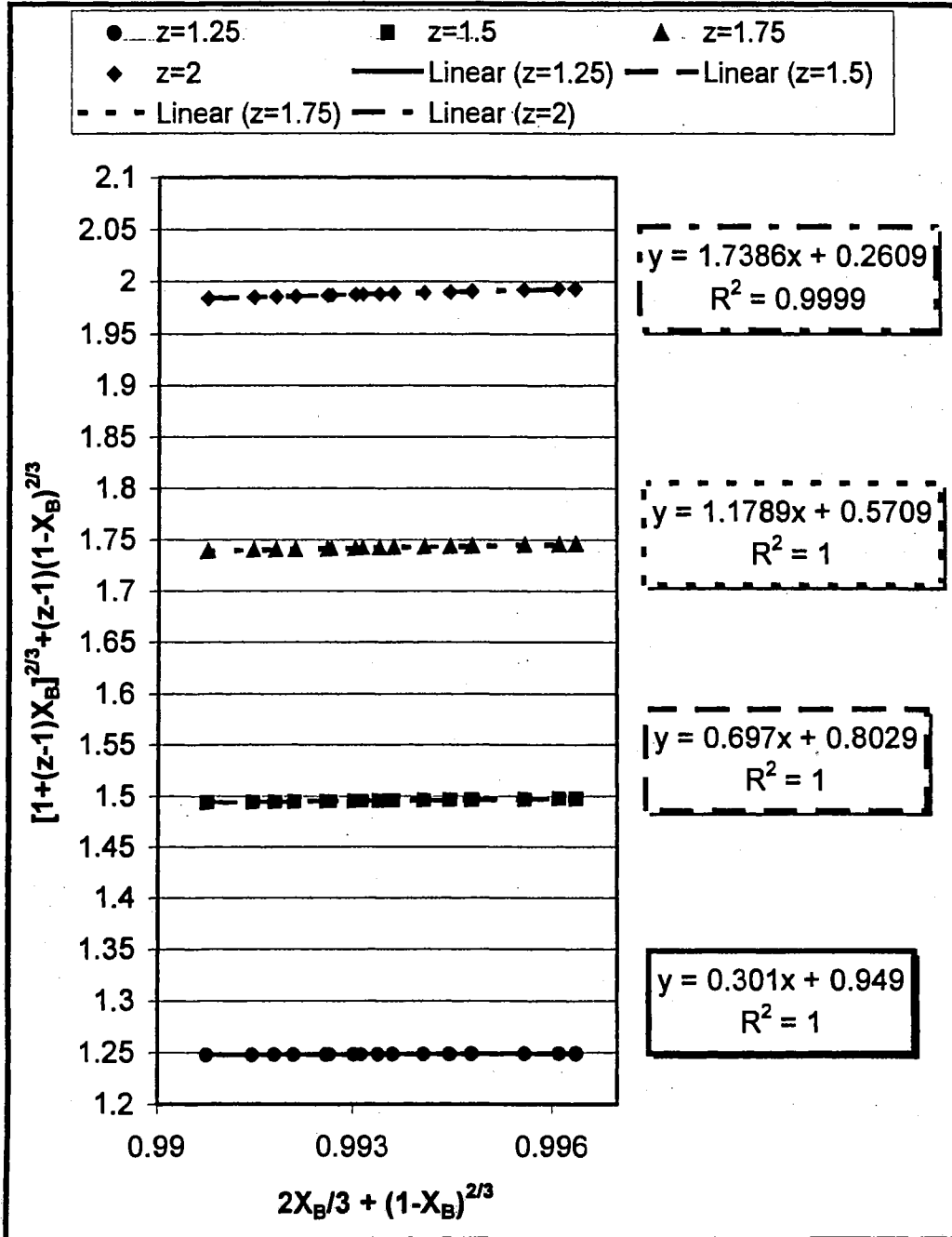


Figure 82. Comparison of Gingstling's and Carter's equations for the conversion of D₂O ice nanocrystals to 2NH₃.D₂O at 102 K.

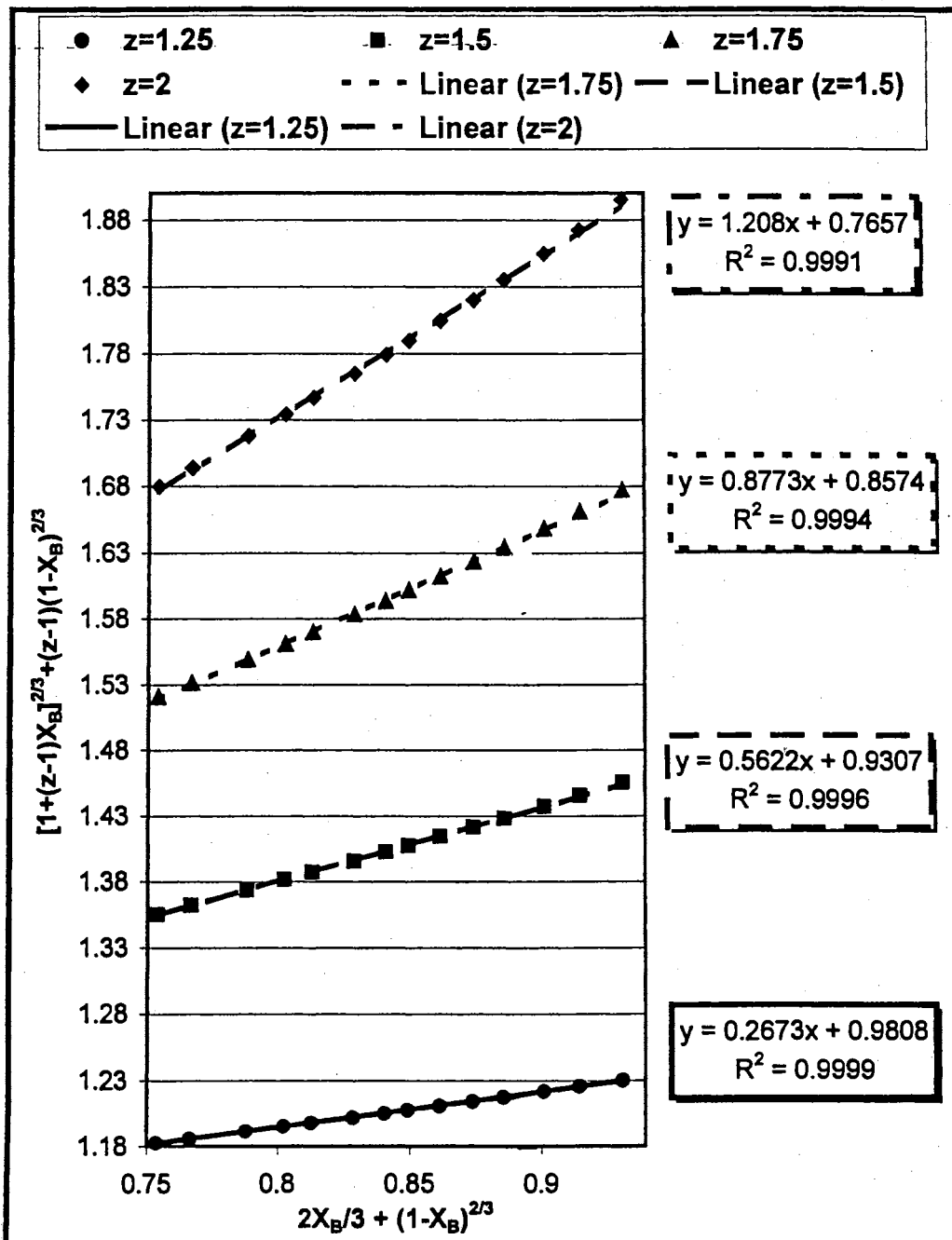


Figure 83. Comparison of Gingstling's and Carter's equations for the conversion of D₂O ice nanocrystals to 2NH₃.D₂O at 112 K.

4. Conversion of H₂O Ice Nanocrystals to the Amorphous 2NH₃.H₂O

In Chapter IV, the small difference in the rates between the H₂O ice and D₂O ice was noted. The plot of $1-3(1-X_B)^{2/3}+2(1-X_B)$ versus time at 102 and 105 K is shown in Figure 84. The diffusion coefficients (\mathcal{D}_e) at 102 and 105 K for NH₃ in the 2NH₃.H₂O are calculated as 3.21×10^{-18} and 1.35×10^{-18} cm²/sec, respectively.

5. Conversion of D₂O Ice Nanocrystals to 2ND₃.D₂O

The plot of $1-3(1-X_B)^{2/3}+2(1-X_B)$ versus time at 102 and 105 K is shown in Figure 85 and the diffusion coefficients are calculated as 1.27×10^{-18} cm²/sec at 102 K and 3.06×10^{-18} cm²/sec at 105 K.

The plot of $1-3(1-X_B)^{2/3}+2(1-X_B)$ versus time at 107 and 110 K is shown in Figure 86 and the diffusion coefficients are found as 2.08×10^{-17} cm²/sec at 107 K and 8.60×10^{-17} cm²/sec at 110 K.

The ratio of diffusion coefficient of NH₃ and ND₃ is calculated as;

$$\mathcal{D}_{e \text{ NH}_3} / \mathcal{D}_{e \text{ ND}_3} = 1.3543 \text{ at } 102 \text{ K}$$

$$\mathcal{D}_{e \text{ NH}_3} / \mathcal{D}_{e \text{ ND}_3} = 3.8562 \text{ at } 105 \text{ K}$$

$$\mathcal{D}_{e \text{ NH}_3} / \mathcal{D}_{e \text{ ND}_3} = 3.3125 \text{ at } 107 \text{ K}$$

$$\mathcal{D}_{e \text{ NH}_3} / \mathcal{D}_{e \text{ ND}_3} = 3.7325 \text{ at } 110 \text{ K}$$

If the reaction rate is controlled by the diffusion of ammonia through the solid hydrate product, rate should be affected by an association of ammonia with

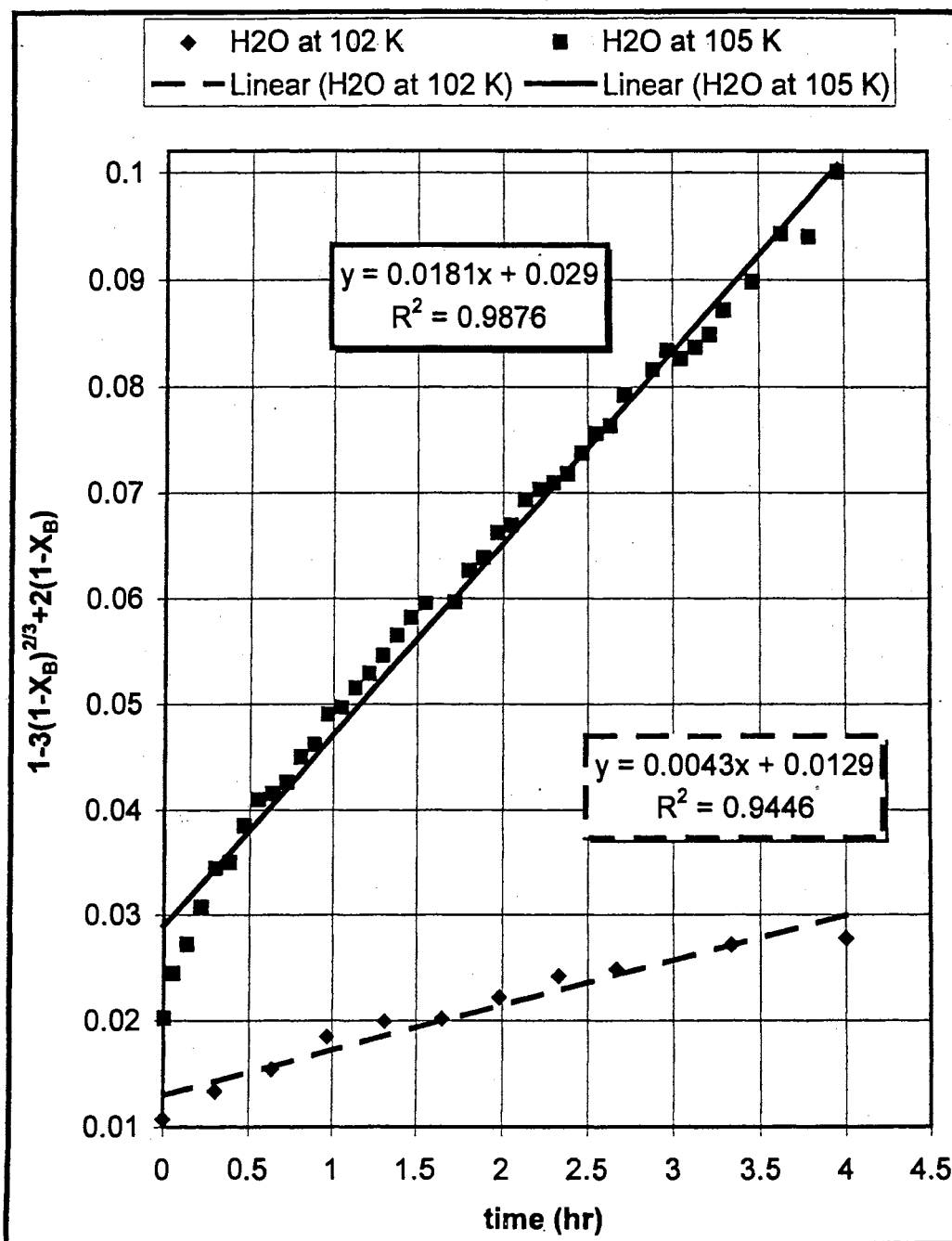


Figure 84. Plots of $[1-3(1-X_B)^{2/3}+2(1-X_B)]$ versus time for the conversion of H₂O ice nanocrystals to the amorphous 2NH₃.H₂O.

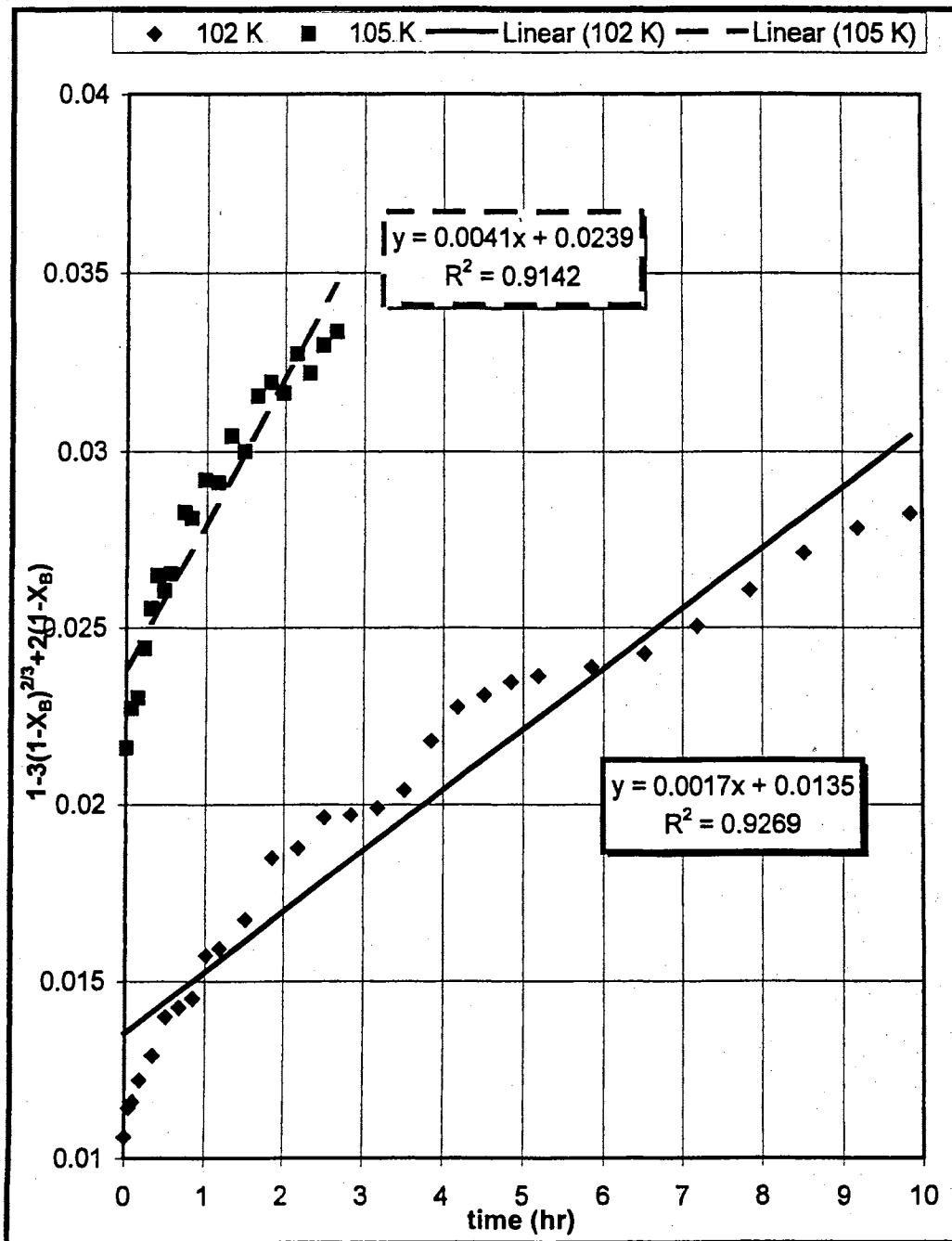


Figure 85. Plots of $[1-3(1-X_B)^{2/3}+2(1-X_B)]$ versus time for the conversion of D_2O ice nanocrystals to the amorphous $2ND_3 \cdot D_2O$.

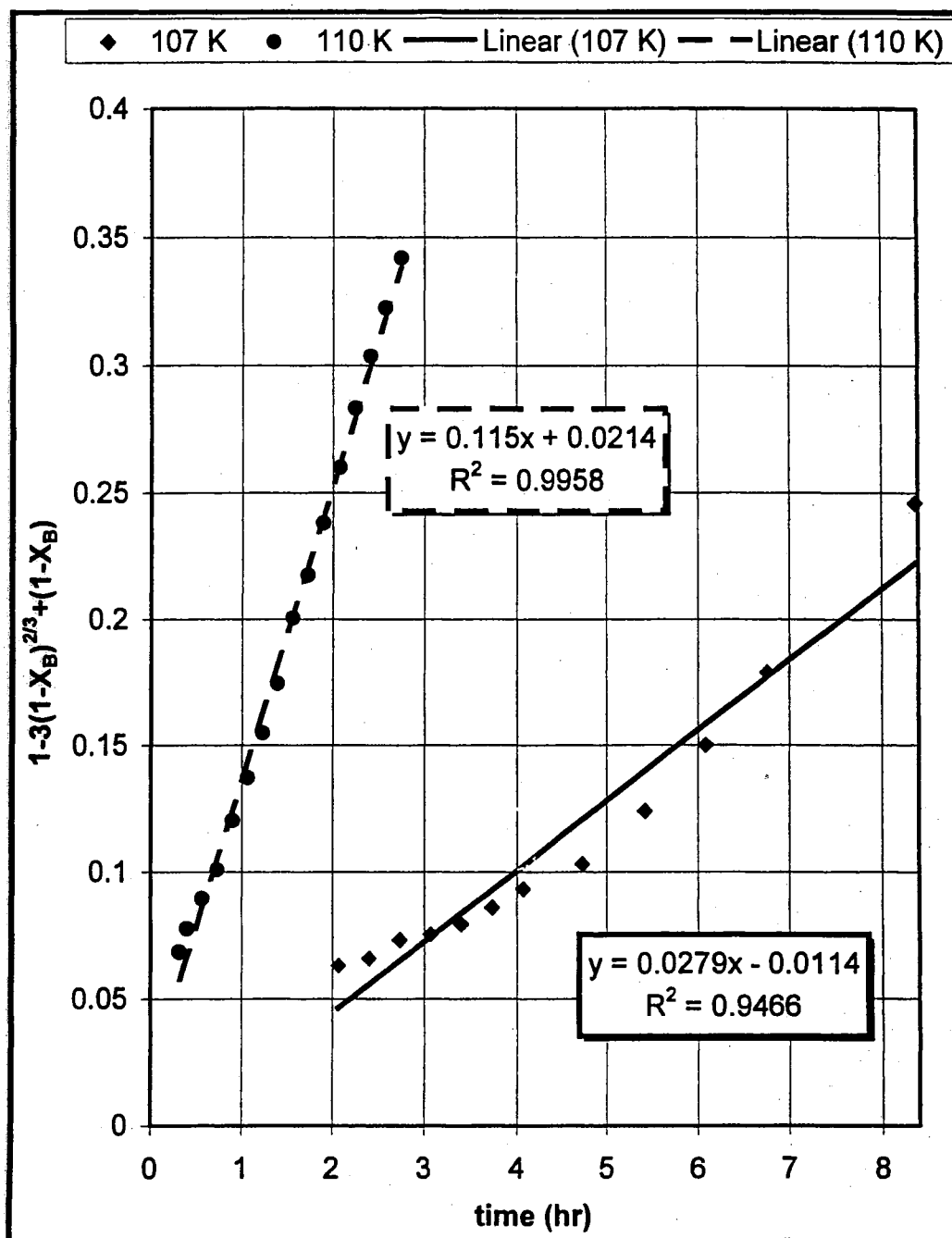


Figure 86. Plots of $[1-3(1-X_B)^{2/3}+2(1-X_B)]$ versus time for the conversion of D_2O ice nanocrystals to the crystalline $2ND_3 \cdot D_2O$.

the ammonia and water within the hydrate network. Therefore, it is expected that this difference comes from the zero-point energy difference for association of NH_3 and ND_3 .

6. Errors in the Results

The major sources of errors in the determination of the diffusion coefficients may be divided into two sections: In the first part, the errors comes from the measurements of the fraction of reacted ice (X_B) placed in the equation of $[1-3(1-X_B)^{2/3}+2(1-X_B)]$ to find the diffusion coefficients. In the second part, the errors are in the determination of the constants in the factor $(6bD_eC_{Ag}/\rho_B R^2)$ of the shrinking core equation.

6.1. Errors in Determination of Fraction of Reacted Ice

The main source of error in the first part is in evaluating the spectroscopic measurements; the fraction of reacted ice, as discussed in the previous chapter, was found using the product band intensity measured against the original sample spectrum. Although, a base line correction was used to measure accurately these peak intensities, since these are broad peaks, some error may originate here.

The second main error in determination of the fraction of reacted ice is the difference spectrum between the partially reacted ice and bare ice spectra since we were deciding to stop subtraction with naked eye. The only requirement that we followed to find the subtraction factor was the disappearance from the hydrate

spectrum of the main ice band at 2424 cm^{-1} . Furthermore, as noted before, since the NH_3 and ND_3 samples contained contaminant (NH_2D), this contaminant interfered with the subtraction of ice from the partially reacted ice spectrum.

6.2. Errors in Determination of Constants in the Equation of $(6bD_eC_{Ag}/\rho_B R^2)$

When the data were analyzed, the size of the ice particles (R) was assumed to be 25 nm. However, there is a distribution of the particle size that may be given by a Gaussian type of plot with a width of 10 nm where from ~20 nm. That is, diameters of few particles are smaller than 15 nm or larger than 35 nm. Putting 15 and 35 nm values into the equation, the diffusion coefficient is calculated for these cases as;

$$D_e = 1.37 \times 10^{-18} \text{ for 35 nm particle diameter at 102 K}$$

$$D_e = 6.19 \times 10^{-19} \text{ for 15 nm particle diameter at 102 K}$$

which gives average diffusion coefficient as $1.98 \times 10^{-18} \text{ cm}^2/\text{sec}$ at 102 K. For 25 nm particle diameter, the diffusion coefficient has been calculated as 1.72×10^{-18} at 102 K.

7. Summary

The conversion of ice nanocrystals to the hemihydrate of ammonia may be thought as the heterogeneous reaction between the $\text{NH}_3(\text{g})$ and the spherical ice nanocrystals. The diffusion of ammonia through the hydrate layer is rate limiting for this conversion and the diffusion of ammonia occurs primarily via a molecular mechanism.

It was shown that the experimental data obtained in this research correlated very well with “shrinking core model for spherical particles” (equation 20) developed by Yagi and Kunii (1955) and “the diffusion kinetics of reactions in spherical particles” (equation 33) by Ginstling and Brounshtein (1950). These two models assume the particle size does not change throughout the reaction. Furthermore, including the volume change did not change the results obtained from this research.

The activation energies for the diffusion of NH_3 through the amorphous and crystalline hydrates were determined as 15.13 kcal/mol and 12.12 kcal/mol, respectively.

There seems to be only a small isotopic effect on the reaction rate when the D_2O and H_2O are compared. If this small difference is a D-isotope effect, it occurs due to the association of ammonia with the water part of the hydrate while the ammonia molecule is diffusing through the hydrate.

There is a deuterium isotope effect on the reaction rate when NH_3 was replaced by ND_3 . This comes from the difference of zero-point energy for association of ammonia molecules with the hydrate and the difference in the mass of the H- and D- containing ammonia.

CHAPTER VI

CONCLUSION AND DISCUSSION

1. Introduction

In this chapter, the results of the study of NH_3 – ice reaction are summarized and compared with the literature on other strong (penetrating) adsorbates; namely HCl and HNO_3 . To evaluate the credibility of the magnitude of diffusion and activation energies for the solid state reactions, values for in ice H_2O will be examined, then, future studies will be considered.

2. Conclusions

The conversion of ice nanocrystals to the hydrates of ammonia is a heterogeneous gas-solid process. Two methods were used to prepare FTIR samples: in the first method, an ~ 1.0 micron thick network of ice nanocrystals was deposited onto IR transparent windows and then exposed to ammonia vapor in the range 115-123 K. In the second method, the ice particles were mixed with ammonia particles at 90 K and the subsequent reaction was measured in the range 100-112 K. For both methods, the rate of thermal vaporization of ammonia was fast enough to allow measurement of the kinetics for the conversion of ice nanocrystals to the hydrates of ammonia by monitoring the FTIR spectra as a function of time. However, the first method resulted in formation of the monohydrate of ammonia ($\text{NH}_3 \cdot \text{H}_2\text{O}$) and the second one produced the hemihydrate of ammonia ($2\text{NH}_3 \cdot \text{H}_2\text{O}$).

It is suggested that the first step for the formation of the hydrate is the nucleation of the hydrate phase and the solid hydrate is monohydrate or hemihydrate, depending on the concentration of ammonia in the critical cluster. Furthermore, it is shown based on the experimental evidence that the conversion of the ice nanocrystals to either hydrate proceeds via a molecular mechanism.

It was concluded that the vapor pressure of ammonia is rate limiting for the conversion of ice nanocrystals to the monohydrate of ammonia. The reaction rate was constant, which clearly indicates that one factor, constant during the reaction, should control the reaction rate.

For the conversion of ice nanocrystals to the hemihydrate of ammonia, the rate-limiting step is the diffusion of ammonia through the hemihydrate of ammonia that forms on the surface of the ice particles. It was shown that the experimental results correlate successfully with the "shrinking core model". The diffusion coefficient of ammonia in the amorphous crust were evaluated in the range $1.72 \times 10^{-18} - 5.82 \times 10^{-17} \text{ cm}^2 \text{sec}^{-1}$ at 102-107 K and the activation energy was found as $\sim 15 \text{ kcal/mol}$ for the conversion of D_2O ice nanocrystals to the amorphous $2\text{NH}_3 \cdot \text{D}_2\text{O}$. By comparison, the diffusion coefficient was in the range $6.89 \times 10^{-17} - 8.81 \times 10^{-16} \text{ cm}^2 \text{sec}^{-1}$ at 107-110 K and the activation energy was $\sim 12 \text{ kcal/mol}$ for the conversion of D_2O ice nanocrystals to the crystalline $2\text{NH}_3 \cdot \text{D}_2\text{O}$.

3. Literature Review for the Kinetic Studies with Ice

As discussed in the first chapter, HCl, HNO_3 and NH_3 are strong

(penetrating) adsorbates with a capability to break the water-water bonding in the ice due to the comparable adsorbate-water bonding, therefore, they can convert ice to a hydrate.^{23,24}

Perhaps, one of the critical conclusion of this study is the diffusion of ammonia through the hydrate crust is rate limiting for the conversion of ice nanocrystals to particles of the hemihydrate of ammonia.

Several researchers have studied kinetics of conversion of ice to the hydrate of HCl with a wide variety of methods and the diffusion of HCl was calculated from these measurements. However, there may be a misconception in the interpretation of the experimental results, since most of these authors are speak of the diffusion of HCl in the ice, rather than in the hydrate.

For instance, Koehler *et. al.*⁵³ used FTIR to determine the kinetics of formation of the hexahydrate of HCl from the thin film of ice at 158 K. Actually, they used FTIR to plot the uptake of HCl as a function of film thickness (the uptake of HCl in their study was calculated from one of the calibrated bands of the hexahydrate, and using the intensity difference between the partially HCl reacted ice and the bare ice). Since they observed that for the thicker films, the uptake of HCl by ice does not increase they concluded that the uptake of HCl is diffusion limited. They calculated the diffusion coefficient of HCl in the ice from $D=x^2/2t$, where D is the diffusion coefficient, x is the film thickness and t is the time. Since the film thickness and time is known, the diffusion coefficient is found $\sim 2 \times 10^{-12} \text{ cm}^2 \text{ sec}^{-1}$ at 158 K.

Horn and Sully⁸ also investigated the reaction and diffusion of HCl using

attenuated total internal reflection IR spectroscopy (ATR-IR). They used H_3O^+ band intensity in the difference spectrum between the partially reacted HCl spectrum and the bare ice spectrum. The diffusion coefficient of HCl in the ice is calculated a $1.5 \times 10^{-15} \text{ cm}^2 \text{ sec}^{-1}$ at 160 K. Moreover, it is believed in this study that the diffusion of HCl in the ice proceeds via ionic diffusion mechanism which is based on the diffusion of H_3O^+ and Cl^- .

The diffusion coefficient HCl in a thin film of ice was found to be $1 \times 10^{-5} \text{ cm}^2 \text{ sec}^{-1}$ at 185 K by Molina *et. al.*³ They monitored the rate of diffusion in the ice crystals by measuring the HCl concentration spectroscopically at 185 nm with a mercury lamp-dielectric filter-solar blind photomultiplier assembly.

Thibert and Domine⁵⁴ found the diffusion coefficient of HCl in ice at 258 K was $1 \times 10^{-12} \text{ cm}^2 \text{ sec}^{-1}$.

It should be noted here, all of these studies were done with thin films of ice. However, it does not matter whether the bulk ice or particle is used since this does not change the mechanism, but certainly, it changes the rate (since the greater particle surface-to-volume ratio accelerates the reaction). It is widely accepted that exposure of ice to HCl at levels above of a monolayer coating results in ionization of HCl. Hydrogen chloride forms an ionic hydrate which is either amorphous or crystalline, depending on the temperature. At high temperatures and low HCl concentration, the solid product is generally the hexahydrate of HCl.^{23,54} Therefore, the diffusion of HCl, after the initial rapid reaction with the ice surface, should occur in the hydrate not in the ice.

Thibert and Domine¹³ studied also HNO_3 kinetics. The diffusion coefficient

of HNO_3 in the ice was found as $1 \times 10^{-11} \text{ cm}^2/\text{sec}$ at 238 K and $2 \times 10^{-10} \text{ cm}^2/\text{sec}$ at 265 K. The activation energy was calculated as 13 kcal/mol. A similar argument, as for HCl, can be made for HNO_3 , since HNO_3 also converts ice to the ionic hydrates. Therefore, the diffusion of HNO_3 occurs in the hydrate of HNO_3 , not in the ice.

4. Diffusion of HDO in Ice

To compare the magnitude of the diffusion coefficient and activation energy in the solid state reactions, a study of diffusion of HDO in ice by Livingston *et.al.*⁵⁵ can be taken into account. The diffusion coefficient of HDO in the ice was found as $2.2 \times 10^{-16} - 3.9 \times 10^{-14} \text{ cm}^2/\text{sec}$ for temperatures of 153-170 K and a diffusion activation energy was 17 kcal/mol.

If one considers the heat of vaporization of ice and ammonia, which are ~ 11 for ice and ~ 7 for ammonia, a similar relation between the activation energies and heats of vaporization (17 vs 11 kcal/mol for HDO and 12 vs 7 kcal/mol for ammonia) can be found.

5. Future Studies

As mentioned in parts of this study, this research will be a basis for a computer simulation to understand the molecular level aspects of the hydrate formation stages, like adsorption, penetration and conversion.

NH_3 is a good candidate for this purpose; since the molecular nature of the penetration and conversion simplifies the computer simulation, in contrast to

HCl and HNO₃. As shown for the low reaction temperature samples, the conversion of ice to the amorphous hemihydrate of ammonia was achieved by using approximately six monolayers of ice at 102 K. That is, the data for the molecular transport in the near surface region of ice is available after this research so that it also simplifies the computer simulation.

As shown in this study, the experimental results correlate successfully with the "shrinking core model". The same study can be done for HCl and HNO₃ to find the diffusion coefficient of these adsorbates that may make a clearer picture of the diffusion mechanism, and the importance of diffusion through the hydrate must rather than in ice.

REFERENCES

1. Hobbs, V. P. "Ice Physics" Oxford, Great Britain: Clarendon Press; 1974.
2. Lal, M., Clark, A. H. and Lips, A. "Inhibition of Ice Crystal Growth by Preferential Peptide Adsorption: A Molecular Modeling Study." Faraday Discuss, Vol. 95, p.299, 1993.
3. Molina, J. M., Tso, T.-L., Molina, L. T., and Wang, F. C.-Y., "Antarctic Stratospheric Chemistry of Chlorine Nitrate, Hydrogen Chloride, and Ice: Release of Active Chlorine." Science, Vol. 238, p. 1233, 1987.
4. Tolbert, M. A., Rossi, M. J., and Golden, D. M., "Antarctic Ozone Depletion Chemistry: Reactions of N_2O_5 with H_2O and HCl on Ice Surfaces." Science, Vol. 240, p. 1018, 1988.
5. Iraci, L. T., Middlebrook, A. M., Wilson, M. A., and Tolbert, M. A., "Growth of nitric acid hydrates on thin sulfuric acid films." Geophysical Res. Lett., Vol. 21, p. 867, 1994.
6. Graham, J. D., and Roberts, J. T., "Interaction of Hydrogen Chloride with an Ultrathin Ice Film: Observation of Adsorbed and Absorbed States." J. Phys. Chem., Vol. 98, p. 5974, 1994.
7. Delzeit, L., Rowland, B., and Devlin, J. P., "Infrared Spectra of HCl Complexed/Ionized in Amorphous Hydrates and at Ice Surfaces in the 15-90 K Range." J. Phys. Chem., Vol. 97, p. 10312, 1993.
8. Horn, A. B., and Sully, J., "Reaction and Diffusion in Heterogeneous Atmospheric Chemistry Studied by Attenuated Total Internal Reflection IR Spectroscopy." J. Chem. Soc., Faraday Trans., Vol 93(16), p. 2741, 1997.
9. Kroes, G.-J., and Clary, D.C., "Sticking of HCl and $ClOH$ to Ice: A Computational Study." J. Phys. Chem., Vol. 96, p. 7079, 1992.
10. Geiger, F. M., Hicks, J. M., and de Dios, A. C., "Ab Initio Study of $HOCl$, HCl , H_2O , and Cl_2 Interacting with Four Water Molecules." J. Phys. Chem., Vol. 102, p. 1514, 1998.
11. Bussolin, G., Casassa, S., Pisani, C., and Ugliengo, P., "Ab Initio Study of HCl and HF Interaction with Crystalline Ice. I. Physical Adsorption." J. Chem. Phys., Vol. 108, p. 9516, 1998.

12. Tolbert, M. A., and Middlebrook, A. M., "Fourier Transform Infrared Studies of Model Polar Stratospheric Cloud Surfaces: Growth and Evaporation of Ice and Nitric Acid/Ice." J. Geophysical Res., Vol. 95, p. 423, 1990.
13. Thibert, E., and Domine, F., "Thermodynamics and Kinetics of Solid Solution of HNO₃ in Ice." J. Phys. Chem., Vol. 102, p. 4432, 1998.
14. Lunine, J. I., "Chemistry in the Outer Solar System." C&EN, Special Report, p. 41, 1995.
15. Lewis, J. S., "The Clouds of Jupiter and the NH₃-H₂O and NH₃-H₂S Systems." Icarus, Vol. 10, p. 365, 1969.
16. Rowland, B., Kadagathur, N. S., and Devlin, J. P., Buch, V., Feldman, T., Wojcik, M. J., "Infrared Spectra of Ice Surfaces and Assignment of Surface-Localized Modes from Simulated Spectra of Cubic Ice." J. Chem. Phys., Vol. 102, p. 8328, 1995.
17. Devlin, J. P., Buch, V., "Surface of Ice As Viewed from Combined Spectroscopic and Computer Modeling Studies." J. Phys. Chem., Vol. 99, p. 16534, 1995.
18. Kroes, G.-J., "Surface Melting of the (0001) Face of TIP4P Ice." Surface Science, Vol. 275, p. 365, 1992.
19. Delzeit, L., Devlin, J. P., and Buch, V., "Structural Relaxation Rates Near the Ice Surface: Basis for Separation of the Surface and Subsurface Spectra." J. Chem. Phys., Vol. 107, p. 3726, 1997.
20. Rowland, B., Kadagathur, N. S., and Devlin, J. P., "Infrared Spectra of CF₄ Adsorbed on Ice: Probing Adsorbate Dilution and Phase Separation with the ν_3 Transverse-Longitudinal Splitting." J. Chem. Phys., Vol. 102, p. 13, 1995.
21. Delzeit, L., Devlin, M. S., Rowland, B., Devlin, J. P., and Buch, V., "Adsorbate-Induced Partial Ordering of the Irregular Surface and Subsurface of Crystalline Ice." J. Phys. Chem., Vol. 100, p. 10076, 1996.
22. Rowland, B., Fisher, M., and Devlin, J. P., "Probing Icy Surfaces with the Dangling-OH-Mode Absorption: Large Ice Clusters and Microporous Amorphous Ice." J. Chem. Phys., Vol. 95, p. 1378, 1991.
23. Delzeit, L., Powell, K., Uras, N., and Devlin, J. P., "Ice Surface Reactions with Acids and Bases." J. Phys. Chem., Vol. 101, p. 2327, 1997.

24. Uras, N., Rahman, M., and Devlin, J. P., "Covalent HCl at the Surface of Crystalline Ice at 125 K: The Stable Phase at Submonolayer Levels." J. Phys. Chem., Vol. 102, p. 9375, 1998.
25. Devlin, J. P., Uras, N., Rahman, M., and Buch, V., "Covalent and Ionic States of Strong Acids at the Ice Surface." To be published.
26. Ritzhaupt, G. and Devlin, J. P., "Infrared Spectra of Nitric and Hydrochloric Acid Hydrate Thin Films." J. Phys. Chem., Vol. 95, p 90, 1991.
27. Staats, P. A., Morgan, H. W., "Infrared Spectra of Solid Ammonia." J. Chem. Phys., Vol.31, p. 553, 1959.
28. Wolff, H., Rollan, H.-G., and Wolff, E., "Infrared Spectra and Vapor pressure Isotope Effect of Crystallized Ammonia and Its Deuterium Derivatives." J. Chem. Phys., Vol.55, p. 1373, 1971.
29. Ferraro, J. R., Sill, G., and Fink, G., "Infrared Intensity Measurements of Cryodeposited Thin Films of NH₃, NH₄HS, H₂S, and Assignments of Absorption Bands." Applied Spectroscopy, Vol. 34, p. 525. 1980.
30. Latajka, Z., Scheiner, S., "Structure, Energetics, and Vibrational Spectrum of H₃N••HOH." J. Phys. Chem., Vol.94, p. 217, 1990.
31. Langlet, J., Caillet, J., and Caffarel, M., "A Perturbational Study of Some Hydrogen-Bonded Dimers." J. Chem. Phys., Vol.103, p. 8043, 1995.
32. Donaldson, D. J., "Adsorption of Atmospheric Gases at the Air-Water Interface. I. NH₃." J. Phys. Chem., Vol.103, p. 62, 1999.
33. Hu, J. H., Davidovits, P., Worsnop, D. R., Zahniser, M. S., and Kolb, C. E., "Entry of Gas Molecules into Liquids." Faraday Discuss, Vol.100, p. 65, 1995.
34. Olovsson, I., and Templeton, D. H., "The Crystal Structure of Ammonia Monohydrate." Acta Cryst. Vol. 12, p. 827, 1959.
35. Bertie, J. E., and Shehata, M. R., "The Infrared Spectra of NH₃.H₂O and ND₃.D₂O at 100 K." J. Chem. Phys., Vol.83, p.1449, 1995.
36. Siemons, W. J. and Templeton, D. H., "The Crystal Structure of Ammonia oxide." Acta Cryst. Vol. 7, p. 194, 1954.
37. Bertie, J. E., and Devlin, J. P., "The Infrared Spectra and Phase Transitions ND₃.D₂O between 100 and 15 K." J. Chem. Phys., Vol.81, p.1559, 1984.

38. Bertie, J. E., and Shehata, M. R., "Ammonia Dihydrate: Preparation, X-Ray Powder Diffraction Pattern and Infrared Spectrum of $\text{NH}_3 \cdot 2\text{H}_2\text{O}$ at 100 K." J. Chem. Phys., Vol.81, p.27, 1984.
39. Gomes, W., "Definition of Rate Constant and Activation Energy in Solid State Reactions." Nature, Vol. 192, p. 865, 1961.
40. Sharp, J. H., Brindley, G. W., and Narahari Acar, B. N., "Numerical Data for Some Commonly Used Solid State Reaction Equations." Journal of American Ceramic Society, Vol. 49, p. 379, 1966.
41. Budnikov, P. P. and Ginstling, A. M., "Principles of Solid State Chemistry; Reaction in Solids" London: Maclaren & Sons, Ltd; 1968.
42. Szafran, M. and Dega-Szafran, Z., "A Critical Review of the Isotope Effect in IR Spectra." J. Mol. Struct., Vol. 321, p. 57, 1994.
43. Melander, L., "Isotope Effects on Reaction Rates." New York: The Ronald Press Com.; 1960.
44. Wiberg, K. B., "The Deuterium Isotope Effect." Chem. Revs. Vol. 55, p. 713, 1955.
45. Bigeleisen, J., "The Relative Reaction Velocities of Isotopic Molecules." J. Chem. Phys., Vol.17, p.675, 1949.
46. Kirshenbaun, I. and Urey, H. C. "The Differences in the Vapor Pressures, Heats of Vaporization and Triple Points of Nitrogen (14) and Nitrogen (15) and of Ammonia and Trideuteroammonia." J. Chem. Phys., Vol. 10, p. 706, 1942.
47. Rowland, B. and Devlin, J. P., "Spectra of Dangling OH Groups at Ice Cluster Surface and Within Pores of Amorphous Ice." J. Chem. Phys., Vol. 94, p. 812, 1991.
48. Jorgensen, P. J., Wadsworth, M. E., and Cutler, I. B., "Oxidation of Silicon Carbide." J. Am. Ceramic Soc., Vol. 42, p. 613, 1959.
49. Levenspiel, O. "Chemical Reaction Engineering" New York: John Wiley & Sons, Inc; 1962, p. 364).
50. Ginstling, A. M. and Brounshtein, B. I. "Concerning the Diffusion Kinetics of Reactions in Spherical Particles." J. of Appl. Chem. USSR, Vol. 23, p. 1327, 1950.

51. Carter, R. E., "Kinetic Model for Solid-State Reactions." J. Chem. Phys., Vol. 34, p. 2010, 1960
52. Carter, R. E., "Addendum: Kinetic Model for Solid-State Reactions." ibid., Vol. 35, p. 1137, 1961.
53. Koehler, B. G., Middlebrook, A. M., McNeil, L. S., and Tolbert, M. A., "FTIR Studies of the Interaction of HCl with Model Polar Stratospheric Cloud Films." J. Geophys. Res., Vol. 98, p. 10563, 1993.
54. Banham, S. F., Sodeau, J. R., Horn, A. B., McCoustra, M. R. S., and Chesters, M. A., "Adsorption and Ionization of HCl on an Ice Surface." J. Vac. Sci. Technol. A, Vol. 14, p. 1620, 1996.
55. Livingstone, F. E., Whipple, G. C., and George, S. M., "Diffusion of HDO into Single-Crystal H_2^{16}O Ice Multilayers: Comparison with H_2^{18}O ." J. Phys. Chem. B, Vol. 101, p. 6127, 1997.

APPENDIX

Table 6

Fraction of reacted ice versus time for $2\text{NH}_3 \cdot \text{D}_2\text{O}$ from the first method.

100 K		102 K		105 K		107 K		110 K		112 K	
time (hr)	reacted ice	time (hr)	reacted ice	time (hr)	reacted ice	time (hr)	reacted ice	time (hr)	reacted ice	time (hr)	reacted ice
0	0.083	0	0.098	0	0.128	0	0.200	0	0.287	0	0.205
0.083	0.094	0.083	0.114	0.083	0.163	0.133	0.263	0.016	0.336	0.033	0.255
0.183	0.099	0.25	0.131	0.183	0.198	0.25	0.304	0.05	0.405	0.066	0.296
0.35	0.104	0.583	0.150	0.316	0.229	0.366	0.333	0.1	0.477	0.1	0.342
0.533	0.111	0.933	0.167	0.416	0.243	0.483	0.363	0.166	0.536	0.133	0.377
0.683	0.116	1.266	0.181	0.5	0.255	0.65	0.400	0.216	0.579	0.166	0.415
0.833	0.122	1.6	0.192	0.6	0.269	0.833	0.427	0.266	0.640	0.2	0.451
1.2	0.127	1.933	0.199	0.7	0.280	1	0.445	0.316	0.703	0.233	0.478
1.516	0.134	2.266	0.207	0.8	0.299	1.166	0.478	0.366	0.748	0.266	0.514
1.85	0.141	2.616	0.213	0.866	0.312	1.333	0.515	0.416	0.820	0.3	0.561
2.183	0.145	2.95	0.218	0.966	0.319	1.5	0.571	0.466	0.879	0.333	0.593
2.516	0.151	3.283	0.226	1.166	0.336	1.666	0.608			0.366	0.636
2.85	0.155	3.95	0.231	1.266	0.343	1.833	0.644			0.4	0.700
3.183	0.16	4.616	0.238	1.383	0.352	2	0.697			0.433	0.738
3.55	0.164	5.283	0.246	1.5	0.363	2.166	0.742				
4.033	0.171	7	0.265	1.633	0.370						
4.366	0.174			1.783	0.380						
4.7	0.178			1.95	0.391						
5.45	0.183			2.1	0.406						
5.85	0.186			2.316	0.414						
6.666	0.193			2.516	0.427						
7.666	0.198			2.733	0.438						
8.25	0.203			2.933	0.461						
8.666	0.205			3.4	0.489						
9	0.209			3.6	0.505						
9.5	0.212			3.766	0.516						
9.833	0.214			3.933	0.528						
10.75	0.216			4.133	0.534						
11.16	0.219			4.3	0.545						
6											
11.58	0.220			4.466	0.555						
				4.633	0.563						
				4.8	0.575						
				4.966	0.582						

Table 7

Fraction of reacted ice versus time for $2\text{NH}_3 \cdot \text{D}_2\text{O}$ from the second method.

105 K		107 K		110 K		112 K	
time (hr)	reacted ice	time (hr)	reacted ice	time (hr)	reacted ice	time (hr)	reacted ice
0	0.244	0.366	0.080	0.05	0.425	0	0.205
0.083	0.256	0.483	0.086	0.1	0.455	0.033	0.255
0.183	0.278	0.65	0.098	0.166	0.491	0.066	0.296
0.316	0.296	0.833	0.111	0.216	0.531	0.1	0.342
0.416	0.309	1	0.124	0.266	0.563	0.133	0.377
0.5	0.310	1.166	0.137	0.316	0.597	0.166	0.415
0.6	0.326	1.333	0.149	0.366	0.637	0.2	0.451
0.7	0.326	1.5	0.165	0.416	0.664	0.233	0.478
0.8	0.330	1.666	0.185	0.466	0.698	0.266	0.514
0.866	0.337	1.833	0.204			0.3	0.561
0.966	0.341	2	0.222			0.333	0.593
1.166	0.359					0.366	0.636
1.266	0.362					0.4	0.700
1.383	0.363					0.433	0.738
1.5	0.370						
1.633	0.381						
1.783	0.383						
1.95	0.394						
2.1	0.395						
2.316	0.401						
2.516	0.410						
2.733	0.416						
2.933	0.425						
3.4	0.439						
3.6	0.447						
3.766	0.453						
3.933	0.457						
4.133	0.470						
4.3	0.472						
4.466	0.482						
4.633	0.483						
4.8	0.490						
4.966	0.498						

Table 8

Fraction of reacted ice versus time for $2\text{NH}_3\cdot\text{H}_2\text{O}$ from the second method.

$2\text{NH}_3\cdot\text{H}_2\text{O}$ at 102 K		$2\text{NH}_3\cdot\text{H}_2\text{O}$ at 105 K			
time (hr)	Fraction of reacted ice	time (hr)	Fraction of reacted ice	time (hr)	Fraction of reacted ice
0	0.172	0	0.232	1.883	0.394
0.3	0.191	0.05	0.254	1.966	0.400
0.633	0.204	0.133	0.267	2.05	0.402
0.966	0.222	0.216	0.282	2.133	0.409
1.316	0.231	0.3	0.298	2.216	0.411
1.65	0.232	0.383	0.300	2.3	0.413
1.983	0.242	0.466	0.313	2.383	0.415
2.333	0.253	0.55	0.322	2.466	0.420
2.666	0.256	0.633	0.325	2.55	0.425
3.333	0.267	0.716	0.328	2.633	0.426
4	0.269	0.8	0.337	2.716	0.433
7	0.287	0.883	0.340	2.883	0.439
		0.966	0.350	2.966	0.443
		1.05	0.352	3.05	0.441
		1.133	0.358	3.133	0.444
		1.216	0.362	3.216	0.447
		1.3	0.367	3.3	0.452
		1.383	0.373	3.466	0.458
		1.466	0.378	3.633	0.467
		1.55	0.382	3.8	0.467
		1.716	0.382	3.966	0.48
		1.8	0.391		

Table 9

Fraction of reacted ice versus time for $2\text{ND}_3\cdot\text{D}_2\text{O}$ from the second method.

$2\text{ND}_3\cdot\text{D}_2\text{O}$ at 102 K		$2\text{ND}_3\cdot\text{D}_2\text{O}$ at 105 K		$2\text{ND}_3\cdot\text{D}_2\text{O}$ at 107 K		$2\text{ND}_3\cdot\text{D}_2\text{O}$ at 110 K	
time (h)	Fraction of reacted ice	time (h)	Fraction of reacted ice	time (h)	Fraction of reacted ice	time (h)	Fraction of reacted ice
0	0	0	0.240	0.233	0.282	0.316	0.406
0.05	0.663	0.066	0.245	0.316	0.291	0.4	0.429
0.1	1.327	0.15	0.247	0.4	0.299	0.566	0.457
0.183	2.433	0.233	0.254	0.483	0.302	0.733	0.481
0.35	4.646	0.316	0.259	0.583	0.309	0.9	0.518
0.516	6.858	0.4	0.264	0.666	0.313	1.066	0.548
0.683	9.071	0.483	0.262	0.75	0.324	1.233	0.575
0.85	11.28	0.566	0.264	0.85	0.334	1.4	0.604
1.016	13.49	0.733	0.272	1.016	0.356	1.566	0.638
1.183	15.70	0.816	0.271	1.233	0.359	1.733	0.658
1.516	20.13	0.983	0.276	1.4	0.373	1.9	0.681
1.85	24.55	1.15	0.275	1.733	0.384	2.083	0.704
2.183	28.98	1.316	0.281	2.066	0.392	2.25	0.726
2.516	33.40	1.483	0.279	2.4	0.399	2.416	0.744
2.85	37.83	1.65	0.286	2.733	0.418	2.583	0.760
3.183	42.25	1.816	0.288	3.066	0.424	2.75	0.776
3.516	46.68	1.983	0.286	3.4	0.433		
3.85	51.10	2.15	0.291	3.733	0.449		
4.183	55.53	2.316	0.289	4.066	0.465		
4.516	59.95	2.483	0.292	4.733	0.486		
4.85	64.38	2.65	0.293	5.416	0.526		
5.183	68.80			6.083	0.568		
5.85	77.66			6.75	0.610		
6.516	86.51			8.366	0.69		
7.183	95.36						
7.85	104.2						
8.516	113.0						
9.183	121.9						
9.85	130.7						

d

VITA

Nevin Uras

Candidate for the Degree of

Doctor of Philosophy

Thesis: A MECHANISTIC AND KINETIC STUDY: CONVERSION OF ICE NANOCRYSTALS TO NANOPARTICLES OF THE HYDRATES OF AMMONIA

Major Field: Chemistry

Biographical:

Personal Data: Born in Pamukova, Sakarya, Turkey, On June 26, 1972, the daughter of Ismail and Mukaddes Uras.

Education: Graduated from Pamukova High School, Pamukova, Sakarya, Turkey in June 1989; received Bachelor of Science degree in Chemistry from Anadolu University, Eskisehir, Turkey in October 1989 and June 1993, respectively. Completed the requirements for the Master of Science degree with a major in Chemistry at Oklahoma State University in July, 1997. Completed the requirements for the Doctor of Philosophy degree with a major in Chemistry at Oklahoma State University in December, 2001.

Experience: Employed by Oklahoma State University, Department of Chemistry as a graduate research assistant; Oklahoma State University, Department of Chemistry, 1997 to present.

Professional Membership: American Chemical Society.